Exploring the potential of a rice NLR pair to engineer novel effector recognition specificities

Rafał Zdrzałek

A thesis submitted to the University of East Anglia for the degree of Doctor of Philosophy

John Innes Centre

September 2021

Moim rodzicom…

Abstract

Plants suffer from various diseases, which cause significant yield losses in crops annually. Pathogens secrete effectors that interact with host targets and manipulate plant metabolism to promote the infection. Translocated effectors can be perceived by plant immune receptors termed NLRs (nucleotide-binding, leucine-rich repeat), restricting pathogen spread.

The rice NLR pair Pik-1/Pik-2 confers resistance to the fungal pathogen *Magnaporthe oryzae* by perceiving variants of the AVR-Pik effector. This recognition is mediated via direct interaction between AVR-Pik and an integrated HMA (heavy metal associated) domain within Pik-1.

In this work, I predominantly used biochemical and structural approaches to characterise several aspects of rice/*M. oryzae* interactions. I investigated the working model of the Pikp-1/Pikp-2 pair and demonstrated they function via a finely tuned cooperation that requires all domains of both NLRs for function. Moreover, I showed both NLRs require their intact P-loop and MHD-like motifs, and they can associate, before and after the perception of the AVR-PikD effector.

I also investigated the interaction between *M. oryzae* effectors from the PWL family, and their potential target OsHIPP43 (rice HMA-containing isoprenylated plant protein 43). I demonstrated that PWL effectors bind OsHIPP43 with micro to nanomolar affinity. I generated the chimeric receptor Pikm-1^{OsHIPP43} and showed that it can perceive all tested PWL effectors in a transient expression system. Additionally, I determined the crystal structure of the PWL2/OsHIPP43 complex. This structure revealed that PWL2 belongs to the MAX effector superfamily. I demonstrated the binding between PWL2 and OsHIPP43 cannot be easily compromised, which has implications for engineering disease resistance.

Finally, I showed that the recently identified rice blast effector AVR-Pias represents a new structural class of *M. oryzae* effector.

These findings can inform future rational design of NLRs with novel recognition specificities. In turn, this can help provide continuous new solutions for tackling ever-evolving plant pathogens worldwide.

Author's declaration

The research presented in this thesis was entirely conducted by the author at the John Innes Centre, unless specific acknowledgements are given in relevant sections of this work.

Results presented in Chapter 3 have contributed to the following publication, which is included in the appendices:

ZDRZALEK, R., KAMOUN, S., TERAUCHI, R., SAITOH, H. & BANFIELD, M. J. 2020. The rice NLR pair Pikp-1/Pikp-2 initiates cell death through receptor cooperation rather than negative regulation. PLoS One, 15, e0238616.

Table of Contents

Abstract 5
Author's declaration 7
Index of Figures 15
Index of Tables 17
Acknowledgements 19
Abbreviations 21
1 General Introduction 27
1.1 Plants are constantly threatened by pathogens 27
1.2 The majority of plants are resistant to majority of pathogens 28
1.2.1 Early responses are triggered by cell-surface immunity 28
1.3 Effectors are pathogens' weapons to promote infection 29
1.3.1 Effectors can rapidly evolve 29
1.3.2 Characteristic features of effectors can help to identify new candidates 29
1.3.3 Effectors can target different host components 30
1.3.4 Structural biology helps to identify new effectors and determine their activities 31
1.3.5 The *Magnaporthe oryzae* effector repertoire is likely diverse 34
1.4 NLRs are important in defence responses to effectors 34
1.4.1 The canonical architecture of NLRs consists of three domains 35
1.4.2 NLRs can recognise effectors via different mechanisms 36
1.4.3 NLRs can work as singletons, in specialised pairs or in networks 39
1.4.4 NLRs form resistosomes upon activation 40
1.5 Gene transfer and protein engineering can be used for deploying novel resistance 43
1.6 Rice NLR pair Pik-1/Pik-2 recognises rice blast effector AVR-Pik via integrated HMA domain 44
1.7 Aims and objectives 47
2 Materials and Methods 51
2.1 Cloning and DNA manipulation 51
2.1.1 Gene synthesis 51
2.1.2 DNA amplification 51
2.1.3 Agarose gel/ DNA electrophoresis 52
2.1.4 Purification from agarose 52
2.1.5 In-Fusion cloning 53

2.1.6 Golden Gate cloning 53
2.2 Bacteria transformation 55
2.2.1 *E. coli* transformation 55
2.2.2 *Agrobacterium tumefaciens* transformation 55
2.2.3 Antibiotics 56
2.3 Protein production and purification 56
2.3.1 Protein production in *E. coli* 56
2.3.2 Purification of PWL2/OsHIPP43 complex 58
2.3.3 Production of ^{15}N labelled protein 58
2.3.4 SDS-PAGE 58
2.4 In vitro techniques 59
2.4.1 Analytical Size-Exclusion Chromatography (SEC) 59
2.4.2 Isothermal Titration Calorimetry (ITC) 59
2.4.3 Circular dichroism (CD) 59
2.4.4 Trypsin digest 60
2.4.5 Mass spectrometry 61
2.5 Crystallography, structure solution and analysis 61
2.5.1 X-ray crystallography 61
2.5.2 Cross-seeding 61
2.5.3 X-ray data processing 62
2.5.4 Protein interface analyses 62
2.5.5 Root Mean Squared Deviation (RMSD) 62
2.5.6 NMR data collection and structure solution 62
2.6 Plant techniques 63
2.6.1 Growth of *Nicotiana benthamiana* 63
2.6.2 Agroinfiltration 64
2.6.3 Cell death assays 64
2.6.4 Coimmunoprecipitation (CoIP) 65
2.6.5 Western blot 65
3 NLRs Pikp-1 and Pikp-2 work via cooperation rather than negative regulation to deliver cell death responses in planta 69
3.1 Introduction 69
3.2 Results 71
3.2.1 All domains of Pikp-1 and Pikp-2 are required for receptor activation 71
3.2.2 Intact P-loop and MHD motifs are required for Pikp-1 and Pikp-2 function 75
3.2.3 Pikp-1 and Pikp-2 form homo- and hetero-complexes in planta 78

3.3 Discussion....82
3.3.1 Roles of individual domain can often be distinguished....82
3.3.2 Different NLRs have different requirements for intact nucleotide-binding motifs..83
3.3.3 Oligomerisation is common feature for NLRs....84
4 Biochemical characterisation of PWL2 and OsHIPP43 interaction....89
4.1 Introduction....89
4.2 Results....91
4.2.1 PWL2 can be purified from *E. coli*....91
4.2.2 Circular dichroism spectroscopy suggests PWL2 has low percentage of secondary structure features....94
4.2.3 Yeast-2-Hybrid screen identifies a potential interactor for PWL2....97
4.2.4 OsHIPP43 can be purified from *E. coli*....98
4.2.5 Circular dichroism spectrum of OsHIPP43 displays features of a folded protein...101
4.2.6 PWL2 and OsHIPP43 interact with nanomolar affinity....102
4.2.7 PWL2-2 and PWL2-3 can be purified from *E. coli*....106
4.2.8 PWL2-2 and PWL2-3 interact with OsHIPP43 with nanomolar affinity....111
4.3 Discussion....112
4.3.1 PWL2 may be highly unstructured without its interactor....112
4.3.2 Natural resistance to PWL2 seems not to be mediated by OsHIPP43....113
4.3.3 Different effectors bind HMA-containing proteins with different affinity....113
5 A chimeric Pikm-1 receptor, Pikm-1^{OsHIPP43}, demonstrates novel recognition of the PWL2 effector....117
5.1 Introduction....117
5.2 Results....119
5.2.1 Pikm-1^{OsHIPP43} chimeric receptor is auto-active....119
5.2.2 Chimeric receptor Pikm-1^{OsHIPP43} can perceive PWL2 in Pikp-2 dependent manner 121
5.2.3 All tested alleles of PWL2 are recognised by Pikm-1^{OsHIPP43}/Pikp-2....122
5.3 Discussion....123
5.3.1 Sequence alterations in NLRs can lead to auto-activity....123
5.3.2 Correlation of affinity with strength of immune response is not always clear....124
5.3.3 Exchange of NLR integrated domain can be powerful tool to engineer novel resistance in plants....124
6 The crystal structure of the PWL2/OsHIPP43 complex....127
6.1 Introduction....127
6.2 Results....128
6.2.1 PWL2/OsHIPP43 complex can be purified from *E. coli*....128

6.2.2 Crystallisation of PWL2/OsHIPP43 complex 130
6.2.3 X-ray data collection and structure determination 138
6.2.4 The crystal structure of the PWL2/OsHIPP43 complex 142
6.2.5 Validation and functional analysis of the PWL2/OsHIPP43 crystal structure 147
6.3 Discussion 156
6.3.1 PWL2 might be intrinsically disordered protein that folds upon binding to its interactor 156
6.3.2 PWL2 possesses MAX fold and large C-terminal extension 157
6.3.3 Binding between PWL2 and OsHIPP43 cannot be easily compromised 158
7 Recognition specificity of chimeric receptor Pikm-1^{OsHIPP43} 163
7.1 Introduction 163
7.2 Results 165
7.2.1 Purification of PWL1 and PWL4 165
7.2.2 Purification of PWL3 167
7.2.3 PWL1, PWL3 and PWL4 bind OsHIPP43 in vitro 169
7.2.4 In planta recognition of PWL1, PWL3 and PWL4 by chimeric Pikm-1^{OsHIPP43} 172
7.3 Discussion 175
7.3.1 What makes OsHIPP43 an interesting target for PWL effectors? 175
7.3.2 HMA proteins as susceptibility factors 176
7.3.3 Effectors from the PWL family might be structurally conserved 176
8 The solution structure of AVR-Pias 181
8.1 Introduction 181
8.2 Results 182
8.2.1 AVR-Pias can be purified from *E. coli* 182
8.2.2 Intact mass spectrometry revealed that AVR-Pias was truncated 185
8.2.3 Purification of AVR-PiasΔ21 187
8.2.4 The solution structure of AVR-Pias 193
8.3 Discussion 195
8.3.1 Correlation of sequence conservation with the structure 195
8.3.2 Finding the interactor for AVR-Pias is crucial for establishing its activity 196
9 General Discussion 201
9.1 Plant diseases can become pandemic too 201
9.2 Pathogen's effector repertoire can be structurally diverse 201
9.3 One model does not fit them all 202
9.4 The discovery of the integrated domains (IDs) offers new insights into plant immunity and NLR engineering 202

9.5 New recognition specificity does not always correlate with resistance in the field.....204
9.6 GMO acceptance is slowly increasing worldwide.....205
9.7 Closing remarks.....206
References.....207
Appendix.....231

Index of Figures

Figure 1.1 Symptoms of rice blast disease. 28
Figure 1.2 MAX effectors share a structural fold with no sequence similarity. 33
Figure 1.3 Different models of effector recognition in plants. 38
Figure 1.4 Oligomeric states of different NLRs. 42
Figure 2.1 Schematic representation of the Pikm-1- integrated domain acceptor vector. 54
Figure 2.2 Scoring scale used for cell death assays 65
Figure 3.1 All the domains are required for Pikp-1/Pikp-2 system to function. 73
Figure 3.2 All the domains are required for Pikp-1/Pikp-2 system to function. 74
Figure 3.3 Intact P-loop and MHD-like motifs are required for Pikp-1/Pikp-2 to function. 77
Figure 3.4 Pikp-1 and Pikp-2 associate in homotypic manner. 79
Figure 3.5 Presence of AVR-PikD does not disrupt the homo-association of Pikp-1 and Pikp-2. 80
Figure 3.6 Pikp-1 and Pikp-2 hetero-associate prior to and upon recognition of the effector. 81
Figure 4.1 PWL2 can be purified from *E. coli.* 93
Figure 4.2 Typical CD spectra of basic secondary structures of polypeptide chains. 95
Figure 4.3 PWL2 has low percentage of secondary structures. 96
Figure 4.4 PWL2 interacts with OsHIPP43 in Y2H. 97
Figure 4.5 Sequence alignment of OsHIPP43 and Pikm-1-HMA. 99
Figure 4.6 OsHIPP43 can be purified from *E. coli.* 100
Figure 4.7. CD spectrum of OsHIPP43 suggests that the protein is well ordered. 101
Figure 4.8 OsHIPP43 interacts with PWL2, but not with AVR-PikD in vitro. 103
Figure 4.9 PWL2 binds OsHIPP43 with nanomolar affinity. 105
Figure 4.10. PWL2-2 can be purified from *E. coli.* 107
Figure 4.11. PWL2-3 can be purified from *E. coli.* 109
Figure 4.12 Sequence alignment and CD spectra of PWL2 alleles. 110
Figure 4.13 PWL2-2 and PWL2-3 bind OsHIPP43 with nanomolar affinity. 111
Figure 5.1 Scheme of integration of OsHIPP43 into Pikm-1 background to engineer recognition towards PWL2. 118
Figure 5.2 Pikm-1^{OsHIPP43} receptor is auto-active in presence of Pikm-2, but not in presence of Pikp-2. 120
Figure 5.3 Pikm-1^{OsHIPP43} receptor triggers strong cell death in response to PWL2, but not to AVR-PikD. 121
Figure 5.4 Pikm-1^{OsHIPP43} receptor triggers strong cell death response upon recognition of PWL2, PWL2-2 and PWL2-3. 122
Figure 6.1 Purification of PWL2/OsHIPP43 complex from *E. coli.* 129
Figure 6.2 Limited proteolysis of the PWL2/OsHIPP43 complex. 132
Figure 6.3 Identification of truncated fragments of PWL2/OsHIPP43 complex. 134
Figure 6.4 Initial screens and conditions used for crystallisation of PWL2/OsHIPP43 complex resulted in crystalline precipitate. 135

Figure 6.5 Optimisation of crystallisation conditions. 136
Figure 6.6 Crystals of PWL2/OsHIPP43 complex. 137
Figure 6.7 Ramachandran plots for the PWL2/OsHIPP43 structure. 141
Figure 6.8 Crystal structure of PWL2/OsHIPP43 complex. 143
Figure 6.9 Analysis of interaction interface of the PWL2/OsHIPP43 complex. 145
Figure 6.10 PWL2 forms a vast binding interface with OsHIPP43. 146
Figure 6.11 All single mutants of PWL2 are perceived by the chimeric Pikm-1^{OsHIPP43} receptor. 148
Figure 6.12 Septuple mutant PWL2^{SNDEYWY} is not perceived by chimeric Pikm-1^{OsHIPP43} receptor. 149
Figure 6.13 CD spectrum of PWL2 and PWL2^{SNDEYWY}. 150
Figure 6.14 Analytical size-exclusion chromatography traces of PWL2 and PWL2^{SNDEYWY}. 151
Figure 6.15 PWL2^{SNDEYWY} does not bind OsHIPP43 in vitro. 152
Figure 6.16 CD spectrum of PWL2 and PWL2^{SNW}. 153
Figure 6.17 Analytical size-exclusion chromatography traces of PWL2 and PWL2^{SNW}. 154
Figure 6.18 PWL2^{SNW} binds OsHIPP43 with nanomolar affinity. 155
Figure 6.19 Dali homology search using PWL2 as query. 157
Figure 6.20 Superposition of selected structures with PWL2/OsHIP43 complex. 159
Figure 7.1 Alignment of PWL effector family. 164
Figure 7.2 Purification of PWL effectors from *E. coli.* 166
Figure 7.3 CD spectrum of PWL1Δ13, PWL2 and PWL4. 167
Figure 7.4 Purification of PWL3Δ10 from *E. coli.* 168
Figure 7.5 PWL1 and PWL4 bind OsHIPP43 with nanomolar affinity. 170
Figure 7.6 PWL3 binds OsHIPP43 with micromolar affinity. 171
Figure 7.7 PWL1, PWL2, PWL3 and PWL4 are perceived by the chimeric Pikm-1^{OsHIPP43} receptor. 172
Figure 7.8 Truncated and diffrentially tagged PWL effectors are perceived by Pikm-1^{OsHIPP43}. 174
Figure 7.9 Structure prediction of PWL1, PWL3 and PWL4. 177
Figure 8.1 Purification of AVR-Pias from *E. coli.* 183
Figure 8.2 Initial crystallisation screens and conditions used for crystallisation of AVR-Pias resulted in crystalline precipitate. 184
Figure 8.3 Mass spectrometry analysis of AVR-Pias revealed an N-terminal truncation. 186
Figure 8.4 Purification of AVR-PiasΔ21 from *E. coli.* 188
Figure 8.5 CD spectrum of AVR-PiasΔ21. 189
Figure 8.6 Final size-exclusion chromatography step of purification of ^{15}N-labelled AVR-PiasΔ21. 191
Figure 8.7 NMR Structure of AVR-Pias. 194
Figure 8.8 Dali homology search did not find any significant similarity of AVR-Pias to other known structures. 194
Figure 8.9 AVR-Pias is prevalent in pathogen population. 196

Index of Tables

Table 2-1 Reaction mix for DNA amplification using VELOCITY DNA Polymerase 51

Table 2-2 Reaction mix for DNA amplification using MyTaq™ Polymerase 52

Table 2-3 Components of Golden Gate reaction..... 55

Table 2-4 Reaction conditions of Golden Gate cloning 55

Table 2-5 List of antibodies used in this work..... 66

Table 6-1 Initial screens and conditions used for crystallisation of PWL2/OsHIPP43 complex. 130

Table 6-2 Initial screens and conditions used for crystallisation of PWL2Δ10/OsHIPP43 complex. 135

Table 6-3. X-ray data collection and refinement statistics for PWL2Δ/OsHIPP43 complex. 139

Table 8-1 Crystallisation screens and conditions used for crystallisation of AVR-Pias. 184

Table 8-2 Crystallisation screens and conditions used for crystallisation of AVR-PiasΔ21. 189

Table 8-3 Refinement statistics for NMR structure of AVR-Pias..... 192

Acknowledgements

I would like to start with thanking my supervisor, Professor Mark Banfield, for making this journey possible, and for the entire support throughout the past four years. For all the guidance and shared wisdom, for patience, for keeping me focused, and all the words of encouragement whenever I was in doubt. Without all that, this work would not be possible. I would also like to thank my supervisory committee, Saskia Hogenhout and Adam Bentham for all the support and advice during our meetings.

I would like to thank all the members of the Banfield Lab, past and present, who have always been a source of support, advice, experience, and fun. In particular, I would like to thank Adam Bentham and Nitika Mukhi, two excellent scientists who helped me to shape a lot of ideas and improve my technical skills over the last four years. I am also grateful for the opportunity to supervise a Summer School student, Poppy Smith, who also contributed to this work, and worked with me on protein purification.

I would like to thank all the members of the #BLAST OFF team: Kamoun Lab, Talbot Lab, and Moscou Lab, for the discussion, and for sharing their experience and resources. Special thanks to Vincent Were, Yohann Petit-Houdenot, Thorsten Langner and Abbas Maqbool for sharing their resources and first-hand experiences.

Results in Chapter 8 would not be possible without our overseas collaborators: Ryohei Terauchi's group in Japan and Andre Padilla in France. I am very grateful for the opportunity of the collaboration with them, and I look forward to further collaboration.

I would like to express my gratitude to scientific support stuff that contributed to this work. Clare Stevenson for technical support with ITC and fishing out my precious protein crystals. Julia Mundy for CD analysis and troubleshooting the crystallisation screens set up. Dave Lawson for X-ray data collection. Jan Sklenar for MS analysis. Tracey Hannant and entire media kitchen staff for tens (if not hundreds) of litres of media. Andrew Davies and Phil Robinson from the JIC photography department. Horticulture service, and many more, for all the work that goes "behind the scenes" to enable the research that happens at the John Innes Centre.

Finally, I would like to thank my Beach Squad: Isa, Mimi and Lira, who made this journey much more fun than expected. I hope we all stay in touch after this is over, coz we still have some travelling to do together!

Abbreviations

A_{280}	absorbance at 280nm
ADP	adenosine diphosphate
AI	Arabinose Inducible
ATP	adenosine triphosphate
AU	absorbance units
AVR	avirulence protein
BIC	biotrophic interfacial complex
CC	coiled coil
CD	circular dichroism
cDNA	complementary DNA
CDS	coding sequence
Da (kDa)	Dalton (kiloDalton)
DAMP	damage associated molecular pattern
dATP	deoxyadenosine triphosphate
DNA	deoxyribonucleic acid
dNTP	deoxyribonucleotide triphosphate
dpi	days post-infiltration
DTT	dithiothreitol
EDTA	ethylenediaminetetraacetic acid
FOG	Ficoll and Orange G
FT	Flow through
GMO	Genetically modified organism
HA	haemagglutinin
HEPES	4-(2-hydroxyethyl)-1-piperazineethanesulfonic acid
HF	HellFire (6xHis, 3xFlag)
HIPP	heavy metal associated isoprenylated plant protein
HMA	heavy metal associated
HPP	heavy metal associated plant protein

HR	hypersensitive response
HRP	horseradish peroxidase
ID	integrated domain
IMAC	immobilised metal affinity chromatography
IP	immunoprecipitation
IPTG	isopropyl β-D-1-thiogalactopyranoside
IRRI	International Rice Research Institute
ITC	isothermal titration calorimetry
JCSG	Joint Centre for Structural Genomics
LB	lysogeny broth (Luria-Bertani)
LDS	lithium dodecyl sulphate
LRR	leucine rich repeat
LysM	lysine motif
MALS	Multi-angle Light Scattering
MAMP	microbe associated molecular pattern
MAPK	mitogen-activated protein kinase
MAX	Magnaporthe AVRs and ToxB-like
MBP	maltose binding protein
NB-ARC	nucleotide binding Apaf-1, R protein, CED4 shared
NLR	nucleotide-binding leucine rich repeat
NMR	nuclear magnetic resonance
NTA	nitrilotriacetic acid
OD_{600}	optical density measured at a wavelength of 600nm
PBS	phosphate-buffered saline
PCR	polymerase chain reaction
PDB	Protein Data Bank
PISA	protein interfaces, surfaces and assemblies
PRR	pattern recognition receptor
PTI	pattern triggered immunity
PVDF	polyvinylidene difluoride

R	(disease) resistance
RLK	receptor-like kinase
RLP	receptor-like protein
RMSD	root-mean-square deviation of atomic positions
RNA	ribonucleic acid
ROS	reactive oxygen species
SDS-PAGE	sodium dodecyl sulphate-polyacrylamide gel electrophoresis
SEC	Size-exclusion chromatography
SPR	surface plasmon resonance
STAND	signal transduction ATPase with numerous domains
TAE	tris-acetate-EDTA
TBS	tris-buffered saline
TIR	TOLL/interleukin-1 receptor
TLS	translation-libration-screw
T3SS	type III secretion system
UV	ultraviolet
v/v	volume/volume
w/v	weight/volume
WT	wild type

1

General Introduction

1 General Introduction

1.1 Plants are constantly threatened by pathogens

Plants, like humans and animals, can suffer from various diseases. They are attacked by a wide range of pathogens and pests, including viruses, bacteria, filamentous pathogens (oomycete and fungi), nematodes and insects (Scholthof et al., 2011, Dean et al., 2012, Fisher et al., 2012, Mansfield et al., 2012, Kamoun et al., 2015, Bentham et al., 2020). This is of economic importance, as plant diseases can cause up to 30% loss of the yield in crops world-wide every year, which in turn have an impact on food supply chains and prices (Savary et al., 2019). Crops are protected from pathogens largely via chemicals. However, this approach is not sustainable in the long-term due to the impact on environment and high costs. Genetic resistance in plants offers an alternative approach for crop protection that is environmentally friendly and sustainable (van Esse et al., 2020).

Rice (*Oryza sativa*) is a staple crop for more than half of the world population (Pennisi, 2010, Liu et al., 2014), nearly 500 million metric tons of rice are consumed worldwide every year. Production of rice is constantly threatened by various pathogens, out of which the most economically important is filamentous ascomycete fungus *Magnaporthe oryzae* (syn. *Pyricularia oryzae* (Dean et al., 2012)), the causal agent of the blast disease (**Figure 1.1**). It is estimated that rice blast causes around 6% loss of rice yield globally (Savary et al., 2019). Apart from rice, *M. oryzae* can infect more than 50 different grass species, including barley, millet and weeping lovegrass (Langner et al., 2018). It also displays the ability to jump from one host to another. A good example is wheat blast that first appeared in Brazil in 1985, likely following a host jump from *Lolium sp.* to common wheat (Inoue et al., 2017). Increasing global trade allows for pathogens to spread on different continents, which can classify them as pandemics. In 2016, wheat blast emerged in Bangladesh (Islam et al., 2016, Ceresini et al., 2018), threatening the entire wheat production in this country, but also posing a threat of spreading to India, which is world's second largest wheat producer (Islam et al., 2019, Islam et al., 2020). Most recently, wheat blast has also been reported in Zambia (Tembo et al., 2020), indicating that *Magnaporthe oryzae* poses a significant threat globally. Current strategies for blast management include quarantines, fungicides, good agricultural practices and deploying genetic resistance (Singh et al., 2021).

1.2 The majority of plants are resistant to majority of pathogens

This phenomenon is sometimes called a non-host resistance; however, it is not a precise term (Panstruga and Moscou, 2020). Plants possess a range of structural characteristics and physical barriers like leaf cuticle (Yu et al., 2019), epicuticular waxes (Ishiga et al., 2013), cell wall of a specific composition (Engelsdorf et al., 2017) or display a characteristic stomatal patterning and closure (Melotto et al., 2017), which all can prevent the pathogen from infection.

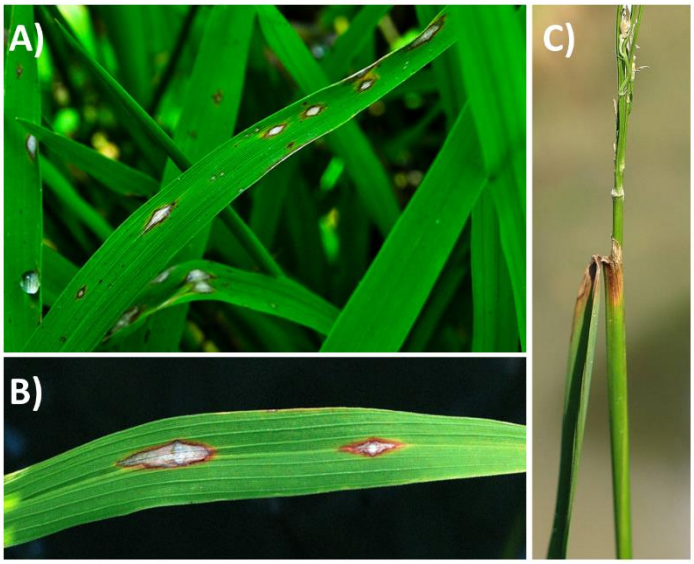

Figure 1.1 Symptoms of rice blast disease.

A) *and* ***B)*** *Typical grey lesions on leaves.* ***C)*** *Collar blast characterised by brow necrotic lesions. Pictures taken from International Rice Research Institute (http://www.knowledgebank.irri.org/training/fact-sheets/pest-management/diseases/item/blast-leaf-collar)*

1.2.1 Early responses are triggered by cell-surface immunity

Plants can also induce defence responses upon early detection of pathogens via extracellular receptors. Cell-surface immunity consists of two major components: membrane-localized receptor-like kinases (RLKs) and receptor-like proteins (RLPs) that detect signatures of non-self as signs of infection (Jones and Dangl, 2006). These receptors monitor the extracellular environment for microbial-associated molecular patterns (MAMPs) or damage-associated molecular patterns (DAMPs), hence they are also known as pattern recognition receptors (PRRs) (Saijo et al., 2018, Kanyuka and Rudd, 2019). MAMPs are molecules found in a broad group of microorganisms that are generally conserved and integral to the structure or function of the microbes, e.g., flagellin in bacteria or chitin in fungi (Boller and Felix, 2009). DAMPs are plant-derived molecules whose presence indicates microbial attack, e.g., cell-wall components, ATP, or certain sugars (Hou et al.,

2019). Frequently, PRRs require coreceptors to transduce the perception of microbes into a defence response (Böhm et al., 2014, Macho and Zipfel, 2014). The specific ligands (MAMPs and DAMPS) can be perceived by cell-surface receptors at nanomolar concentrations, which in turn initiates downstream signalling cascades and responses, including cytosolic Ca^{2+} bursts, production of reactive oxygen species (ROS), activation of mitogen-activated protein kinases (MAPKs) and changes in expression of various defence related genes (Lu and Tsuda, 2021). These responses are very often sufficient to prevent the majority of pathogens from infecting the plants and are generally referred to as pattern-triggered immunity (PTI).

1.3 Effectors are pathogens' weapons to promote infection

To counteract these immune responses and manipulate host's metabolism for their own benefit, pathogens evolved effectors. Effectors are secreted molecules (most often proteins, but small RNAs and secondary metabolites have also been described (Collemare et al., 2019) that can act either in the apoplast or in the plant cells (Toruño et al., 2016). Many apoplastic effectors are cysteine-rich proteins, and they often target host proteases (Wang and Wang, 2018). The intracellular effectors can act in various plant cell compartments, manipulating the cellular machinery and interfering with immunity hubs (Lo Presti and Kahmann, 2017, El Kasmi et al., 2018, Derevnina et al., 2021, Pandey et al., 2021).

1.3.1 Effectors can rapidly evolve

Genes encoding effectors are often located in parts of genome that are evolutionarily dynamic, associated with structural variation and instability of the genome (Allen et al., 2004, Langner et al., 2021). This feature allows the effector genes to undergo constant selection pressure and evolve via different mechanisms including translocation, duplication, presence/absence polymorphism and diversification (Allen et al., 2004, Raffaele et al., 2010, Raffaele and Kamoun, 2012, Huang et al., 2014, Dong et al., 2015, Yoshida et al., 2016, Inoue et al., 2017). The capacity of plant pathogens to rapidly adapt to novel habitats and hosts, and break resistance via accelerated evolution poses a serious challenge for disease management and creates the constant need for implementing new resistance genes in the field.

1.3.2 Characteristic features of effectors can help to identify new candidates

Frequently, effectors do not share strong amino acid sequence similarity with each other or with other known proteins. However, they sometimes share some overall features that can help identify new effector candidates. Gram-negative bacteria deliver effectors to host cells via the Type III secretion system (T3SS). This requires an export signal (also known as signal peptide) at the N-terminus of the effector (Wang et al., 2011). Although this signal does not constitute a specific

amino acid sequence, it can be reliably identified by certain amino acid patterns. Its presence is indicative of secreted proteins, therefore underlies the identification of potential effectors and effector repertoires in many bacterial pathogens. Type III secreted effectors often contain catalytic domains and can target a variety of signal transduction pathways and immune components. Known modifications of immunity elements include proteolysis, ADP ribosylation, and ubiquitination among others (Büttner, 2016).

In oomycetes, the best described effector family (based on the presence of translocation signal) is the RXLR family. In these effectors, the N-terminal export signal is followed by an RXLR sequence (where X can be any amino acid). The RXLR sequence has been shown to be important for the effectors' translocation, e.g., mutation is this motif prevented the translocation of the AVR3 effector from *Phytophtora infestans* (Whisson et al., 2007). However, the C-terminal domains of these effectors are highly diverse and many of these effectors' roles in pathogenicity are yet to be determined.

The apparent absence of conserved motifs necessary for translocation into the host cell has made identifying fungal effectors more challenging. The infection patterns displayed by fungal pathogens are quite diverse and they use various mechanisms to deliver the effectors. For instance, *Ustilago maydis* delivers effectors via the hyphal tip (Bielska et al., 2014, Ludwig et al., 2021), whereas *M. oryzae* develops a special structure called biotrophic interfacial complex (BIC) (Eseola et al., 2021). The characteristics shared by many experimentally validated effectors, such as small size, high cysteine content and genomic location, have traditionally been used to predict effectors from fungal secretomes (Lo Presti et al., 2015, Saunders et al., 2012, Nemri et al., 2014). More recently, new approaches have been developed to identify new potential effectors, which include machine learning methods (Sperschneider et al., 2018, Sperschneider et al., 2016) and searches based on predicted structures (de Guillen et al., 2015).

1.3.3 Effectors can target different host components

Many of the effectors that have been functionally characterised suppress plant immune signalling, alter host metabolic modification, or reprogram transcription. One of the better characterised set of effectors are those from *P. infestans*. Effectors EPI1, EPI10, EPIC2B, EPIC1 and AVR-blb2 all function as inhibitors of the apoplastic proteases that are involved in plant immunity (Tian et al., 2004, Tian et al., 2005, Tian et al., 2007, Song et al., 2009, Kaschani et al., 2010, Kaschani and Van der Hoorn, 2011, Bozkurt et al., 2011). The RXLR effector, PexRD2, suppresses the activity of MAPKKK ε kinase domain (King et al., 2014), which is involved in immune signalling. PexRD24 suppresses host's immunity by interaction with three protein phosphatase 1 catalytic (PP1c)

isoforms and their relocalization to the nucleoplasm from the nucleolus, which decreases levels of salicylic acid (SA) and jasmonic acid (JA) (Boevink et al., 2016). AVRcap1b effector can suppress the response triggered by auto-active immunity receptors NRC2 and NRC3 (Derevnina et al., 2021). Additional examples of *P. infestans* effectors are discussed in (Wang and Jiao, 2019), where the known effector repertoire of *Phytohtora sp*. is reviewed.

Multiple effectors can target similar host proteins, sometimes even within one pathogen. Such redundancy could offer a certain buffer, in case that one of the effectors becomes recognised by the host. One example of a plant protein that is targeted by multiple effectors is the RPM1-Interacting Protein 4 (RIN4). This protein is located at the plasma membrane (El Kasmi et al., 2017) and acts as a regulator of plant immunity. It has been shown that several pathogen effectors can cleave RIN4 or introduce post-translational modifications, altering its role in plant immunity (Axtell and Staskawicz, 2003, Chung et al., 2011, Chung et al., 2014).

On the other hand, it has been also demonstrated that individual effectors can target various host proteins. For instance, HopZ1a effector from *Pseudomonas syringae* can acetylate multiple host targets, including tubulin and JAZ proteins. Modification of tubulin interferes with transport of various proteins, including immunity related, whereas modification of JAZ proteins induces their degradation, which leads to downregulating signalling pathways regulated by salicylic acid (Lee et al., 2012, Jiang et al., 2013). Furthermore, it has been shown that *M. oryzae* effector AvrPiz-t interacts with at least four different host targets. These include a bZip-type transcription factor, APIP5 (Wang et al., 2016), two RING E3 ubiquitin ligases, APIP6 and APIP10 (Park et al., 2012, Park et al., 2016), and APIP12, which has a homology to the nucleoporin protein Nup98 (Tang et al., 2017).

1.3.4 Structural biology helps to identify new effectors and determine their activities

Structural studies of effectors can be also a powerful tool in identifying effector candidates and deciphering effector functions and evolutionary trajectories. Bioinformatic analyses coupled with structural studies have recently identified structures of several bacterial effectors secreted via T3SS, displaying distinct enzymatic folds- AvrRpt2 from *P. syringae* was confirmed a cysteine protease (Bartho et al., 2019), HopBA1 was shown to be an esterase (Nishimura et al., 2017), and XopAI from *Xanthomonas sp.* was confirmed an ADP-ribosyltransferase (Liu et al., 2019). These examples highlight how diverse catalytic strategies pathogens can deploy to promote the infection.

Several effectors of filamentous plant pathogens display structural folds similar to proteins of determined functions, such as LysM domain-containing proteins (Ecp6) and carbohydrate binding proteins (Avr4) (Giraldo and Valent, 2013, Lo Presti et al., 2015). Interestingly, filamentous

pathogens also possess a range of effectors that can share a conserved fold, despite sharing low sequence similarity. The two most known structural families of effectors, defined by the adopted fold, are the RXLR-WY (and RXLR-LWY) and MAX effectors (Mukhi et al., 2020).

The WY domain is characterised by the overrepresentation of Trp and Tyr residues in conserved positions (Jiang et al., 2008, Boutemy et al., 2011). The WY fold is present in many oomycete effectors, which can display high functional diversity and low sequence similarity (Chou et al., 2011, Yaeno et al., 2011, Maqbool et al., 2016). Moreover, structural variations (such as tandem multiplications) of this fold have also been observed (He et al., 2019), suggesting that this fold may serve as a structural platform to enable the rapid evolution and diversification of the effectors (Franceschetti et al., 2017). Almost half of the Phytophthora RXLR effectors are predicted to contain the WY fold (Win et al., 2012). This fold has been also found in effectors from other oomycete pathogens, including proteins that lack the RXLR motif (Wood et al., 2020). Therefore, it can be used as a good predictor for effector candidates in oomycete genomes.

The MAX effectors are characterised by six-stranded β-sandwich fold. This is a shared structural feature for all *M. oryzae* effectors, of which structures have been determined to date (de Guillen et al., 2015, Bentham et al., 2021a). These effectors include AVR-Pik, APikL2, AVR-Pia, AVR1-CO39, AVR-Pib and AvrPiz-t (Zhang et al., 2013b, Maqbool et al., 2015, Ose et al., 2015, Guo et al., 2018, Zhang et al., 2018, Bentham et al., 2021a). Interestingly, this fold is also shared by ToxB, a toxin from the fungus *Pyrenophora tritici-repentis* (Nyarko et al., 2014), to which these effector family owes the name “MAX” (Magnaporthe AVR and ToxB effectors) (**Figure 1.2**).

Despite having a similar structure, most of *M. oryzae* effectors target distinct host proteins. As mentioned previously, AvrPiz-t modulates the plant ubiquitination system and manipulates gene expression by interacting with a variety of host targets (Park et al., 2012, Park et al., 2016, Wang et al., 2016, Tang et al., 2017). AVR-Pik, AVR-Pia and AVR1-CO39 have been shown to directly bind to proteins containing a heavy metal associated (HMA) domain, however the exact role of that interaction remains to be determined. The precise mechanism of action of ToxB is also unknown, however it has been shown to cause chlorosis on expression in host plants (Figueroa Betts et al., 2011).

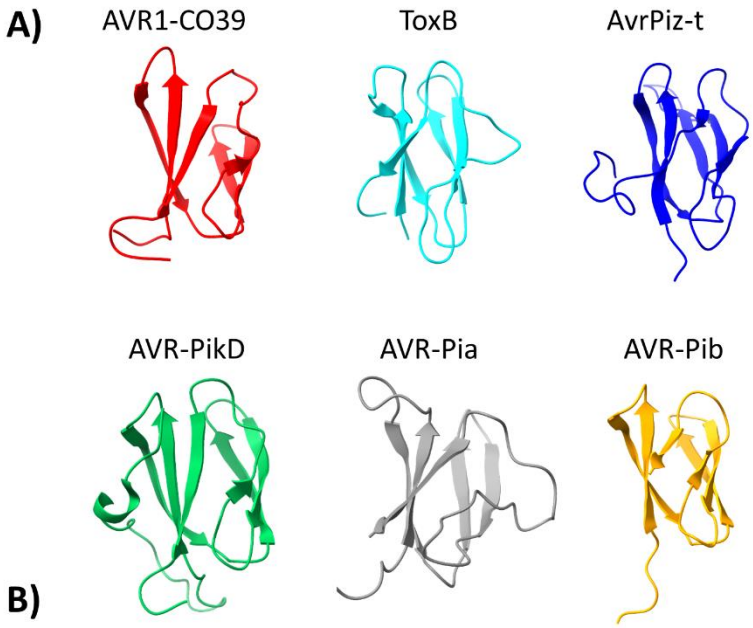


```
AVR1-CO39----------------------------MAWKDCIIQRYKDGDVNN-----------IYT     21
ToxB       ---------------------------------NCTANILNINEVVIATGCVP------AG     22
AvrPiz-t   ------------------------------SFVQCNHHL------------------LYN     12
AVR-PikD   METGNKYIEKRAIDLSRERDPNFFDHPGIPVPECFWFMFKNNVRQDAGTCYSSWKMDMKV     60
AVR-Pia    ----------------APARFCVYYDGHLPATRVLLMYVRIGTTAT----I------TAR     34
AVR-Pib    ------------------TQVTILKK----GERITWVEVPKGESRE----F------NIR     28

AVR1-CO39ANRNEEITI-EEYKVFVNE------------------------ACHPYPV---ILPDRSV     53
ToxB       GNLIIRVGSDH-----------------------------SYLIRATVSCGLSLNPSQSF     53
AvrPiz-t   GRHWGTIRKKAGWAVRFYEEKPGQPKRLVAICKNASPVHCNYLKCTNLAAGFSAGTSTDV     72
AVR-PikD   GPNWVHIKSDDNCNL---S--GDFPP--------------GWIVLGKKRPGF--------     93
AVR-Pia    GHEFEVEAKDQNCKVILTN--GKQAP--------------DWLAAEPY------------     66
AVR-Pib    GKYFTVSVSDDGTPSIS----------------------------GSKYTVE---------     52
           .

AVR1-CO39LSGDFTSAYADDDESC 69
ToxB       INGES----LASGGRC 65
AvrPiz-t   LSSGT----VGS---- 80
AVR-PikD   ---------------- 93
AVR-Pia    ---------------- 66
AVR-Pib    ---------------- 52
```

Figure 1.2 MAX effectors share a structural fold with no sequence similarity.

A) *Structure representation of MAX effectors, as deposited in PBD database. AVR1-CO39 (5ZNG); ToxB (2MM2); AvrPiz-t (2LW6); AVR-PikD (6G10); AVR-Pia (6Q76); AVR-Pib (5Z1V); structures were prepared using ChimeraX software.* ***B)*** *Sequence alignment of the presented effectors showing no similarity between them.*

1.3.5 The *Magnaporthe oryzae* effector repertoire is likely diverse

Apart from the MAX effectors listed above, *M. oryzae* carries many other potential effectors (Petit-Houdenot et al., 2020). Over the years, several effectors have been identified and described, although the level of detail differs from case to case. The PWL2 (Pathogenicity towards Weeping Lovegrass 2) effector was first identified in 1995 and described as host determining factor, as *M. oryzae* strains carrying this effector are not able to infect weeping lovegrass (*Eragrostis curvula*), but could infect rice and barley (Kang et al., 1995, Sweigard et al., 1995). AVR-Pii is small effector that was cloned via association genetics in 2009 (Yoshida et al., 2009). Although its precise function is not known, it has been shown to specifically bind to specific Exo70 alleles, which can form part of the plant exocyst complex. This effector is also indirectly recognised by the Pii-1/Pii-2 NLR pair (Fujisaki et al., 2015, Fujisaki et al., 2017). Recently, a new, small, cysteine-rich effector has been reported, designated as AVR-Pias, which is recognised by a cognate rice NLR pair Pias-1/Pias-2 (Shimizu et al., 2021). However, no further studies have been conducted on this protein. A more extensive list of identified *M. oryzae* effectors can be found (along with references) in (Guo et al., 2019). From the effectors mentioned in this paragraph, AVR-Pii is the best studied so far, and little research has been done on PWL2 and AVR-Pias. Hence, PWL2 and AVR-Pias will be subjects of study in this thesis.

1.4 NLRs are important in defence responses to effectors

During evolution, plants have acquired resistance (R) genes that encode proteins able to specifically recognise certain effectors and trigger immune responses, preventing infection and the spread of disease. Hence, many characterised effectors have been named avirulence (AVR) proteins, which can be a confusing term for researchers entering the plant-pathogen interactions field. However, in the absence of the cognate plant immune receptor, these effectors still enhance the pathogenicity of the pathogens.

The majority (~60%) of cloned Resistance (R) genes encode NLR (Nucleotide-binding Leucine-rich Repeats) proteins (Kourelis and van der Hoorn, 2018), which are intracellular receptors able to recognise cytoplasmic effectors. This recognition often leads to a localised programmed cell death response (also known as Hypersensitive Response (HR)) that restricts spread of the pathogen.

NLR receptors are part of the immune system in both plants and animals, although they are thought to have evolved independently in a convergent manner (Yue et al., 2012). Interestingly, animal NLRs trigger immune responses upon recognition of non-self and modified-self molecules, similar to plant PRRs, while plant NLRs recognise pathogen/strain specific effectors delivered to their cells (Broz and Dixit, 2016).

1.4.1 The canonical architecture of NLRs consists of three domains

NLR proteins belong to the STAND (Signal Transduction ATPase with Numerous Domains) protein family. The canonical architecture of plant NLRs consists of three domains: C-terminal leucine-rich repeat domain (LRR), a central NB-ARC (nucleotide-binding Apaf-1, R protein, CED4-shared) domain, and a variable N-terminal domain. In plants, the N-terminus typically consists of either a TOLL/interleukin-1 receptor (TIR) domain or a coiled coil (CC) domain, which classifies them to two main subfamilies: TIR-NLRs (or TNLs) and CC-NLRs (or CNLs). Recently, an additional subfamily has been distinguished in the literature, with CC domain with homology to RPW8 (resistance to powdery mildew 8), forming a separate subfamily of CC_R-NLRs (or RNLs) (Duxbury et al., 2016, Bentham et al., 2020).

The C-terminal Leucine-Rich Repeat (LRR) domain is mainly thought to have two functions. Firstly, it can carry out a regulatory function, as its deletion can cause constitutive NLR activation (also known as auto-activation) in several plant and animal receptors (Ade et al., 2007, Faustin et al., 2007). This was further verified by determining the crystal structure of the mammalian NLRC4 receptor, which revealed that direct contact between the LRR and the NB domains was underlying the auto-inhibition mechanism (Hu et al., 2013). Secondly, the LRR domains have also been shown to be involved in direct and indirect recognition of effectors and specificity determination (Jia et al., 2000, Dodds et al., 2006). This has been shown for flax NLRs L5/L6/L7, where swapping fragments of LRR domains between these receptors changed the specificity towards the AVRL-567 effector variants from flax stem rust pathogen *Melampsora lini* (Ellis et al., 1999).

The central NB-ARC domain is thought to function as a molecular switch that operates via ADP/ATP exchange upon the pathogen recognition (Takken and Goverse, 2012, Jones et al., 2016, Meunier and Broz, 2017). Several well conserved motifs involved in ADP/ATP binding can be distinguished within this domain, including the Walker A motif (also known as the P-loop), the Walker B motif and MHD motif. Mutations in these motifs often affect the functionality of NLRs (making them either non-functional or auto-active), therefore nucleotide association has long been thought to be essential for NLR activity (Tameling et al., 2002, Tameling et al., 2006, Takken et al., 2006, Takken and Goverse, 2012).

The N-terminal domains, CC and TIR have been long thought to be involved in downstream signalling, as both types of domain are able to trigger immune responses when transiently overexpressed alone in model plant *Nicotiana benthamiana* (Collier et al., 2011, Maekawa et al., 2011, Williams et al., 2014, Casey et al., 2016, Baudin et al., 2017, Lee et al., 2021). Recent discoveries shed light on their mechanism of action. In the case of CC domains, it was shown that

upon activation they form can a funnel that inserts into the plasma membrane and acts as an ion channel (Lee et al., 2020b, Bi et al., 2021). TIR domains have been shown to possess NADase activity, which depletes the plant cell of the NAD^+ pool, which in turn leads to cell death in yet unresolved way. Interestingly, one of the bacterial defence systems against phages also relies on TIR proteins that indirectly act via depleting the cells of NAD (Ofir et al., 2021).

1.4.2 NLRs can recognise effectors via different mechanisms

Detection of pathogen effectors by plant NLRs can be very specific and can occur via various mechanisms. To date, three main models of effector recognition have been described (Cesari, 2017, Kourelis and van der Hoorn, 2018), depending on whether the effector is perceived directly by the NLR or via an intermediate host protein (**Figure 1.3**).

Several plant NLRs have been reported to directly bind effectors. For example, *M. oryzae* effector AVR-Pita interacts with the LRR domain of the rice NLR Pi-ta (Jia et al., 2000) and AVRL-567 variants from *M. lini* were shown to interact directly with specific proteins encoded in the flax resistance locus L (NLRs L5, L6 and L7) (Dodds et al., 2004).

However, in other cases, instead of directly interacting with effectors, NLRs monitor the state of the virulence target and detect the modification introduced by the effectors. This is referred to as the “guardee model”. In this scenario, the guardees are host proteins important for various plant processes, including defence mechanisms. A good example is mentioned in section **1.3.3 (p. 30)** protein RIN4 that can be targeted by multiple pathogens. In Arabidopsis, the status of RIN4 is monitored by the NLR RPM1 (resistance to *Pseudomonas syringae pv. maculicola* 1), which can detect various states of the protein and trigger downstream immune responses. (Mackey et al., 2002, Axtell and Staskawicz, 2003, Chung et al., 2011, Liu et al., 2011, Chung et al., 2014, Lee et al., 2015).

Sometimes, plant NLRs can monitor the status of protein that does not seem to carry any other biological function than interacting with an effector. Such proteins are known as “decoys” and are thought to have evolved to mimic real pathogen targets. Their status is monitored by NLRs that trigger an immune response upon detection of decoy modification. This model is known as the “decoy model” and its advantage over the “guardee model” is that the effectors are not interfering with important host metabolic pathways (or that interference is decreased due to mistargeting of the effectors) (van der Hoorn and Kamoun, 2008, Kourelis et al., 2020).

A good example of decoy model is the protein kinase PBS1. PBS1 does not appear to carry any biological function, as its mutations do not show any measurable phenotypes in plants. It is,

however, targeted for cleavage by multiple effectors, and this is recognised by the NLR RPS5 (Resistance to Pseudomonas Syringae 5), which triggers immune responses upon detection of the cleavage (Shao et al., 2003, Ade et al., 2007, Kim et al., 2016). Another example is a range of plant pseudokinases targeted by different effectors from *Xanthomonas campestris*. The state of these proteins is monitored by the NLR ZAR1 (HopZ-Activated Resistance 1) that can be found in both *Arabidopsis thaliana* and *N. benthamiana* (Seto et al., 2017, Wang et al., 2015b, Wang et al., 2019a, Wang et al., 2019b).

In addition to the three canonical domains present in plant NLRs, a subset of these immune receptors possesses additional, unconventional domains. Initially they were described as "integrated decoys", as they were hypothesised to share a common origin with the effector targets. Such integration of decoys would allow for the direct recognition of the effectors by NLRs, enabling more efficient response (Cesari et al., 2014a). However, to avoid the assumption that all these domains serve as baits and have no other function, they are more broadly referred to as "integrated domains" (Wu et al., 2015).

Integrated domains have been estimated to be present in 3.5-5.2% of higher plant NLR proteins (Kroj et al., 2016, Sarris et al., 2016). These domains are quite diverse and include (but are not limited to) BED domains, WRKY domains, HMAs, thioredoxins and kinases (Grund et al., 2019, Andersen et al., 2020, Chen et al., 2021). Moreover, they are found to be integrated at different positions of the NLRs, not only at N- and C-termini, but also between the canonical domains. It is thought that integration of unconventional domains into the NLR architecture occurred independently multiple times during evolution. Interestingly, research on grass NLRs with integrated domains revealed an amino acid motif upstream of the integration, which might have enabled the integration of unconventional domains (Bailey et al., 2018). The mechanism underlying these integrations remains to be elucidated.

In the majority of reported cases, the integrated domain has been shown to directly interact with an effector. The *A. thaliana* RRS1 receptor contains an integrated WRKY domain at its C-terminus, which directly interacts with the effectors AvrRps4 (from *P. syringae pv. pisi*) and PopP2 (from *R. solanacearum*) to trigger immune responses (Sarris et al., 2015, Mukhi et al., 2021). The rice NLR proteins Pik-1 and RGA5 both contain an integrated HMA (heavy metal associated) domain that can directly bind the cognate *M. oryzae* effectors AVR-Pik and AVR-Pia/AVR1-CO39, respectively (Maqbool et al., 2015, Ortiz et al., 2017, Guo et al., 2018, De la Concepcion et al., 2018). Arabidopsis RPP1 directly recognises the ATR1 effector from *Hyaloperonospora arabidopsidis* via an integrated C-JID (C-terminal jelly roll and Ig-like domain) domain (however, there is an ongoing debate,

whether this domain is actually an “integrated domain”, therefore it is often referred to as post-LRR domain (PL)) (Ma et al., 2020).

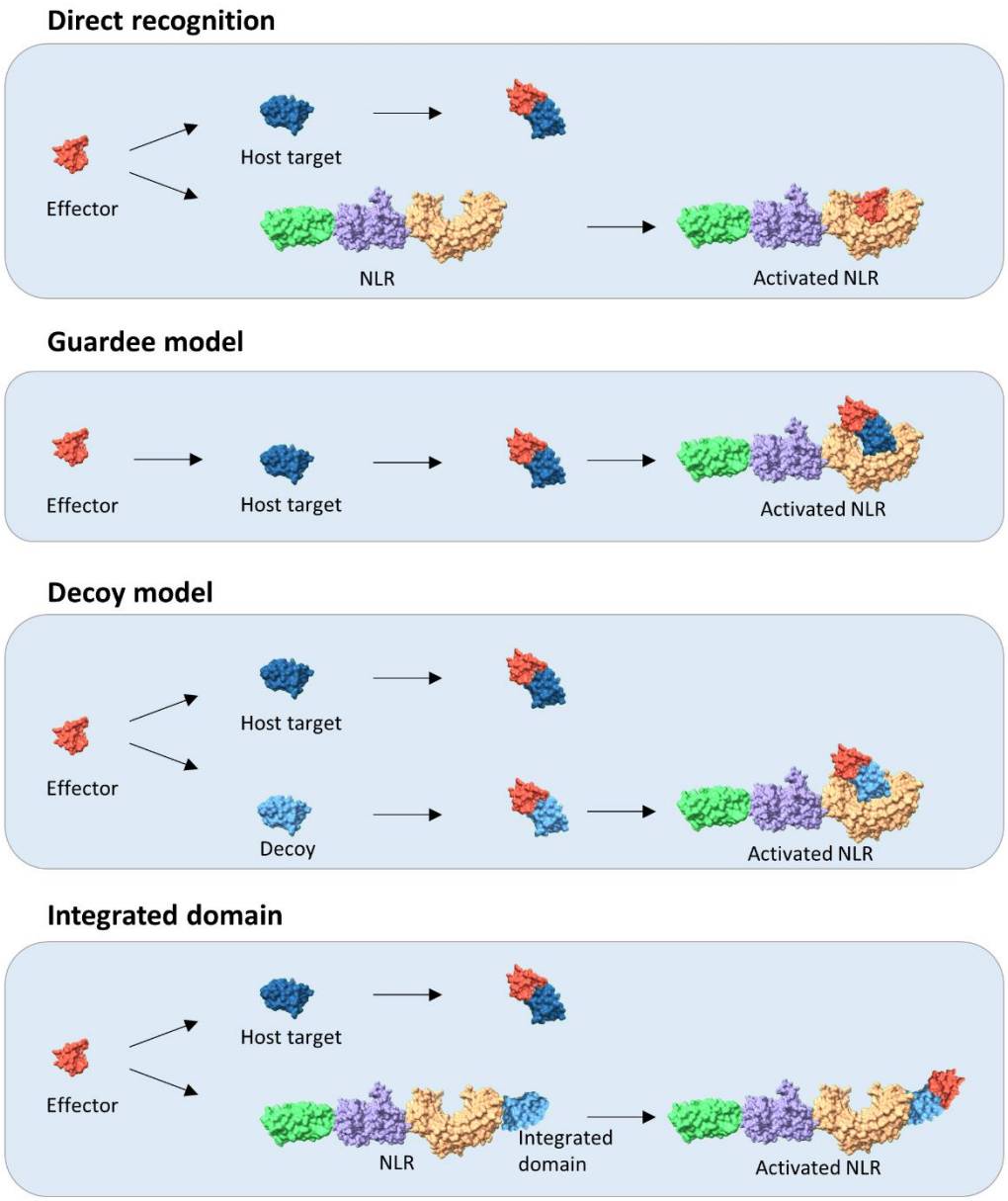

Figure 1.3 Different models of effector recognition in plants.

The NLR presented in the figure does not represent actual NLR structure. Different colours within the NLR structure represent individual NLR domains: green - CC, purple - NB-ARC, orange – LRR. Adapted from (Bentham et al., 2020).

1.4.3 NLRs can work as singletons, in specialised pairs or in networks

NLRs, and other resistance genes, were initially reported to work as single units, according to Flor's gene-for-gene model (one Resistance (R) gene for one avirulence gene) (Flor, 1971).

So-called "singleton" NLRs are receptors that trigger cell death responses in heterologous systems by overexpressing them in the presence of their cognate effector. Examples include *A. thaliana* NLRs RPS5 and RPP13 that recognise effectors AvrPphB (from *P. syringae*) and ATR13 (from *Hyaloperonospora arabidopsidis*), respectively (Ade et al., 2007, Leonelli et al., 2011). Moreover, different alleles of barley MLA (mildew locus A) proteins can directly recognise corresponding alleles of powdery mildew effector AVRa (Saur et al., 2019). These "singleton" NLRs are capable of both recognising (sensing) the presence of an effector and triggering downstream immune responses.

Apart from NLR receptors working as singletons, an increasing number of studies indicate that genetic architecture underpinning plant immunity can be more complex and additional components, including additional NLRs, can be required to deliver responses to a pathogen (Eitas and Dangl, 2010, Wu et al., 2018).

Contrary to NLRs that work as singletons, which are capable of both sensing the effectors and triggering the immune response, some NLRs specialised to carry only one of these functions. NLRs that are specialised in recognising the pathogen are usually referred to as "sensors". Sensor NLRs need partner NLRs that are specialised in delivering the immunity response. These partner NLRs are usually referred to as "helpers" (Adachi et al., 2019b, Jubic et al., 2019). Sensor and helper NLRs can work in highly specialised pairs (often genetically linked, sharing the regulatory elements (Eitas and Dangl, 2010, Griebel et al., 2014)) or form more intricate immune networks where multiple sensor NLRs can work together with diverse helper NLRs (Wu et al., 2017, Wu et al., 2018, Castel et al., 2019).

Several paired NLRs have been described to date, with two main modes of action described, based on the auto-activity of the helper NLR. Arguably, the best characterised NLR pairs are rice RGA5/RGA4 (Cesari et al., 2014b, Cesari et al., 2013) and Arabidopsis RRS1/RPS4 (Narusaka et al., 2014, Sarris et al., 2015, Huh et al., 2017, Ma et al., 2018). They share similar working mechanism, where the helper NLR (RGA4 and RPS4) is auto-active, and this auto-activity is repressed by presence of the sensor NLR (RGA5 and RRS1). The inhibition is released upon recognition of the cognate effector by the sensor. This model is therefore based on negative regulation.

A different model has been suggested for the rice Pik-1/Pik-2 pair (Białas et al., 2018). The helper NLR (Pik-2) is not auto-active when overexpressed alone, therefore this pair is thought to work via cooperation rather than negative regulation. However, this system is not as well characterised as the other described NLR pairs, and will be a subject of investigation in Chapter 3 of this work. A cooperation model has been also suggested for mammalian NAIP2/NLRC4 inflammasomes (Broz and Dixit, 2016), where NAIP2 functions as a sensor of bacterial patterns (Kofoed and Vance, 2011, Tenthorey et al., 2017) and NLRC4 is recruited to trigger downstream immune responses (Hu et al., 2015, Zhang et al., 2015).

1.4.4 NLRs form resistosomes upon activation

Initial studies on NLRs revealed that receptor activation involves ADP/ATP exchange within the NB-ARC domain. It has been suggested that NLRs are initially in an inactive, ADP-bound state, maintained via intra and intermolecular interactions (Tameling et al., 2002, Maekawa et al., 2011). Effector recognition would then lead to a switch of the ADP-bound inactive state for an ATP-bound active state, probably by inducing conformational changes that enable ADP/ATP exchange (Tameling et al., 2002, Takken et al., 2006, Williams et al., 2011, Bernoux et al., 2016).

Until recently, the knowledge about mechanisms of plant NLR function and activation were based on studies conducted on individual domains (Bentham et al., 2018, Casey et al., 2016, Cesari et al., 2016, Maekawa et al., 2011, Zhang et al., 2017a). Moreover, several studies indicated that plant NLRs can also associate in homo- and hetero-typic manner, both prior to and after effector recognition (Mestre and Baulcombe, 2006, Schreiber et al., 2016, El Kasmi et al., 2017, Huh et al., 2017). However, it was unclear whether that association represented active oligomeric structures, as has been observed in mammalian inflammasomes or apoptosomes.

A recent breakthrough in biochemical studies of plant NLRs shed light on their activation and post-activation events leading to immune signalling. The Cryo-EM structures of Arabidopsis ZAR1, RPP1 (Recognition of *Peronospora parasitica* 1) and *N. benthamiana* Roq1 (Recognition of XopQ 1) revealed that upon the effector recognition they form oligomeric structures named “resistosomes”, which is reminiscent of the oligomeric inflammasomes and apoptosomes, formed by mammalian NLRs (Wang et al., 2019a, Wang et al., 2019b).

ZAR1 belongs to a CC-NLR family and recognises at least three bacterial effectors via association with various pseudokinases. One of these effectors is AvrAC, delivered by *Xanthomonas campestris pv. campestris.* Before effector recognition, ZAR1 remains in an inactive, ADP-bound state, forming a heterodimer with the pseudokinase RKS1. AvrAC uridylylates a cytoplasmic kinase, PBS1-like protein 2 (PBL2), which subsequently binds to the ZAR1-RKS1 complex (as $PBL2^{UMP}$). Binding of

PBL2^{UMP} induces conformational changes in the NB-ARC domain of ZAR1 which leads to the release of ADP from the receptor, allowing binding of ATP (Wang et al., 2019b). This in turn induces oligomerisation of the ZAR1-RKS1-PBL2^{UMP} complex, which forms a pentameric wheel-like resistosome (Wang et al., 2019a) (**Figure 1.4 A**). Analysis of the cryo-EM structure of the ZAR1 resistosome revealed that the α1 helices of the CC domains undergo a conformational change upon oligomerisation and form a 5-helix funnel-like structure that projects outwards. Initially, it was suggested that this structure could cause cell death response due to plasma membrane perforation (activated ZAR1 localises at the plasma membrane), as has been observed in certain cell-death causing toxins (Wang et al., 2019a, Burdett et al., 2019a). However, there is growing evidence that this structure could be forming ion channels, which would cause ion influx to the cell (the studies mainly point towards calcium ions), causing a cell death (Lee et al., 2020b, Bi et al., 2021). Interestingly, this mechanism seems to be working for both plants and animals, as auto-active mutant of plant NLR NRG1 (N requirement gene 1) can also induce calcium influx and subsequent cell-death in human cell lines (Jacob et al., 2021b).

RPP1 (Recognition of *Peronospora parasitica* 1) is a TIR-NLR that recognises ATR1 effector from oomycete pathogen *Hyaloperonospora arabidopsidis* (previously *Peronospora parasitica*) (Botella et al., 1998, Asai et al., 2015, Steinbrenner et al., 2015). The Cryo-EM structure revealed that RPP1 oligomerizes upon recognition of ATR1 and forms a tetrameric ring-like resistosome, consisting of four RPP1 and four ATR1 molecules (**Figure 1.4 B**). The oligomerisation of the receptor is entirely mediated by subdomains of RPP1. In addition to canonical NLR domains, RPP1 possesses post-LRR domain at its C-terminus. Structural search showed that this domain adopts a β–jelly roll and Ig-like fold, therefore it has been designated as C-JID (C-terminal jelly roll and Ig-like domain). This domain, together with LRR domain, is responsible for mediating the interaction with ATR1 (Ma et al., 2020). It has been previously suggested that TIR-NLRs deliver the cell death response via depleting the NAD^+ pool in the cell upon the activation (Essuman et al., 2018, Horsefield et al., 2019, Wan et al., 2019). This has been also confirmed by studies on RPP1, which showed that activated RPP1 (but not RPP1 in absence of the ATR1 effector) displays NADase activity and can hydrolyse NAD^+ in vitro. This activity is driven by oligomerisation of the TIR domains, as it has been shown that increased concentration of TIR domains alone can also display NADase activity in vitro (where oligomerisation was likely driven by higher concentration of the protein). To achieve NADase activity, the TIR domains are positioned in a specific way in the active resistosome. Two symmetric TIR homodimers are packed in a specific way, leading to formation of two asymmetric head-to-tail TIR homodimers. Surprisingly, in the active state, RPP1 binds ADP instead of ATP at its P-loop motif. Although this might be an effect of intrinsic ATPase activity of RPP1, other interactions between NB-ARC domains

of RPP1 monomers have been suggested to compensate for loss of ATP-mediated stabilization of the resistosome (Ma et al., 2020).

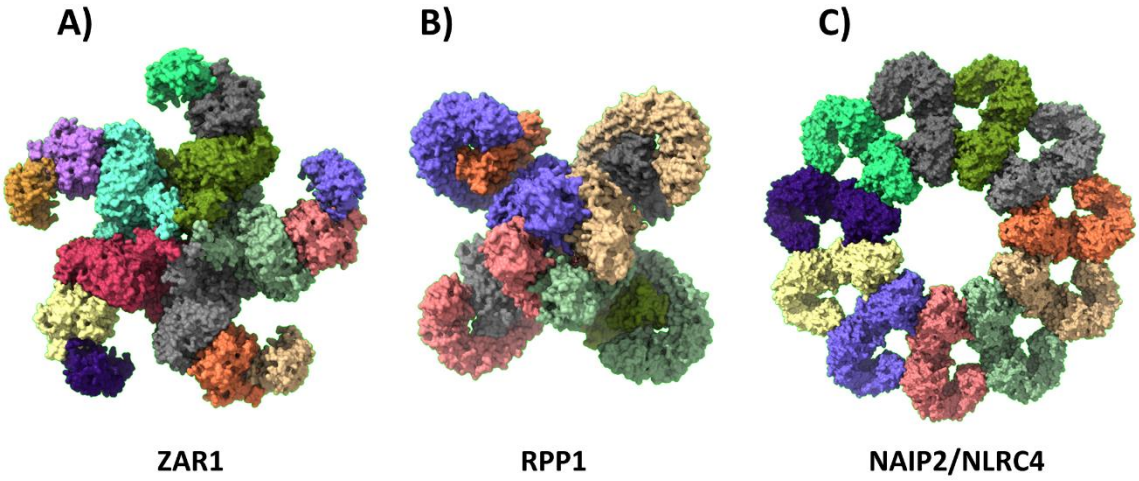

Figure 1.4 Oligomeric states of different NLRs.

A) *Pentameric ZAR1 structure in complex with RKS1 and PBL2^{UMP} (6J5W).* ***B)*** *Tetrameric structure of RPP1 in complex with ATR1 (7CRC).* ***C)*** *Inflammasome formed by activated NAIP2/NLRC4 (3JBL).*

A similar structure to RPP1 has been described for the TIR-NLR Roq1 that recognises the *Xanthomonas euvesicatoria* type III effector XopQ. XopQ binds to the LRR and post-LRR (PL) domain of Roq1, which alters the conformational state of the NB-ARC domain. This change allows for the release of ADP and ATP to bind at the P-loop site (in contrast to RPP1 structure, ATP molecule was found in the Roq1 resistosome). Interestingly, the PL region of Roq1 also resembles the immunoglobulin-like or jelly-roll fold, as observed in the RPP1 structure. Roq1 oligomerises into ring-like tetramer, where TIR domains form a two-fold assembly of “dimer of dimers”, as seen in RPP1 structure (Martin et al., 2020).

Although determining the Cryo-EM structures of the first CC-NLR and TIR-NLRs was a major breakthrough, these structures represent receptors that function as singletons. To date, it is hard to extrapolate the mechanism of activation of ZAR1 or Roq1 to paired NLRs or to the NLRs that function in networks. It is possible that different mechanisms could apply for these receptors, for instance, similar to mammalian NAIP2/NLRC4 inflammasomes (**Figure 1.4 C**), where a single molecule of NAIP2 is assembled with multiple copies of NLRC4, therefore providing a scaffold for oligomerisation of other units (Zhang et al., 2015). Moreover, it has been reported that both CC-NLRs and TIR-NLRs can act via certain downstream signalling components and there is increasing evidence that they interact directly (Huh et al., 2017, Zhai et al., 2019, Townsend et al., 2018, Xu et

al., 2014, Chang et al., 2013, Liu et al., 2015). This suggests that NLRs can act via various mechanisms, and we are only at the beginning of the path leading to understanding the biology and mechanistic details of plant NLRs.

1.5 Gene transfer and protein engineering can be used for deploying novel resistance

Continuous progress in discovering and describing new immunity receptors enables finding new solutions for plant health improvement. PRR receptors tend to recognise conserved patterns from pathogens and act via conserved signalling pathways, therefore they offer numerous opportunities to transfer the resistance between different plant species. For example, expression of rice cell-surface receptor Xa21 in tomato, sweet orange and banana increased resistance to *Xanthomonas sp*. (Mendes et al., 2010, Afroz et al., 2010, Tripathi et al., 2014). EFR receptor (from Arabidopsis) conferred novel resistance to bacterial pathogens when it was transferred to tomato and rice (Lacombe et al., 2010, Schoonbeek et al., 2015, Kunwar et al., 2018). Further, transfer of allelic receptor FLS2 from wild grape to tobacco conferred resistance to the crown-gall pathogen *Agrobacterium tumefaciens* (Furst et al., 2020). Based on these advances, cell-surface receptors can be a good source of novel and broad-spectrum resistance that can be transferred between plant species (Tian et al., 2020).

Apart from PRRs, simple transfer of NLRs between species has also been reported to be successful in conferring novel resistance. Originally identified in pigeon pea (*Cajanus cajan*) receptor CcRpp1 (*Cajanus cajan* Resistance against *Phakopsora pachyrhizi* 1) conferred full resistance in soybean to pathogen of Asian Soybean Rust, *Phakopsora pachyrhizi* (Kawashima et al., 2016). Further, transfer of resistance genes from wild potato species conferred resistance to late blight pathogen in common potato (Witek et al., 2016, Ghislain et al., 2019). Constant improvement of genomic technologies (Jupe et al., 2013, Bevan et al., 2017) and structure-based predictions (Zheng et al., 2021), enables more and more efficient mining the genomes of wild plant species and identification of new resistance genes, however breeding the resistance into elite cultivar crops is still a slow process (Steuernagel et al., 2016, Rodriguez-Moreno et al., 2017, Arora et al., 2019). Moreover, transfer of newly identified resistance genes to other plant species often appears to be ineffective (lack of response). Since many NLRs might function in pairs or networks (Castel et al., 2019, Wu et al., 2018), newly discovered NLRs may require specific genetic context to successfully confer resistance (Chae et al., 2014, Hurni et al., 2014, Stirnweis et al., 2014). Furthermore, NLRs usually have a precise recognition specificity, recognising race-specific effectors. Because of that, rapidly evolving pathogens may relatively quickly escape recognition by modifying their effector repertoire (Yoshida et al., 2016, De la Concepcion et al., 2018).

An alternative approach to developing new resistance genes is to modify the toolkit that has evolved in nature. Engineering of NLRs has been attempted on multiple occasions, using different approaches. The first trials focused on random mutagenesis of NLRs to expand their recognition, however it turned out to be largely unsuccessful (Farnham and Baulcombe, 2006, Harris et al., 2013, Segretin et al., 2014, Giannakopoulou et al., 2015).

Expanding the knowledge about mechanisms of effector recognition and NLR activation has recently enabled more focused and precise approaches to engineering novel resistance, not only via modification of NLRs, but also via engineering decoys. An excellent example is engineering of novel resistance mediated by the RPS5 receptor. RPS5 monitors the state of protein kinase PBS1 (Shao et al., 2003, Ade et al., 2007), which is targeted by the effector AVRPphB from *P. syringae.* AVRPphB is a protease and specifically cleaves PBS1, and this activity is detected by the RPS5. It has been shown that replacing the AVRPphB cleavage site in PBS1 with the cleavage site of different effector protease, can alter the recognition specificity mediated by RPS5 (Kim et al., 2016). Moreover, a PBS1 variant containing the cleavage site of the NIa protease (delivered by soybean mosaic virus) could be cleaved by this protease, and this further triggered a cell death response in soybean protoplasts, likely via an RPS5 ortholog (Helm et al., 2019). Furthermore, AVRPphB can also induce immune responses in wheat and barley, suggesting that PBS1 orthologs are also monitored in different plant species. Therefore, engineering PBS1 variants with various protease cleavage sites could be a promising tool to develop resistance to a subset of pathogens that deliver proteases to their hosts (Carter et al., 2019, Pottinger et al., 2020, Pottinger and Innes, 2020).

1.6 Rice NLR pair Pik-1/Pik-2 recognises rice blast effector AVR-Pik via integrated HMA domain

Rice paired NLRs Pik-1 and Pik-2 confer resistance to *Magnaporthe oryzae* strains carrying AVR-Pik effectors. Pik-1 and Pik-2 are genetically linked, as they are arranged in a head-to-head orientation in the genome (on the long arm of chromosome 11), and they share the same promoter (Ashikawa et al., 2008).

Pik-2 has a canonical CC-NLR architecture. However, Pik-1 possesses an integrated heavy metal associated (HMA) domain that is located between the CC and NB-ARC domains. The HMA is widely conserved in living organisms, and can be found in both prokaryotes and eukaryotes. It is generally involved in detoxification or transport of various heavy metals (Zhang et al., 2020). HMA domains typically contain a metal-binding motif, comprising residues MXCXXC (where X represents any amino acid). The cysteine residues are responsible for binding and coordinating the heavy metal (Arnesano et al., 2001). Structures of HMA-containing proteins revealed that they typically adopt

an αβ-sandwich fold comprised of a four-stranded antiparallel β-sheet and two α-helices. This fold is often referred to as a "ferredoxin-like" (Gitschier et al., 1998). Apart from Pik-1, the HMA domain has been also found to be integrated in another NLR, RGA5. Interestingly, in RGA5, the HMA is located at the C-terminus of the receptor (Ortiz et al., 2017, Guo et al., 2018).

To date, eight Pik-1/Pik-2 alleles have been described: Pikp, Pikm, Pik*, Pik*-KA, Pikh, Piks, Pike and Pi1 (Ashikawa et al., 2008, Yuan et al., 2011, Zhai et al., 2011, Ashikawa et al., 2012, Hua et al., 2012, Zhai et al., 2014, Chen et al., 2015), and they share between 95% and 99% amino acid sequence similarity. Importantly, the most polymorphic region between the alleles is the HMA domain.

The AVR-Pik effector was cloned using an association genetics approach (Yoshida et al., 2009). Initially, five alleles of AVR-Pik were identified (designated A-E), differing in between 1 and 4 amino acid positions. Further analysis found that all the AVR-Pik alleles (apart from AVR-PikB) could be found in isolates from all over the world, including Asia, Europe, America and Africa, indicating that AVR-Pik effectors are widely present in pathogen populations (Kanzaki et al., 2012). Recently, an additional allele has been described, named AVR-PikF (Longya et al., 2019, Li et al., 2019).

Different Pik alleles have different recognition specificity towards the AVR-Pik alleles. For example, the Pikp allele can only recognise AVR-PikD, whereas Pikm can recognise AVR-PikD, AVR-PikA and AVR-PikE. Interestingly, none of the known Pik alleles can recognise AVR-PikC or AVR-PikF, which means that *M. oryzae* carrying one of these effectors can infect rice varieties containing any Pik allele.

Biophysical studies of AVR-PikD/Pikp-1-HMA interaction revealed that these two proteins interact in vitro. This means that the integrated HMA domain of Pik-1 receptors can recognise the effectors directly, therefore Pik-1 acts as a classical "sensor" in this NLR pair. Pik-1 is only able to trigger cell death responses upon effector recognition in the presence of Pik-2 protein, therefore Pik-2 acts as a classical "helper" (Maqbool et al., 2015).

Structural studies of the AVR-PikD/Pikp-1-HMA complex identified important residues involved in binding between these two proteins. A single mutation in AVR-PikD, H46E, was able to disrupt the binding to Pikp-1-HMA in vitro, which was further correlated with lack of recognition in a transient expression system. Moreover, *M. oryzae* carrying the AVR-PikD^{H46E} mutant was not recognised by rice cultivar K60 that naturally possesses the Pikp-1/Pikp-2 pair (Maqbool et al., 2015). These results indicate that interaction between the integrated HMA domain and the AVR-Pik effector is necessary for activation of resistance mediated by the Pik NLRs.

Pikp-1-HMA binds AVR-PikD with high affinity, and weakly interacts with AVR-PikE (although that does not translate into resistance in planta), while Pikm-1-HMA binds AVR-PikD, AVR-PikE and AVR-PikA effectors (De la Concepcion et al., 2018). Determining crystal structures of Pikm-1-HMA with these three effectors allowed identification of important residues involved in binding between the HMA domain and the effectors, and explains the differences in the interaction profiles between Pikp-1-HMA and Pikm-1-HMA. Furthermore, these data enabled engineering the interaction interface present in Pikm-1-HMA onto Pikp-1-HMA, which extended its recognition profile to AVR-PikE and AVR-PikA effectors (De la Concepcion et al., 2019). These results provided an important proof-of-concept that we can use structural biology in engineering novel recognition specificities in NLRs.

The binding between AVR-Pik and the integrated HMA domains suggests that an HMA-containing proteins might be biological targets of these effectors. Over 100 small HMA-containing proteins (abbreviated as small HMAs or sHMAs for simplicity) have been identified in rice. Broadly, they can be divided into two families: heavy metal associated isoprenylated plant proteins (HIPPs) and heavy metal associated plant proteins (HPPs). In addition to one or more HMA domains, HIPPs also contain a C-terminal CaaX isoprenylation motif (where “a” represents an aliphatic amino acid, and X represents any amino acid), whereas HPPs lack this motif (de Abreu-Neto et al., 2013).

A yeast-2-hybrid screen aiming at identifying putative biological targets of AVR-PikD identified several HMA-containing proteins, including OsHIPP19, OsHIPP20, OsHPP04 and OsHPP03 (Oikawa et al., 2020). Interestingly, other tested alleles AVR-PikA, AVR-PikC and AVR-PikE also bound OsHIPP19 and OsHIPP20, suggesting that they might be a biological target for all the AVR-Pik effectors. In addition, it has been demonstrated that AVR-PikF also binds to OsHIPP19 (Maidment et al., 2021). It has been shown that presence of AVR-PikD can stabilise OsHIPP19 and OsHIPP20, and affects their localisation in the plant cell. Although the exact mechanism of how interaction between AVR-Pik and sHMA proteins promotes disease is not known, it has been shown that a knockout of OsHIPP20 reduces rice susceptibility to *M. oryzae*, suggesting that sHMA proteins can be susceptibility genes (Oikawa et al., 2020).

1.7 Aims and objectives

Advancing our comprehension of plant-pathogen interactions requires research on both sides of the conflict. A better understanding of plant immune receptors combined with knowledge about pathogen effectors and effectors' targets can inform and enable rational design of NLRs to engineer novel recognition specificities and offer new solutions for improving the food security. In this work, I investigate different aspects of molecular interactions between rice and the rice blast fungus *Magnaporthe oryzae*.

In Chapter 3, I investigate the working model of rice NLR pair Pikp-1/Pikp-2 that has been suggested to deliver the cell death response via cooperation rather than negative regulation.

In Chapter 4, I characterise biochemically the interaction between different alleles of *M. oryzae* effector PWL2 and their potential interactor rice protein OsHIPP43.

In Chapter 5, I investigate the potential of engineering new recognition specificity of Pikm-1 by exchanging its integrated HMA domain for OsHIPP43-HMA - a potential biological target of PWL2.

In Chapter 6, I describe the crystal structure of PWL2/OsHIPP43 complex and the interactions that underpin the binding between these two proteins. I also show that the interaction between PWL2 effector and OsHIPP43 cannot be easily compromised.

In Chapter 7, I investigate whether other *M. oryzae* effectors from the PWL family can also interact with OsHIPP43, and whether the approach of engineering novel recognition specificity presented in Chapter 5 can be also applied to these effectors.

In Chapter 8, I describe the solution structure of the recently discovered effector AVR-Pias, which represents a new effector class from *M. oryzae.*

2

Materials and Methods

2 Materials and Methods

2.1 Cloning and DNA manipulation

All generated constructs were verified by Sanger sequencing. The service was provided by Genewiz or Eurofins Genomics companies.

2.1.1 Gene synthesis

The DNA sequence coding each PWL2 mutant was commercially synthesised by Integrated DNA Technologies as a gBlocks Gene Fragment. The DNA fragments were designed with *BsaI* restriction sites and appropriate overhangs, therefore could be directly used as level 0 constructs for an assembly of level 1 constructs for in planta expression (with C-terminal tags) using Golden Gate cloning. For generating constructs for protein expression, the synthesised DNA fragments were used as templates for amplification of DNA fragments with appropriate overhangs that enable the cloning with N-terminal tags.

2.1.2 DNA amplification

DNA fragments destined for downstream cloning were amplified using high fidelity, proof reading VELOCITY DNA polymerase (Bioline), allowing 30 s/kb of extension time. The reaction components are listed in **Table 2-1**

Table 2-1 Reaction mix for DNA amplification using VELOCITY DNA Polymerase

Component	Quantity
5 x VELOCITY Buffer	10 µl
Forward primer	3 µl (at 10 µM)
Reverse primer	3 µl (at 10 µM)
Template DNA	1 µl with 10 ng of DNA
VELOCITY DNA Polymerase	1 µl
dNTP	1 µl (at 1 µM)
Water	31 µl

To perform colony PCR, MyTaq DNA polymerase (Bioline) was used according to the manufacturer's guidelines, allowing 30 s/kb of extension time. MyTaq DNA polymerase uses a premixed buffer that contains $MgCl_2$, dNTPs, and a gel loading dye. The reaction components are listed in **Table 2-2**. As a DNA template, single, isolated bacterial colonies were added to the mixture. To release the DNA from bacteria, the initial denaturation was extended to 5 min.

Table 2-2 Reaction mix for DNA amplification using MyTaq Polymerase

Component	Quantity
5 x MyTaq Buffer	4 µl
Forward primer	1 µl (at 10 µM)
Reverse primer	1 µl (at 10 µM)
Template DNA	Bacterial cells
MyTaq Polymerase	0.5 µl
Water	13.5 µl

2.1.3 Agarose gel/ DNA electrophoresis

1% (w/v) agarose gel (in TAE buffer; 40 mM Tris-acetate pH 8.0, 1.0 mM EDTA) with Midori^{Green} Advance DNA stain (Nippon Genetics Europe; 1 µl stain / 25 ml agarose) was used to confirm and/or separate the desired PCR products. MyTaq Red PCR buffer contains the loading dye, therefore samples obtained using this buffer were loaded directly on a gel. Other DNA samples were mixed with loading dye 4xFOG (12% (w/v) Ficoll 400, 0.25% (w/v) Orange G) before loading on a gel. The electrophoresis was carried out at a constant voltage of 100 V in TAE buffer. Subsequently samples were visualised under UV light.

2.1.4 Purification from agarose

After electrophoresis, DNA bands of interest were cut out from the agarose gel using a razor blade. To purify the DNA from the gel fragment, NucleoSpin Gel and PCR Clean-up kit (Macherey-Nagel) was used according to the manufacturer's instructions.

2.1.5 In-Fusion cloning

For protein production in *E. coli*, genes of interest were cloned into pOPIN vectors (Berrow et al., 2007) by In-Fusion cloning. Protein coding sequences were amplified with primers introducing overhangs matching the cloning acceptor plasmid. 100 ng of linearized vector and 100 ng of purified PCR fragment were combined with 1 µl of 5x In-Fusion HD enzyme premix and adjusted to final reaction volume 5 µl with water. The reaction mix was incubated at 42 °C for 30 min and subsequently transformed into chemicompetent *E. coli* STELLAR cells.

2.1.6 Golden Gate cloning

Golden Gate cloning was used to generate constructs for transient expression in *N. benthamiana* (Engler et al., 2014) and several constructs for protein production in *E. coli* (Bentham et al., 2021b). The full length NLRs (wild type and chimeric) were cloned under control of *A. tumefaciens* mannopine synthase (mas) promoter and terminator. Individual NLR domains were cloned under control of CaMV35S promoter. Full length Pik-1 NLRs and Pik-1 individual domains were C-terminally tagged with 6xHis/3xFlag (HellFire, HF) tag, full length Pik-2 and Pik-2 individual domains were C-terminally tagged with an HA tag. Expression of the effectors was driven by the *A. thaliana* Ubi10 promoter with a 35S terminator, and all the effectors were tagged with 4xMyc tag. AVR-PikD was tagged N-terminally and all PWL effectors were tagged C-terminally, unless stated otherwise. All constructs were cloned into acceptor vector pICH47751.

The selected constructs for protein production in *E. coli* obtained via Golden Gate cloning are listed in the relevant Results sections, and were cloned as described in (Bentham et al., 2021b).

The Golden Gate cloning method is a single-pot digestion-ligation reaction that allows assembly of multiple DNA fragments in a desired order. The reaction uses type IIS restriction enzymes that recognise specific asymmetric DNA sequences and cleave outside of the recognition site, leaving four base pair single stranded overhangs (Engler et al., 2008, Weber et al., 2011, Engler et al., 2014). Subsequently, the DNA fragments are ligated by the T4 DNA ligase, and the assembly order is dictated by the complementarity of the overhangs. This method requires that the DNA templates used for construct assemblies are free from endogenous restriction sites (*BpiI* and *BsaI* sites). The process of removing the restriction site (by introducing mutations) is referred to as domestication.

The standard Golden Gate components are usually defined as level 0, level 1 or level 2, based on their content. Level 0 modules carry single genetic components such as promoters, epitope tags, terminators and coding sequences. These can be assembled into level 1 constructs that contain complete functional transcriptional units. Importantly, level 1 acceptor vectors are binary vectors, therefore can be used in both bacteria (for plasmid amplification or protein expression) and plants

(for protein expression). Hence, level 1 constructs are broadly used for transient expression of proteins in planta, allowing optimisation of that expression, by straightforward assembly of given gene of interest with various promoters, terminators and tags. Level 1 constructs can be further assembled into level 2 constructs that contain multiple transcriptional units. This can be used for stable plant transformation, as alongside the gene of interest, a separate selectable marker cassette can be present. The order of assembly is determined by the level 1 acceptor vectors and the overhang they expose upon digestion. *BpiI* enzyme is used for generation of level 0 and level 2 constructs; *BsaI* is used for generation of level 1 constructs.

This method can be adapted to create unique acceptor vectors. For instance, Pikm-1 has been incorporated into level 0 acceptor vector, with the original Pikm-1-HMA domain exchanged for the RFP selection cassette flanked by *BpiI* restriction sites (**Figure 2.1**). The generated construct allows replacing this cassette with any DNA sequence, therefore, generating a level 0 construct carrying Pikm-1 receptor with integrated domain of interest in place of the original HMA domain. Such chimeric receptor would be a level 0 construct, ready for further assembly into level 1 construct with regulatory elements of choice. Using this method, I generated the Pikm-1^{OsHIPP43} receptor, where I inserted the OsHIPP43 sequence in place of the RFP selection cassette in the described acceptor vector. This acceptor vector has been designed and prepared by Dr. Mark Youles (The Sainsbury Laboratory).

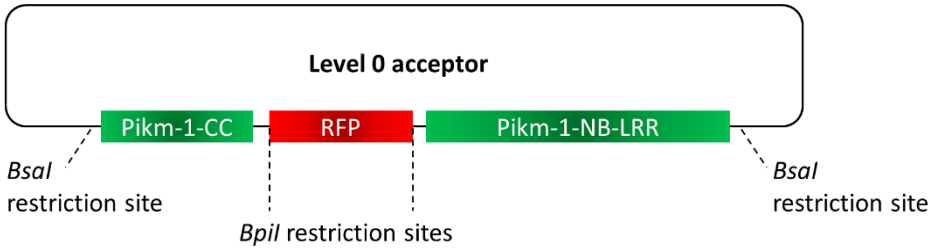

Figure 2.1 Schematic representation of the Pikm-1- integrated domain acceptor vector.

BpiI restriction enzyme can be used in Golden Gate reaction to replace the RFP selection cassette with any integrated domain. Subsequently, the chimeric Pikm-1 construct can be put together with epitope tag and regulatory elements of choice into a level 1 construct.

To assemble the level 1 constructs, 100 ng acceptor plasmid was used. The level 0 modules were added in a 2:1 (level 0 construct : acceptor vector) molar ratio. The components of the digestion-ligation reaction are listed in **Table 2-3**. The final volume of the reaction was 20 µl. The protein coding sequence of interest was added to the mixture in form of purified PCR product (amplified with appropriate overhangs and restriction sites). The conditions of the reaction are listed in **Table**

2-4. After completed reaction, 2 µl of the reaction mix was used to transform chemicompetent *E. coli* STELLAR cells.

Table 2-3 Components of Golden Gate reaction

Component	Quantity
Acceptor plasmid	100 ng
Level 0 parts	2:1 molar ratio of insert:acceptor
Bovine Serum Albumin (1 mg/ml)	1.5 µl
T4 DNA ligase buffer (NEB)	1.5 µl
T4 DNA ligase (NEB)	1 µl
BsaI or BpiI (NEB)	1 µl

Table 2-4 Reaction conditions of Golden Gate cloning

Temperature	Time	
37 °C	20 s	
37 °C	3 min	X 27 cycles
16 °C	4 min	
50 °C	5 min	
80 °C	5 min	

2.2 Bacteria transformation

2.2.1 *E. coli* transformation

1-2 µl of a plasmid/reaction mix was added to the 30 µl of chemically competent *E. coli* STELLAR cells (thawed on ice). Transformation mix was incubated in 42 °C for 60 s and immediately resuspended in 1 ml of room-temperature LB medium. The mix was incubated for 1 hour in 37 °C with agitation (200 rpm) for cell recovery. Subsequently, 100 µl of the suspended bacteria were plated on the LB plate containing relevant antibiotics and the plate was incubated at 37 °C overnight.

2.2.2 *Agrobacterium tumefaciens* transformation

Electrocompetent *Agrobacterium tumefaciens* cells were transformed using electroporation. Plasmid DNA was mixed with the bacteria and transferred into pre-chilled 2 mm electroporation

cuvette (Geneflow/Cell Projects). The cells were transformed by supplying 2500 V pulse using an Eppendorf Electroporator 2510. Immediately after electroporation, cells were resuspended in 1 ml of LB and incubated at 28 °C with agitation (200 rpm) for 2-3 hours. 100 µl of the suspended bacteria were plated on the LB plate containing relevant antibiotics and the plate was incubated at 28 °C for at least two days.

2.2.3 Antibiotics

1000X stocks of kanamycin (30 mg/ml), carbenicillin (100 mg/ml), gentamycin (50 mg/ml), and spectinomycin (100 mg/ml), were prepared by dissolving in deionised water. A 1000X stock of rifampicin (50 mg/ml), was prepared by dissolving in 100% DMSO, and a 1000X stock of chloramphenicol (34 mg/ml) was prepared by dissolving in ethanol. Prepared solutions were filter-sterilised (Minisart 0.22µm filters (Sartorius)).

2.3 Protein production and purification

2.3.1 Protein production in *E. coli*

OsHIPP43, PWL2/OsHIPP43 complex and AVR-Pias constructs in pOPIN (Berrow et al., 2007, Bentham et al., 2021b) protein expression vectors were transformed into *E. coli* SHuffle cells (Lobstein et al., 2012), and all PWL effectors (including PWL2 mutants) were transformed into BL21-AI One Shot (Arabinose Inducible) *E. coli* cells (Invitrogen). To prepare the pre-culture, 100 ml of LB medium (supplied with appropriate antibiotics) was inoculated with bacteria carrying the plasmid of interest, and incubated overnight at 37 °C. The next day, 5 ml of the pre-culture was added to 1 L of LB medium in 2 L baffled Erlenmeyer flask with appropriate antibiotics and incubated with shaking (160 rpm) at 37 °C (AI strain) or 30 °C (SHuffle strain) until the OD reached 0.6 - 0.8. Then the temperature was decreased to 18 °C and cultures were induced with 1 mM IPTG (SHuffle strain) or 0.2% arabinose (AI strain), and incubated overnight. 8 L of cultures were grown per construct, unless stated otherwise.

Allowing at least 18 hours of growth post-induction, cells were harvested by centrifugation (10 min, 7500 x g) and resuspended in ice-cold lysis buffer (A1 buffer (150 mM Tris-HCl pH 8.0, 500 mM NaCl, 5% glycerol, 50 mM glycine and 20 mM imidazole)), freshly supplemented with cOmplete EDTA-free Protease Inhibitor Cocktail). Subsequently, the cells were lysed by sonication using a Vibra-Cell sonicator (SONICS) with a single 13 mm probe, with the cells resting on ice. The sonication was set at 1 s pulse / 3 s pause for 10 min (total time of pulses), with amplitude set on 40%.

To obtain the soluble fraction, the lysate was centrifuged at 45000 x g for 30 min at 4 °C. The supernatant was loaded onto ÄKTAxpress to perform immobilised metal affinity chromatography (IMAC), directly followed by size-exclusion chromatography (SEC). 5 ml HisTrap HP NTA column (GE Healthcare) pre-equilibrated in A1 buffer was used for the IMAC step. After loading the sample (lysate), the column was washed with 100 ml of A1 buffer (also referred to as washing buffer). A1 buffer contains low concentration of imidazole that should help to prevent binding of the proteins with weak affinity to the nickel resin. After the washing step, the proteins were eluted with 25 ml of elution buffer B1 (A1 buffer supplemented with 500 mM imidazole), and immediately loaded onto a SEC column equilibrated with A4 buffer (20 mM HEPES pH 7.5 and 150 mM NaCl). The SEC step was performed on a Superdex 75 HiLoad 26/600 column (GE Healthcare). Elution from the column was collected in 8 ml fractions, containing proteins separated by size. The elution of the proteins was monitored by measuring the absorption at 280 nm. The fractions were subsequently analysed by SDS-PAGE to inspect the presence of the proteins.

Samples containing the proteins of interest (POI) were combined and incubated overnight with recombinant human rhinovirus (HRV) 3C protease at 4 °C to remove the affinity/solubility tag. The protease was added in 10 µg of protease / 1 mg of POI ratio. After the cleavage, the untagged protein of interest was separated from the cleaved tag and the protease (the 3C protease contains 6xHis tag) by affinity chromatography using 5 ml HisTrap HP NTA column (GE Healthcare). If proteins were initially tagged with an MBP tag, additional MBPTrap HP dextrin sepharose column (GE Healthcare) was used in the process, attached in tandem with HisTrap column. Both columns were equilibrated in SEC (A4) buffer. The sample was passed through the columns using peristaltic pump at speed around 4 ml/min. The initial flow through (ca. 8-15 ml, referred to as Flow Through 1 (FT1)) was collected to assess the “dead” volume of the column. The subsequent flow through was collected altogether (referred to as Flow Through 2 (FT2)). This fraction should contain majority of the untagged protein of interest, unless it displays weak affinity to one of the columns. The columns were subsequently washed with 45 ml A1 buffer that contains higher amount of salt and low concentration of imidazole; both components can help to elute the proteins with low affinity to the columns. Elution from the washing step was collected into three 15 ml fractions (referred to as Wash 1, Wash 2 and Wash 3). 15 ml of elution buffers (B1 for HisTrap column and 0.5 M NaOH for MBPTrap™ column) were passed through the column to elute the remaining proteins, which allows to assess the efficiency of the process (and any losses in yield). The collected fractions from the process were analysed by SDS-PAGE and fractions containing protein of interest were combined and concentrated down to 5 ml using 20 ml VivaSpin concentrators (Sartorius) with a cut-off depending on the molecular weight of the protein of interest.

Following the concentration, the sample was loaded on an ÄKTAxpress system at 4 °C for a second SEC. This step was performed on smaller column Superdex 75 HiLoad 16/600 (GE Healthcare), which allows collection of smaller fractions (2 ml), therefore enables more precise selection of least contaminated samples. The SEC was run again in A4 buffer (20 mM HEPES pH 7.5 and 150 mM NaCl).

Subsequently, the selected fractions were analysed by SDS-PAGE. Fractions containing purified proteins (or least contaminated) were combined and concentrated using 20 ml and 500 µl VivaSpin concentrators (Sartorius), with a cut-off depending on the molecular weight of the protein of interest. Samples were concentrated down to concentrations desired for biophysical analysis or crystallography trials (usually ca. 10 mg/ml (if possible)), flash frozen in liquid N_2 and stored at -70 °C.

2.3.2 Purification of PWL2/OsHIPP43 complex

To produce PWL2/OsHIPP43 complex in *E. coli* the proteins were co-expressed in the SHuffle cells following co-transformation of pOPINM:PWL2 and pPGC-K:OsHIPP43 (untagged). Cells were grown in LB medium, with antibiotic selection for both plasmids. Cells were induced, harvested and purification was conducted as described above. As the pPGC-K:OsHIPP43 construct did not produce a protein with an affinity tag, OsHIPP43 could be only purified when bound to PWL2.

2.3.3 Production of ^{15}N labelled protein

E. coli SHuffle strain carrying pOPIN-M:AVR-PiasΔ20 was inoculated from a glycerol stock into 100 ml of LB medium and incubated overnight at 37 °C with shaking (200 rpm). The following day, 10 ml of the pre-culture was inoculated per 1 L (8 L total) of minimum medium M9, supplemented with $^{15}NH_4Cl$ and appropriate antibiotic. To prepare the ^{15}N labelled M9 medium:

Per 500 ml of MQ water, 3 g Na_2HPO_4, 1.5 g KH_2PO_4 and 0.25 g NaCl were added, and the mix was autoclaved.

Subsequently, 1ml of 1 M $MgSO_4$, 50 µl of 1 M Ca_2Cl_2, 500 µl of 2.5% thiamine, 2.5ml of 0.2% biotine, 10 ml of 50% glycerol, 3 ml of 50% glucose and 2.5 ml of 20% $^{15}NH_4Cl$ were added cold.

The cultures were incubated at 30 °C until OD_{600} reached 0.5. Then the temperature was set to 18 °C and cultures were induced with 1 mM IPTG and grown overnight.

2.3.4 SDS-PAGE

Gradient 4% - 20% pre-cast RunBlue TEO-Tricine SDS Mini gels (Expedeon) were used for resolving proteins from plant extracts. 16% gels were used for resolving proteins during the purification from

E. coli. Samples were mixed with RunBlue 4x LDS Sample Buffer supplied with 100 mM DTT, incubated 95 °C for 10 min, loaded on a gel, and run with 1x RunBlue TEO-Tricine SDS running buffer at 90 – 130 V. Samples from *E. coli* expression and purification were incubated with InstantBlue Coomassie Protein Stain (Expedeon) at room temperature for at least 1 h for visualisation. The excess of the dye was then rinsed off with water and the gel was imaged using a GeneSys G:Box (Syngene). Samples derived from plant extracts were subjected to further western blot analysis (see section **2.6.5, p.65**).

2.4 In vitro techniques

2.4.1 Analytical Size-Exclusion Chromatography (SEC)

Analytical SEC experiments were carried out at 4 °C using a Superdex 75 10/300 GL column (GE Healthcare) equilibrated in A4 running buffer (20 mM HEPES pH 7.5, 150 mM NaCl). PWL2 and OsHIPP43 were mixed in a 1:1 molar ratio and incubated on ice for 1 h. Sample volume of 110 µl was injected on a column. For analysis of individual proteins, samples were loaded at concentration of 1 mg/ml (110 µl). The samples passed through the column at a flow rate of 0.5 ml/min. 0.5 ml fractions were collected for further SDS-PAGE analysis. The protein elution profile was monitored by measuring the absorbance at 280 nm.

2.4.2 Isothermal Titration Calorimetry (ITC)

ITC experiments were conducted using a MicroCal PEAQ-ITC (Malvern, UK). The PWL effectors were placed in experimental cell at 20 µM and titrated with OsHIPP43 at 300 µM. Both proteins were in A4 buffer (20 mM HEPES, pH 7.5, 150 mM NaCl) from the same batch, ensuring that the buffer is exactly the same and does not interfere with the measurements. Every ITC experiment was conducted at 25 °C. In each run, a single injection of 0.5 µL of OsHIPP43 was followed by 19 injections of 2 µl injections in 150 s intervals, with stirring (750 rpm). Experiments were repeated three times each. The raw titration data was analysed by AFFINIMeter software (Pineiro et al., 2019) that integrated the datasets, removed noise, corrected the baseline and calculated the ΔH and K_a parameters. For visualisation, the data was plotted using R v3.4.3 (https://www.r-project.org/) and the graphic package ggplot2 (Wickham, 2016).

2.4.3 Circular dichroism (CD)

After purification, proteins are in the buffer used for the final SEC step (20 mM HEPES pH 7.5, 150 mM NaCl). Both HEPES and chloride ions absorb in the far UV (<200 nm), hence the purified proteins needed to be exchanged into a phosphate buffer (20 mM potassium phosphate, pH 7.5). The buffer

exchange was carried out either via overnight dialysis using 0.5 ml Slide-A-Lyzer Dialysis Cassettes (Thermofisher) with 3.5 kDa molecular weight cut-off or by repeated cycles of dilution and concentration using a VivaSpin centrifugal concentrator (Sartorius). The final sample was concentrated to ca. 0.5 mg/ml and diluted, if necessary, during the measurements.

Circular dichroism was performed by Ms Julia Mundy, at JIC Biophysical Analysis Platform. The spectra were measured on a Chirascan Plus CD Spectrometer (Applied Photophysics) at wavelengths 180 – 260 nm, with measurement taken every 1 nm; the temperature was set to 20 °C. Three spectra per protein were obtained, averaged and the blank measurement was subtracted. The software reports the final data in milidegrees, which were subsequently converted into mean residue molar ellipticity (MRME), to correct the measurement for protein concentration. The conversion equation was as follows:

$$MRME = \frac{MRW * \theta obs}{10 * d * c}$$

Where:

MRW - Mean residual weight (~110 Da)

Θ_{obs} - measured ellipticity (deg)

d - pathlength (cm)

c – protein concentration (g/ml)

2.4.4 Trypsin digest

Stock solution of trypsin (Sigma) was prepared at 1 mg/ml in 1 mM HCl. 5 µl of the stock solution was added to an Eppendorf tube. Subsequently, as series of 1:3 dilution in PBS (137 mM NaCl, 2.7 mM KCl, 10mM Na_2HPO_4, 1.8 mM KH_2PO_4, pH 7.4) was prepared, with each tube containing 5 µl of diluted trypsin solution. To each tube, 20 µl of protein solution (either PWL2+OsHIPP43 or PWL2 alone) was added at concentration of 0.2 mg/ml, so the total reaction volume was 25 µl. The samples were incubated at 23 °C for 30 min. The reaction was stopped by adding 7 µl of stopping buffer (4x Loading Dye supplemented with 100 µM DTT and 5x solution of cOmplete EDTA-free Protease Inhibitor Cocktail), incubated at 95 °C for 10 in and 15 µl of the mix was loaded on a gel for the SDS-PAGE analysis.

2.4.5 Mass spectrometry

Intact mass spectrometry and peptide mapping / fingerprinting was performed by Dr. Jan Sklenar in The Sainsbury Laboratory. For the intact mass spectrometry, around 100 µg of protein sample was precipitated with 80% Acetone at -20 °C (for at least an hour) and spun down. For peptide mapping, a single band of interest was excised from polyacrylamide gel after SDS-PAGE and Coomassie staining.

2.5 Crystallography, structure solution and analysis

2.5.1 X-ray crystallography

Commercially available crystallization trials were set up using sitting drop, vapor diffusion method. Trials were set up in 96 well plates, allowing two proteins (or two protein concentrations) per screen, using an Oryx nano robot (Douglas Instruments, United Kingdom). Plates were kept at 20°C. Amongst many tested proteins and conditions, the only crystals were obtained for PWL2Δ10/OsHIPP43 complex in ProPlex crystallisation screen (Molecular dimensions) condition H5 (1.2 M Potassium sodium tartrate tetrahydrate, 0.1 M Tris 8.0) 13 days after initial set up. For data collection, three crystals were harvested by Dr. Clare Stevenson, dipped in a buffer containing the crystallisation condition supplemented with 20% ethylene glycol (cryoprotectant), and flash-frozen in liquid nitrogen.

2.5.2 Cross-seeding

Seeding is a process of addition of small protein crystal fragments (seeds) into the sitting drop in a crystallography screen. These seeds can act as nucleation points and enable formation of protein crystals more efficiently. Usually, the seeds are derived from the same proteins as the target protein that is intended to be crystallised. However, cross seeding is also possible, if crystals of the target protein are not available. In this case, seeds from different proteins can be used. As the seeds are very small and only serve as initiation point for crystal formation, the majority of subsequently formed crystals are made of the protein of interest which will be mainly responsible for the obtained diffraction pattern in an X-ray data collection. Therefore, the signal from the seed in a crystal will be reduced to noise.

Crystallisation trials of the PWL2/OsHIPP43 complex involved cross seeding. The seeds were derived from initial crystals of sHMA94/AVR-PikF complex, kindly provided by Dr. Adam Bentham (Bentham et al., 2021a). The seed stock is obtained by diluting the sitting drop with crystals with 2 µl of buffer

identical to crystallisation condition and transferring the drop into a tube with 48 µl of that buffer. The tube is then vortexed to shatter the crystals.

2.5.3 X-ray data processing

X-ray diffraction data were collected at beamline I04 of the synchrotron facility Diamond Light Source (Oxford, UK). Data reduction was carried out using the autoPROC (Native data, (Vonrhein et al., 2011)), and xia2.multiplex (S-SAD data, (Gildea and Winter, 2018, Beilsten-Edmands et al., 2020)) pipelines with the scaled (but unmerged) data imported and processed with AIMLESS (as implemented in CCP4i2) (Winn et al., 2011, Evans and Murshudov, 2013). The structure was solved by the SAD method using the CRANK2 pipeline as implemented in CCP4i2 (Skubák and Pannu, 2013, Skubák et al., 2018). This model was then used to solve the Native dataset (that was obtained at higher resolution) by molecular replacement with PHASER (McCoy et al., 2007). To arrive at the final structure, a series of manual rebuilding, refinement and validation steps were carried out using REFMAC (Murshudov et al., 2011) and COOT (Emsley et al., 2010). The structure was validated with MolProbity (Chen et al., 2010) and tools implemented in COOT.

2.5.4 Protein interface analyses

Protein interface analysis was carried out using QtPISA (Krissinel, 2015). The software determines the interactions parameters and visualise them graphically as interaction radar. The polygon area represents the likelihood that the interface is a part of a biologically relevant assembly. The key interface properties are compared to statistical distributions derived from the PDB. The centre of the radar represents zero, therefore any radar area close to centre (or within the 50% probability area) is considered of low probability of biological relevance.

2.5.5 Root Mean Squared Deviation (RMSD)

RMSD is a measure of the average distance between superimposed atoms of two structures. RMSDs were automatically calculated by ChimeraX software, upon superposition of the structures using the 'match maker' command. The command was used as default, allowing rejection of outliers, therefore the RMSD value given for any structure superposition is accompanied by the number of atoms that were aligned in the process.

2.5.6 NMR data collection and structure solution

NMR data for AVR-Pias were collected at 20 °C on Bruker Avance III 700 MHz and 800 MHz spectrometers equipped with a 5 mm z-gradient TCI cryoprobe.

AVR-Pias at concentration 0.5-2.0 mM (^{15}N-labeled or not) was submitted for NMR data collection in 25 mM sodium phosphate buffer (pH 6.8), 150 mM NaCl, 1 mM DTT with 10% D_2O for the lock.

^{1}H chemical shifts were referenced directly to the methyl resonance of DSS, while ^{13}C and ^{15}N chemical shifts were referenced indirectly to the absolute $^{13}C/^{1}H$ and $^{15}N/^{1}H$ frequency ratio, respectively. Each NMR spectrum was processed with TopSpin (Bruker) and analysed with CINDY (v2.1 Padilla, Univ. Montpellier).

Sidechain and backbone resonance assignments were performed using standard 3D [^{1}H, ^{15}N] NOESY-HSQC, 3D [^{1}H, ^{15}N] TOCSY-HSQC and 3D HNCO experiments performed on the ^{15}N-labeled protein sample in combination with 2D [^{1}H, ^{1}H] NOESY, 2D [^{1}H, ^{13}C] TOCSY experiments performed on unlabelled protein sample.

CYANA 3.9 (Güntert, 2004) was used for automated NMR structure calculations to assign NOE cross-peaks identified on NOESY spectra (mixing time 150-250 ms).

Sidechain $\chi 1$ and backbone Φ/Ψ torsion angles constraints were obtained from a database search procedure on the basis of backbone (^{15}N, H_N, $^{13}C'$, 13Cα, Hα and $^{13}C\beta$ chemical shifts using TALOS-N (Shen and Bax, 2013). Hydrogen bond restraints were derived using standard criteria based on the amide ^{1}H / ^{2}H exchange experiments. Following identification, the hydrogen bond was enforced using the following restraints: ranges of 2.7–3.0 Å for d(N,O), and 1.8–2.0 Å for d(N-H,O). The disulphide pairings (Cys-53/Cys-83 and Cys-57/Cys-79) were unambiguously identified from a statistical analysis of the distance between Cβ -Cys atoms of a set of preliminary structures. Disulphide bond restraints were added in the range: 2.0–2.1 Å for d(Sγ - Sγ) and 3.0–3.1 Å for d(Cβ - Sγ).

A total of 200 three-dimensional structures were generated using the torsion angle dynamics protocol of CYANA 3.9 from 1201 NOEs, 28 hydrogen bond, 6 disulphide bond and 93 angular restraints for AVR-PiasΔ21. The 20 best structures (based on the final target penalty function values) were minimized with CNS 1.2 according the RECOORD procedure (Nederveen et al., 2005) and analysed with PROCHECK (Laskowski et al., 1993). The RMSDs were calculated with MOLMOL (Koradi et al., 1996).

2.6 Plant techniques

2.6.1 Growth of *Nicotiana benthamiana*

Nicotiana benthamiana plants were grown in a controlled environment room with a 16 hours photoperiod, constant temperature 22 °C and relative humidity set to 80%. 4-week-old plants were used for agroinfiltrations.

2.6.2 Agroinfiltration

Agrobacterium tumefaciens strain GV3101 carrying the construct of interest was streaked out from a glycerol stock on a LB plate with appropriate antibiotics and incubated at 28 °C for two days prior to infiltration. Grown bacteria were gently scraped from the plate and resuspended in the infiltration buffer (10 mM MES (2-(N-morpholine)-ethanesulfonic acid) pH 5.6, 10 mM $MgCl_2$, freshly added 150 µM acetosyringone). Alternatively, bacteria from the glycerol stock were inoculated in 10 ml of LB medium and incubated for two days prior infiltration at 28 °C with shaking (200 rpm). Subsequently, the culture was spun down (5 min, 3500 x g) and resuspended in the infiltration buffer.

Following the initial measurement of OD_{600}, bacteria were mixed in desired combinations to have to OD_{600} in the final mix as following: Agrobacteria carrying NLRs and individual NLR domains were infiltrated at OD_{600} = 0.4 and bacteria carrying the effectors - at OD_{600} = 0.4. Each infiltration mix contained Agrobacteria carrying p19 constructs at OD_{600} = 0.1, which serves as silencing suppressor and enhances the expression of the proteins of interest. The prepared agrobacteria were infiltrated into the leaves of 4-week-old *N. benthamiana* leaves using needleless 1 ml syringes.

2.6.3 Cell death assays

At 5 dpi, detached agroinfiltrated *N. benthamiana* leaves were imaged under UV light (abaxial side). The UV images were taken using a Nikon D4 camera with a 60 mm macro lens, exposure was set at ~10 s at F14 and ISO set 1600. A Kodak Wratten No. 8 filter was used, with white balance set to 6250 degrees Kelvin. The UV light was supplied with Blak-Ray longwave (365 nm) B-100AP spotlight lamps, actively moved around the leaves for even illumination.

Each infiltration spot was scored (0 to 6) for cell death occurrence, according to the scale published in (Maqbool et al., 2015), also presented in **Figure 2.2**. Scoring data was plotted individually for each sample as dot plots using R v3.4.3 (https://www.r-project.org/) and the graphic package ggplot2 (Wickham, 2009). Every dot represents an individual data point / score. All dots are plotted around their given cell death score (size of the circle at given score is proportional to the number of dots within), each dot has a distinct colour corresponding to the biological replicate.

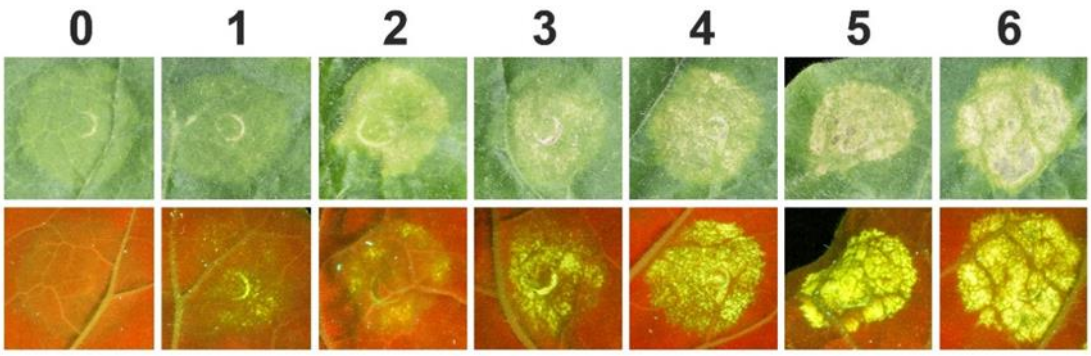

Figure 2.2 Scoring scale used for cell death assays

Figure displayed as presented in (Maqbool et al., 2015).

2.6.4 Coimmunoprecipitation (CoIP)

Proteins of interest were transiently expressed in 4-weeks old *N. benthamiana* plants via agroinfiltration of entire leaves. At 3 days post infiltration (dpi), the transformed leaves were harvested, flash frozen in liquid nitrogen and ground to fine powder in a mortar. The obtained powder was mixed with the ice-cold extraction buffer (GTEN (10% glycerol, 25 mM Tris pH 7.5, 1 mM EDTA, 150 mM NaCl)), freshly supplemented with 0.1% Tween 20 (Sigma), 2% w/v PVPP, 1x protease inhibitor cocktail (Sigma) and 10 mM DTT) in 2 g of tissue / 1 ml of buffer ratio and vortexed. The samples were centrifuged at 4500 x g for 30 min at 4 °C and subsequently the supernatant was passed through a 0.45 µm syringe filter (Minisart). The presence of each protein before the immunoprecipitation (the input) was determined by SDS-PAGE/western blot.

To immunoprecipitate the proteins of interest, 25 µl of pre-washed in the IP buffer (GTEN with 0.1% Tween 20) M2 anti-FLAG magnetic beads (Sigma, M8823) was added to 1.5 ml of filtered plant extract and incubated at 4 °C on a rotary mixer for 1 hour. Then the resin was separated from the extract using magnetic rack and the extract was carefully removed using a syringe with a needle. The resin was washed by resuspension in the IP buffer and separated again using the magnetic rack. The washing step was performed five times. After last wash, samples were gently spun down, resuspended in 30 µl of LDS Runblue sample buffer, incubated at 70 °C for 10 min, spun down and 15 µl of sample was loaded on a gel for western blot analysis.

2.6.5 Western blot

Proteins from the SDS-PAGE gel were transferred onto a PVDF (polyvinylidene difluoride) membrane (pre-activated in methanol for 1 min) using Trans-Blot Turbo transfer system (Bio-Rad) according to the manufacturer's protocol. After protein transfer, the membrane was incubated with the blocking buffer (5% w/v skimmed milk in TBS-T (50 mM Tris-HCl pH 8.0, 150 mM NaCl,

0.1% Tween-20)) at 4 °C for 1 hour, with agitation. Subsequently, the membrane was incubated with appropriate antibodies (diluted in the blocking buffer according to manufacturer's protocol) overnight. The next day, the membrane was washed with TBS-T buffer (3 x 20 min at room temperature with agitation). As the used primary antibodies were conjugated with HRP (horseradish peroxidase) (**Table 2-5**), the protein could be directly visualised using the two LumiBlue ECL Extreme reagents (Expedeon) pre-mixed in 1:1 ratio (300 µl of the mix per membrane). An ImageQuant LAS 500 spectrophotometer (GE Healthcare) was used to detect the chemiluminescence. To visualise the total protein load, membrane was stained with Ponceau red stain (0.1% w/v Ponceau S in 5% v/v acetic acid). The excess of the stain was removed after 15-20 min of incubation by multiple washes with water.

Table 2-5 List of antibodies used in this work.

Antibody	Company
α-FLAG	Cohesion Biosciences
α-HA	Invitrogen
α-V-5	Invitrogen
α-Myc	Santa Cruz Biotechnology

3

NLRs Pikp-1 and Pikp-2 work via cooperation rather than negative regulation to deliver cell death responses in planta

3 NLRs Pikp-1 and Pikp-2 work via cooperation rather than negative regulation to deliver cell death responses in planta

3.1 Introduction

Pikp-1 and Pikp-2 are a well-studied pair of NLRs from rice. Both these proteins belong to CC-NLR class and are both required to trigger immune responses upon the perception of the rice blast pathogen effector protein AVR-PikD. Pikp-2 has a canonical plant NLR architecture and consists of CC, NB-ARC and LRR domains. Pikp-1 possesses an additional, unconventional integrated HMA domain between the CC and NB-ARC domains that binds directly the effector. Due to the ability to directly bind the effector, Pikp-1 functions as a "sensor" in this NLR pair, while Pikp-2 functions as a "helper".

Many studies support a conceptual framework for the function of each of the domain found in NLR immune receptors, although the roles and requirements for these domains can vary from one NLR to another. CC domains are involved in downstream signalling and initiating the cell death response, supported by experiments demonstrating their ability to trigger these responses when expressed in planta alone (Casey et al., 2016, Wroblewski et al., 2018, Lee et al., 2020a). CC domains have been also reported to self-associate (Maekawa et al., 2011, Wang et al., 2015c, Wang et al., 2021a), associate with CC domains of other, paired NLRs (Cesari et al., 2014b), guardee proteins (Ade et al., 2007) and potential downstream interactors (Hao et al., 2013, Hamel et al., 2016, Baudin et al., 2017, Townsend et al., 2018). In the first reported cryo-EM structure of a full length NLR, that of ZAR1, it was shown that CC domains can undergo a conformational change upon NLR activation. This conformational change resulted in the α1 helix of the ZAR1-CC filling out of the core structure in oligomeric state (forming a funnel on self-association) (Wang et al., 2019a). The funnel formed by the oligomeric α1 helices has been suggested to mediate association with the plasma membrane and form an ion channel (Burdett et al., 2019a). Recent discoveries indicate that the CC domains might indeed form a specific Calcium-influx channel (Bi et al., 2021, Jacob et al., 2021a), which has been suggested to be the mechanism underlying the cell death response (Lee et al., 2020b).

The central NB-ARC domain is thought to be the molecular switch of the NLR as it can adopt significantly different conformations depending on the bound nucleotide (Bernoux et al., 2016,

Zhang et al., 2017b, Wang et al., 2019b). Within the NB domain several well-conserved motifs can be distinguished, including the P-loop and MHD motifs, both of which are involved in nucleotide binding and/or exchange. Mutations in these sequences can have diverse effects on protein function and localisation. Mutation of the P-loop motif impairs nucleotide binding and often results in loss of protein function (Dinesh-Kumar et al., 2000, Howles et al., 2005, Bai et al., 2012). Moreover, mutations in the P-loop of RPM1 caused loss of its ability to self-associate and impaired plasma-membrane localisation (El Kasmi et al., 2017). The MHD motif in the ARC2 is predicted to act as a phosphate sensor and be involved in nucleotide-dependent conformational changes. Mutations in this motif often lead to constitutive activity (usually described as auto-activation) of NLRs (Bendahmane et al., 2002, Kawano et al., 2010, Gao et al., 2011, Roberts et al., 2013). Although the role and mechanism of binding and sensing ADP/ATP by the NB-ARC domain is relatively well investigated, its role in some NLRs does not seem to be crucial for the protein function and therefore remains somewhat elusive (mutation of P-loop does not always impair NLR's function) (Bonardi et al., 2011, Cesari et al., 2014b, Wu et al., 2016, Steele et al., 2019, Wang et al., 2019b, Martin et al., 2020).

The C-terminal LRR domains have been shown to play mainly two roles. Firstly, they can play important roles in intramolecular interactions, very often being responsible for auto-inhibition in cooperation with NB-ARC domain (Rairdan and Moffett, 2006, Qi et al., 2012, Slootweg et al., 2013, Qi et al., 2018). Interestingly, similar patterns can also be found in mammalian NLRs (Hu et al., 2015, Bentham et al., 2017, Burdett et al., 2019b). Secondly, they can play a role in both direct and indirect effector recognition. For instance, direct interaction has been shown between AVR-Pita and LRR domain of Pita NLR in Yeast-2-Hybrid (Jia et al., 2000), whereas indirect interaction can be observed in ZAR1 structure, where the LRR domain is involved in formation of the pre-activation complex of ZAR1-RKS1 that can perceive uridylylated PBL2 ($PBL2^{UMP}$) catalysed by the AvrAC effector (Wang et al., 2019a, Wang et al., 2019b).

In the literature, two cases of genetically linked NLR pairs are relatively well studied: CC-NLRs RGA5 and RGA4 from rice, with integrated HMA (Heavy Metal Associated) domain and TIR-NLRs RRS1 and RPS4 from Arabidopsis, with integrated WRKY domain. It has been shown that they share similar modes of action. One of the proteins of the pair (helper) is auto-active when expressed alone, and this auto-activity is inhibited by the second NLR (sensor) via direct interactions. Upon recognition of the effector this suppression is released, leading to cell death (Williams et al., 2014, Cesari et al., 2014b). Moreover, these pairs can form pre- and post-activation complexes that are crucial for NLR function (Cesari et al., 2014b, Huh et al., 2017).

Molecular interactions underpinning recognition of specific AVR-Pik effector alleles, and corresponding Pik NLRs, have been well studied (Maqbool et al., 2015, De la Concepcion et al., 2018, De la Concepcion et al., 2019, De la Concepcion et al., 2021b). However, how effector perception translates into response in the context of full-length receptors remains unclear. The Pik-2 (helper) NLR does not display the characteristic auto-activity observed on expression of other genetically linked helper NLRs like RGA4 and RPS4 (Maqbool et al., 2015). Therefore, it has been suggested that the Pik-1/Pik-2 NLR pair works via cooperation, rather than negative regulation (Białas et al., 2018). However, the details of this cooperation, as well as requirements for particular domains in both receptors remain elusive.

In this Chapter, I set out to investigate the roles and requirements of individual domains of the NLR pair Pikp-1/Pikp-2 in triggering the cell death response in planta. I also determine the requirements for P-loop and MHD motifs in the receptor activity. Finally, I investigate the roles of homo- and hetero- association of the two NLRs in planta, and how the receptor oligomerisation is affected by the presence of the AVR-PikD effector.

3.2 Results

3.2.1 All domains of Pikp-1 and Pikp-2 are required for receptor activation

It has previously been shown that the cell death response mediated by Pik-1/Pik-2 NLR pair upon perception of AVR-Pik effectors can be recapitulated using transient expression in leaves of the model plant *Nicotiana benthamiana* (Maqbool et al., 2015, De la Concepcion et al., 2018, De la Concepcion et al., 2019). To achieve this, the proteins are overexpressed using *Agrobacterium tumefaciens* mediated transformation (from now on referred to as agroinfiltration). The presence of cell death is usually recorded between 3-5 dpi (days post infiltration). Upon cell death, plant cells accumulate phenolic compounds that fluoresce under UV light, allowing for a clear distinction between healthy and collapsed tissue. The intensity of the cell death can be scored visually, according to a scale originally developed in (Maqbool et al., 2015).

To investigate the roles and requirements for the individual domains of Pikp-1 (CC, HMA, NB-ARC and LRR) and Pikp-2 (CC, NB-ARC and LRR) in triggering cell death, I set out to transiently express each of these in *N. benthamiana*. Sequences encoding these domains (as defined as in (Maqbool et al., 2015)) were PCR-amplified and assembled into expression constructs using Golden Gate cloning (Engler et al., 2008). Each domain was placed under the control the viral constitutive promoter CaMV35S and tagged at the C-terminus with the HellFire tag (6xHis + 3xFlag (HF), for Pikp-1 domains) or HA tag (for Pikp-2 domains). Full length Pikp-1, Pikp-2 and AVR-PikD constructs for expression were kindly provided by Dr. Juan Carlos de la Concepcion, and were used as described

in (Maqbool et al., 2015). Briefly, the NLRs were cloned and expressed under control of the *mas* (mannopine synthase promoter derived from *A. tumefaciens*) promoter and C-terminally tagged with HF and HA tag (for Pikp-1 and Pikp-2 respectively). Expression of the AVR-PikD effector was driven by the AtUbi10 promoter (ubiquitin promoter derived from Arabidopsis), and the protein was cloned to be expressed with an N-terminal 4xMyc tag.

I found that none of the individual domains of either Pikp-1 or Pikp-2 triggered a cell death response when expressed on their own. Further, I did not observe any cell death response on expression of any of the individual domains in the presence of the corresponding paired NLR and/or effector (**Figure 3.1 A; Figure 3.2 A, B**). Western blot analysis showed that all the proteins accumulated to detectable levels (**Figure 3.1 C**). Subsequently, I set out to look for a minimum functional unit of the Pikp-1/Pikp-2 system that would be able to trigger the cell death response. I systematically truncated Pikp-1 or Pikp-2 at relevant domain boundaries and expressed them alone or in the presence of the corresponding paired NLR and/or effector. For all these combinations I did not observe any cell death responses on expression (**Figure 3.1 B, Figure 3.2 A, B**), despite the proteins accumulating in plant tissues to detectable levels (**Figure 3.1 C**). I only observed a cell death response when full length Pikp-1 and Pikp-2 were co-expressed in the presence of AVR-PikD. These results suggest that the Pikp-1/Pikp-2 pair work together to deliver cell death responses upon perception of the effector, and all domains are required for this cooperation.

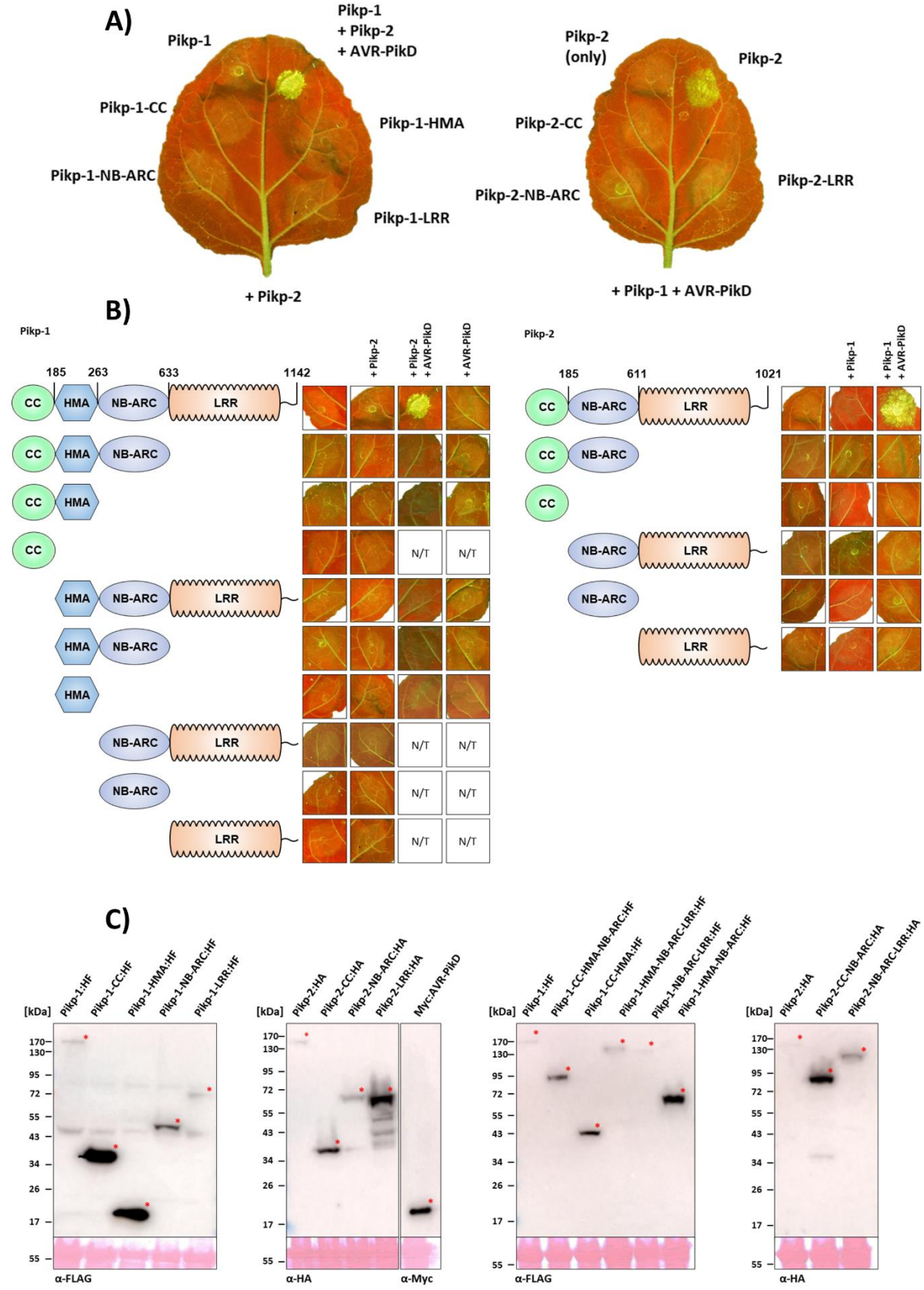

Figure 3.1 All the domains are required for Pikp-1/Pikp-2 system to function.

Indicated proteins were transiently overexpressed via agroinfiltration. Leaf pictures were taken at 5 dpi under the UV light, which allows to visualise the cell death response as green fluorescence. ***A)*** *Representative leaves show that only full length Pikp-1/Pikp-2 can trigger cell death response in presence of the AVR-PikD effector. None of the individual domains of Pikp-1/Pikp-2 tested were able to tigger cell death response.* ***B)*** *Boxes with representative infiltration sites show that none of the truncated variants of Pikp-1 or Pikp-2 tested were able to tigger cell death response. Combinations of constructs without HMA domain were not tested (N/T) in presence of the effector.* ***C)*** *Western blot showing that all the proteins were expressed and accumulated to detectable level.*

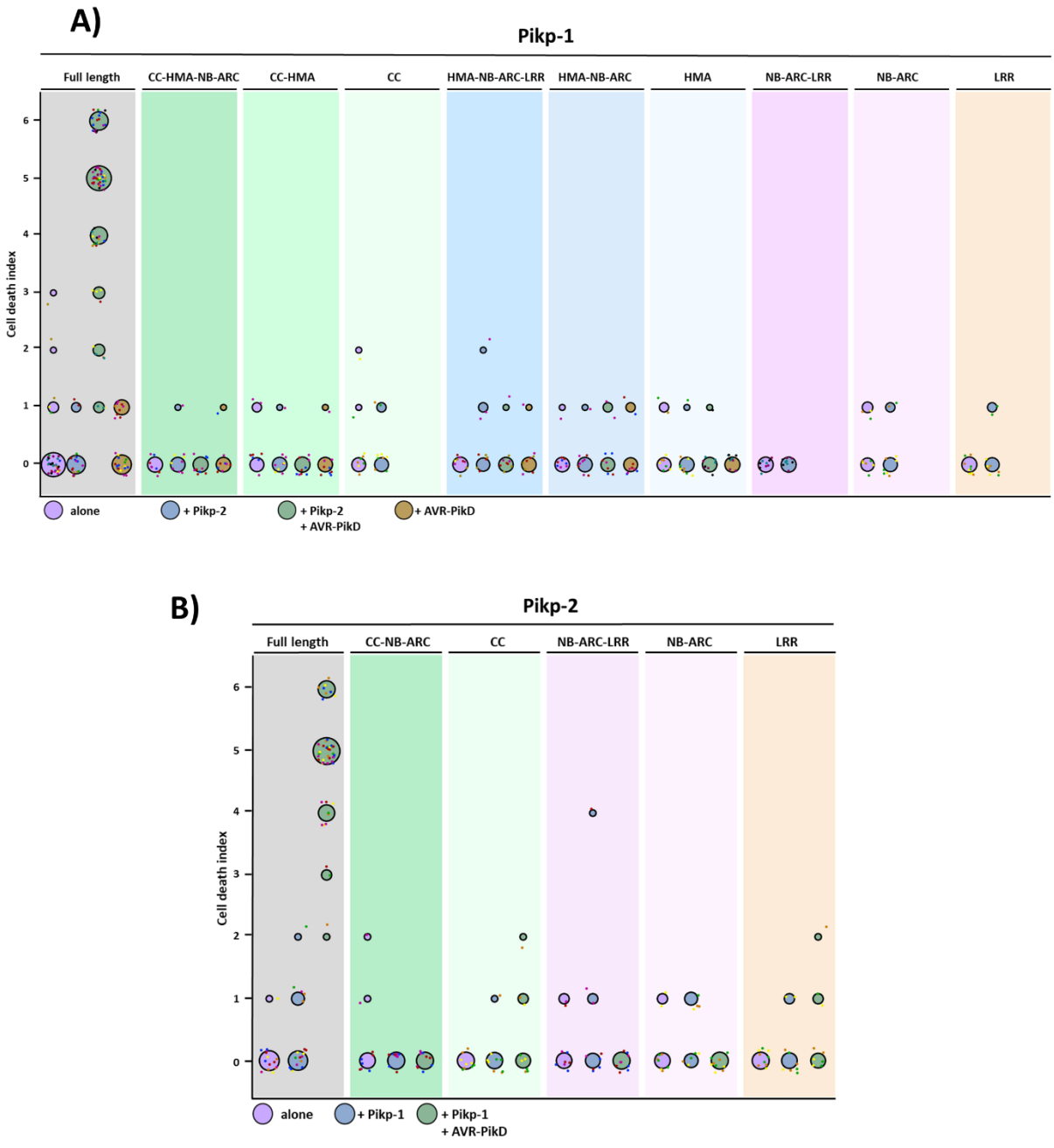

Figure 3.2 All the domains are required for Pikp-1/Pikp-2 system to function.

*Quantification of the cell death assay presented in **Fig 3.1** shown as dot plots, for Pikp-1 **(A)** and Pikp-2 **(B)** respectively. All dots are plotted around the cell death score (size of the circle at given score is proportional to the number of dots within), each dot has a distinct colour corresponding to the biological replicate. Experiments were conducted in 3 biological replicates with at least 2–3 technical replicates.*

3.2.2 Intact P-loop and MHD motifs are required for Pikp-1 and Pikp-2 function

To further characterise the Pikp-1/Pikp-2 system, I set out to investigate the requirements for a functional nucleotide-binding pocket in Pikp-1 and Pikp-2 for receptor activity. To test this, lysine to arginine mutations were introduced into the highly conserved P-loop motif present in nucleotide-binding proteins, generating Pikp-1^{K296R} and Pikp-2^{K217R} variants (constructs were generated and provided by Dr. Josephine Maidment and Dr. Juan Carlos de la Concepcion). These mutations sterically block nucleotide binding, and have previously been shown to impair NLR function (Tameling et al., 2002, Howles et al., 2005, Williams et al., 2011, Bai et al., 2012). The mutants were placed under control of the CaMV35S promoter and tagged with HF tag (Pikp-1 variants) or HA tag (Pikp-2 variants) at the C-terminus. When expressed in *N. benthamiana* via agroinfiltration, neither of these mutants was able to trigger the cell death response, including when expressed in the presence of the paired NLR and the AVR-PikD effector (**Figure 3.3 A, B, C, D**). This reveals that both Pikp-1 and Pikp-2 require an intact P-loop for cell death activity. Expression of all proteins was confirmed by Western Blot (**Figure 3.3 E**). Please note that in previous Western Blots (**Figure 3.1 C**) no observable background bands at relevant heights were detected, therefore the Western Blots presented below are cropped to relevant regions for simplicity and no negative control was included for these experiments.

Another widely conserved motif in nucleotide-binding proteins is the MHD (methionine-histidine-aspartate) motif located in ARC2 region of the NB-ARC NLR domain. This motif is a part of the nucleotide binding pocket, and the histidine is responsible for binding and positioning of β-phosphate of ADP, and the aspartate is involved in coordination binding, and thought to be involved in keeping the receptor in inactive state prior to effector perception (van Ooijen et al., 2008). The MHD motif is classically defined as Met-His-Asp, however the residues comprising this motif in plant NLRs can vary. In Pikp-1/Pikp-2 system, this motif is less conserved, and therefore I will refer to it as the MHD-like motif. In Pikp-1, the MHD-like motif consists of Ile-His-Pro (IHP) residues, while in Pikp-2 it comprises Val-His-Asp (VHD) residues. In many cases this motif is involved in auto-inhibition of NLR and mutation of either histidine or aspartate leads to auto-activity and constitutive cell death in absence of the pathogen perception (de la Fuente van Bentem et al., 2005, van Ooijen et al., 2008, Takken and Goverse, 2012). To investigate the importance of the MHD-like motif for Pikp-1 and Pikp-2 activity, I set out to test how the introduced mutations would affect the proteins'

function. Triple mutants Pikp-1$^{599IHP601\rightarrow AAA}$ and Pikp-2$^{557VHD559\rightarrow AAA}$, and an additional single mutant Pikp-2^{D559V} were provided by Dr. Josephine Maidment and Dr. Juan Carlos de la Concepcion. Overexpression of these genes alone did not result in auto-activity and cell death (**Figure 3.3 A, B, C, D**). To determine whether auto-activity could occur in the presence of the paired NLR, I expressed the mutants in the presence of corresponding MHD-like mutants and intact NLRs, but I did not observe cell death in any of these combinations (**Figure 3.3 A, B, C, D**). Moreover, overexpression of these constructs in the presence of the corresponding wild-type NLR and AVR-PikD effector led to loss-of-function, as no cell death was observed in the assay (**Figure 3.3 A, B, C, D**). All proteins were expressed to detectable levels, as confirmed by western blot analysis (**Figure 3.3 E**). These results demonstrate that wild-type MHD-like motifs are required for both Pikp-1 and Pikp-2 to trigger cell death responses.

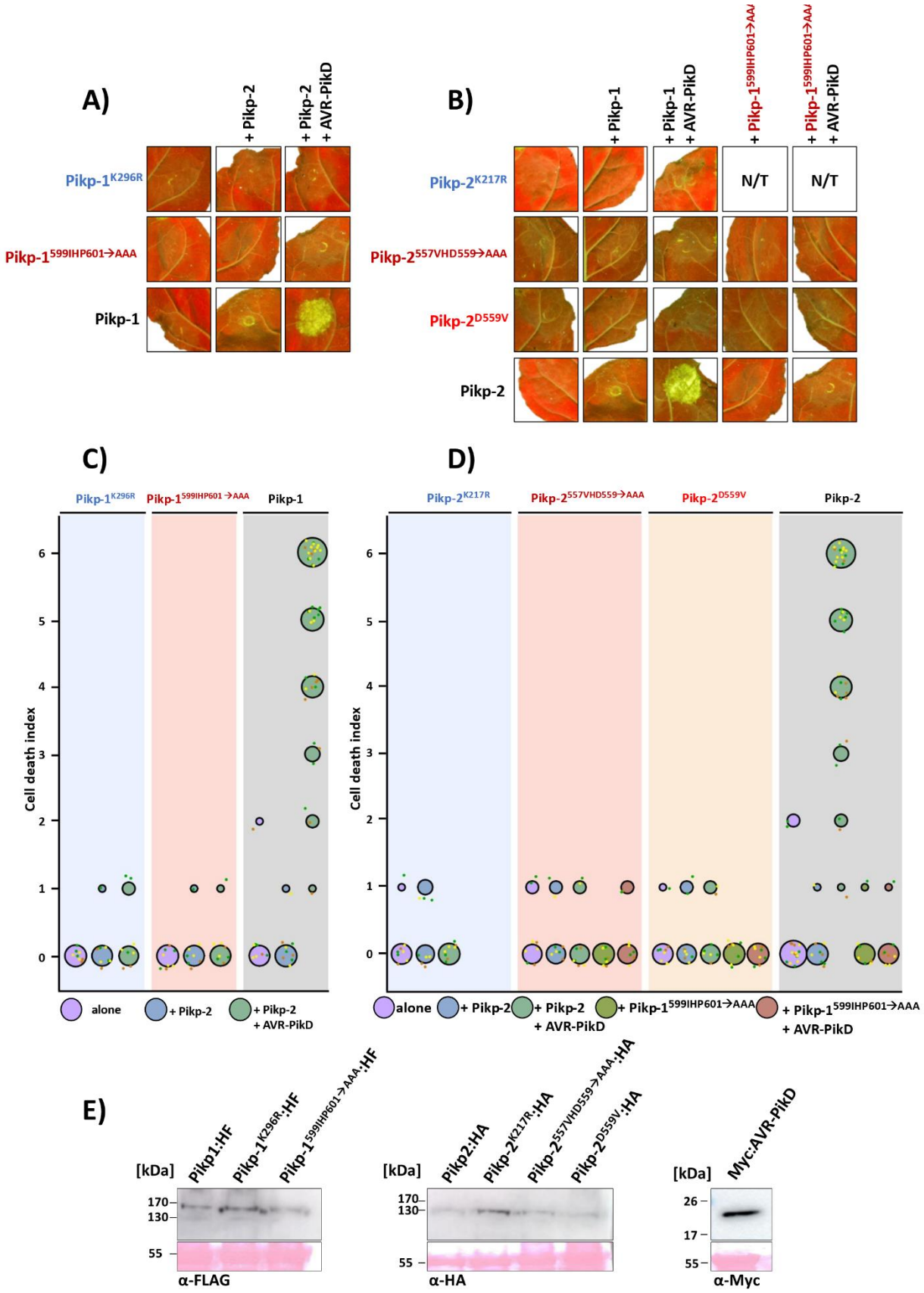

Figure 3.3 Intact P-loop and MHD-like motifs are required for Pikp-1/Pikp-2 to function.

A) *Mutation of P-loop motif in Pikp-1 results in loss of cell death response upon perception of AVR-PikD. Mutation of the MHD-like motif in Pikp-1 does not lead to auto-activity, and results in loss of cell death response upon perception of AVR-PikD.* ***B)*** *Mutation of P-loop motif in Pikp-2 results in loss of cell death response upon perception of AVR-PikD. Mutation of the MHD-like motif in Pikp-2 does not lead to auto-activity, and results in loss of cell death response upon perception of AVR-PikD.* ***C), D)*** *Quantification of the cell death assay presented in* ***A), B)*** *shown as dot plots, for Pikp-1* ***(C)*** *and Pikp-2* ***(D)*** *respectively. All dots are plotted around the cell death score (size of the circle at given score is proportional to the number of dots within), each dot has a distinct colour corresponding to the biological replicate. Experiments were conducted in 3 biological replicates with at least 2–3 technical replicates.* ***E)*** *Western blot showing that all the proteins were expressed and accumulated to detectable level.*

3.2.3 Pikp-1 and Pikp-2 form homo- and hetero-complexes in planta

Paired NLRs can form homo- and hetero-complexes in planta (Cesari et al., 2014b, Huh et al., 2017). I tested whether Pikp-1 and Pikp-2 can also form such complexes using co-immunoprecipitation (co-IP) assays. This was investigated both prior to and upon effector perception. Two differentially tagged Pikp-1 (with FLAG tag and V-5 tag) and Pikp-2 constructs (with FLAG tag and HA tag) were generated under the control of *mas* promoter in the Golden Gate system and expressed in *N. benthamiana* via agroinfiltration in relevant combinations. The barley NLR MLA10 (expressed with a FLAG tag) was used as a negative control for interactions (construct provided by Dr. Hiroaki Adachi, The Sainsbury Laboratory). Following expression, the protein complexes were extracted and immunoprecipitated using α-FLAG resin. All FLAG-tagged NLRs were expressed, and immunoprecipitated as expected (**Figure 3.4 A, B** lower and top panels). Pikp-1:V-5 was pulled down with Pikp-1:FLAG via the α-FLAG resin, but not on co-expression with MLA10:FLAG or when expressed alone (**Figure 3.4 A**). This shows that Pikp-1 associates specifically with itself (Pikp-1:V-5 with Pikp-1:FLAG) and not with another unrelated NLR, or with α-FLAG resin in non-specific manner. Similar results were observed for Pikp-2 (**Figure 3.4 B**). A strong band of Pikp-2:HA was observed only following pull-down with Pikp-2:FLAG, indicating self-association of the protein (Pikp-2:HA with Pikp-2:FLAG). I observed a very faint band of Pikp-2:HA with MLA10:FLAG, however, a similar band can be observed where Pikp-2:HA is expressed alone, indicating possible weak non-specific binding to the resin. This result indicates that Pikp-2 self-associates in a specific manner.

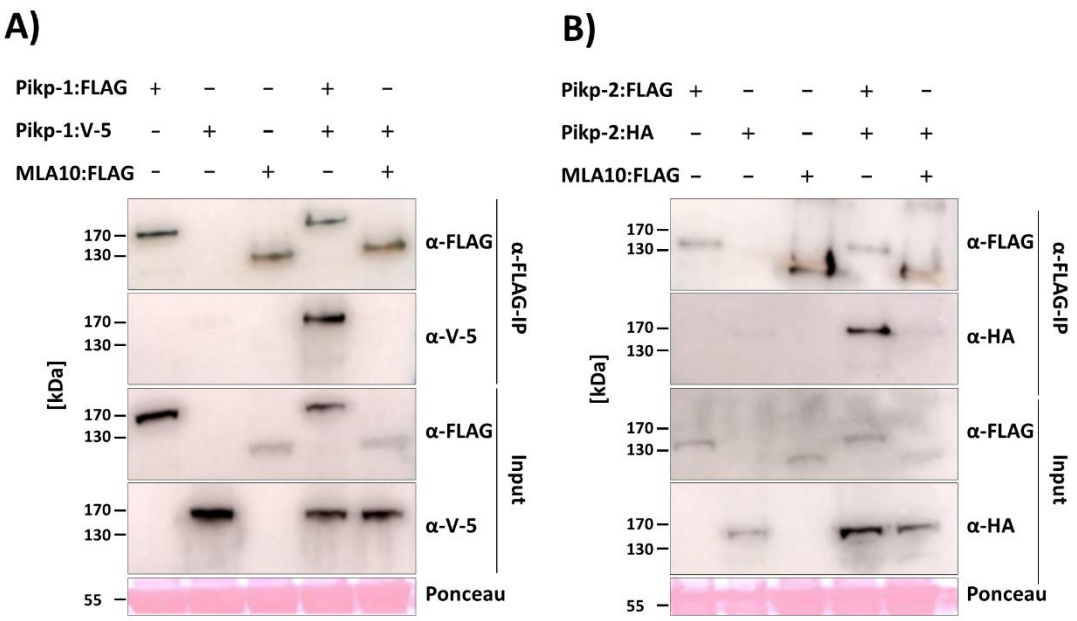

Figure 3.4 Pikp-1 and Pikp-2 associate in homotypic manner.

All the proteins were transiently expressed in N. benthamiana via Agroinfiltration. ***A)*** *Pikp-1:FLAG, Pikp-1:V5 and MLA10:FLAG and* ***B)*** *Pikp-2:FLAG, Pikp-2:HA and MLA10:FLAG were expressed alone or in relevant combinations. Subsequently anti-FLAG immunoprecipitation (αFLAG-IP) was performed, followed by Western Blot detection with relevant antibodies (upper panel). Lower panel (Input) confirms presence of all the proteins in extracts prior to immunoprecipitation. Experiments were repeated at least 3 times with similar results.*

To test whether presence of the AVR-PikD effector might affect the self-association of either Pikp-1 or Pikp-2, I co-expressed these NLRs in presence of AVR-PikD and its non-binding mutant AVR-PikD^{H46E} (Maqbool et al., 2015), which served as a negative control. All the proteins accumulated to detectable levels and FLAG-tagged proteins were pulled down appropriately (**Figure 3.5 A, B**). AVR-PikD coimmunoprecipitated with Pikp-1 as expected, but it did not affect the self-association of the Pikp-1 itself, as strong band of Pikp-1:V-5 could be observed following pull-down with Pikp-1:FLAG (**Figure 3.5 A**, upper panel). No co-precipitation with Pikp-1:FLAG was observed for AVR-PikD^{H46E} mutant. Further, as expected, I did not observe an interaction between AVR-PikD and Pikp-2, and the presence of the effector did not affect self-association of Pikp-2 (**Figure 3.5 B**, upper panel). These results show that presence of AVR-PikD does not affect the self-association of Pikp-1 or Pikp-2, and AVR-PikD associates with the sensor NLR Pikp-1 in planta, but not the helper Pikp-2.

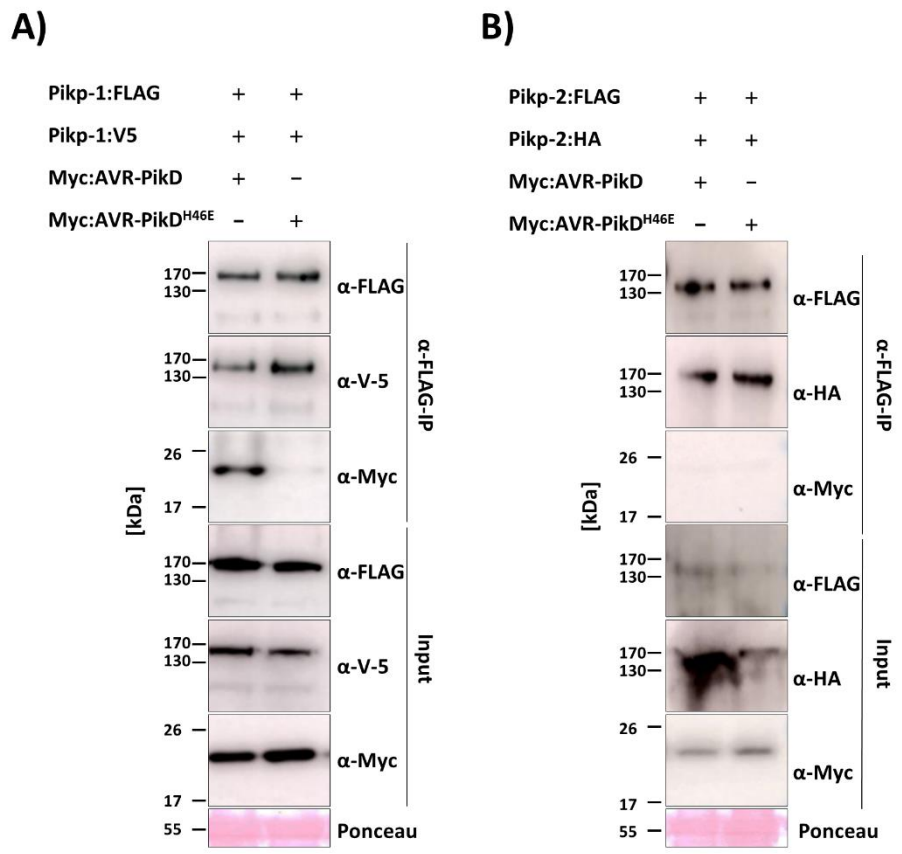

Figure 3.5 Presence of AVR-PikD does not disrupt the homo-association of Pikp-1 and Pikp-2.

All the proteins were transiently expressed in N. benthamiana via Agroinfiltration. ***A)*** *Pikp-1:FLAG, Pikp-1:V5, Myc:AVR-PikD and Myc:AVR-PikD^{H46E} and* ***B)*** *Pikp-2:FLAG, Pikp-2:HA, Myc:AVR-PikD and Myc:AVR-PikD^{H46E} were expressed in relevant combinations. Subsequently anti-FLAG immunoprecipitation (α-FLAG-IP) was performed, followed by Western Blot detection with relevant antibodies (upper panel). Lower panel (Input) confirms presence of all the proteins in extracts prior to immunoprecipitation. Experiments were repeated at least 3 times with similar results.*

Next, I tested whether Pikp-1 and Pikp-2 can associate with each other to form hetero-oligomeric complexes. To test this, I co-expressed these proteins as described above (using MLA10 as a negative control) and performed α-FLAG pull down. Pikp-2:HA co-precipitated specifically with Pikp-1:FLAG, but not with MLA10:FLAG, indicating that Pikp-1 and Pikp-2 can associate (**Figure 3.6 A**).

To investigate how the presence of AVR-PikD may affect formation of hetero-complexes between Pikp-1 and Pikp-2, I co-expressed Pikp-1:V-5, Pikp-2:FLAG and Myc:AVR-PikD and performed α-FLAG pull down (note: in this case Pikp-2:FLAG is immunoprecipitated). As shown in **Figure 3.6 B**, upper panel, all three proteins could be detected following α-FLAG coimmunoprecipitation, indicating that they form tri-partite complex, where Pikp-2 associates with Pikp-1, which at the same time is

bound to the AVR-PikD effector (but not to AVR-PikD^{H46E} mutant). This suggests that signalling competent unit in the Pikp-1/Pikp-2 system most likely comprises each of these three proteins in planta.

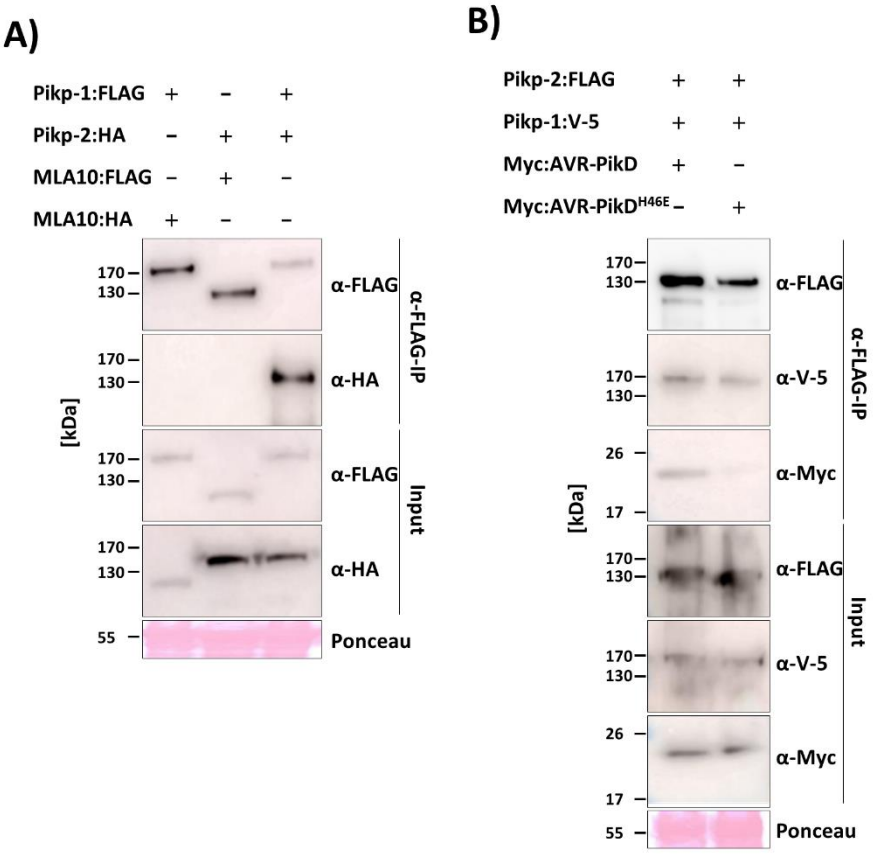

Figure 3.6 Pikp-1 and Pikp-2 hetero-associate prior to and upon recognition of the effector.

All the proteins were transiently expressed in N. benthamiana via Agroinfiltration. ***A)*** *Pikp-1:FLAG, Pikp-2:HA, MLA10:FLAG and MLA10:HA and* ***B)*** *Pikp-2:FLAG, Pikp-1:V5, Myc:AVR-PikD and Myc:AVR-PikD^{H46E} were expressed in relevant combinations. Subsequently anti-FLAG immunoprecipitation (αFLAG-IP) was performed, followed by Western Blot detection with relevant antibodies (upper panel). Lower panel (Input) confirms presence of all the proteins in extracts prior to immunoprecipitation. Experiments were repeated at least 3 times with similar results.*

3.3 Discussion

In this Chapter, I demonstrated that the NLRs Pikp-1 and Pikp-2 form a fine-tuned system that differs from other well characterised paired NLRs to work via a cooperation rather than negative regulation mechanism. All domains of both the sensor and helper NLRs are indispensable for receptor function. Moreover, mutations in well-characterised motifs, P-loop and MHD-like, in either of the proteins, abolished the ability of the receptor complex to trigger the cell death response, suggesting that Pikp-1/Pikp-2 requires functional ADP/ATP exchange system for its activity. Finally, I showed that Pikp-1 and Pikp-2 can associate in homo- and hetero-typic manner, and upon recognition of the AVR-PikD effector, a tri-partite Pikp-1/Pikp-2/AVR-PikD complex is formed.

3.3.1 Roles of individual domain can often be distinguished

The N-terminal domains of specific NLRs have been observed to trigger cell death when overexpressed in planta (Howles et al., 2005, Maekawa et al., 2011, Wang et al., 2015c, Casey et al., 2016, Wroblewski et al., 2018, Lee et al., 2021). However, this activity was not observed for the CC domains of Pikp-1 or Pikp-2. For the CC-domain constructs, all 4 helices predicted to be important for the folding of the protein were included (Bentham et al., 2018, Burdett et al., 2019a). Further, no cell death response was observed upon co-expression of full-length Pikp-1 with the Pikp-2 CC domain (with or without AVR-PikD). This is considered a biologically relevant test for CC domain-mediated cell death in a paired NLR, compared to expression of the CC domains fused to GFP/YFP that proved to be a successful strategy in some cases (Krasileva et al., 2010, Hamel et al., 2016, Baudin et al., 2017). The ability of CC domains to mediate cell death appear to be finely tuned. Studies on the barley NLR MLA10 showed that a single amino acid change in length of the CC domain construct determined the capacity for mediating a cell death response (Casey et al., 2016). Moreover, Pikp-2 possesses the MADA motif that has been linked with the ability to trigger cell death (Adachi et al., 2019a). Further studies are required to identify a Pikp-1 or Pikp-2 CC domain construct that triggers a cell death response.

When considering other NLR domains, the NB-ARC domain from NLR Rx was able to trigger a cell death response upon overexpression (Rairdan and Moffett, 2006). However, the NB domains of Pikp-1 or Pikp-2 did not promote this activity. For the NLR RPS5 it was shown that CC-NB-ARC construct could mediate cell death on overexpression (Ade et al., 2007). This result suggests that the LRR domain is involved in auto-inhibition of this NLR (Qi et al., 2012, Qi et al., 2018). However, corresponding constructs from Pikp-1 and Pikp-2 did not show this activity, neither on their own nor when expressed with the effector. Moreover, when lacking the LRR domain of either Pikp-1 or

Pikp-2, the entire complex lost the ability to initiate a cell death response on perception of the effector.

Altogether, these results show that all the domains are indispensable for the cooperation and function of the Pikp-1/Pikp-2 receptor complex. It also highlights the necessity for additional studies to understand the molecular mechanistic basis of Pikp-1/Pikp-2 activation, and the function of diverse genetically linked NLRs more generally.

3.3.2 Different NLRs have different requirements for intact nucleotide-binding motifs

An intact P-loop motif has been shown to be necessary for many NLRs reported to work as singletons (Dinesh-Kumar et al., 2000, Bai et al., 2012), but it is not always required for paired or NLRs part of extended networks (Cesari et al., 2014b, Williams et al., 2014, Wu et al., 2017). In other genetically linked pairs, RGA5/RGA4 and RRS1/RPS4, only the helper NLR protein requires intact P-loop for the activity, whereas it is redundant for the function of the sensor. For the CC_R-type helper NLRs, ADR1 and NRG1, which work downstream of several other NLRs (not genetically linked) (Castel et al., 2019), an intact P-loop motif was not required (Bonardi et al., 2011, Wu et al., 2019), but it was required for NLRs responsible for pathogen recognition. The requirement of Pikp-1/Pikp-2 for an intact P-loop is similar to the Solanaceous NRC network, where NRC proteins work downstream of other NLRs and both components require this motif for their function (Wu et al., 2017). The requirement for intact P-loop motif in both Pikp-1 and Pikp-2 may provide an additional layer of regulation of the system. Mutations in the P-loop might prevent appropriate protein folding by affecting ADP binding, and ADP/ATP exchange could be more important for perception of the effector by this system, possibly determined by the position of the integrated HMA domain between CC and NB-ARC domains.

Residues of the MHD motif are involved in binding ADP, which stabilises the inactive state of NLR (Steele et al., 2019, Wang et al., 2019b, Ma et al., 2020, Martin et al., 2020). Mutation of this motif can lead to auto-activity of the protein, observable as constitutive cell death response in the absence of the effector (Roberts et al., 2013). This motif is less conserved in Pikp-1 (IHP) although largely conserved in Pikp-2 (VHD). Interestingly, mutations in these sequences did not result in auto-activation of Pikp-1 or Pikp-2, and the proteins were not able to respond to the presence of the AVR-PikD effector. In both RGA5 and RGA4, the MHD-like motif is also less conserved, and comprises residues Leu-His-His (LHH) in RGA5 and Thr-Tyr-Gly (TYG) in RGA4. The presence of Glycine (G) in the third position of the MHD-like motif was shown to be responsible for auto-activity of RGA4 (Cesari et al., 2014b). Introducing mutations into MHD-like motif of RGA5 did not abolish its ability to repress RGA4. In the ZAR1 structure, the MHD residues stabilise the ADP-bound

inactive state of protein, but they do not participate in the binding of dATP in an active state. The Cryo-EM structure of the TIR-NLR RPP1 revealed that in the active state the MHD motif binds ADP (Ma et al., 2020), but RPP1 displays an ATPase activity. It is possible that hydrolysis of ATP may play a role in Pikp-1/2 system, and therefore intact nucleotide-binding pocket is required for both proteins. It is also possible that mutation of MHD-like motif in Pikp-1 and Pikp-2 results in a loss of function rather than auto-activity, probably because these mutations do not support the protein conformation required to translate effector perception into cell death.

3.3.3 Oligomerisation is common feature for NLRs

Plant NLRs can form both homo- and hetero-oligomeric complexes. Tomato Prf, maize Rp1-D21 and Arabidopsis RPM1 and RPS5 NLRs have been shown to self-associate both prior to and after effector recognition (Ade et al., 2007, Gutierrez et al., 2010, Ntoukakis et al., 2014, Wang et al., 2015a, El Kasmi et al., 2017). The tobacco TIR-NLR N shows effector-induced oligomerisation (Mestre and Baulcombe, 2006). For some receptors, their N-terminal domains have been shown to oligomerise, inferring that these NLRs require homotypic interactions for their function. Self-association of TIR domains were shown for several NLRs, including L6 (Bernoux et al., 2011), RPP1 (Schreiber et al., 2016) and SNC1 (Zhang et al., 2017a). For CC domains, the self-oligomerisation has been shown in several cases, including MLA10 (Maekawa et al., 2011), Sr33, Sr50 (Casey et al., 2016) and ZAR1 (Baudin et al., 2017). The Cryo-EM structure of ZAR1 showed oligomerisation into a pentameric structure called the “resistosome” on activation (Wang et al., 2019a). In the inactive state, ZAR1 remains in the complex with pseudokinase RKS1 in 1:1 ratio. Binding of $PBL2^{UMP}$ (decoy kinase uridylylated by AvrAC effector) by the RKS1 leads to conformational changes within the single unit of ZAR1:RKS1 complex and allows formation of the oligomer. A similar mechanism may operate in the Pikp system, where Pikp-1 remains associated with itself and Pikp-2, and upon the recognition of AVR-PikD, the whole complex undergoes a conformational change to form a signalling competent unit composed of three proteins. However, how many monomers of each NLR are involved in formation of such a complex remains unknown. In context of other genetically linked NLRs, in the RGA5/RGA4 pair both proteins can associate in a homo- and hetero-typic manner and this association is not disrupted by perception of the effector. For the paired TIR-NLRs RRS1 and RPS4, only the RRS1 is able to form homotypic complexes, whereas RPS4 can self-associate only in the presence of RRS1. At present, multiple models are possible for the activated Pikp-1/Pikp-2 complex, including a Pikp-1/Pikp-2 dimer, multiple copies of the dimer forming higher order complex, or a model where Pikp-1 acts as a scaffold to initiate oligomerisation of Pikp-2 similar to the mechanism seen for NAIP5/NLRC4 (Tenthorey et al., 2017) and NAIP2/NLRC4 (Zhang et al., 2015). To address more accurately the mechanism of cooperation between Pikp-1 and Pikp-2, and how this complex

perceives the effector to initiate cell death, further biochemical and structural studies are required, but this research is beyond the scope of this work presented in this thesis.

4

Biochemical characterisation of PWL2 and OsHIPP43 interaction

4 Biochemical characterisation of PWL2 and OsHIPP43 interaction

4.1 Introduction

Investigating functions and properties of effectors is important to better understand how pathogens overcome the host's immune system and promote disease spread. Analysis of genomic sequences and gene expression patterns have allowed identification of hundreds of effector candidates from fungi and oomycete pathogens (Giraldo and Valent, 2013). However, since majority of fungal effectors share low sequence similarity with each other or with other proteins with established activities (e.g., enzymes), prediction of their function remains challenging. Despite the lack of sequence similarity, proteins can adopt similar domain architectures, and structural conservation can be a better indicator of shared function than sequence. Therefore, determining structures of effectors can contribute to understanding their activities, and can also reveal which residues may be involved in their recognition by plant receptors. Combined with comparative analysis of allelic variants, structure and in planta assays can identify functionally relevant regions of effectors (Zhang et al., 2018). Subsequently, when combined with structural studies of the corresponding NLR or biological target, that knowledge might enable engineering of receptor to extend recognition of the pathogen (De la Concepcion et al., 2019).

PWL2 (Pathogenicity towards Weeping Lovegrass) is an effector from *M. oryzae*, first identified in 1995 using map-based cloning (Sweigard et al., 1995). *M. oryzae* strains containing PWL2 cannot infect weeping lovegrass (*Eragrostis curvula*), but can infect rice and barley. The role of PWL2 in pathogenicity is unknown and might be redundant, as *pwl2* deletion mutants gain virulence on weeping lovegrass but do not show any known fitness cost. A lack of known resistance "in the field" towards PWL2 has resulted in high occurrence of the effector in the pathogen population. Over 95% of rice-infecting isolates tested carry this effector (doctoral thesis of Dr. Vincent Were), making it an interesting target for engineering resistance in crops. Since weeping lovegrass has been shown to be resistant to *M. oryzae* strains carrying PWL2, some advances have been made towards identifying and cloning the gene responsible for resistance, however no results have been published to date. PWL2 occurs in pathogen populations with allelic variation, with two other described variants known as PWL2-2 and PWL2-3 that are not recognised by any known weeping lovegrass or rice accession. Importantly, PWL2-3 allele is present in majority of isolates causing wheat blast that currently poses a major threat to wheat production in Bangladesh and neighbour countries (Islam

et al., 2016). Moreover, wheat blast disease was recently also reported in Zambia, Africa, therefore can be now considered a pandemic pathogen (Tembo et al., 2020, Singh et al., 2021).

This project initially started with attempts to purify and crystallise the PWL2 effector only. While the initial work was being conducted, Dr. Yohann Petit in the Kamoun Lab (The Sainsbury Laboratory) discovered a potential interactor of PWL2 in a Yeast-2-Hybrid screen. This protein turned out to be heavy metal associated isoprenylated plant protein 43 (OsHIPP43), derived from rice. Since many of effector structures to date have been determined in complex with their interactors, I decided to use this opportunity and investigate further the interactions between PWL2 and OsHIPP43. This section will focus on confirming and characterising the interaction between these two proteins in vitro and, furthermore, will investigate whether this interaction might also occur between other reported alleles of PWL2, PWL2-2 and PWL2-3.

4.2 Results

4.2.1 PWL2 can be purified from *E. coli*

The native sequence of secreted proteins (including effectors) contains a signal peptide, characterised by high number of hydrophobic residues, which decreases the solubility and stability of the protein. Moreover, signal peptide is usually cleaved from the protein upon secretion, and does not perform any other biological function. Therefore, for in vitro studies, it is common to express and purify proteins without the signal peptide (here I predicted the signal peptide sequence using SignalP 5.0 software (http://www.cbs.dtu.dk/services/SignalP/)). The desired nucleotide sequence, encoding $PWL2^{22-145}$ was PCR-amplified using a DNA construct provided by Dr. Vincent Were (The Sainsbury Laboratory) as a template, and cloned into the pOPIN-F vector by In-Fusion cloning system (see Material and Methods, **p. 53**).

The pOPIN-F:PWL2 construct produces a recombinant protein with an N-terminal hexa-histidine (6xHis) tag that enables purification by immobilised metal affinity chromatography (IMAC), most commonly on immobilised Nickel resin (Ni-NTA). The 6xHis tag is followed by 3C protease cleavage site (LEVLQGP) that allows removal of the tag after initial purification steps. 3C protease is derived from human rhinovirus (HRV) and cleaves between glutamine (Q) and glycine (G) (of the sequence above), therefore leaves a Gly-Pro “scar” on the final protein product.

An initial expression screen showed that *E. coli* BL21-AI (Arabinose Inducible) strain was the best system for expression of PWL2 (data not shown). Competent cells were transformed with the pOPIN-F:PWL2 construct, grown in LB medium and expression was induced with 0.2% arabinose. The cells were harvested by centrifugation (10 min, 7500 x g), suspended in lysis buffer, and lysed by sonication. To clarify the lysate and obtain the soluble fraction, the sample was subjected to another centrifugation (45 min, 45000 x g).

To purify the protein of interest, the clarified lysate was loaded onto an ÄKTAxpress system, where it was subjected to IMAC, directly followed by size-exclusion chromatography (SEC). Using SEC, we can separate the proteins based on their shape and size. The injected sample of interest flows through the column filled with resin composed of cross-linked agarose and dextran matrix. This matrix forms pores of various sizes that can be occupied by smaller molecules. Therefore, larger molecules like proteins (and protein complexes) can travel through the column faster and elute earlier, as they do not occupy the small free spaces between the beads, which would result in their retention in the column. Smaller proteins and molecules can fill the pores of the beads, what results in their longer retention in the resin and overall later elution from the column.

The presence of the protein before and after purification steps was inspected by sodium dodecyl sulphate polyacrylamide gel electrophoresis (SDS-PAGE). A 6xHis:PWL2 band could be seen in Whole Cell and Soluble fractions, even though the protein was significantly diluted and contaminated by other bacterial proteins (**Figure 4.1 A**), indicating that the protein was expressed and soluble. Subjecting the lysate to IMAC resulted in concentration of the protein of interest, as it could be seen eluting in subsequent SEC between 180-280 ml not as a single peak, but as a trailing trace, indicating potential low affinity between the protein and the resin of the SEC column. Samples collected from across the trace were also run on a gel, confirming the presence of the protein, as the band of expected size (17.9 kDa) was visible on the gel after Coomasie staining (**Figure 4.1 A**). To remove the 6xHis tag from the PWL2, samples containing the protein were pooled together and incubated overnight with the 3C protease at 4°C. SDS-PAGE analysis of the protein confirmed the successful tag removal, as the slightly lower band could be observed, comparing to the sample before cleavage (**Figure 4.1 B**). To separate the cleaved 6xHis tag and the 6xHis-tagged 3C protease from the PWL2, the sample was run through an IMAC column, where 6xHis tag, 3C protease and uncleaved PWL2 should bind to the resin, allowing the protein of interest to flow through the column. Since there is a possibility that untagged protein retains some affinity to the IMAC resin, the column was washed with the lysis buffer (containing 20 mM imidazole and higher NaCl concentration than the SEC buffer) and the Wash fractions were collected. Indeed, PWL2 seems to moderately bind to the column and none of the protein could be seen in Flow Through fractions. Part of the protein was detected in the Wash fractions, but also a significant part of PWL2 was retained on the column and eluted only with high imidazole, along with 3C protease and other contaminants (**Figure 4.1 B**). Recovering the protein from the IMAC elution fraction would require a buffer exchange and subsequent repetition of downstream purification steps and therefore extending the entire purification process. Such extended protein manipulation may lead to protein degradation. I estimated that combined Wash fractions contained enough protein for downstream analysis and proceeded with them only. To recover higher amount of PWL2 from the IMAC purification in the future, extended washing step is required. This can be achieved through increased volume or time of washing in the current condition, or optimisation the washing buffer towards higher imidazole content.

The Wash fractions containing PWL2 were subjected to a second SEC, to separate them further from contaminants, but also to exchange the buffer (See section **2.3.1**, **p. 56**) that would be more suitable for downstream analysis. SDS-PAGE analysis of the fractions from the elution peak showed that PWL2 was purified to a satisfactory level, with only few contaminants that might be a result of

protein instability (**Figure 4.1 C**). To obtain the final sample, I combined the samples with best protein-of-interest:contamination ratio (represented by lanes 2-7 on the gel (**Figure 4.1 C**)).

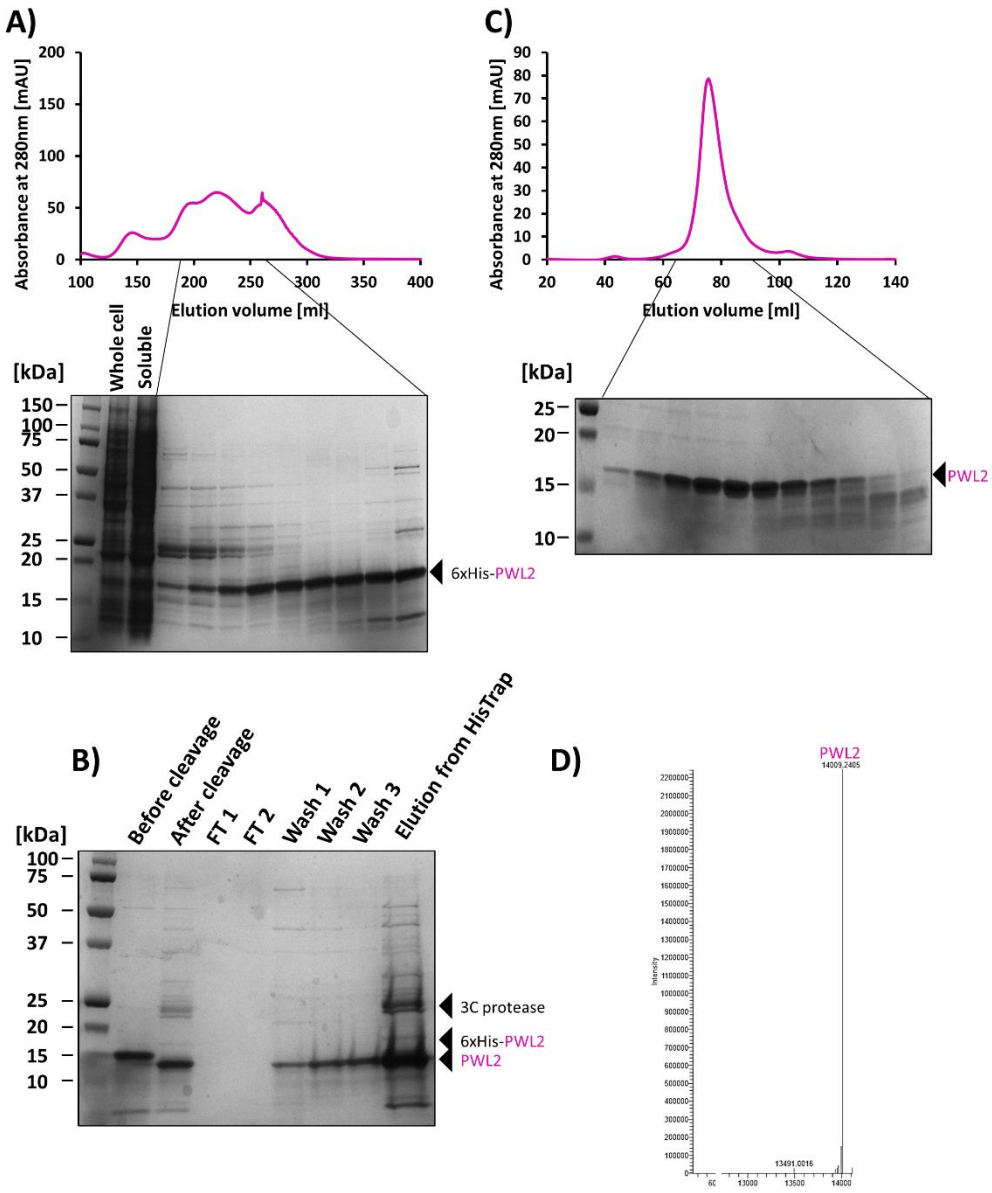

Figure 4.1 PWL2 can be purified from *E. coli.*

A) *SDS-PAGE gel showing Whole Cell and Soluble fractions from E. coli expressing pOPIN-F:PWL2. Further lanes show fractions corresponding to the indicated fragment of SEC trace.* ***B)*** *SDS-PAGE gel showing fractions before and after cleavage of the tag, and subsequent steps of manual purification.* ***C)*** *SDS-PAGE gel showing fractions from final SEC.* ***D)*** *Intact mass spectrometry analysis of the purified sample. The detected mass (14009.24 Da) exactly matches predicted monoisotopic mass of PWL2 (14009.26 Da).*

To confirm the protein identity, the sample was given to TSL Proteomics Team, where it was analysed by intact mass spectrometry and subjected for trypsin digest and peptide mapping. The intact MS result showed a major peak at 14009.24 Da, precisely matching the predicted mass of PWL2 (14009.26 Da) (**Figure 4.1 D**). This was further confirmed by 100% coverage of the protein sequence by the peptide mapping experiment.

4.2.2 Circular dichroism spectroscopy suggests PWL2 has low percentage of secondary structure features

To enable biochemical and biophysical analysis of a protein in vitro, it is important that at the end of the purification process the protein is properly folded and maintains appropriate secondary structure. Analysis of PWL2 sequence by the PSIPRED software suggests that this protein could be mainly formed by loop regions, as majority of the sequence is designated as "coils" (e.g., Tyr-32 to Arg-42, Gly-56 to Tyr-81 and Gly-91 to His-113) (**Figure 4.3 A**). Moreover, homology search with PHYRE2 server failed to detect any potential secondary structures or conserved protein folds. To detect the presence of secondary structures in protein, techniques like circular dichroism (CD) can be used. CD is a spectroscopic technique used to detect and characterise (to certain degree) the secondary structures of proteins and other structural features of optically active chiral molecules. Such molecules can differentially absorb right and left circularly polarised light. By measuring these differences in absorption at specific wavelengths in the UV range (typically 180-260 nm), we can draw conclusions about protein secondary structure content. Certain structures give a characteristic spectrum. α-helices show a positive peak at 192 nm and two negative peaks at 208 nm and 222 nm, while β-sheets are characterised by a positive peak between 195-200 nm and a negative peak around 215-219 nm. A large negative peak around 195-200 nm is characteristic for random coils (**Figure 4.2**) (Wei et al., 2014, Micsonai et al., 2015). Apart from recognising certain features of the obtained spectra by hand, this can be submitted for deconvolution by software, such as BeStSel (Micsonai et al., 2021). Since the final SEC buffer contains chloride ions and HEPES- two molecules that strongly absorb in far UV, the purified PWL2 was exchanged into phosphate buffer (10 mM potassium phosphate, pH 7.5) by overnight dialysis prior to the experiment. The final result from the CD analysis was obtained by subtracting the "blank" measurement (buffer only) from the protein containing sample, and subsequently converting the millidegrees to mean residue molar ellipticity (MRME), to correct for protein concentration.

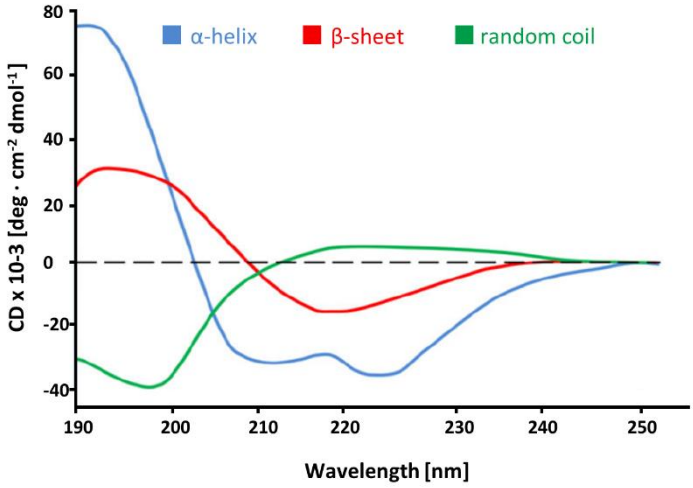

Figure 4.2 Typical CD spectra of basic secondary structures of polypeptide chains.

Adapted from (Wei et al., 2014).

The CD spectrum of PWL2 shows a large negative peak between 197-202 nm, suggesting low percentage of secondary structures or that the majority of the protein might be disordered (**Figure 4.3 B**). However, the spectrum does not reach a positive value in a wide range (205-250 nm), which suggests that some secondary features can be present in the PWL2 structure. Further analysis with BeStSel software confirmed these estimations and suggested that helices and sheets constitute 24.6% and 11.7% of the structure, respectively, whereas Turns and "Other" possible structures would make up to 63.6% of the structure. These results are in agreement with previously reported attempts of purification and characterisation of one of the alleles of PWL2, where Schneider and colleagues suggested that misfolding of the protein might be a mechanism of recognition escape by the pathogen (Schneider et al., 2010). However, since we know that this PWL2 allele can be recognised by certain plant accessions, I considered other explanations. I hypothesised that this protein might simply be misfolded as a result of the heterologous expression system or might be unstructured in solution, and only becomes properly folded upon binding to its target. As the potential target for this effector was identified at that time, I investigated the latter idea.

A)

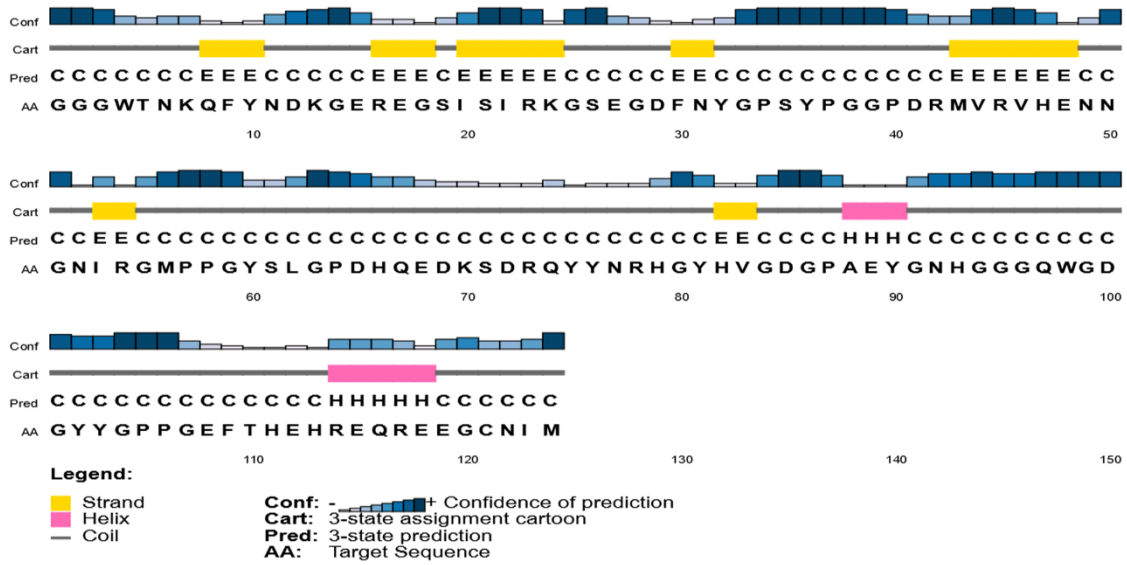

B)

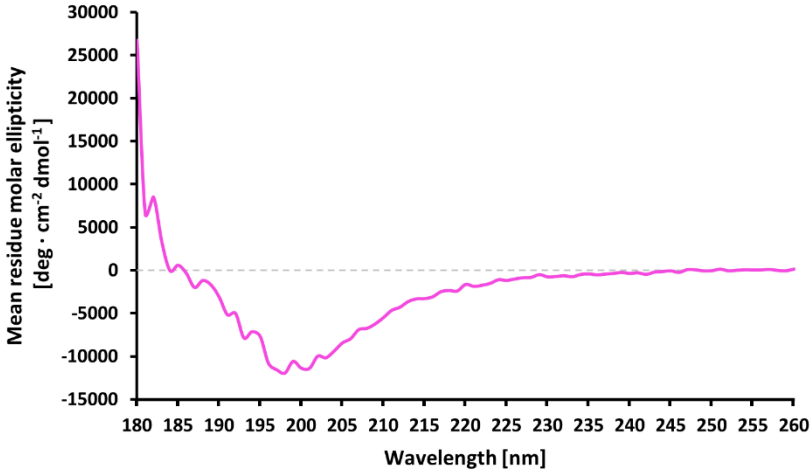

Figure 4.3 PWL2 has low percentage of secondary structures.

A) *Secondary structure features prediction with PSIPRED. Analysis shows low percentage of predicted secondary structures.* ***B)*** *CD spectrum of PWL2. Analysis of the spectrum suggests that PWL2 has low percentage of secondary structures or might be partially unstructured in solution.*

4.2.3 Yeast-2-Hybrid screen identifies a potential interactor for PWL2

The following experiment was designed and conducted by Dr. Yohann Petit and Dr. Thorsten Langner in The Sainsbury Laboratory. They designed and built two libraries of genetic constructs: one composed of *M. oryzae* effectors and one with HMA-containing proteins from rice. Both libraries were published and deposited online (Petit-Houdenot et al., 2020), and the constructs are available upon request. Subsequently they screened these libraries against each other in Yeast-2-Hybrid screen, looking for potential interactions. One potential candidate for interactor for PWL2 emerged from this screen, initially designated as Os01g0507700 (**Figure 4.4**). When searched in NCBI database, this accession revealed a protein called Heavy metal associated Isoprenylated Plant Protein 20 (HIPP20)- an HMA-containing protein found initially in a rice cultivar Nipponbare. However, when I retrieved this protein's sequence and searched it against an available database of partially characterized HPPs and HIPPs published by (de Abreu-Neto et al., 2013), I found out that it has been described as OsHIPP43, and can be found in The Rice Genome Annotation Project designated as LOC_Os01g32330. To remain consistent with published literature, I decided to follow the latter naming system, and name the new protein of interest as OsHIPP43.

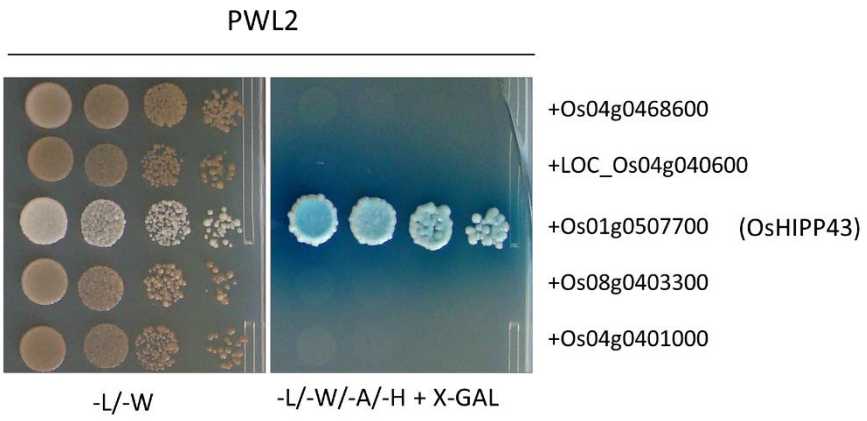

Figure 4.4 PWL2 interacts with OsHIPP43 in Y2H.

Yeast-2-Hybrid screen identified OsHIPP43 as potential interactor for PWL2. Blue colonies on selective medium (–L/-W/-A/-H + X-GAL) indicates positive interaction between the two tested proteins. Experiment conducted by Dr. Y. Petit.

4.2.4 OsHIPP43 can be purified from *E. coli*

Full length OsHIPP43 consists of 151 amino acids, with the HMA domain initially identified as sequence between Met-37 to Ala-90, according to a BLAST search. This domain was included in the truncated construct tested in Y2H screen, which spanned the sequence Arg-26 to Thr-99. To increase the probability of obtaining stable and soluble protein for in vitro work (and at the same time to enable the HMA integration into full length receptor background, described in detail in the next Chapter), I defined boundaries of this HMA domain based on comparison with the Pikm-1-HMA, for which a crystal structure is available. Sequence alignment with Clustal OMEGA software of full length OsHIPP43 (**Figure 4.5 A**) (or the shorter fragment of OsHIPP43 used in Y2H (**Figure 4.5 B**)) with the Pikm-1-HMA did not give a consensus answer and showed different alignments, depending on the length of the sequence in query. To resolve this, I defined the boundaries for this construct based on crystal structures of other HMA domains and used the structure prediction software PHYRE2 (Kelley et al., 2015). When submitted as the full sequence, PHYRE2 predicted OsHIPP43 as an HMA-domain containing protein, and built a model based on the Pikm-1-HMA domain (automatically detected). The result showed that the sequence aligned was two amino acids longer than used in Y2H screen (Arg-26 to Thr-101) (**Figure 4.5 C**). Therefore, I decided to use these boundaries for cloning and further analysis. Henceforth, for simplicity, OsHIPP43-HMA$^{26\text{-}101}$ construct in any work described, will be referred to as OsHIPP43, unless stated otherwise.

The sequence described above was PCR-amplified (using a construct provided by Dr. Yohann Petit as a template) and cloned into pOPIN-M vector via In-Fusion cloning system. pOPIN-M, apart from adding the 6xHis tag to the protein of interest, adds a maltose binding protein (MBP) tag, that promotes solubility and can be used for affinity chromatography. The 6xHis+MBP tag can be cleaved by 3C protease, leaving the same Gly-Pro “scar” on the final protein product as for pOPIN-F. The developed construct was transformed into competent *E. coli* SHuffle strain that has been previously successfully used by other members of the Lab to produce HMA proteins. After the expression and harvesting the cells, initial purification steps were identical to those described for PWL2.

The MBP tag is relatively large (42 kDa) and is known for its solubility properties, hence it can significantly boost the expression of the protein of interest. This can be seen in the gel for 6xHis-MBP-OsHIPP43 (**Figure 4.6 A**). A large band of around 50 kDa can be seen in Whole Cell and Soluble fractions, and can be further seen as a main protein eluting from the SEC column (**Figure 4.6 A**). The indicated fractions were combined, and the tag was cleaved with 3C protease.

A)

```
CLUSTAL O(1.2.4) multiple sequence alignment

OsHIPP43_full_length      MGVLDSLSDMCSLTETKEALKLRKKRPLQTVNIKVKMDCEGCERRVKNAVKSMRGVTSVA  60
Pikm-1-HMA                ------------------------GGEMQKIVFKIPMVDDKSRTKAMSLVASTVGVHSVA  36
                                                  :*.: :*: *  : .. :. . * *  ** ***

OsHIPP43_full_length      VNPKQSRCTVTGYVEASKVLERVKSTGKAAEMWPYVPYTMTTYPYVGGAYDKKAPAGFVR  120
Pikm-1-HMA                IAGDLR--------------DQVVVVGDGI----------DSINLVSALRKKVGPAMFLE  72
                          :  .                ::*  .*..           :   *..  .* .** *:.

OsHIPP43_full_length      GNPAAMADPSAPEVRYMTMFSDENVDSCSIM       151
Pikm-1-HMA                VSQVKE-D-----------------------       79
                           . .   *
```

B)

```
CLUSTAL O(1.2.4) multiple sequence alignment

OsHIPP43-HMA_from_Y2H     -RPLQTVNIKVKMDCEGCERRVKNAVKSMRGVTSVAVNPKQ------------------- 40
Pikm-1-HMA                GGEMQKIVFKIPMVDDKSRTKAMSLVASTVGVHSVAIAGDLRDQVVVVGDGIDSINLVSA 60
                             :*.: :*: *  : .. :. . * *  ** ***:  .

OsHIPP43-HMA_from_Y2H     --SRCTVTGYVEASKVLERVKSTGKAAEMWPYVPYT 74
Pikm-1-HMA                LRKKVGPAMFLEVSQVKED----------------- 79
                            .:   : ::*.*:* *
```

C)

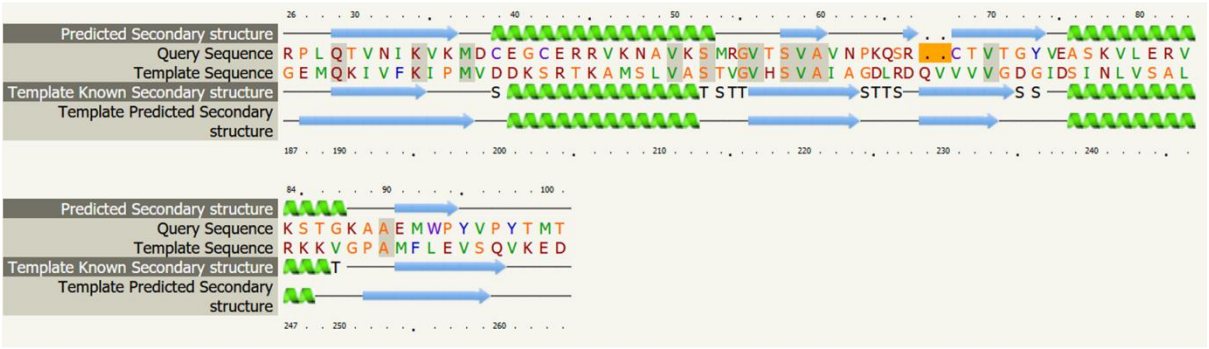

Figure 4.5 Sequence alignment of OsHIPP43 and Pikm-1-HMA.

Sequence alignment of full length OsHIPP43 ***(A)*** *and OsHIPP43-HMA (from Y2H screen)* ***(B)*** *with Pikm-1-HMA with CLUSTAL OMEGA reveals no significant similarities between the aligned proteins and does not lead to defining the ultimate boundaries for OsHIPP43-HMA to be studied in vitro.* ***C)*** *Analysis of OsHIPP43 sequence by PHYRE2. The software detected the HMA motif and built a homology model on template of Pikm-1-HMA. Sequence alignment with the template suggested including two more residues in the structure, when compared with the fragment used in Y2H screen.*

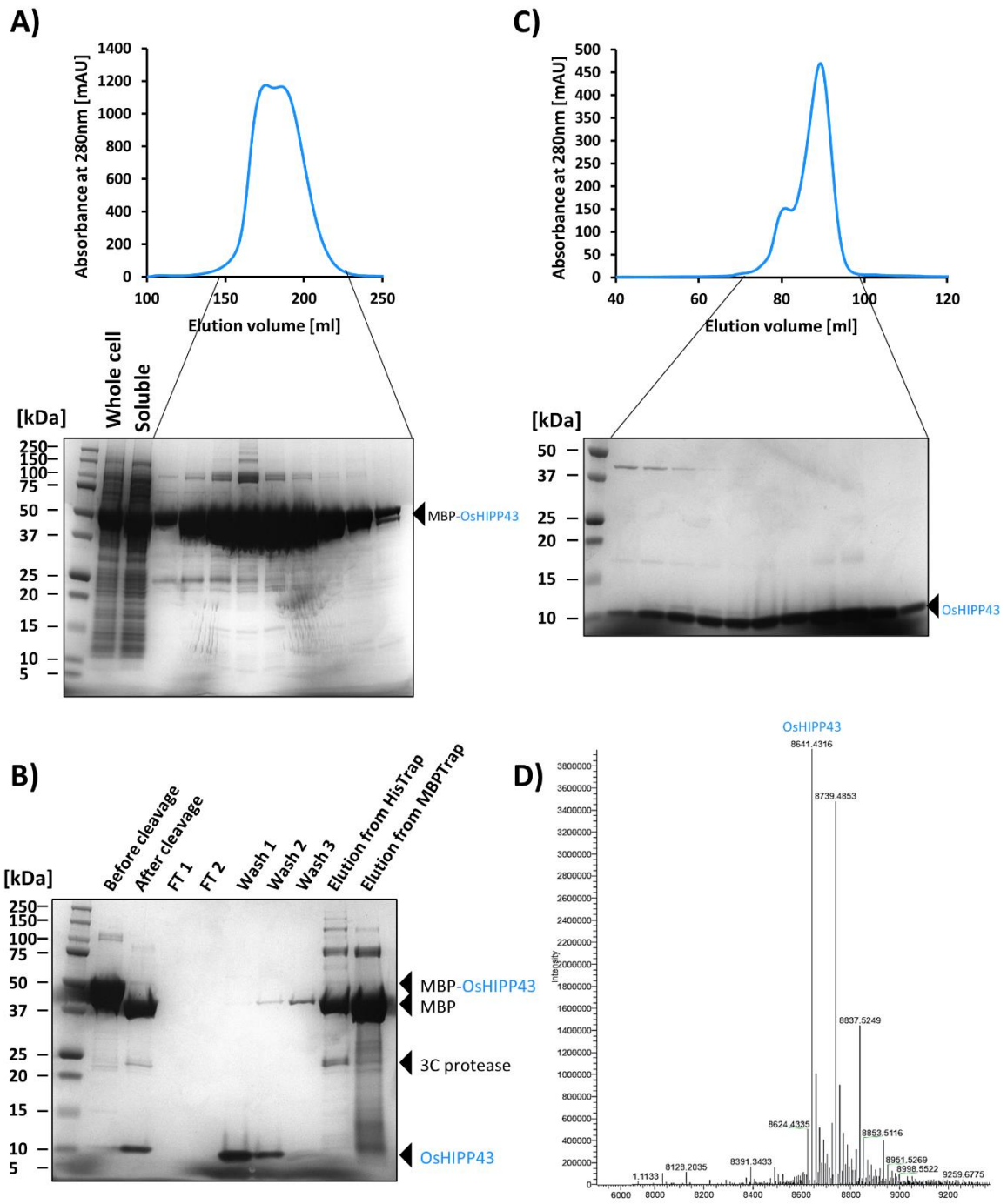

Figure 4.6 OsHIPP43 can be purified from *E. coli.*

A) *SDS-PAGE gel showing Whole Cell and Soluble fractions from E. coli expressing pOPIN-M:OsHIPP43. Further lanes show fractions corresponding to the indicated fragment of SEC trace.* ***B)*** *SDS-PAGE gel showing fractions before and after cleavage of the tag, and subsequent steps of manual purification.* ***C)*** *SDS-PAGE gel showing fractions from final SEC.* ***D)*** *Intact mass spectrometry analysis of the purified sample. The detected (8641.43 Da) mass almost exactly matches predicted monoisotopic mass of OsHIPP43 (8642.45 Da).*

To remove the cleaved tag, the solution was passed through MBPTrap and HisTrap columns in tandem. The MPBTrap column allows to remove the majority of the MBP tag from the sample. The adjacent IMAC column removes the 6xHis-tagged 3C protease and other contaminations with high affinity to that resin, but also any remaining 6xHis-MBP tag. Similar to PWL2, OsHIPP43 also weakly binds to the IMAC column, and was eluted with the low imidazole buffer in the Wash fractions (**Figure 4.6 B**). The sample containing protein of interest was further subjected to size-exclusion chromatography (SEC) and yielded a protein of satisfactory yield and purity for further analysis (**Figure 4.6 C**).

The identity of the protein was confirmed by Mass Spectrometry, where the major peak of 8641.43 Da could be observed, which matches almost exactly the predicted mass of OsHIPP43 (8642.45 Da) (**Figure 4.6 D**) (experiment conducted by Dr. Jan Sklenar).

4.2.5 Circular dichroism spectrum of OsHIPP43 displays features of a folded protein

The CD spectrum of OsHIPP43 indicates that the protein is well folded, and displays features of both α-helices and β-sheets (**Figure 4.7**). The main negative peak between 205-210 nm and slight drop around 220 nm indicate presence of helices, whereas major positive peak at 190-195 nm is very likely a contribution of β-sheets. Interestingly, despite having clear characteristics of spectrum of a folded protein, analysis with the BeStSel software suggested combined helices and β-sheets contribute only to 38% of the protein structure.

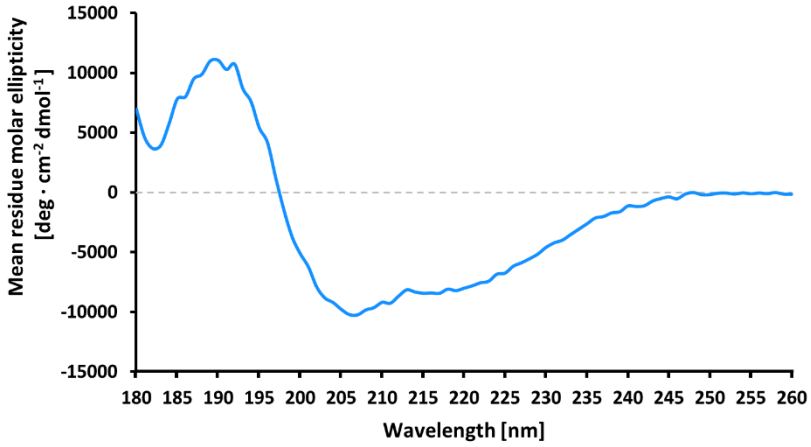

Figure 4.7. CD spectrum of OsHIPP43 suggests that the protein is well ordered.

CD analysis OsHIPP43. The obtained spectrum displays features of α-helices and β-sheets, indicating that OsHIPP43 is well ordered.

4.2.6 PWL2 and OsHIPP43 interact with nanomolar affinity

Next, I sort to confirm the interaction between the PWL2 and OsHIPP43 in vitro using purified proteins. To qualitatively answer this question, I used analytical size-exclusion chromatography. This technique functions on the same basis as the preparative SEC described in section **4.2.1, p. 91**. Based on this principle, complex formation between two proteins can be investigated using a column of a higher resolution. When two (or more) proteins form a complex, they form a single unit of a higher molecular mass (that by default should be also larger in size) than the individual monomers. Such complex will likely behave as a larger molecule, and will elute from the column faster (observed as shift of the elution peak to the left) than the single components. The elution of the proteins can be monitored by measuring the absorbance at 280 nm and the elution profiles from single runs can be plotted and compared. OsHIPP43 alone elutes from the column around 15.9 ml, whereas PWL2 elutes at approximately 13 ml, as indicated by the chromatography peaks (**Figure 4.8 A**). When these proteins were combined in an equimolar ratio, a clear shift of the peak to the left could be observed, when compared with single OsHIPP43 run. Additionally, in the OsHIPP43+PWL2 sample, no small peak was observed at 15.9 ml elution volume, indicating that the entirety of OsHIPP43 was in complex with PWL2. The SDS-PAGE analysis shows the presence of both proteins coeluting at the volume of 13.5 ml, which confirms the complex formation (**Figure 4.8 B**). Interestingly, when compared with PWL2 alone, the elution peak of the complex shifted to the right, suggesting formation of a smaller molecule. This is counterintuitive, as one would usually expect that the complex formed between two proteins should be bigger than its individual units (**Figure 4.8 A**). One possible explanation for this is that PWL2 alone can self-associate, and therefore elutes as a bigger complex (dimer of PWL2 would have a mass of approx. 28 kDa, whereas in complex with OsHIPP43 it would be ca. 22 kDa). However, we have no direct evidence to support this hypothesis and additional experiments, like Size-exclusion Chromatography coupled with Multi Angle Light Scattering (SEC-MALS), would have to be conducted to investigate this phenomenon. As a negative control, I tested whether OsHIPP43 would interact with the *M. oryzae* effector- AVR-PikD (the purified protein was provided by Dr. Juan Carlos de la Concepcion). As can be observed (**Figure 4.8 C**, upper panel), a sample containing OsHIPP43 and AVR-PikD elutes as two distinct peaks. One at 15.9 ml, characteristic for OsHIPP43, and another peak at around 17.8 ml, representing AVR-PikD. Fractions from the peaks were further analysed by SDS-PAGE. This shows a clear distinction between the two proteins, indicating that they do not form a complex in vitro (**Figure 4.8 C**, lower panel). Very weak bands from OsHIPP43 can be seen on the gel apparently coeluting with AVR-PikD, suggesting a very weak interaction. However, a very small peak can be also observed at this elution volume when OsHIPP43 was run alone, indicating that this is not indicative of potential interaction.

Interestingly, AVR-PikD (11.8 kDa), despite being a larger protein, as indicated on a gel, elutes later than OsHIPP43 (8.5 kDa). One possible explanation for this is that AVR-PikD interacts with the resin of the chromatography column in an unspecific manner, probably via hydrophobic interactions. This elution pattern is in agreement with published data on this effector, and therefore does not raise concerns about potential disorder of AVR-PikD (disordered protein can display properties of small molecules and have higher retention time). Another possible explanation might be that OsHIPP43 behaves as a homodimer in solution (17 kDa), however, similarly to PWL2, we do not have any direct evidence for this.

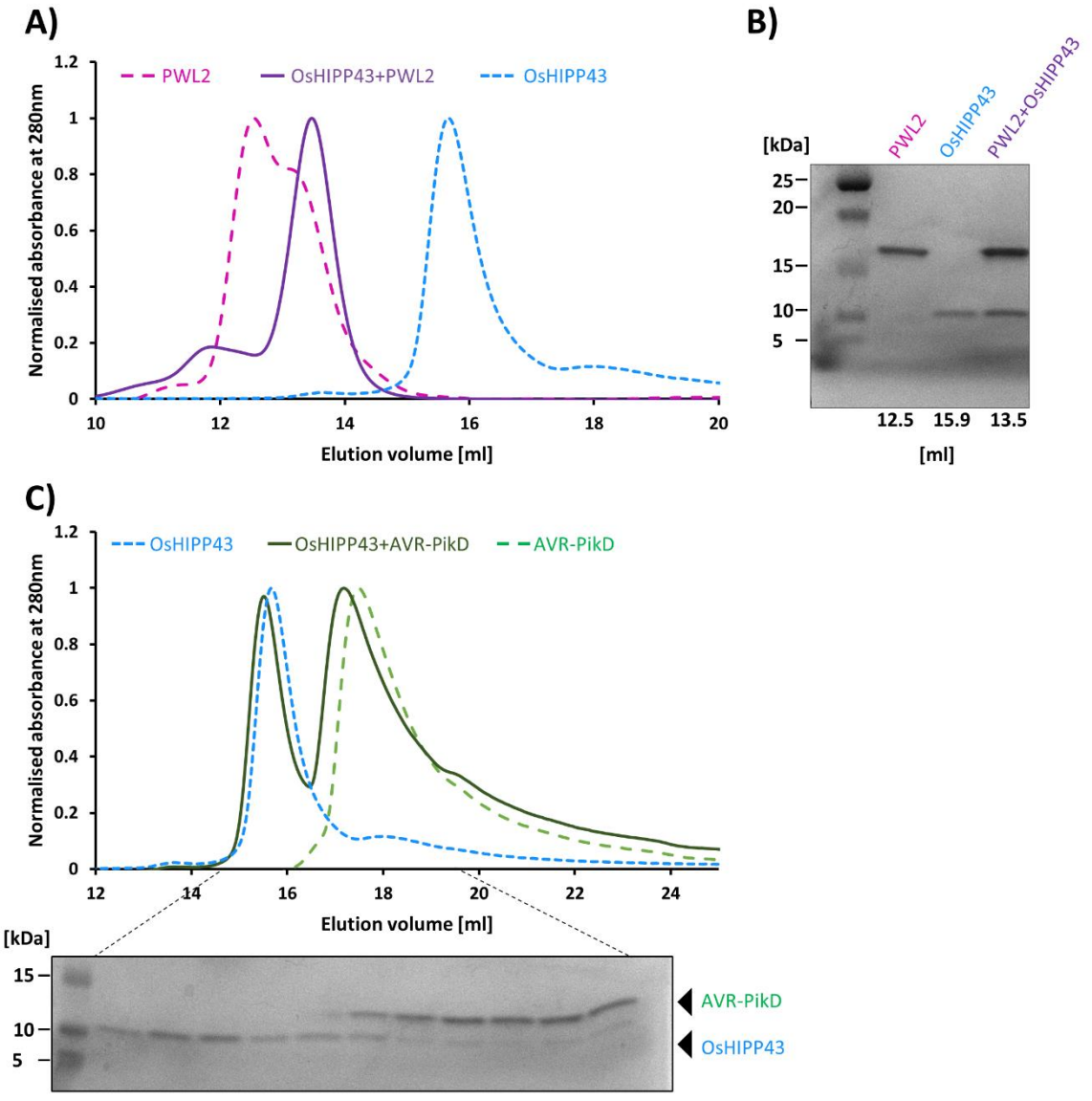

Figure 4.8 OsHIPP43 interacts with PWL2, but not with AVR-PikD in vitro.

Size-exclusion chromatography traces of analysed proteins and protein complexes. ***A)*** *PWL2+OsHIPP43 sample displays clear shift of the elution peak to the left, when compared to the OsHIPP43 sample alone, indicating a complex formation. PWL2 alone sample elutes sooner than the complex, suggesting it might be self-aggregating.* ***B)*** *SDS-PAGE gel of showing the proteins eluting*

at the indicated volumes (from individual runs), confirming complex formation (middle line). ***C)*** *Mixed OsHIPP43+AVR-PikD elute as two distinct peaks that correspond to individually run OsHIPP43 and AVR-PikD, indicating that they do not interact and form a complex in vitro.*

Analytical size-exclusion chromatography is a technique that allows qualitative detection of protein-protein interaction. However, for comparative studies, and to enable any future engineering of interactions, more quantitative approach is needed to characterise the interactions between proteins of interest. Biophysical techniques like surface plasmon resonance (SPR) and isothermal titration calorimetry (ITC) can be used to measure the strength of interactions between two molecules. ITC is a technique based on measuring the heat exchanged (either absorbed or produced) upon binding between two molecules. The amount of heat exchanged by the system is measured as amount of energy that is required to be delivered in order to restore the temperature of the experimental cell (where the binding occurs) to the temperature of the reference cell, and is output as function of energy delivered over time (µcal/s). Hence, the isotherm of exothermic reactions (releasing heat), will occur as a series of negative peaks, as the energy required to restore the equilibrium is negative (to decrease the temperature of the experimental cell). ITC is a powerful tool that allows measuring several parameters and thermodynamic properties of the studied process, like equilibrium constant (K), enthalpy (ΔH), entropy (ΔS), and Gibbs energy.

PWL2 was placed in the experimental cell at concentration of 20 µM and the OsHIPP43 in the syringe at concentration of 300 µM. OsHIPP43 was injected into PWL2 solution in 18 2 µl aliquots, in 150s intervals and the heat change was monitored over time. The negative peaks of the isotherm indicate that the reaction was exothermic (**Figure 4.9,** upper panel). The results obtained in triplicates were analysed using the AFFINImeter software (Pineiro et al., 2019). This programme allows to integrate raw ITC data and obtain desired kinetic parameters of the reaction. Data integration by this software includes (but is not limited to) noise removal, baseline correction, calculation of uncertainty for each datapoint of equilibrium isotherm, global fitting of replicates within the experiment, calculation of association constant K_a and calculation of molar enthalpy change ΔH and stoichiometry N. Importantly, this software also corrects for the heat of dilution, which might have an effect of potential of monomer/dimer equilibrium shift upon concentration change (dilution of the sample upon injection to the cell). These data are obtained from the saturated part of the isotherm, where no more heterocomplexes are formed upon injections.

Fitting the obtained data and further analysis by the AFFINImeter showed that interaction between PWL2 and OsHIPP43 has association constant K_a = 6.7154x10^6 M^{-1}. To obtain the dissociation constant K_d that is a standard parameter reported for biophysical interactions, we need to perform

simple mathematical operation $K_d = 1/K_a$. That means that binding strength between PWL2 and OsHIPP43 is at nanomolar range, and has the K_d = 191 nM (**Figure 4.9**). Such strong binding indicates that this interaction is specific, and encourages further investigation, especially in context of future in planta work. Remarkably, this reaction has also a relatively high molar enthalpy change ΔH = -67.6 kcal/mol. This might be possibly a result of folding upon binding of PWL2, as previously hypothesised. The experiments above indicate that both proteins, PWL2 and OsHIPP43 can be expressed and purified, therefore are suitable for in vitro studies. Moreover, I showed that they can form a complex in vitro and they interact with nanomolar affinity.

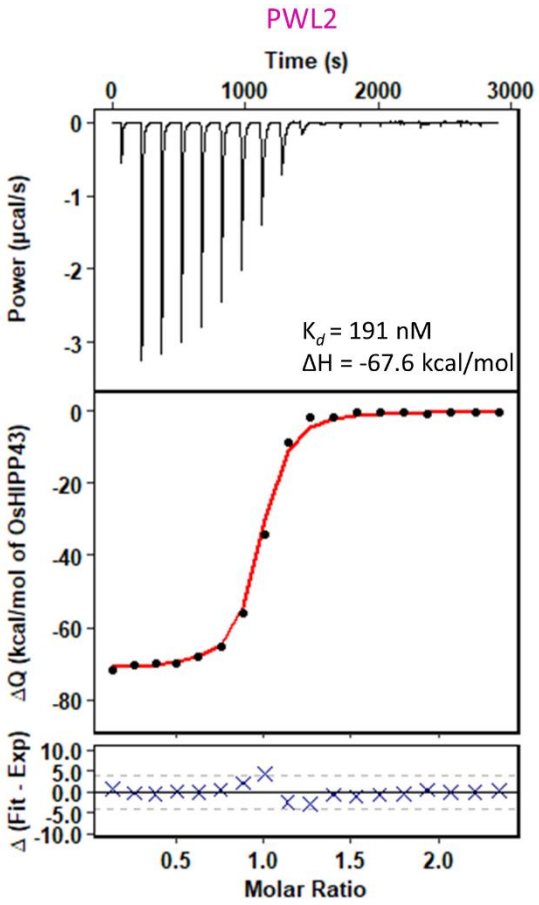

Figure 4.9 PWL2 binds OsHIPP43 with nanomolar affinity.

In vitro binding affinity between PWL2 and OsHIPP43 was measured by ITC. Upper panel- representative isotherm showing heat exchange upon the injection of the HMA into the cell containing the effector. Middle panel- Integrated heats of injection from the technical replicates and global fit to a single site binding model calculated using AFFINImeter. Lower panel- calculated difference between predicted value of measurement (by global fit) and actual measurement.

4.2.7 PWL2-2 and PWL2-3 can be purified from *E. coli*.

The published literature and doctoral thesis of Dr. Vincent Vere shows that other alleles of PWL2 have been identified and reported (Sweigard et al., 1995). These alleles, called PWL2-2 and PWL2-3 are not recognised by any known weeping lovegrass or crop accession. It is interesting, especially in case of PWL2-2, that the recognition specificity is only dependent on single residue polymorphism, Asp90Asn, that seems to be relatively mild, given the nature of these amino acids. Furthermore, PWL2-3 possesses mutations in the same region and in place of 89EDKS92, has a sequence QDQI (for the alignment, see **Figure 4.12 A, p. 110**), and also carries additional Asn32His substitution. Since no resistance gene against these effectors has been cloned, or even resistant plant accessions identified, it is of great interest to investigate this system further. By exploring the potential of these effectors to bind to OsHIPP43 we can investigate the use of this HMA domain as a potential integrated decoy to engineer resistance against pathogens carrying these effectors. If the binding of the HMA is compromised, we can speculate that a homologue of OsHIPP43 might be involved in mediating resistance found in weeping lovegrass and the introduced mutations are in fact selected to disrupt this interaction. To answer this, I set out to purify PWL2-2 and PWL2-3 and measure the potential affinity to OsHIPP43 and compare it with PWL2.

To purify PWL2-2, I used the same strategy that proved successful in purification of PWL2. I amplified by PCR the gene of interest using a DNA construct provided by Dr. Vincent Were as a template. I cloned the desired coding sequence into the pOPIN-F vector and transformed it into competent *E. coli* BL21-AI strain and followed the protocol previously described. Following the IMAC + SEC, an intense band of ca. 16 kDa was observed on the SDS-PAGE gel, indicating that protein of interest was expressed and purified by IMAC successfully (**Figure 4.10 A**). After overnight cleavage with 3C protease, sample was passed through the IMAC column to remove the cleaved tag, the protease, and any additional contaminations. As described previously, PWL2-2 also displayed weak affinity to the IMAC column and needed to be eluted with the Wash buffer containing imidazole at low concentration (**Figure 4.10 B**). A final SEC step resulted in a high yield of protein (**Figure 4.10 C**). However, some contamination was observed on the gel, most likely as an effect of protein degradation, indicated by progressive set of bands below the bands of interest. To obtain the final sample, only samples with the best protein-of-interest:contamination ratio were chosen (lanes 3-7 from the SEC, **Figure 4.10 C**), yielding a sample with satisfactory purity. The identity of the protein was assessed by intact mass spectrometry, that showed the main peak of 14008.25 Da, exactly matching the estimated monoisotopic mass of PWL2-2 (14008.27 Da).

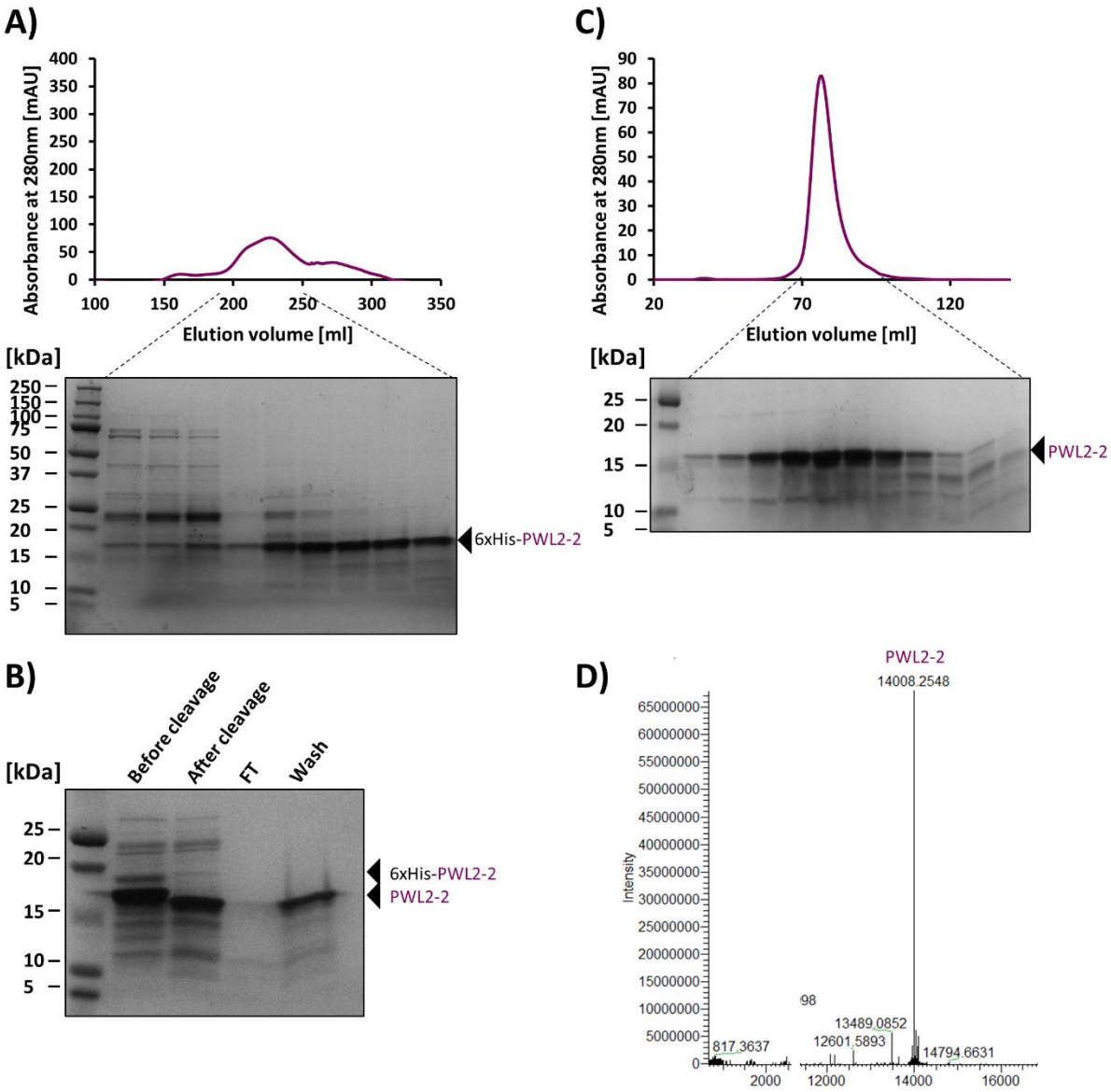

Figure 4.10. PWL2-2 can be purified from *E. coli.*

A) *SDS-PAGE gel showing fractions corresponding to the indicated fragment of SEC trace of PWL2-2 purification.* ***B)*** *SDS-PAGE gel showing fractions before and after cleavage of the tag, and subsequent steps of manual purification.* ***C)*** *SDS-PAGE gel showing fractions from final SEC.* ***D)*** *Intact mass spectrometry analysis of the purified sample. The detected mass (14008.25 Da) exactly matches predicted monoisotopic mass of PWL2-2 (14008.27 Da).*

The assembly of DNA via In-Fusion is a well-established system for cloning new constructs for protein expression. However, creating new acceptor vectors that would allow cloning the protein of interest with a wider variety of tags is laborious and therefore limits the number of available vectors and plasticity of the system. To improve these factors, we moved to the Golden Gate cloning system that simplifies the development of new elements (e.g., genetic constructs carrying tags for protein expression) and hence allows to increase the possibilities and variety of DNA constructs that can be used (Bentham et al., 2021b). This allowed me to introduce the GB1 tag (derived from streptococcal protein G) that has proved to be successful by other members of the Group in boosting the expression of the proteins of interest. The coding sequence of PWL2-3 was PCR-amplified and assembled with N-terminal 6xHis-GB1-3C-cleavage-site into pPGN-C vector using Golden Gate cloning. The obtained construct was transformed into BL21-AI *E. coli* strain and subsequent expression and purification steps were performed as previously described.

After initial IMAC purification followed by SEC, two peaks were observed at elution volume of around 210 ml and 290 ml (data not shown). Fractions across the two peaks were analysed by SDS-PAGE, revealing that PWL2-3 was spread across all of the tested fractions (**Figure 4.11 A**). Such elution profile indicates that the protein might be transiently self-associating or has weak affinity to the resin that slows down its flow through the column. The fractions containing PWL2-3 were pooled together, subjected for overnight 3C cleavage and run through IMAC column as described previously. Interestingly, this allele of PWL2 has weaker affinity to the IMAC resin and the majority of the protein passed through the column and was detected in the Flow Through fraction (**Figure 4.11 B**). The most likely explanation for this change points towards the polymorphic region of PWL2-3 where EDKS residues are changed for QDQI (meaning charged glutamate and lysine that might be contributing to weak binding to the resin, are changed for non-charged glutamines). The fractions containing PWL2-3 were pooled, concentrated and subjected for the second SEC. Interestingly, this time the protein came out as a single peak, and its purity was further assessed by SDS-PAGE (**Figure 4.11 C**). The gel shows a protein of satisfactory yield and purity that is suitable for downstream analysis. The identity of the protein was again assessed by intact mass spectrometry, which showed the main peak of 14188.33 Da, exactly matching the estimated monoisotopic mass of PWL2-3.

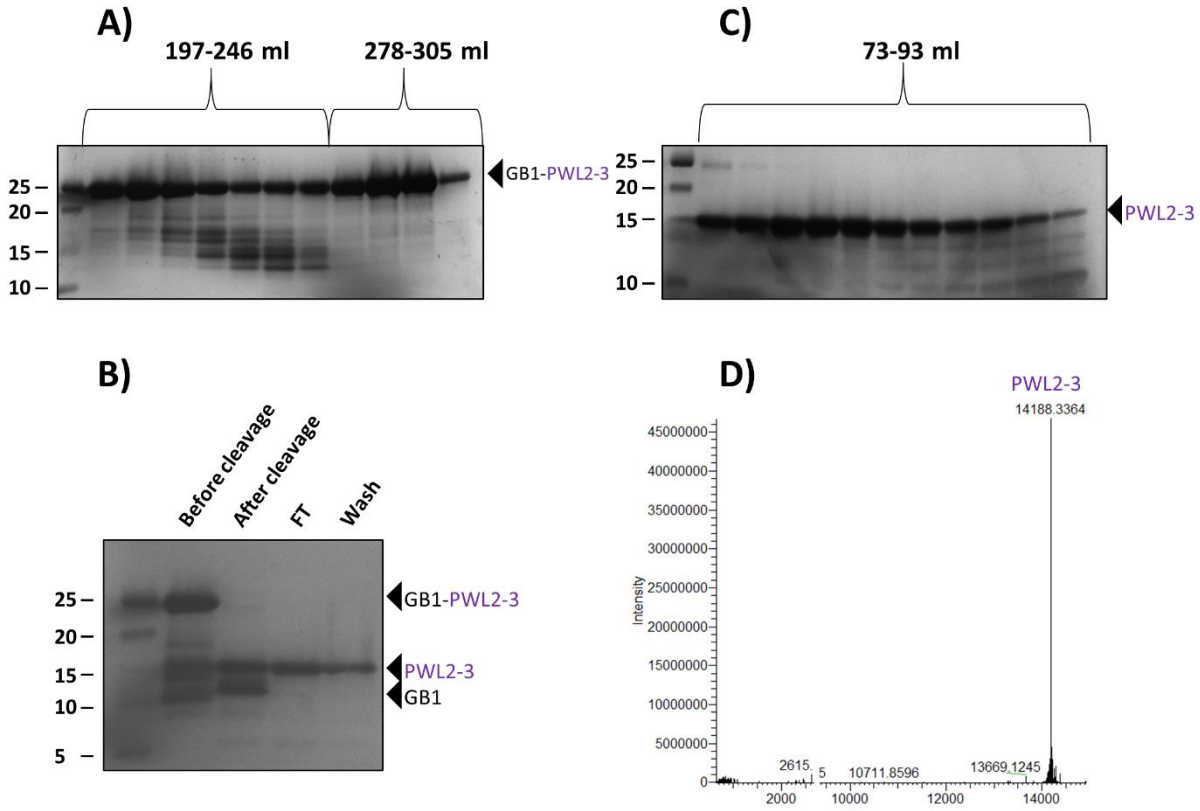

Figure 4.11. PWL2-3 can be purified from *E. coli*.

A) *SDS-PAGE gel showing fractions corresponding to the indicated fragment of elution volume of PWL2-3.* ***B)*** *SDS-PAGE gel showing fractions before and after cleavage of the tag, and subsequent steps of manual purification.* ***C)*** *SDS-PAGE gel showing fractions from final SEC.* ***D)*** *Intact mass spectrometry analysis of the purified sample. The detected mass (14188.33) exactly matches predicted monoisotopic mass of PWL2-3 (14188.33 Da).*

Both PWL2-2 and PWL2-3 were analysed by CD spectroscopy. The CD spectrum obtained showed very similar pattern as previously described for PWL2, indicating that all these proteins have similar folding patterns (**Figure 4.12 B**).

A)

```
PWL2-3  GGGWTHKQFYNDKGEREGSISIRKGSEGDFNYGPSYPGGPDRMVRVHENNGNIRGMPPGY  60
PWL2    GGGWTNKQFYNDKGEREGSISIRKGSEGDFNYGPSYPGGPDRMVRVHENNGNIRGMPPGY  60
PWL2-2  GGGWTNKQFYNDKGEREGSISIRKGSEGDFNYGPSYPGGPDRMVRVHENNGNIRGMPPGY  60
        *****:************************************************************

PWL2-3  SLGPDHQQDQIDRQYYNRHGYHVGDGPAEYGNHGGGQWGDGYYGPPGEFTHEHREQREEG  120
PWL2    SLGPDHQEDKSDRQYYNRHGYHVGDGPAEYGNHGGGQWGDGYYGPPGEFTHEHREQREEG  120
PWL2-2  SLGPDHQENKSDRQYYNRHGYHVGDGPAEYGNHGGGQWGDGYYGPPGEFTHEHREQREEG  120
        ********::: ************************************************

PWL2-3  CNIM        124
PWL2    CNIM        124
PWL2-2  CNIM        124
        ****
```

B)

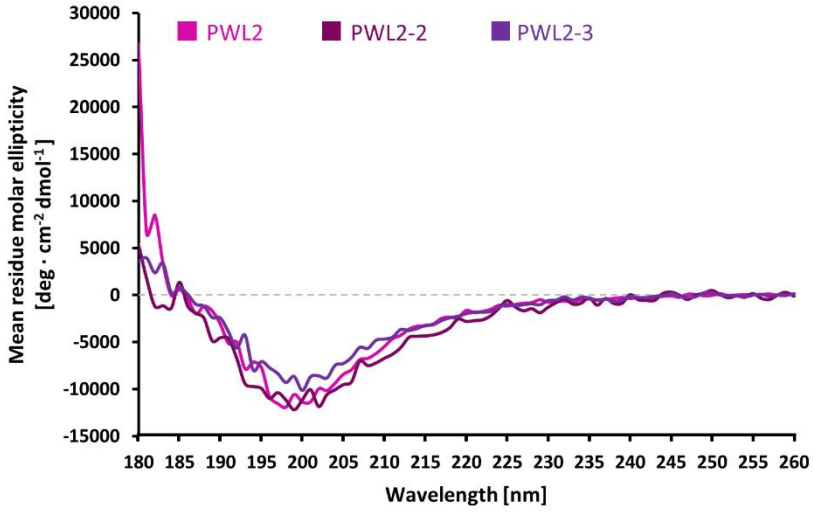

Figure 4.12 Sequence alignment and CD spectra of PWL2 alleles.

A) *Sequence alignment of PWL2 alleles by CLUSTAL OMEGA.* ***B)*** *CD analysis of purified PWL2 alleles. Obtained spectra show that all purified proteins display similar secondary structure features.*

4.2.8 PWL2-2 and PWL2-3 interact with OsHIPP43 with nanomolar affinity

Since PWL2 interaction with OsHIPP43 was successfully measured by ITC, showing that this technique is well suited for this system, I decided to omit the qualitative analysis of PWL2-2 and PWL2-3 interaction with OsHIPP43 by analytical SEC, and directly perform ITC. The experiments were conducted as described previously for PWL2/OsHIPP43 interaction. Analysis of obtained isotherms revealed that both these proteins bind strongly to OsHIPP43, within the nanomolar range: 141 nM and 35 nM for PWL2-2 and PWL2-3 respectively, which is comparable with the binding of PWL2 (191 nM) (**Figure 4.13**). Both these proteins also display high heat exchange upon binding to OsHIPP43 (66.4 kcal/mol and 85.2 kcal/mol for PWL2-2 and PWL2-3, respectively), comparable with the value obtained for PWL2 (67.6 kcal/mol).

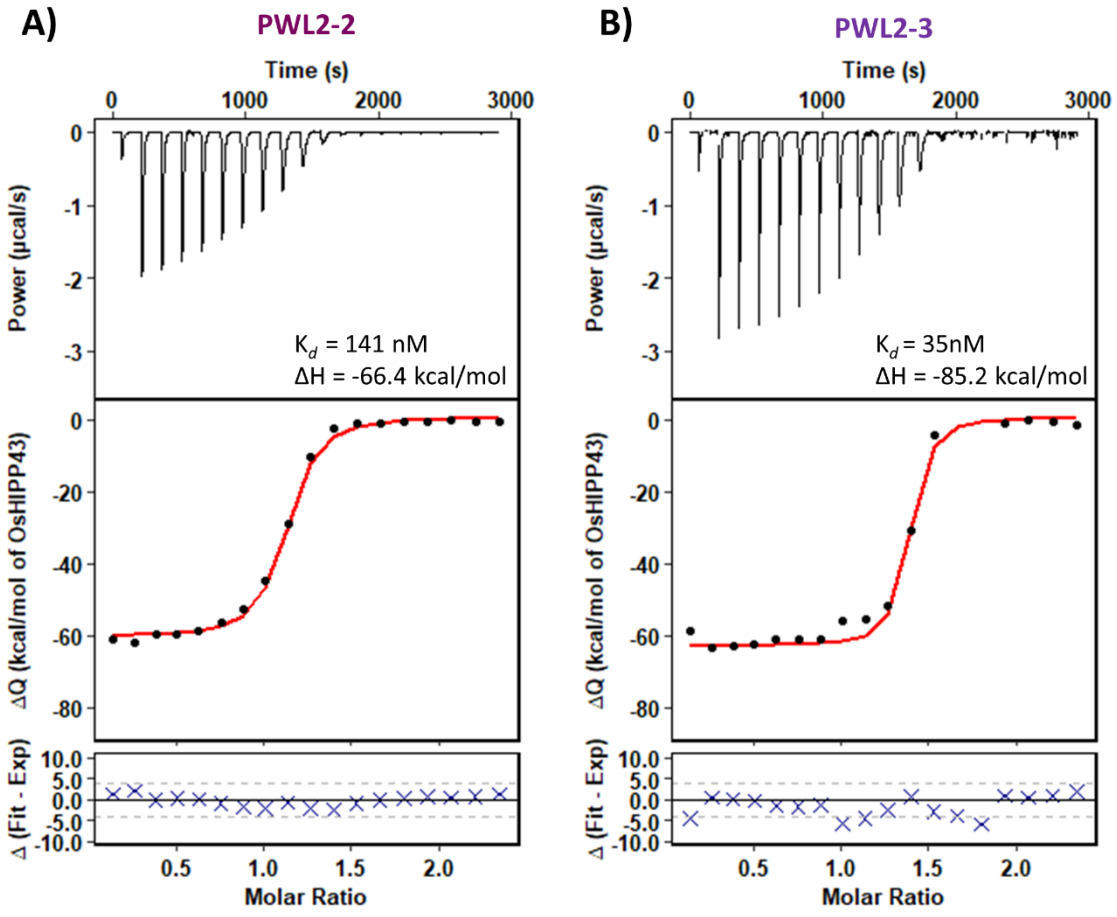

Figure 4.13 PWL2-2 and PWL2-3 bind OsHIPP43 with nanomolar affinity.

In vitro binding affinity between PWL2-2 ***(A)*** *and PWL2-3* ***(B)*** *and OsHIPP43 was measured by ITC. Upper panel- representative isotherm showing heat exchange upon the injection of the HMA into the cell containing the effector. Middle panel- Integrated heats of injection from the technical replicates and global fit to a single site binding model calculated using AFFINImeter. Lower panel- calculated difference between predicted value of measurement (by global fit) and actual measurement.*

4.3 Discussion

In this Chapter, I used biochemical approaches to confirm the interaction between the PWL2 effector from *M. oryzae* and the HMA domain of the rice heavy metal associated isoprenylated plant protein 43 (OsHIPP43), that was initially discovered in Y2H screen by our collaborators. Further, I demonstrated that PWL2 and its alleles, PWL2-2 and PWL2-3, bind to OsHIPP43 with the nanomolar affinity.

4.3.1 PWL2 may be highly unstructured without its interactor

In silico analysis with various software (including PSIPRED and PHYRE2) suggested that PWL2 might have very low percentage of secondary structure, which could be an indication of being unstructured without its binding target or intrinsically disordered. Moreover, analysis with PHYRE2 software did not find any potential homology model, suggesting that either majority of PWL2 is not well folded, or this effector represents entirely new structural features. Subsequent analysis of purified PWL2 with Circular Dichroism Spectroscopy further supported the hypothesis that this protein indeed is does not have high secondary structures content. To confirm that some secondary features are present in the structure, additional experiments could be conducted that measure the folding state of protein while deliberately unfolding it, e.g., by gradual increase of the temperature. These data are in agreement with results reported by (Schneider et al., 2010), who also attempted to purify and characterise one of the PWL2 alleles. The allele they investigated, called PWL2-D, was similar to described in this work PWL2-2, that carries D90N mutation. Additionally, PWL2-D was also carrying Cys142Ser substitution. However, since PWL2 sequence only possesses one cysteine residue, it was unlikely that that mutation was playing a great role in contribution to overall structure stabilisation, as no potential disulphide bridges can be formed. Schneider and colleagues managed to purify and analyse PWL2-D by CD spectroscopy, and reported that this protein seems to be disordered. As this allele is not recognised by any weeping lovegrass accession, they hypothesised that misfolding the effector was a potential mechanism for escaping the recognition, and therefore restoring the pathogenicity of *M. oryzae* towards weeping lovegrass. The discovery of potential interactor for PWL2 allowed me to test this hypothesis. All three alleles described in this work were shown to strongly bind the OsHIPP43, indicating that the mutations introduced into different alleles do not prevent proper folding, and still allow binding to the potential target. The most likely explanation of these observations is that PWL2 is intrinsically disordered and folds properly upon binding to its target. This hypothesis can be further supported by the relatively high heat exchange of the interaction measured by ITC, to which refolding of PWL2 might be contributing.

4.3.2 Natural resistance to PWL2 seems not to be mediated by OsHIPP43

The interaction between effectors and HMA domains has been reported in the literature multiple times (Maqbool et al., 2015, Varden et al., 2019, Oikawa et al., 2020, Maidment et al., 2021, Bentham et al., 2021a). The integrated decoy hypothesis suggests that HMA domain has been integrated independently into NLR backgrounds at least twice during evolution (in Pik alleles and in RGA5, both conferring resistance to *M. oryzae* carrying AVR-Pik and AVR-Pia effectors respectively), by which plants gained potential of direct recognition of the effectors. It has also recently been reported that several alleles of AVR-Pik effectors can bind to HMA-containing protein called OsHIPP19 (Oikawa et al., 2020). A recent study shows that rice HIPPs, including OsHIPP43, show increased expression during infection (Oikawa et al., 2020). However, whether they play a role in immune responses or are highjacked by the pathogen to promote disease remains to be elucidated. It has been shown multiple times that HPPs/HIPPs can be susceptibility factors, and silencing these genes can lead to increased resistance to certain pathogens, not only to fungi, but also to pathogens from across other kingdoms (Zschiesche et al., 2015, Cowan et al., 2018, Radakovic et al., 2018, Oikawa et al., 2020). Therefore, it would not be a great surprise if interaction between one of the rice blast effectors and an HMA-containing plant protein would play a significant biological role in plant-pathogen interaction. The role of OsHIPP43 and its homologs in weeping lovegrass in mediating immunity remains a separate question not investigated in this work. It has been shown (doctoral thesis of Dr. Vincent Were) that PWL2-2 and PWL2-3 alleles are not recognised by the accession of weeping lovegrass that is resistant to *M. oryzae* strain carrying PWL2. As I demonstrated in this Chapter, OsHIPP43 binds all the alleles of PWL2 in vitro with nanomolar affinity. That suggests that this protein might not be involved in mediating the immunity response in planta. It is possible that all alleles of PWL2 retained their ability to bind OsHIPP43, by keeping the relevant interface intact, and they escaped recognition by introducing mutations in the interface that was used by potential plant receptor, which is different to the one binding the HMA.

4.3.3 Different effectors bind HMA-containing proteins with different affinity

The strength of the interaction between PWL2 and OsHIPP43 lays within the upper nanomolar range (ca. 200 nM). This affinity is lower than reported for other *M. oryzae* effectors interacting with HMA domains. AVR-PikD was shown to interact with Pikp-1-HMA at K_d = 31 nM (Maqbool et al., 2015) and at K_d = 4,7 nM with Pikm-1-HMA (De la Concepcion et al., 2018). More interestingly, AVR-Pik effectors are demonstrated to interact with OsHIPP19 with subnanomolar affinity (0.7 nM for AVR-PikD and 0.9 nM for AVR-PikF (Maidment et al., 2021). This suggest that the effectors are evolving higher affinity towards their biological targets than demonstrated by results presented in this Chapter. However, the results reported in the literature were obtained by different method

(SPR) and, although the apparent K_d for two interacting proteins should remain the same when measured with different techniques, comparison of those results should be taken with caution. Interestingly, the affinity measured for other effector/integrated HMA domain pair, AVR-Pia/RGA5-HMA was measured by ITC and reported to be within micromolar range (7.8 µM) (Ortiz et al., 2017). This strength of binding was sufficient to elicit cell death responses in planta upon co-expression of RGA5/RGA4/AVR-Pia in *N. benthamiana* plants, although some interaction between the AVR-Pia and other domains of RGA5 might be contributing to this recognition (Ortiz et al., 2017). It would be interesting to see, whether integration of OsHIPP43-HMA domain into NLR background, like Pikm-1, would result in gaining of recognition of the PWL2 effectors and therefore enable an exciting opportunity to develop a novel recognition specificity towards previously unrecognised effectors.

5

A chimeric Pikm-1 receptor, Pikm-1^{OsHIPP43}, demonstrate novel recognition of the PWL2 effector

5 A chimeric Pikm-1 receptor, Pikm-1^{OsHIPP43}, demonstrates novel recognition of the PWL2 effector

5.1 Introduction

Paired NLRs Pik-1 and Pik-2 confer resistance to *Magnaporthe oryzae* carrying specific AVR-Pik effectors. These receptors and effectors each occur in natural allelic series, where certain Pik variants can only bind and recognize certain alleles of AVR-Pik. The recognition specificity is determined by the HMA domain of Pik-1 proteins, and has been extensively investigated (De la Concepcion et al., 2018, De la Concepcion et al., 2021b). The Pikm-1/Pikm-2 pair perceives AVR-PikD, AVR-PikE and AVR-PikA, whereas the Pikp pair only perceives AVR-PikD. Crystal structures of HMA domains in complex with effectors allowed identification of key residues at the binding interfaces responsible for specificity (De la Concepcion et al., 2018). These data allowed engineering of the Pikp-1 binding interface based on Pikm-1 (by Asn261Lys and Lys262Glu substitution, giving rise to a Pikp-1^{NK-KE} receptor) to expand its recognition specificity towards AVR-PikA and AVR-PikE alleles (De la Concepcion et al., 2019). While this work did not generate a novel resistance specificity per se, it provided an important proof of concept that Pik-HMA domains can be altered to change the specificity of these NLRs. This approach has been further explored based on structural knowledge of an sHMA protein called OsHIPP19 in complex with AVR-PikF (Maidment et al., 2021). Combining information from the OsHIPP19/AVR-PikF structure, and the structures of Pikp-1^{NK-KE} bound to multiple AVR-Pik alleles, allowed engineering to expand the recognition specificity to new effector alleles. By introducing an additional Ser258Glu mutation alongside the Pikp-1^{NK-KE} generated the Pikp-1$^{SNK-EKE}$ mutant that was able to perceive the AVR-PikF allele, in addition to previously recognised AVR-PikA, AVR-PikD and AVR-PikE (doctoral thesis of Dr. Josephine Maidment). Notably, AVR-PikF is not recognised by any natural rice accession and therefore the recognition specificity of the Pikp-1$^{SNK-EKE}$ mutant is novel. These structure-guided approaches showed that specific mutations in HMA binding interfaces could expand effector perception. In an alternative approach, integration of the full length OsHIPP19 into the Pikp-1 background resulted in Pikp-2-dependent auto-activity of the receptor, suggesting that a straightforward swapping of an HMA domain in Pik-1 may not always be useful.

In Chapter 4, I confirmed and characterised the binding between the rice HMA-domain-containing protein OsHIPP43 and the *M. oryzae* effector PWL2. In this Chapter I performed experiments to

determine whether this interaction can be used to engineer a Pik NLR that perceives PWL2. I hypothesised that incorporating the OsHIPP43-HMA into a Pikm-1 chassis would enable binding of the PWL2 effector, and that could lead to a cell death response in *N. benthamiana* upon transient co-expression (**Figure 5.1**).

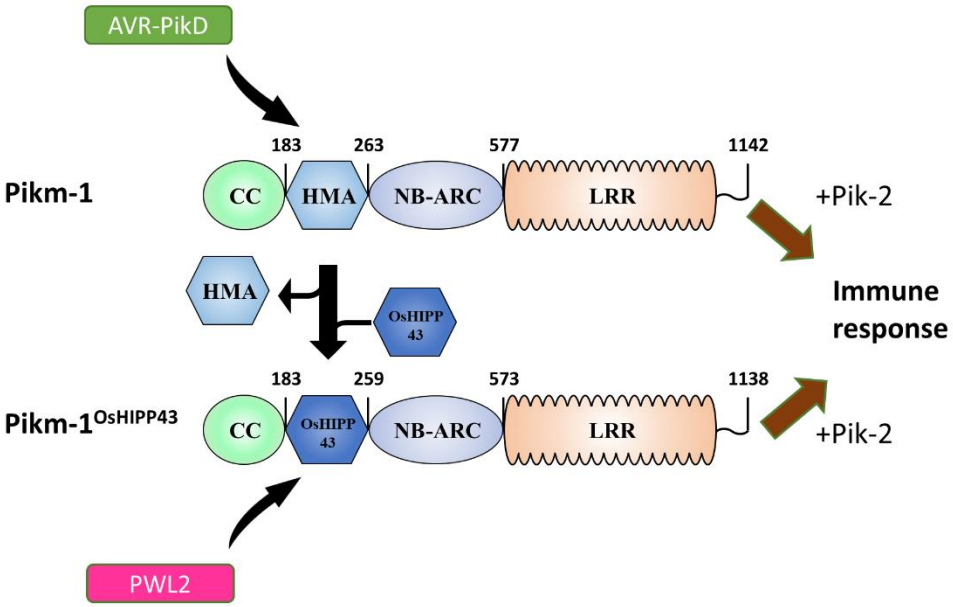

Figure 5.1 Scheme of integration of OsHIPP43 into Pikm-1 background to engineer recognition towards PWL2.

5.2 Results

5.2.1 Pikm-1^{OsHIPP43} chimeric receptor is auto-active

To enable straightforward exchange of the native HMA domain of Pikm-1 for any other HMA domain (or indeed any other gene of interest), a Golden Gate compatible Pikm-1-chassis has been developed (in collaboration with Dr. Mark Youles from TSL SynBio Group, see also Materials and Methods**, p. 53**). The construct was designed as a LVL0 acceptor vector, where an RFP selection cassette was integrated in place of the original Pikm-1-HMA domain (residues 184-263). This selection cassette was flanked by *BpiI* restriction sites allowing for excision and incorporation of any sequence (flanked by appropriate overhangs) using digestion-ligation cloning. Using this system, I placed the OsHIPP43$^{26-101}$ sequence in Pikm-1 chassis, generating Pikm-1^{OsHIPP43} receptor. Subsequently, I generated a LVL1 construct to place the chimeric receptor under the control of the mas promoter and 35S terminator and transformed into electrocompetent cells of *Agrobacterium tumefaciens*. Integration of different HMA domains into the Pikp-1 NLR can result in helper-dependent auto-activity of the receptors (e.g., OsHIPP19, doctoral thesis of Dr. J. Maidment). Interestingly, in this case, auto-activity could be removed by swapping certain residues from OsHIPP19 to those found in Pikp-1 (doctoral thesis of Dr. J. Maidment). However, in a second strategy, auto-activity of chimeric receptors may be alleviated by mismatching NLR alleles in the combination of Pikm-1-chimera and Pikp-2 (interestingly, mismatching Pikp-1 and Pikm-2 results in auto-activity even in the wild type background (De la Concepcion et al., 2021a)). Based on this information, I tested the Pikm-1^{OsHIPP43} receptor for auto-activity in presence of both helper NLRs, Pikm-2 and the mismatched allele Pikp-2 using the well-established *N. benthamiana* system.

Infiltration of the chimeric Pikm-1^{OsHIPP43} receptor in the presence of the corresponding Pikm-2 helper NLR resulted in auto-activity in the absence of the effector (effector-independent cell death, **Figure 5.2,** top right). Interestingly, when Pikm-1^{OsHIPP43} was infiltrated in presence of the mismatched helper allele Pikp-2, effector-independent cell death was not observed (**Figure 5.2**, bottom right). Importantly, the mismatched Pikm-1 with Pikp-2 combination was still responsive to the AVR-PikD effector, suggesting that this combination of NLRs is functional in perceiving the cognate effector. Therefore, mismatching Pikm-1 chimeras with Pikp-2 may present a mechanism for avoiding auto-activity but maintaining perception of effectors.

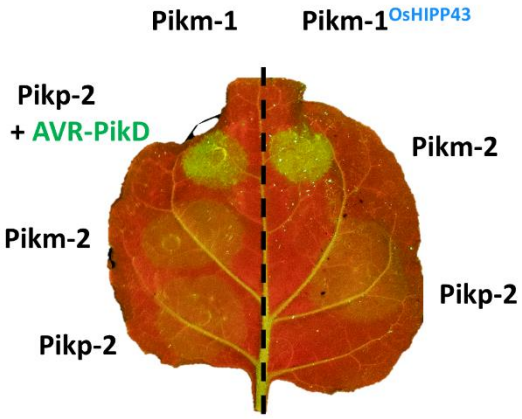

Figure 5.2 Pikm-1^{OsHIPP43} receptor is auto-active in presence of Pikm-2, but not in presence of Pikp-2.

Indicated proteins were transiently overexpressed using agroinfiltration. Leaf picture was taken at 5 dpi under the UV light, which allows to visualise the cell death response as green fluorescence.

5.2.2 Chimeric receptor Pikm-1^{OsHIPP43} can perceive PWL2 in Pikp-2 dependent manner

Next, I set out to test the hypothesis that a Pikm-1^{OsHIPP43}/Pikp-2 combination could trigger cell death in response to recognition of PWL2. For expression in *N. benthamiana*, I cloned PWL2 (with a C-terminal 4xMyc tag) using Golden Gate cloning and placed it under control of AtUbi10 promoter followed by transformation of the expression vector in *A. tumefaciens*. I then co-infiltrated PWL2 with either the Pikm-1 or chimeric Pikm-1^{OsHIPP43} NLRs along with Pikp-2.

In **Figure 5.3** (left side of the leaf) we can observe that wild type Pikm-1 can respond to AVR-PikD in presence of Pikp-2, but cannot recognise the PWL2. Interestingly, upon infiltration of Pikm-1^{OsHIPP43} with Pikp-2 and PWL2 (right side of the leaf), we can observe strong cell death response. Pikm-1^{OsHIPP43} receptor does not recognise the AVR-PikD effector, which agrees with previously obtained results, where no interaction was observed between AVR-PikD and OsHIPPP43 in analytical size-exclusion chromatography. This is an important proof of concept showing that we can use the knowledge about potential targets of effectors to engineer novel recognition specificity in plants.

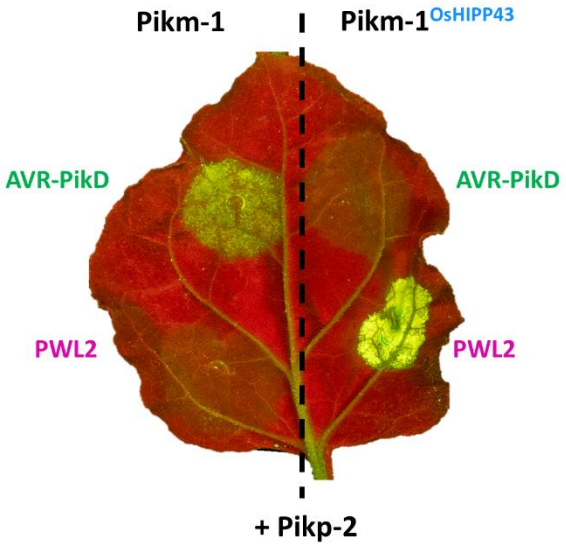

Figure 5.3 Pikm-1^{OsHIPP43} receptor triggers strong cell death in response to PWL2, but not to AVR-PikD.

Indicated proteins were transiently overexpressed using agroinfiltration. Leaf picture was taken at 5 dpi under the UV light, which allows to visualise the cell death response as green fluorescence.

5.2.3 All tested alleles of PWL2 are recognised by Pikm-1^{OsHIPP43}/Pikp-2

The results presented in Chapter 4 showed that all tested alleles of PWL2 bound to OsHIPP43 with similar affinity. Therefore, I tested, whether these alleles could also be recognised by the chimeric receptor. To enable this, I cloned PWL2-2 and PWL2-3 as described for PWL2, and subsequently co-expressed them with Pikm-1^{OsHIPP43} and Pikp-2 in *N. benthamiana*, again using wild type Pikm-1 as a negative control. As expected, Pikm-1 did not respond to any tested PWL2 effector (**Figure 5.4**, left side of the leaf). However, the Pikm-1^{OsHIPP43} chimeric receptor perceived all tested alleles of PWL2, triggering a robust cell death response in each case. These results prove that integration of an HMA domain in the Pik-1 chassis can lead to exciting new opportunities of engineering a novel recognition specificity in plants, even if the sequence conservation of the bespoke HMA domain is very low when compared with wild type Pik-1-HMA.

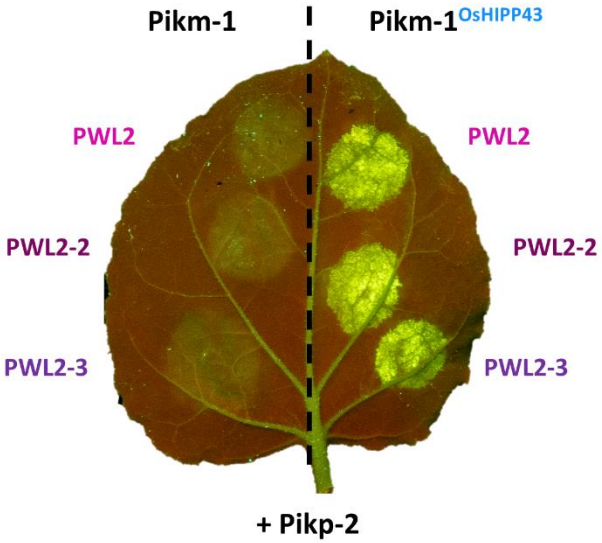

Figure 5.4 Pikm-1^{OsHIPP43} receptor triggers strong cell death response upon recognition of PWL2, PWL2-2 and PWL2-3.

Indicated proteins were transiently overexpressed using agroinfiltration. Leaf picture was taken at 5 dpi under the UV light, which allows to visualise the cell death response as green fluorescence.

5.3 Discussion

In this Chapter, I demonstrated that the integration of OsHIPP43 into the Pikm-1 chassis causes auto-activity in a Pikm-2-dependent manner. This auto-activity can be removed by mismatching the helper allele, using Pikp-2 in place of Pikm-2. The Pikm-1/Pikp-2 NLR combination remains functional in perception of AVR-PikD (De la Concepcion et al., 2021a). Furthermore, I showed that Pikm-1^{OsHIPP43} receptor triggers a robust cell death response upon perception of PWL2, but not AVR-PikD, demonstrating specificity. Finally, I showed that the chimeric Pikm-1^{OsHIPP43} receptor perceives PWL2 alleles PWL2-2 and PWL2-3, which are not recognised by any crop accession reported to date.

5.3.1 Sequence alterations in NLRs can lead to auto-activity

Upon pathogen perception, NLRs very often trigger cell death response. Such dramatic reaction requires tight regulation to prevent a spontaneous auto-activity that can have a drastic effect on plant fitness and overall plant development (Chae et al., 2016, Karasov et al., 2017, Richard and Takken, 2017). Moreover, in case of paired NLRs, mismatching the alleles in an individual plant through crossing might lead to ineffective response to pathogen that might result in susceptibility, which helps the pathogens to spread. When two gene products that cannot function properly together are brought together upon hybridization, the phenomenon called “hybrid necrosis” might occur, which leads to dwarfism, and necrotic and lethal phenotypes (Bomblies and Weigel, 2007, Chae et al., 2014, Tran et al., 2017, Barragan et al., 2019, Vaid and Laitinen, 2019). The role of hybrid necrosis is to reduce the gene flow among incompatible genotypes, and as such, it is long known in agriculture (Hermsen, 1963, Bomblies and Weigel, 2007, Yamamoto et al., 2010). It has been suggested that NLR mismatch is one of the components underlaying the mechanisms of this phenomenon (Bomblies and Weigel, 2007, Ispolatov and Doebeli, 2009). In context of paired NLRs and their adaptation to constantly evolving pathogens, we can hypothesise that they have to maintain balance between diversification that allows recognition of new variants of pathogens and maintaining the fine-tuned regulation of protein assembly leading to immune responses. It has been suggested that helper NLRs (in this case Pik-2 proteins) have evolved to work specifically with their cognate sensor NLRs (Pik-1) and are not always compatible in mixed combinations (De la Concepcion et al., 2021a). Pikm-1 can function with Pikp-2 to trigger a cell death response upon perception of AVR-PikD, but that response is weaker than response triggered by Pikm-1/Pikm-2 or Pikp-1/Pikp-2 pairs (De la Concepcion et al., 2021a). However, when Pikp-1 and Pikm-2 are combined, they trigger constitutive cell death that is independent of the effector. The auto-activity of this complex has been narrowed down to a single amino acid polymorphism (De la Concepcion et al., 2021a). Moreover, it has also been shown that minor modifications of the HMA domain can lead to auto-activity of the Pik NLRs. Deleting Gly-186, or introducing mutation Pro252Asp, into the

HMA domain of Pikm-1 also causes constitutive cell death in a Pikm-2 dependent manner (doctoral thesis of Dr. Juan Carlos de la Concepcion). Interestingly, these changes were introduced in regions of HMA that are not directly involved in binding of the effector. This suggests that the Pik-1/Pik-2 system forms a sophisticated receptor complex, sensitive to subtle changes and appropriate pairing of NLRs. Therefore, careful engineering of HMAs is needed, if the recognition properties of this complex are to be expanded or changed.

5.3.2 Correlation of affinity with strength of immune response is not always clear

I found that the chimeric receptor Pikm-1^{OsHIPP43} can perceive PWL2 and triggers a strong Pikp-2 mediated cell death response in *N. benthamiana*. Interestingly, the binding affinity between PWL2 and OsHIPP43 lies within upper nanomolar range (191 nM), which is lower than apparent K_d measured for AVR-PikD effector interacting with Pik-HMA domains (K_d = 4.7 nM with Pikm-1-HMA and 31 nM with Pikp-1-HMA). However, these values were obtained using different techniques, and caution should be taken when comparing these results. Moreover, there is limitation to which we can compare the two systems, and their correlation between in vitro and in planta studies. For instance, we still do not know whether the dissociation constant (the time that protein remains bound to its interactor) can affect the initiation of downstream signalling, or how differences in binding interfaces contribute to overall conformation changes that initiate the ADP/ATP switch in NLRs and downstream processes leading to immune responses. A first step to answering this question could be determining the crystal structure of PWL2 in complex with OsHIPP43 and comparing it with existing effector/HMA structures.

5.3.3 Exchange of NLR integrated domain can be powerful tool to engineer novel resistance in plants

The integration of OsHIPP43 into the Pik-1/Pik-2 system, which facilitates specificity towards an effector unrelated to AVR-Pik, such as PWL2, is a new concept that shows that we can use existing knowledge about effector targets to engineer novel resistance. Moreover, the chimeric Pikm-1^{OsHIPP43} receptor can recognise also PWL2-2 and PWL2-3, to which no natural resistance has been reported to date. This further strengthens the potential use of this system. However, it is important to note that the results presented here were obtained from a transient expression system, where the experiments were conducted in *N. benthamiana*, and the proteins were overexpressed via agroinfiltration. Although cell death responses in *N. benthamiana* have been correlated with disease resistance in crops (De la Concepcion et al., 2019), such engineered receptors must be further validated using stable NLR transformants in host plants such as rice, barley, or wheat, and challenged by the pathogens of interest (Cesari et al., 2021). Generation of transgenic crops containing the chimeric receptor Pikm-1^{OsHIPP43} is currently ongoing.

6

The crystal structure of the PWL2/OsHIPP43 complex

6 The crystal structure of the PWL2/OsHIPP43 complex

6.1 Introduction

Proteins can adopt similar domain architectures, even if they lack sequence similarity. A well-established example of such phenomenon are MAX effectors from *M. oryzae*, where AVR-PikD, AVR-Pia, AVR-Pib, AvrPiz-t, AVR1-CO39 and APikL2 adopt the same characteristic β-sandwich fold without any significant similarity of their amino acid sequences (Maqbool et al., 2015, Ortiz et al., 2017, Guo et al., 2018, Zhang et al., 2018, Varden et al., 2019, Bentham et al., 2021a). Structural conservation can be a better indicator of shared function than sequence, therefore determining structures of proteins is crucial for understanding their biological functions. Moreover, combining the structural knowledge of allelic variants of the effectors and their corresponding NLRs or biological targets can identify functional relevant regions of effectors (Zhang et al., 2018) and underpin the mechanisms of escape from immune recognition. This in turn can be used to engineer plant immune receptors towards extended recognition of the pathogen (De la Concepcion et al., 2019).

In this Chapter, I set out to purify and crystallise the PWL2/OsHIPP43 complex and determine its 3D structure using X-ray crystallography. Analysis of the resulting structure allowed me to identify important residues responsible for interaction between the PWL2 and OsHIPP43, and revealed that the binding between these two proteins cannot be easily compromised. This knowledge has the potential to contribute to the rational design of HMA-containing NLRs with extended recognition specificities to new effectors.

6.2 Results

6.2.1 PWL2/OsHIPP43 complex can be purified from *E. coli*

To purify PWL2 in complex with OsHIPP43 I co-expressed the proteins in *E. coli.* I introduced PWL2 into the pOPIN-M vector (adding an N-terminal 6xHis-MBP tag that enhances the solubility and expression of the protein) via In-Fusion cloning, and OsHIPP43 into pPGC-K without a tag via Golden Gate cloning (Bentham et al., 2021b). It was hypothesized the strong interaction between PWL2 and OsHIPP43 should allow for the purification of a complex by pulling down only one component. I transformed both constructs into competent *E. coli* SHuffle strain and purified the proteins via immobilised-metal affinity chromatography (IMAC) coupled with size-exclusion chromatography (SEC), as described in Chapter 4, (section **4.2.1, p. 91**; see also Materials and Methods, section **2.3, p. 56**). As can be seen in **Figure 6.1 A**, initial IMAC-SEC resulted in purification of both proteins in complex; the high molecular weight band represents 6xHis-MBP-PWL2 (ca. 50 kDa), and lower molecular weight band represents untagged OsHIPP43 (ca 8 kDa). Overnight cleavage with 3C protease was efficient, as the majority of 6xHis-MBP tag was removed from PWL2 (**Figure 6.1 B**). After tag removal, the complex was further purified by reverse-IMAC purification using MBPTrap and HisTrap IMAC columns in tandem. The tagless PWL2/OsHIPP43 complex displayed a weak affinity to the IMAC column (as individual proteins displayed previously) and could be eluted with low imidazole in the Wash fractions (**Figure 6.1 B**). The cleaved 6xHis-MBP tag, 3C protease and other contaminations were retained on the columns until specifically eluted. Final size-exclusion chromatography resulted in a high yield of pure protein complex, suitable for crystallisation trials (**Figure 6.1 C)**.

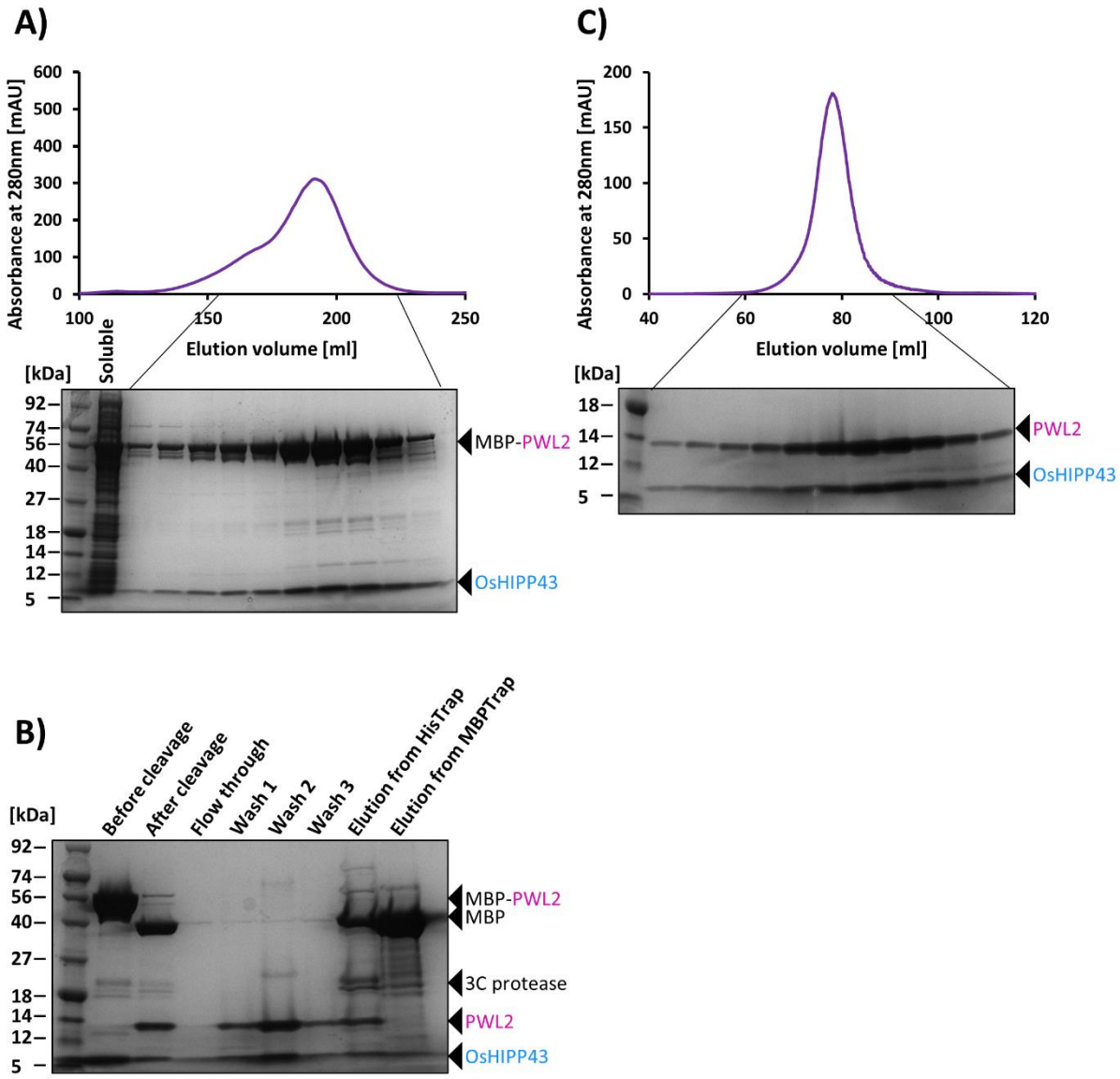

Figure 6.1 Purification of PWL2/OsHIPP43 complex from *E. coli.*

A) *SDS-PAGE gel showing Soluble fraction from E. coli expressing pOPIN-M:PWL2+pPGC-K:OsHIPP43. Further lanes show fractions corresponding to the indicated fragment of size-exclusion chromatography trace.* ***B)*** *SDS-PAGE gel showing fractions before and after cleavage of the tag, and subsequent steps of manual purification.* ***C)*** *SDS-PAGE gel showing fractions from final size-exclusion chromatography.*

6.2.2 Crystallisation of PWL2/OsHIPP43 complex

The Protein Crystallography Platform at the John Innes Centre offers a range of commercially available crystallisation screens and robotics for crystallisation and imaging crystallisation experiments. The crystallisation trials are conducted using the sitting drop vapour diffusion method, and each screen (96-well plate) allows to test two different proteins (or the same protein at two different concentrations). Each screen offers a range of different pH, buffers, precipitants, and additives, which can be found on manufacturers' websites. To begin with, I used the Morpheus and JCSG (Molecular Dimensions) screens, however no crystals were observed. Since no clear preferred conditions were revealed by these initial screens (indicated by occurrence of crystalline precipitate, data not shown), I set up additional crystallisation screens, including Shotgun and ProPlex. The screens and concentrations tested are listed in **Table 6-1.** Unfortunately, none of the tested conditions generated any crystals.

Table 6-1 Initial screens and conditions used for crystallisation of PWL2/OsHIPP43 complex.

Screen	Protein concentration	Additional comments
JCSG	**17 mg/ml and 8.5 mg/ml**	
Morpheus	**17 mg/ml and 8.5 mg/ml**	
Morpheus	**20 mg/ml and 10 mg/ml**	**With cross seeding**
Shotgun	**20 mg/ml and 10 mg/ml**	**With cross seeding**
JCSG	**20 mg/ml and 10 mg/ml**	
ProPlex	**20 mg/ml and 10 mg/ml**	
KISS	**20 mg/ml and 10 mg/ml**	
Shotgun	**58 mg/ml and 29 mg/ml**	
Morpheus	**58 mg/ml and 29 mg/ml**	

All screens are commercially available, apart from the KISS screen, which has been developed by Biophysical Platform in John Innes Centre. Seeds for cross-seeding were derived from crystals of sHMA94/AVR-PikF complex, provided by Dr. Adam Bentham (Bentham et al., 2021a).

Based on previously acquired data, I hypothesised that PWL2 might be highly unstructured or an intrinsically disordered protein that folds properly upon binding to its interactor. Proper folding of the protein is crucial to obtain crystals, as any disordered region within the protein or protein complex could physically interfere with ordering molecules into a lattice, as required for crystal formation. Although I purified PWL2 in complex with OsHIPP43, hoping to promote its stability and

proper folding, the complex did not crystallise. Therefore, I hypothesised that PWL2 does not become completely ordered upon the interaction with OsHIPP43 and there might still be disordered regions that interfere with the crystallisation process. To test this and identify any potential truncation that could be made in order to obtain a well folded complex, I conducted a partial trypsin digest experiment.

Partial trypsin digest is a limited proteolysis process that can be used to remove disordered and unstructured regions from proteins in vitro and can be added directly to crystallisation plate as an additive to perform in situ proteolysis (Dong et al., 2007, Wernimont and Edwards, 2009). Trypsin belongs to the serine protease family, cleaving after lysine and arginine residues, and will most readily cut disordered regions above folded structures (**Figure 6.2 A**). I optimised this approach and set up a limited proteolysis experiment to observe whether trypsin could cleave portions of either of the proteins in the PWL2/OsHIPP43 complex. This would allow subsequent identification (using Mass Spectrometry) of well folded regions of PWL2 and/or OsHIPP43 and redesigning the constructs, potentially increasing the chances of protein crystallisation.

I prepared a trypsin dilution series and incubated it with 4 µg of the PWL2/OsHIPP43 complex, and 4 µg of PWL2 alone, for 30 min at room temperature. I also incubated the samples without the protease at room temperature, and on ice to exclude the possible effect of exposing the sample to higher temperature on degradation. To halt the reaction, a "stopping buffer" was added to each sample (see Materials and Methods Section **2.4.4, p. 60**). Subsequently the samples were boiled and analysed by SDS-PAGE. As can be seen in **Figure 6.2 B**, trypsin digests PWL2 into a smaller product, suggesting that there is a specific region of PWL2 that is potentially unstructured or disordered in the complex with OsHIPP43 and readily available to the protease. I observed the degree of trypsin digest is directly proportional to amount of trypsin added. Interestingly, OsHIPP43 seems to be unaffected, even in higher amounts of trypsin, suggesting OsHIPP43 is well ordered in the complex with PWL2. When PWL2 alone was incubated with trypsin, it was completely degraded, even in the experiment with the smallest amount of protease (**Figure 6.2 C**). These observations agree with the hypothesis that PWL2 majorly consists of loop regions on its own ((Schneider et al., 2010), also section **4.2.2, p.94**) and only becomes properly folded upon the interaction with its binding partner.

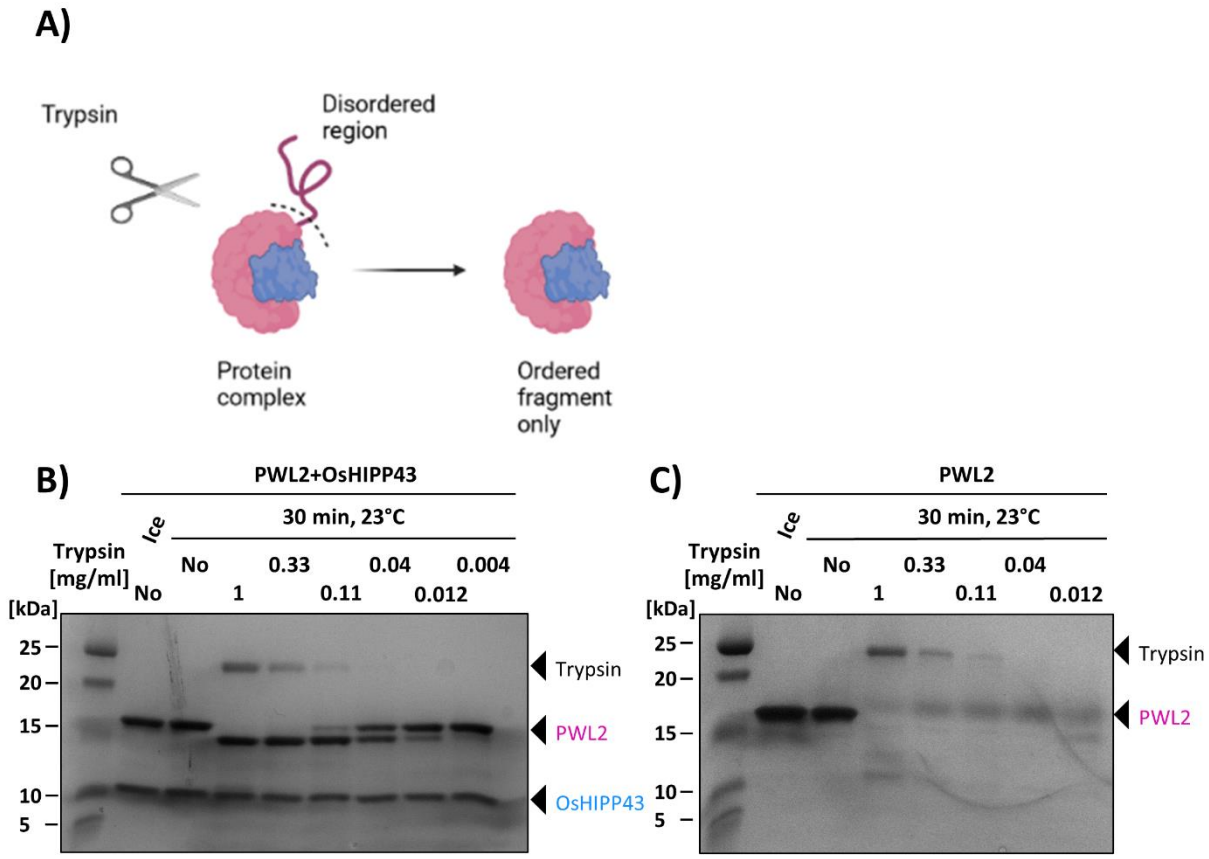

Figure 6.2 Limited proteolysis of the PWL2/OsHIPP43 complex.

A) *Visual representation of partial trypsin digest. Trypsin cuts only into primary protein structure, leaving ordered parts of protein complex intact. Image generated with BioRender.* ***B)*** *Partial trypsin digest of PWL2+OsHIPP43 complex. PWL2 is being truncated down to a stable fragment. The amount of processed PWL2 is directly proportional to amount of trypsin in the sample. OsHIPP43 remains intact.* ***C)*** *Trypsin digest of PWL2 only results in complete digest of the sample.*

To identify the PWL2 fragment that is resistant to proteolysis, the digested sample was prepared for intact mass spectrometry analysis by acetone precipitation. Further, the band representing truncated PWL2 was excised from the SDS-PAGE gel and submitted for peptide mass fingerprinting. The peptide mapping analysis revealed a tryptic peptide was missing from the sample, and indicated that PWL2 was truncated by 10 amino acids at its C-terminus (**Figure 6.3 A**). Analysis of the intact mass spectrum showed a main peak in the sample of 12819.70 Da, which corresponds to the monoisotopic mass of the predicted truncated sequence of PWL2 (12819.78 Da) (**Figure 6.3 B**). A second major peak in the intact mass spectrum, at 8617.35 Da, almost exactly matches the predicted mass of OsHIPP43 (8619.41 Da), indicating that OsHIPP43 was not affected by the trypsin digest (**Figure 6.3 B**). The apparent difference between predicted and measured masses of OsHIPP43 might be a result of possible disulphide bond formation between two cysteines in the OsHIPP43 sequence. The difference between the predicted mass of OsHIPP43 in this experiment and the one reported in Chapter 4 (8642.45 Da vs. 8619.41 Da) is a result of a different construct being used. In Chapter 4, OsHIPP43 was purified with an affinity tag, which after cleavage left glycine-proline scar at the N-terminus of the protein. In this Chapter, OsHIPP43 was cloned without the affinity tag, which required the presence of additional methionine residue at the beginning of the sequence to enable start of translation and expression of the protein.

Following these limited proteolysis experiments I cloned a new truncated construct of PWL2, PWL2Δ10 (missing the C-terminal 10 amino acids), and co-expressed/purified it with OsHIPP43, as described previously (**Figure 6.4 A, p. 135**). I set up several crystallisation screens, as listed in **Table 6-2.** The presence of crystalline precipitation in crystallisation screens can be an indicator of conditions that might result in crystal formation, but are currently sub-optimal. Analysis of the screens that were set-up revealed that most of the precipitates occurred in presence of ammonium sulphate in acidic pH (**Figure 6.4 B, p. 135**). I decided to set up a custom designed optimisation screen with a range of ammonium sulphate (1.0-2.4 M) at acidic pHs (5.5-7.0) (**Figure 6.5 A, p. 136**). This resulted in a similar outcome (mainly crystalline precipitate), as described previously for commercially available screens (**Figure 6.5 B, p. 136**). Overall, these results suggest that truncating of the PWL2 sequence resulted in better folded protein, prone to crystallisation.

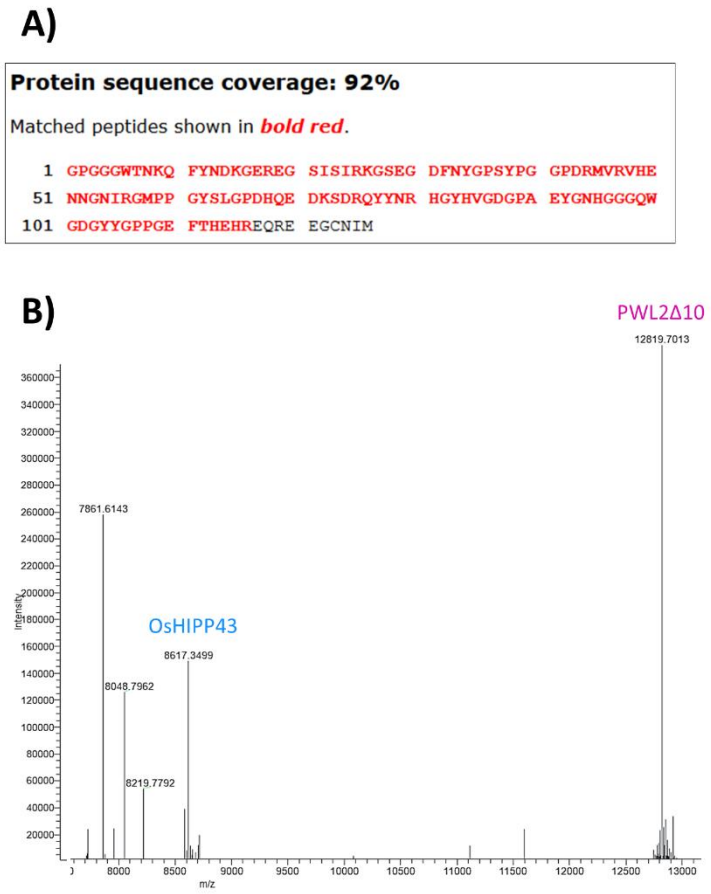

Figure 6.3 Identification of truncated fragments of PWL2/OsHIPP43 complex.

A) *Peptide mapping of PWL2 submitted for partial trypsin digest revealed that PWL2 was truncated at C-terminus by 10 amino acids.* ***B)*** *Intact mass spectrometry analysis of the protein complex submitted for partial trypsin digest. The detected masses precisely match the predicted monoisotopic mass of PWL2Δ10 (12819.78 Da). The peak representing OsHIPP43 (predicted mass 8619.41 Da) is smaller by 2 Da, indicating possible disulphide bond formation and no truncation caused by partial trypsin digest.*

Table 6-2 Initial screens and conditions used for crystallisation of PWL2Δ10/OsHIPP43 complex.

Screen	Protein concentration
JCSG	35 mg/ml and 17.5 mg/ml
Morpheus	35 mg/ml and 17.5 mg/ml
ProPlex	35 mg/ml and 17.5 mg/ml
Shotgun	35 mg/ml and 17.5 mg/ml

All the screens are commercially available.

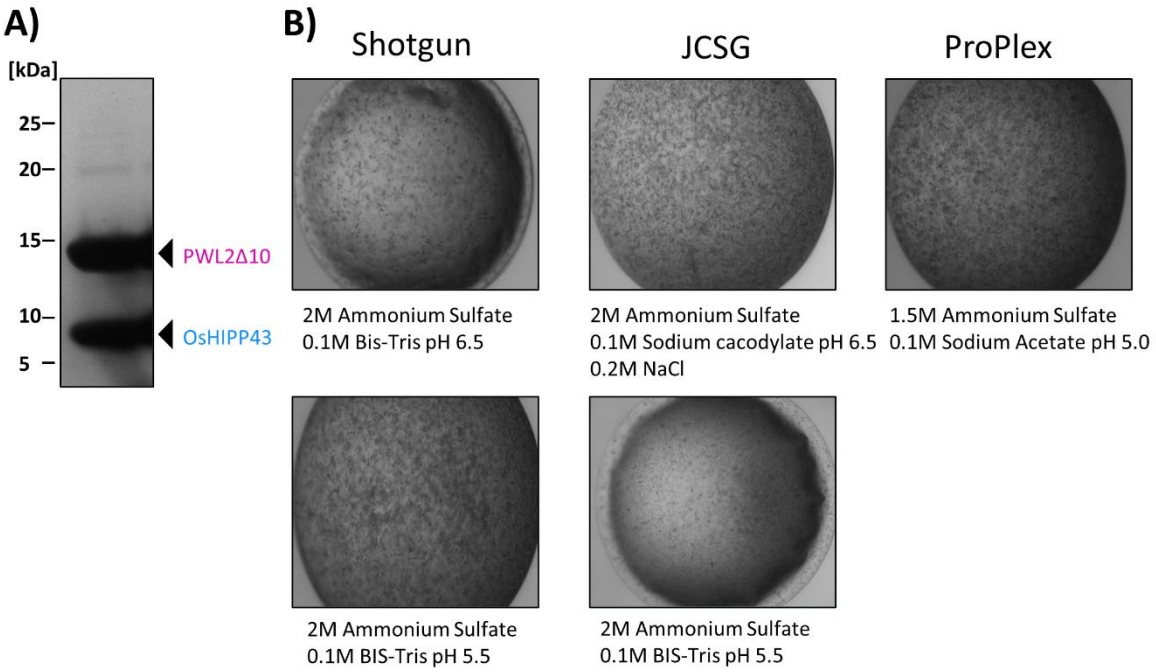

Figure 6.4 Initial screens and conditions used for crystallisation of PWL2/OsHIPP43 complex resulted in crystalline precipitate.

A) *SDS-PAGE gel showing final purified complex of PWL2Δ10/OsHIPP43 complex* ***B)*** *Representative pictures of crystalline precipitates obtained in indicated crystallisation screens.*

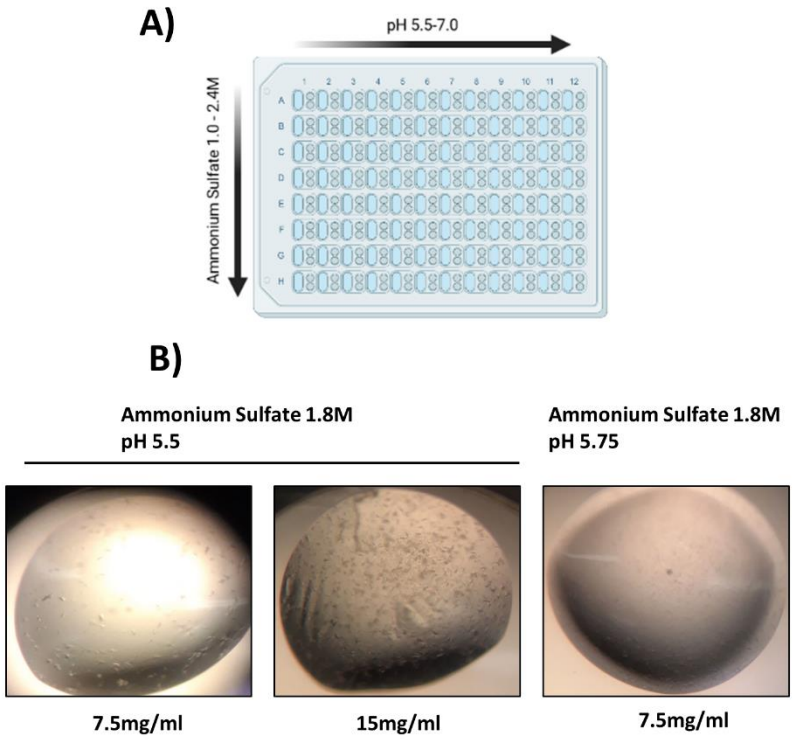

Figure 6.5 Optimisation of crystallisation conditions.

A) *Schematic representation of gradient of ammonium sulphate and pH across the crystallisation screen. Image generated with BioRender.* ***B)*** *Representative pictures of crystalline precipitates obtained in indicated conditions*

Protein crystallisation can be a slow process and require days, months or even years (McPherson, 2017), therefore continuous monitoring of experiments is important. Two weeks after the initial crystallisation set up, rhomboidal-shaped crystals were observed in the ProPlex crystallisation screen (**Figure 6.6 A**). Three of these crystals were harvested by Dr. Clare Stevenson and flash frozen in liquid nitrogen. Buffer identical to crystallisation condition, but supplemented with 20% ethylene glycol, was used as a cryoprotectant. These crystals were sent to the Diamond Light Source synchrotron facility for X-ray data collection.

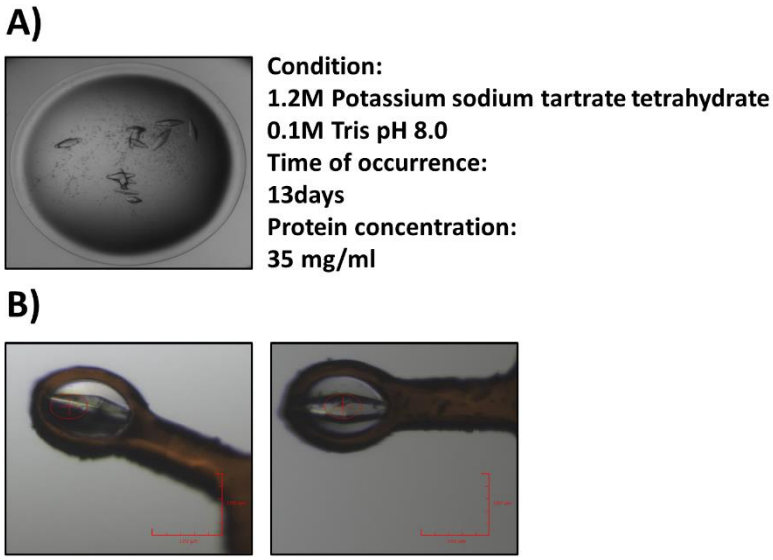

Figure 6.6 Crystals of PWL2/OsHIPP43 complex.

A) *Crystals of PWL2Δ10/OsHIPP43 complex in the crystallisation screen.* ***B)*** *Crystals mounted on the loop prepared for X-ray data collection*

6.2.3 X-ray data collection and structure determination

X-ray diffraction data were collected at beamline I04 of the synchrotron facility. Following preliminary screening, a diffraction dataset was collected for each the harvested crystals at a wavelength of 0.98Å. **Figure 6.6 B** shows one of the crystals mounted in the loop prior to data collection. For each dataset, 3600 images were collected, with an oscillation angle of 0.1°. The dataset with the highest initial resolution was chosen for downstream analysis. Initially, we tried to solve the structure by deriving phases from molecular replacement using the automated MrBUMP pipeline, implemented on ISPyB website (Keegan and Winn, 2007, Keegan and Winn, 2008). However, due to lack of sequence similarity between OsHIPP43 and any other deposited structure of HMA domain, the programme did not find a suitable homology model to build the structure. Moreover, we did not know what could possibly PWL2 look like, therefore we could not use any available structure as a model. Additional attempts to solve the PWL2/OsHIPP43 structure using available structures of HMA domains as templates also failed to position any protein molecules. At this time, we recognised that the PWL2/OsHIPP43 complex contained 11 sulphur atoms present within four cysteine and seven methionine residues. We hypothesised that the anomalous signal from these sulphur atoms may be sufficient to position these atoms and allow structure solution by single-wavelength anomalous diffraction (S-SAD). To do this, the same crystals used for the previous data collection were used, with an X-ray wavelength of 1.9 Å. Remarkably, we were able to collect 12 datasets from one of these crystals. We subsequently focussed on 9 of these datasets, those which showed the best quality, to combine and further analyse. Each of these 9 data sets comprised 3600 images, with an oscillation angle of 0.1°.

Data reduction was carried out using the autoPROC (Native data, (Vonrhein et al., 2011)), and xia2.multiplex (S-SAD data, (Gildea and Winter, 2018, Beilsten-Edmands et al., 2020)) pipelines with the scaled (but unmerged) data imported and processed with AIMLESS (as implemented in CCP4i2) (Winn et al., 2011, Evans and Murshudov, 2013). As expected, unit cell parameters were very similar as the data was collected from the same crystal and were calculated as, a= 63.16, b= 63.16, c= 198.21, α= β= 90, γ=120 for the Native dataset, and a= 63.30, b= 63.30, c= 198.47, α= β= 90, γ=120, for the S-SAD data. Both datasets were processed in the space group P 6_1 2 2 to a maximum resolution of 1.8 Å and 2.8 Å respectively. The overall R_{merge} for the Native and S-SAD datasets are 8.7% and 13.5%, respectively. The overall data collection statistics are presented in **Table 6-3.** Notably, the S-SAD dataset had an overall redundancy of 295.

The structure was solved by the SAD method using the CRANK2 pipeline as implemented in CCP4i2 (Skubák and Pannu, 2013, Skubák et al., 2018). This pipeline built an initial model of the structure, with 188 amino acids successfully positioned, and initial R-factor of 28.25% and R_{free} of 36.35%. This

model was then used to solve the Native dataset (that was obtained at higher resolution) by molecular replacement with PHASER (McCoy et al., 2007). To arrive at the final structure, a series of manual rebuilding, refinement and validation steps were carried out using REFMAC (Murshudov et al., 2011) and COOT (Emsley et al., 2010). At the final stages of refinement, translation-liberation-screw (TLS) parameters were included (setting the TLS groups to be automatically defined), to reflect anisotropic displacement of the defined groups of atoms (Winn et al., 2003). The TLS parameters were refined over 10 cycles prior to the main refinement, with the automatic weighting of the geometric restraints against the experimental data.

Table 6-3. X-ray data collection and refinement statistics for PWL2Δ/OsHIPP43 complex.

Data Collection and Refinement Table

	PWL2/OsHIPP43	**PWL2/OsHIPP43**
Data collection statistics	Native	S-SAD
Wavelength (Å)	0.9795	1.90
Space group	P 6_1 2 2	P 6_1 2 2
Cell dimensions		
a, *b*, *c* (Å)	63.16 63.16 198.21	63.30 63.30 198.47
Resolution (Å)*	54.70-1.80 (1.84-1.80)	54.82-2.80 (2.95-2.80)
R_{merge} (%)	8.7 (169.8)	13.5 (43.3)
$I/\sigma I$	31.1 (2.9)	70.5 (28.3)
Completeness (%)		
Overall	100.0 (100.0)	100.0 (99.8)
Anomalous	100.0 (100.0)	100.0 (100.0)
Unique reflections	22749 (1291)	6420 (888)
Redundancy		
Overall	36.9 (38.4)	295.3 (230.7)
Anomalous	20.3 (20.5)	173.7 (129.2)
CC(1/2) (%)	100.0 (91.5)	99.8 (99.8)
Refinement and model statistics		
Resolution (Å)	54.76-1.8 (1.84 – 1.80)	
R_{work}/R_{free} (%)	18.5 / 21.3	
No. atoms		
Protein	1473	
Ligand	175	
B-factors		
Protein	21.72	
Ligand	45.59	
R.m.s deviations		
Bond lengths (Å)	0.0138	
Bond angles (°)	1.77	
Ramachandran plot (%)**		
Favoured	97.81	
Allowed	2.19	
Outliers	0.00	
MolProbity Score	1.1	

*The highest resolution shell is shown in parenthesis.
**As calculated by MolProbity

The final refined R-factors for the model were 18.5/21.3% (R_{work}/R_{free}). In the final model, residues Gly^{-2}, Pro^{-1} (the remaining residues after tag removal), Gly-22 (at N-terminus) and Arg-135 (at C-terminus) were excluded from the PWL2 structure due to poor electron density defining their position. For the same reason, Met^{-1} was also excluded from the OsHIPP43 structure (the Met residue was added to the sequence to enable the expression of the protein). Therefore, the final structure comprised amino acids Gly-23 to His-134 of PWL2, and Arg-26 to Met-100 of OsHIPP43. Moreover, 203 water molecules were built in the final model.

In addition to the tools available in COOT, I validated the final model using MolProbity (Chen et al., 2010), which assesses the quality of structures based on steric clashes and protein geometry. The phi (ϕ) and psi (ψ) dihedral angles of the amino acids can be graphically represented as a Ramachandran plot, defining the combinations of ϕ and ψ that are favoured in protein structures. The Ramachandran plot for the refined model of PWL2/OsHIPP43 showed that 97.81% (180 out of 183 amino acids) of the residues were in favoured configurations and no outliers were present in the structure (**Figure 6.7**). Amino acid side chain rotamer analysis revealed that only one residue, Ser-56 of PWL2 was classified as an outlier. This residue was inspected, and the electron density did not support any other more favourable rotamer.

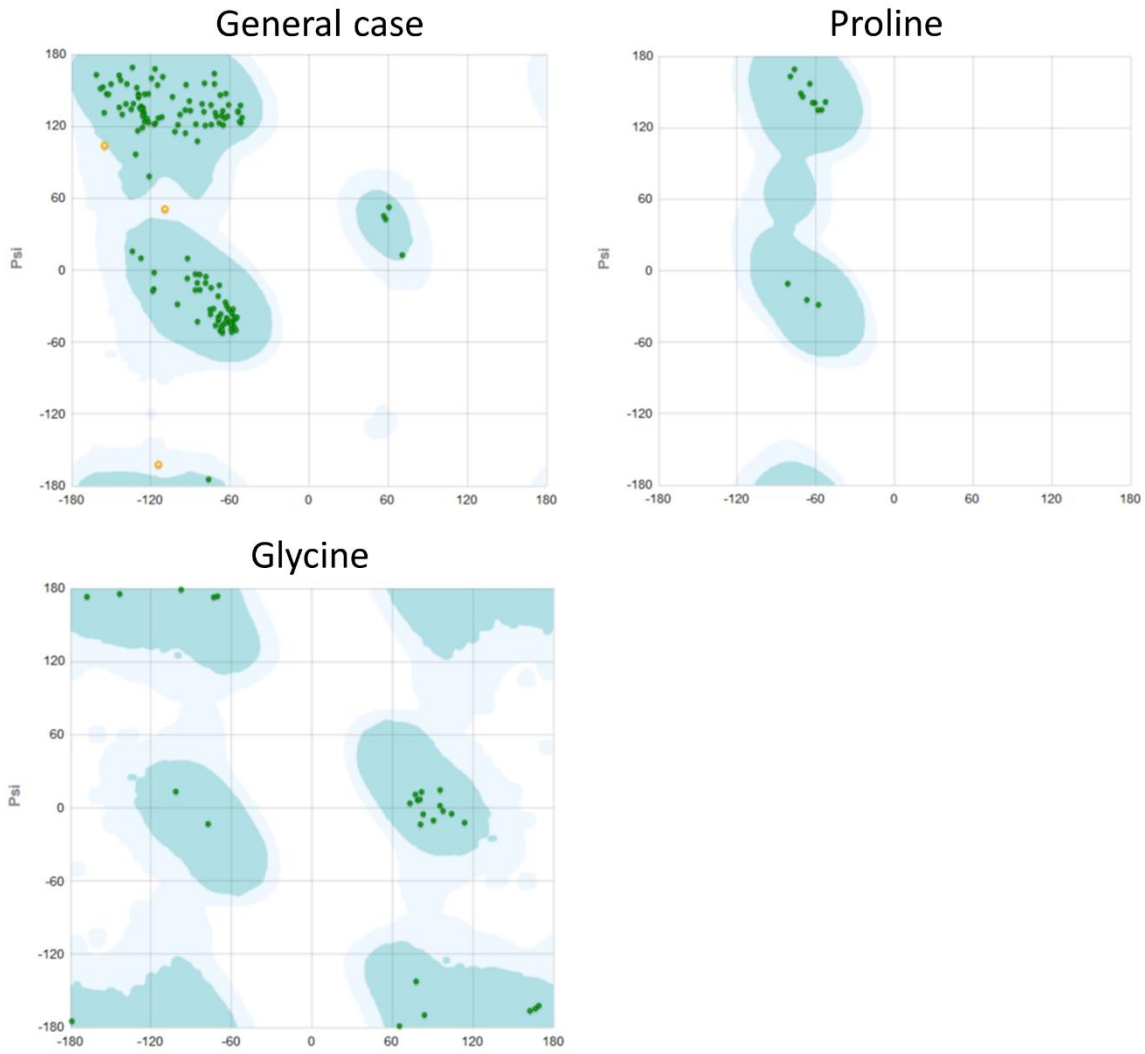

Figure 6.7 Ramachandran plots for the PWL2/OsHIPP43 structure.

All residues were in the allowed regions, with 98.36% (180/183) of the residues lying within favoured regions (green area). Analysis and plots were made by MolProbity.

6.2.4 The crystal structure of the PWL2/OsHIPP43 complex

As expected, the HMA domain of OsHIPP43 adopts the well-characterised HMA fold (Pfam: PF00403) that consists of a four-stranded antiparallel β-sheet and two α-helices. Each of these secondary structures comprise 27.3% of the overall secondary features content of the protein, which is more than calculated from the CD spectrum presented in Chapter 4 (combined β-sheets and α-helices were predicted to constitute 38% of the protein). The metal-binding motif MxCxxC (here MDCEGC) faces away from the interaction interface with PWL2 and lies in a loop between β1 and α1, where the Cys-39 and Cys-42 form a disulphide bridge (**Figure 6.8 A, B, C**).

In the structure of PWL2, three predominant overall structural features can be distinguished (**Figure 6.8 A, B, C**). The N-terminal region adopts a MAX fold, characterized by 6 antiparallel β-strands arranged in a β-sandwich. This fold spans residues Trp-25 to Pro-85. Following the region that adopts the MAX fold, amino acids His-87 to His-100 form an α-helix. Finally, the C-terminal part of the protein (residues Gly-101 to His-134) forms a loop structure without α-helices or β-strands (apart from short β-strand formed between Tyr-111 to Asn-113). Interestingly, this part of PWL2 wraps around the structure of OsHIPP43 forming extensive interactions between the two proteins (**Figure 6.8 A, B, C**). Overall, the content of α-helices, β-sheets and loop regions for PWL2 accounts for 12.3%, 34.2% and 53.5% respectively, which is not in agreement with the interpretation of the CD spectrum presented in Chapter 4, where the proportions of these structures (helices, sheets and loops respectively) were calculated to constitute 24.6%, 11.7% and 63.6% of the protein. However, both results agree that more than half of the PWL2 structure lacks secondary structure features. It is important to remember that analysis of the CD spectrum is only an estimation, and the data was collected for PWL2 only, whereas the structure of PWL2 was obtained in the complex with its interactor.

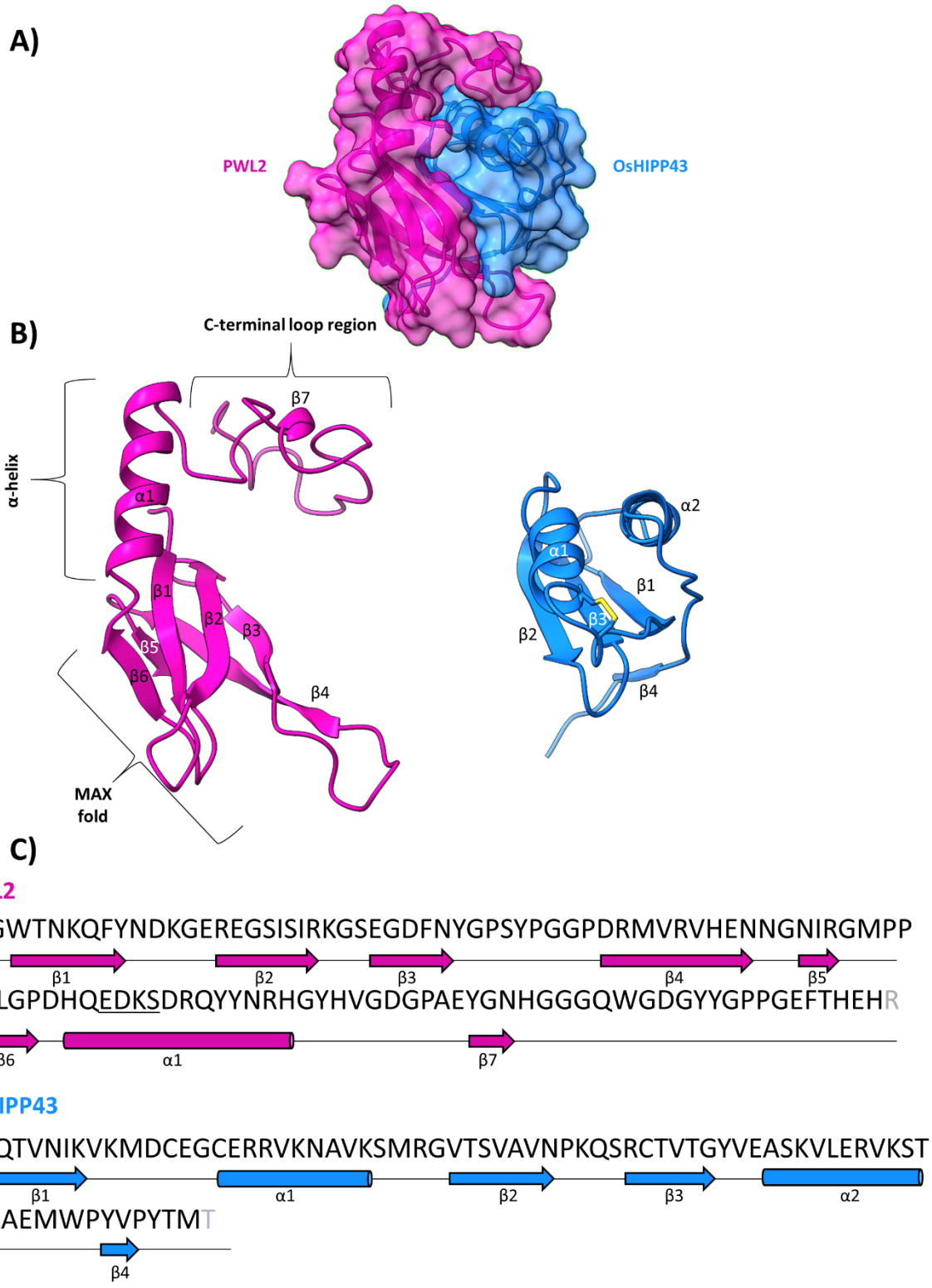

Figure 6.8 Crystal structure of PWL2/OsHIPP43 complex.

A) *The molecular surface of PWL2/OsHIPP43.* ***B)*** *Separate structures of PWL2 (pink) and OsHIPP43 (blue) with indicated secondary structures. The disulphide bridge in OsHIPP43 is represented as yellow bond.* ***C)*** *Secondary structures mapped on proteins' sequences. Underlined residues form the polymorphic region in PWL2 alleles. Residues in grey are not represented in the structure.*

The interface formed between PWL2 and OsHIPP43 is extensive. Analysis using QtPISA (Krissinel and Henrick, 2007, Krissinel, 2010) reveals 25.1% and 38.2% of the total accessible surface area of the effector (1919.2 Å^2) and the HMA domain (2033.9 Å^2) respectively is buried in the complex. The total interface area (the average of the two individual areas) for the PWL2/OsHIPP43 complex is 1976.9 Å^2 (**Figure 6.9**), which is more than twice as large as any of the Pik-HMA/AVR-Pik complexes determined to date. For example, the total interface area of the Pikp-HMA/AVR-PikD complex is 966.6 Å^2 (Maqbool et al., 2015).

The interaction interface between PWL2 and OsHIPP43 is formed by more than a half of the residues of each protein. QtPISA analysis showed that 62 residues (55.4%) of PWL2 and 45 residues (60%) of OsHIPP43 are involved in formation of the interface, and form in total 37 hydrogen bonds and 9 salt bridges (**Figure 6.9**). Upon detailed manual inspection, I identified several residues that are likely to be important for the interaction between PWL2 and OsHIPP43 and these can be grouped into three interfaces (**Figure 6.10**).

The first interface is located in the core part of structure (within the MAX fold region), surrounding β2 of PWL2 and β2 of OsHIPP43. At the beginning of β2 of PWL2, Arg-37 forms a salt-bridge interaction with Glu-43, located at the beginning of α1 of OsHIPP43 (**Figure 6.10**). A large part of this central interface is formed by interaction between backbone atoms of β2 of PWL2 and β2 of OsHIPP43. Additionally, Ser-40 and Ser-42 of PWL2 form hydrogen bonds with Lys-47 located on α1 of OsHIPP43. Finally, Lys-51 (located also on the α1 of OsHIPP43) forms a salt bridge with Glu-89 from α1 of PWL2 (**Figure 6.10**).

The second interface is formed by the loop between β3 and β4 of PWL2. Residues Asn-52 (end of β3) and Asp-62 (beginning of β4) of PWL2 form a range of hydrogen bonds with Asn-32 (located at β1 of OsHIPP43), and Arg-67 and Thr-69 located at β3 of OsHIPP43 (**Figure 6.10**).

Finally, the third interface is formed by the large C-terminal loop region of PWL2 (spanning residues Gly-101 to His-134) that wraps around the structure of OsHIPP43. Tyr-111 (located at the end of short β7) docks into the structure of OsHIPP43, where it is surrounded by Ser-52 and Met-53, positioned on the loop between α1 and β2, and Arg-82, located at α2, of OsHIPP43. Further, Trp-119 and Tyr-123 form stacking interactions with the hydrophobic chain of Arg-54 of OsHIPP43, forming a sandwich-like structure that may contribute to the overall stability of this region (**Figure 6.10**).

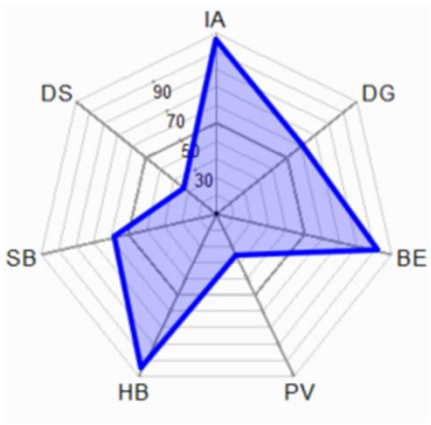

PWL2/OsHIPP43	
IA: Interface area	1976.9 Å
DG: Solvation energy	-7.1 kcal/mol
BE: Binding energy	-26.9 kcal/mol
PV: Hydrophobic P-value	0.3876
HB: Hydrogen bonds	37
SB: Salt bridges	9
DB: Disulphide bonds	0

Figure 6.9 Analysis of interaction interface of the PWL2/OsHIPP43 complex.

Radar plot produced by QtPISA provide a visual representation of the binding interface of the PWL2/OsHIPP43 complex. The polygon area of the radar represents the probability of the interface to be a part of biological assembly based on statistical analysis of all interfaces found in the Protein Data Bank. The parameters represented in the radar are defined in the table underneath the panel.

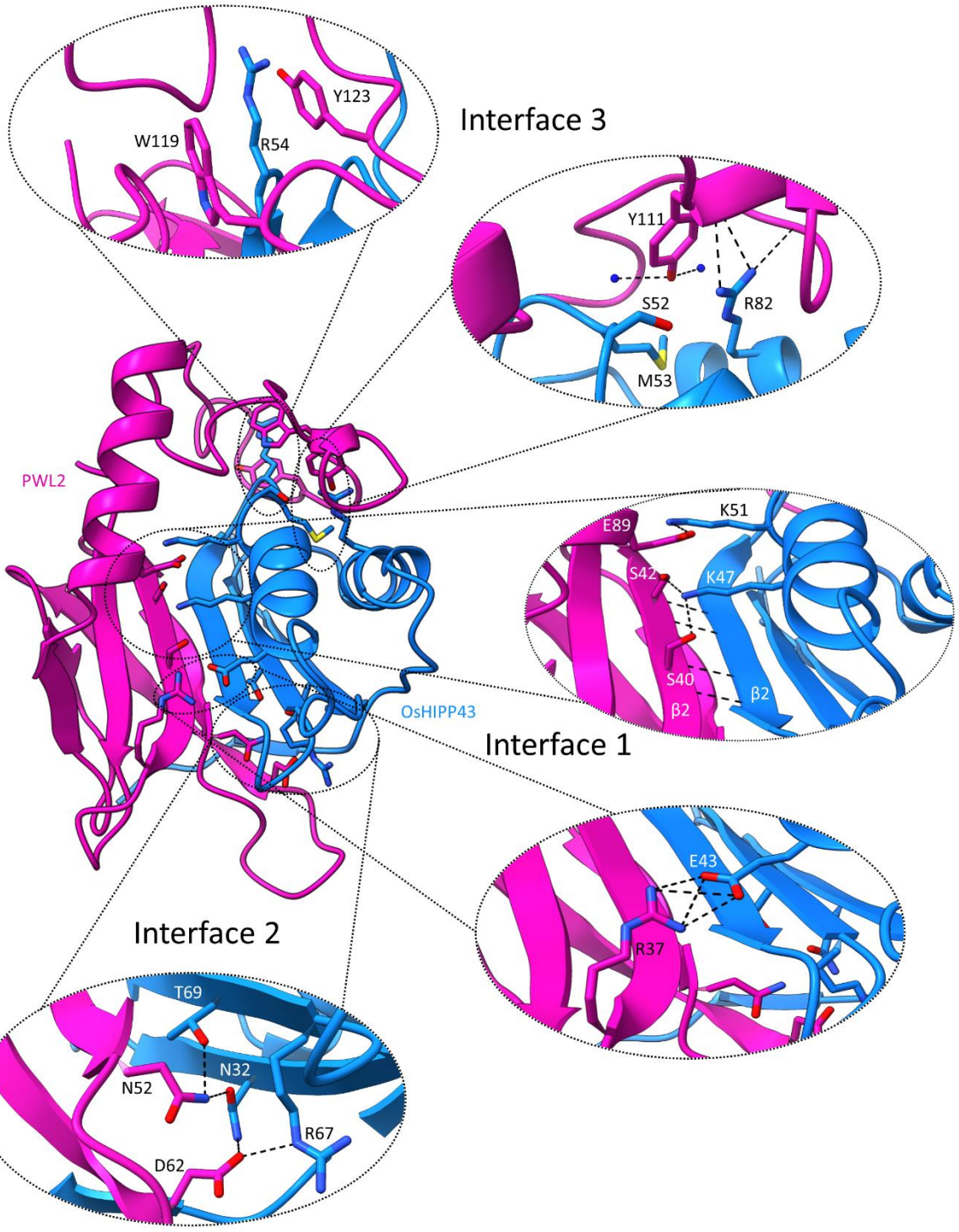

Figure 6.10 PWL2 forms a vast binding interface with OsHIPP43.

PWL2 (pink) wraps around the OsHIPP43 (blue) forming a vast interaction interface. The ovals show a close-up view of the interactions across the interface. Side chains are represented as sticks. Hydrogen bonds are represented as black dashes between the residues. Blue dots represent water molecules.

6.2.5 Validation and functional analysis of the PWL2/OsHIPP43 crystal structure

To identify which residues are crucial for the interaction between the PWL2 and OsHIPP43, I designed seven single point mutations aimed at disrupting the binding between the two proteins. Five mutations were designed to introduce charged and steric clashes across the interface between the proteins: Ser42Arg, Asn52Arg, Asp62Arg, Glu89Arg and Tyr111Arg. The two remaining mutations: Trp119Asp and Tyr123Asp were designed to disrupt the hydrophobic interaction between the aromatic residues of PWL2 and the long side chain of Arg-54 of OsHIPP43. I did not mutate the Arg-37 residue of PWL2 that forms the salt bridge with Glu-43 of OsHIPP43, as I hypothesised that any steric clash introduced in that region could be accommodated, given that this residue is positioned at the surface of the complex.

I tested whether any of the mutants would break the perception of the effector by the chimeric Pikm-1^{OsHIPP43}/Pikp-2 receptor in planta. The coding sequence of PWL2 mutants were synthesised commercially (IDT) and cloned under control of the AtUbi10 promoter and with a C-terminal Myc-tag. These constructs were transformed into *A. tumefaciens* and transiently co-expressed with the Pikm-1^{OsHIPP43}/Pikp-2 NLR pair in *N. benthamiana* plants as described previously in Chapter 1 **(p.119)**. As presented in **Figure 6.11 A**, none of the mutants tested were able to escape perception by the receptor, with all mutants triggering a strong cell death response upon co-expression. AVR-PikD served as a negative control, and did not trigger any responses. Western blot analysis showed that all the effectors were expressed to similar level, apart from PWL2^{Y111R} that could not be detected (**Figure 6.11 B**), despite triggering a cell death response in the in planta assay. This indicates that the PWL2/OsHIPP43 binding interface is complex and single mutations may not overcome the additive effect of the other residues that contribute to binding.

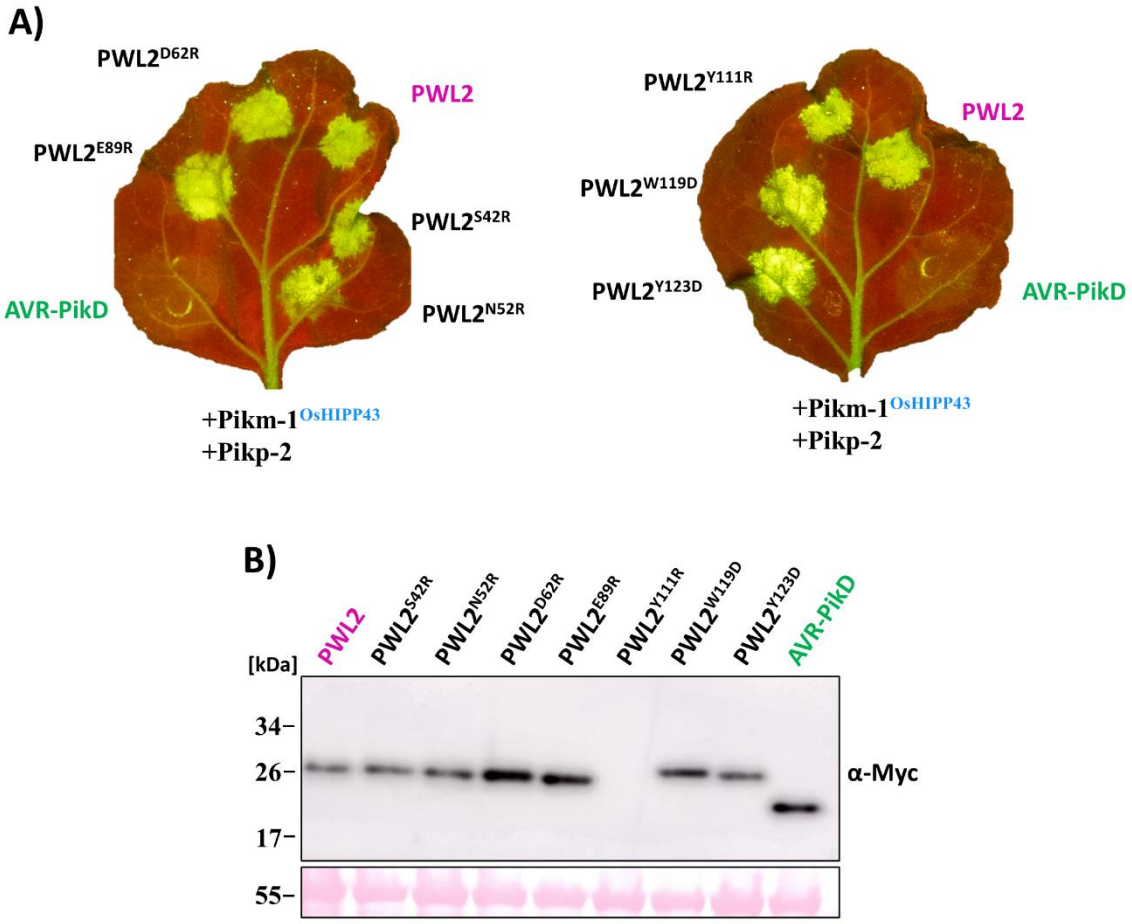

Figure 6.11 All single mutants of PWL2 are perceived by the chimeric Pikm-1^{OsHIPP43} receptor.

Indicated proteins were transiently overexpressed using agroinfiltration. ***A)*** *Leaf picture was taken at 5 dpi under the UV light, which allows to visualise the cell death response as green fluorescence.* ***B)*** *Western blot showing that all the effectors (apart from PWL2^{Y111R}) were expressed and accumulated to detectable level.*

Based on this I hypothesised that introducing a mutation in only one of the interfaces may not be enough to disrupt the binding between PWL2 and OsHIPP43, and several more spatially dispersed mutants may be required. Therefore, I introduced one mutation in each of the described interfaces and designed two triple mutants of PWL2. One mutant carried Ser42Arg, Asn52Arg and Trp123Asp mutations, and was designated as PWL2^{SNW}, while the second mutant combined the Glu89Arg, Asp62Arg and Tyr119Asp mutations, and was designated as PWL2^{EDY}. Additionally, I cloned a septuple mutant that combines all seven mutations previously listed, and this was designated as PWL2^{SNDEYWY}. I cloned PWL2^{SNW}, PWL2^{EDY} and PWL2^{SNDEYWY} and tested whether they can escape perception by the Pikm-1^{OsHIPP43}/Pikp-2 receptor in the cell death assay. Surprisingly, the triple mutants PWL2^{EDY} and PWL2^{SNW} were still perceived and triggered strong cell response when co-

expressed with Pikm-1^{OsHIPP43} and Pikp-2 (**Figure 6.12 A**). Only the septuple mutant PWL2^{SNDEYWY} was not perceived and no longer triggered cell death, despite being expressed and accumulated to the detectable level as shown by western blot analysis (**Figure 6.12 B**). These results show that the binding interface between PWL2 and OsHIPP43 is complex and introducing even triple mutations in the described binding interfaces are not sufficient to break the overall interaction.

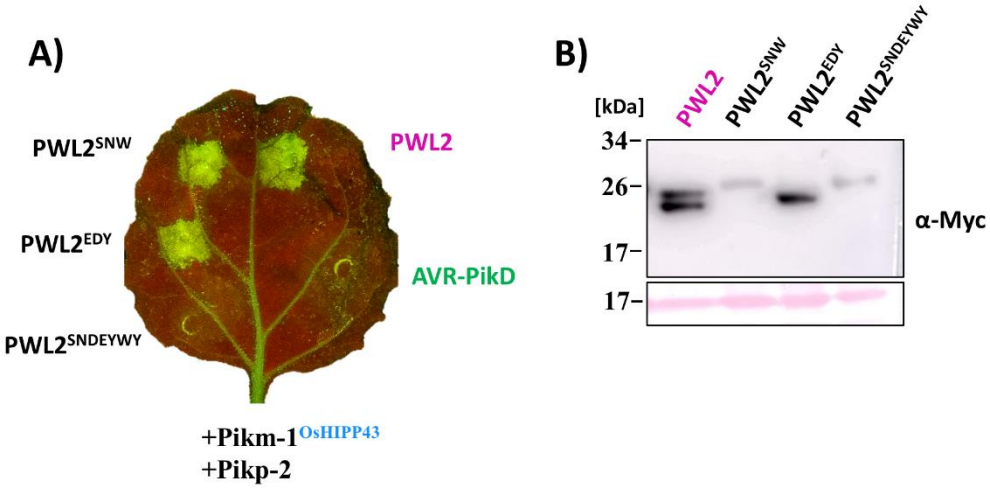

Figure 6.12 Septuple mutant PWL2^{SNDEYWY} is not perceived by chimeric Pikm-1^{OsHIPP43} receptor.

Indicated proteins were transiently overexpressed using agroinfiltration. ***A)*** *Leaf picture was taken at 5 dpi under the UV light, which allows to visualise the cell death response as green fluorescence.* ***B)*** *Western blot showing that all the effectors were expressed and accumulated to detectable level.*

To confirm that the loss of perception in the cell death assay was due to disrupted binding between PWL2^{SNDEYWY} and OsHIPP43, I purified the PWL2^{SNDEYWY} protein and tested whether it would still interact with the OsHIPP43 in the ITC experiment. PWL2^{SNDEYWY} was expressed with a GB1-tag following the protocols previously described (see Chapter 4 (**p. 106**)) and obtained the final protein, which was of sufficient amount and purity for biophysical analyses. Analysis of PWL2^{SNDEYWY} using CD showed that the protein is folded in similar overall pattern as wild type PWL2. This indicates that the introduced mutations did not disrupt the overall protein secondary structure (**Figure 6.13**).

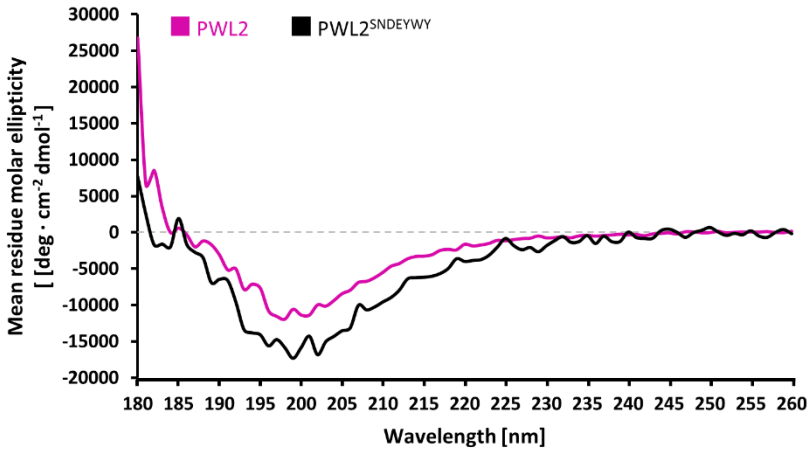

Figure 6.13 CD spectrum of PWL2 and PWL2^{SNDEYWY}.

Analysis of the spectrum suggests that both proteins adopt similar folding pattern.

However, due to potential intrinsically disordered nature of PWL2, the interpretation of this result should be made with caution and other techniques need to be used to confirm that the structural nature of the PWL2^{SNDEYWY} remains similar wild type. To investigate this, I used analytical size-exclusion chromatography to see whether the elution profile of PWL2^{SNDEYWY} remains similar to PWL2. Interestingly, significant shift of the elution peak was observed in the chromatogram, when compared to the wild type PWL2 (**Figure 6.14 A**).

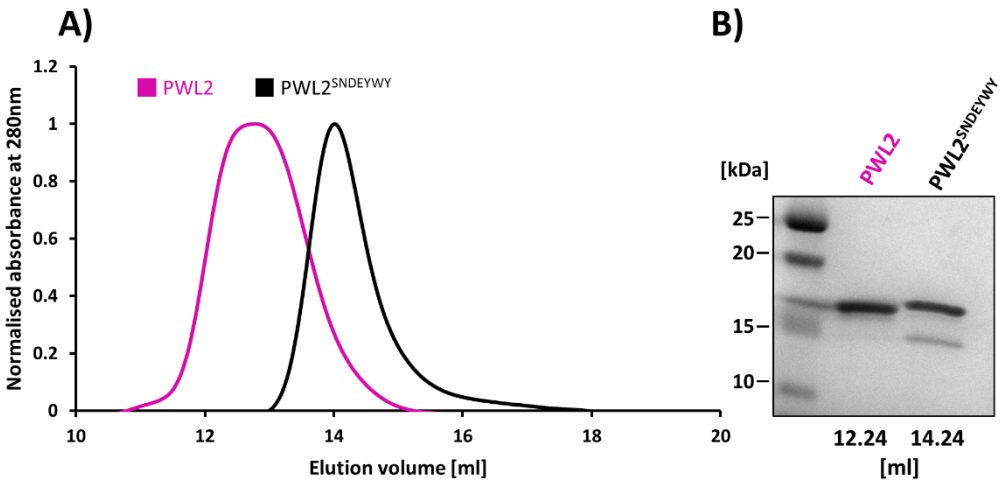

Figure 6.14 Analytical size-exclusion chromatography traces of PWL2 and PWL2^{SNDEYWY}.

Shift of the elution peak of PWL2^{SNDEYWY} indicates that introduced mutations changed the biophysical properties of the protein. ***B)*** *SDS-PAGE gel showing proteins eluted under the peaks.*

This indicates that the PWL2^{SNDEYWY} might adopt a differently folded form compared to wild type. This could affect the retention time on the column, as unfolded proteins can display the properties of smaller proteins (hence the later elution (peak shift to the right) observed for PWL2^{SNDEYWY}). SDS-PAGE analysis of the eluted proteins shows that the shift of the peak is not a result of protein degradation (**Figure 6.14 B**). The other possible explanation is that introduced mutations altered the overall folding of the protein, allowing certain hydrophobic residues to be exposed that could generate nonspecific interactions with the resin of the column and delay elution from the column. Finally, we cannot exclude the possibility that the introduced mutations disrupt the potential self-association properties of PWL2, and the observed elution peak is actually characteristic for the monomeric PWL2. Although at this stage it is hard to conclude how disruptive the introduced mutations were for the overall folding of PWL2, I tested whether it would still interact with OsHIPP43 in an ITC experiment.

ITC experiments were set up as described previously, placing concentrated (300 µM) OsHIPP43 in the syringe and injecting it into the experimental cell containing the purified PWL2^{SNDEYWY} at concentration of 20 µM. As shown in **Figure 6.15**, the binding between the two proteins was completely disrupted, and no heat exchange was measured upon injection. This indicates that PWL2^{SNDEYWY} no longer interacts with OsHIPP43, correlating with lack of perception in the cell death assay.

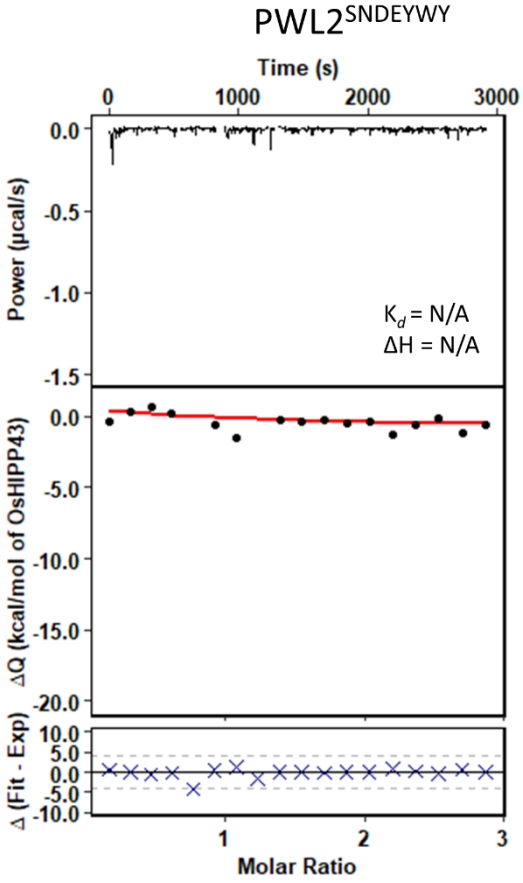

Figure 6.15 PWL2^{SNDEYWY} does not bind OsHIPP43 in vitro.

Upper panel- representative isotherm showing lack of heat exchange upon the injection of the HMA into the cell containing the effector. Middle panel- Integrated heats of injection from the technical replicates and global fit to a single site binding model calculated using AFFINImeter. Lower panel- calculated difference between predicted value of measurement (by global fit) and actual measurement.

As previously discussed, due to the rather extreme changes introduced into PWL2 to generate the PWL2^{SNDEYWY} variant, the disrupted binding with OsHIPP43 might be a result of misfolding of the effector, rather than targeted disruption of the binding interface. To investigate whether structure-guided mutations can decrease the binding affinity between the PWL2 and OsHIPP43 in vitro, I purified and tested in ITC the binding of PWL2^{SNW}, even though this was still perceived by the chimeric Pikm-1^{OsHIPP43} receptor in the cell death assays. I purified the PWL2^{SNW} with a GB1-tag, as described previously. The subsequent analysis of the sample by the CD revealed that PWL2^{SNW} displayed similar secondary features as wild type PWL2 (**Figure 6.16**). Analysis with analytical SEC showed that PWL2^{SNW} was eluting at the same volume as the wild type PWL2 (**Figure 6.17**), indicating that the introduced mutations did not alter the overall folding of the protein and its properties in vitro.

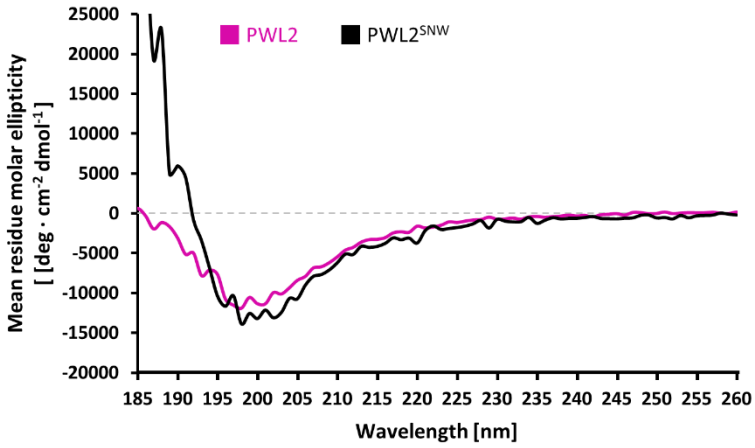

Figure 6.16 CD spectrum of PWL2 and PWL2^{SNW}.

Analysis of the spectrum suggests that both proteins adopt similar folding pattern.

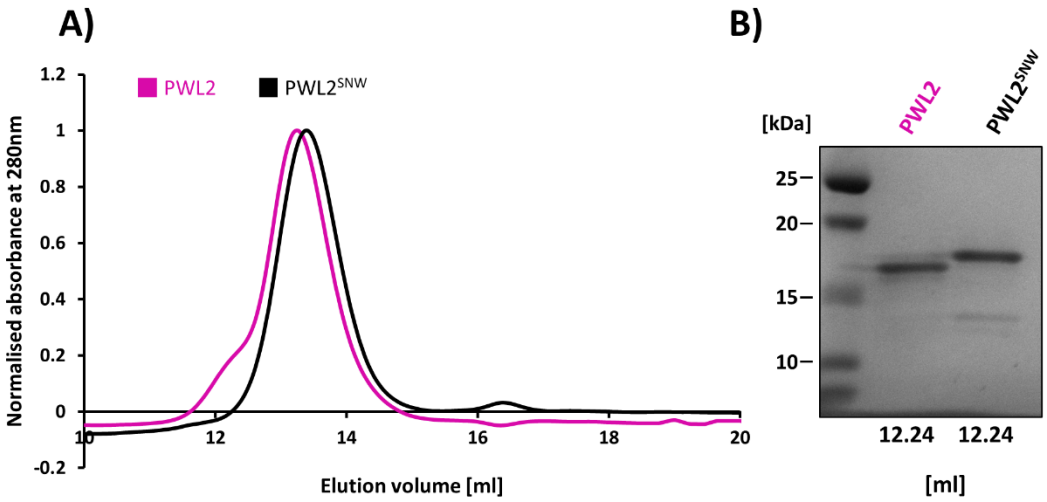

Figure 6.17 Analytical size-exclusion chromatography traces of PWL2 and PWL2^{SNW}.

A) *Shift of the elution peak of PWL2^{SNW} indicates that introduced mutations changed the biophysical properties of the protein.* ***B)*** *SDS-PAGE gel showing proteins eluted under the peaks.*

Using the same experiment setup as described previously, I tested the binding affinity between PWL2^{SNW} and OsHIPP43 by ITC. Interestingly, analysis of the isotherms by the AFFINIMETER software revealed that the proteins still bind with an affinity at the nanomolar range (**Figure 6.18**) (K_d = 357 nM) similar to the the K_d measured for the wild type PWL2 (191 nM).

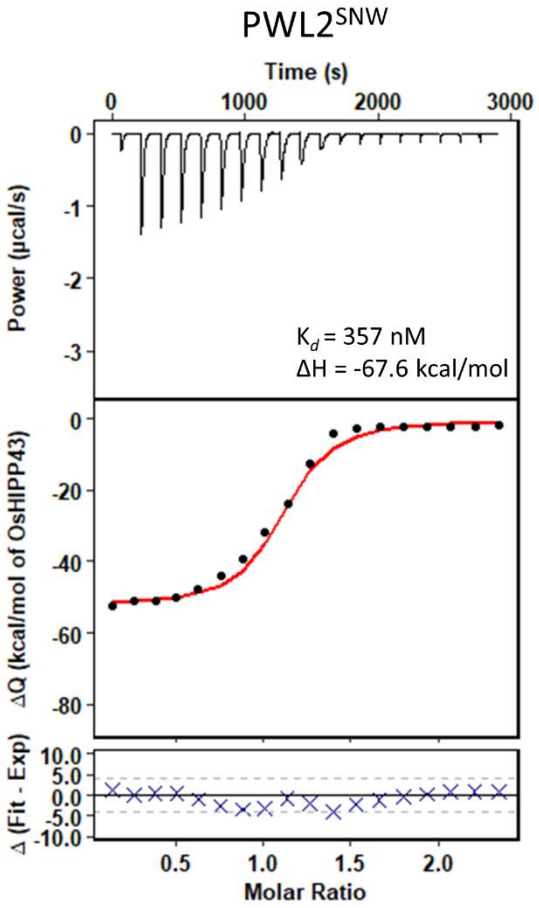

Figure 6.18 PWL2^{SNW} binds OsHIPP43 with nanomolar affinity.

Upper panel- representative isotherm showing heat exchange upon the injection of the HMA into the cell containing the effector. Middle panel- Integrated heats of injection from the technical replicates and global fit to a single site binding model calculated using AFFINImeter. Lower panel- calculated difference between predicted value of measurement (by global fit) and actual measurement.

These results indicate that the binding interface between PWL2 and OsHIPP43 is complex and can accommodate quite severe changes of amino acids designed to introduce steric and charged clashes within the interaction interface. This data suggests that to escape perception by the chimeric Pikm-1^{OsHIPP43} receptor, major changes must be introduced into the effector that might result in its misfolding or changes in its biochemical properties.

6.3 Discussion

In this Chapter, I described the X-ray crystal structure and characterisation of the PWL2 effector in complex with OsHIPP43. PWL2 adopts the characteristic MAX fold and therefore can be classified as a MAX effector, alongside other characterised effectors from *M. oryzae* including: AVR-PikD, APikL2, AVR-Pia, AVR-Pib, AvrPiz-t and AVR1-CO39 (Bentham et al., 2021a). Validation of the crystal structure through structure-guided mutations aimed at breaking the interaction between PWL2 and OsHIPP43 showed that the binding interface between these two proteins is extensive, and all single mutations can be accommodated within the structure, without affecting perception in the cell death assay.

6.3.1 PWL2 might be intrinsically disordered protein that folds upon binding to its interactor

In line with reports previously published in the literature (Schneider et al., 2010), PWL2 lacks major secondary structure features in solution and is readily digested by trypsin. Based on results in Chapter 4, I hypothesised that PWL2 may be highly unstructured in solution (or even intrinsically disordered), but may become fully folded upon binding its interactor. When the PWL2/OsHIPP43 complex was subjected to trypsin digest, I observed a 10 amino acid truncation at the C-terminus, leaving the rest of PWL2, and the entire OsHIPP43, intact. Subsequently, this complex was successfully crystallised. Ultimately, to confirm whether PWL2 is highly unstructured, complementary techniques, such as NMR, could be used (Fu and Vendruscolo, 2015).

Intrinsically disordered proteins (IDPs) are a change in the structure-function paradigm in protein world and are abundant in the proteomes of all the organisms (Uversky, 2010, Xue et al., 2012). They are usually enriched in charged amino acids that stabilise their unfolded state in hydrophilic cytoplasmic environment (Uversky et al., 2000). IDPs that undergo conformational changes in order to perform their biological function are called “inducible foldons” (Uversky, 2019). This can be dependent on several factors like environment (including temperature and pH) (Uversky et al., 1999, Uversky et al., 2002, Permyakov et al., 2003), post-translational modifications (Firman and Ghosh, 2018) or presence of the interactors (Tobi and Bahar, 2005, Zhang et al., 2013a). They can adopt different conformation depending on the interactor (Wright 2009), or part of the protein can remain disordered (fuzzy) (Gunasekaran et al., 2004), where the disordered part can still act as an epoxy for post-translational modifications (Sharma et al., 2015). Interestingly, disordered proteins can still have very high affinity to their interactors (Borg et al., 2007, Borgia et al., 2018).

6.3.2 PWL2 possesses MAX fold and large C-terminal extension

The crystal structure of the PWL2/OsHIPP43 complex revealed PWL2 to be a MAX effector. The characteristic β-sandwich fold of this family is located at the N-terminal part of the protein and is structurally most similar to the AVR-Pib effector (**Figure 6.19, Figure 6.20 A**), according to the Dali search (Holm, 2020), with RMSD 1.19 Å as calculated by ChimeraX software (Pettersen et al., 2021). Unlike the other MAX effectors, PWL2 has a large C-terminal extension that contains an α-helix and loop region that wraps around its interactor, OsHIPP43, in the complex. The α-helix contains residues 89EDKS92 that comprise the polymorphic region between PWL2 alleles. These residues mostly face away from the interface with OsHIPP43, with the exception of Glu-89. Mutating this residue to arginine did not break the interaction between PWL2 and OsHIPP43, suggesting it is not crucial for the interaction. The position of the polymorphic region suggests that OsHIPP43 is not involved in natural resistance to *M. oryzae* isolates expressing PWL2 alleles detected in weeping lovegrass, as it can be predicted that the binding between PWL2 and OsHIPP43 would not be affected by the polymorphisms present in the other alleles of PWL2. Mutations introduced into the C-terminal loop region of PWL2 did not disrupt the binding between PWL2 and OsHIPP43, suggesting that this region can be flexible in accommodating certain changes. The lack of secondary structures in this region raises the question of whether it could fold differently when binding to a different target? To date, we do not have evidence that OsHIPP43 is a biological target of PWL2, and it seems like natural resistance to PWL2 is based on different interface than formed with OsHIPP43 (Sweigard et al., 1995). This implies that there might be an alternative or additional interactor for PWL2 in nature and this interaction might cause the PWL2 to fold alternatively than it is when in complex with OsHIPP43. Although we do not know the biological significance of the PWL2/OsHIPP43 interaction, these findings are still useful for engineering new recognition specificity.

No:	Chain	Z	rmsd	lali	nres	%id	PDB	Description
1:	5z1v-B	6.6	1.9	54	61	20	PDB	MOLECULE: AVRPIB PROTEIN;
2:	6r5j-C	4.8	2.3	57	68	21	PDB	MOLECULE: UNCHARACTERIZED PROTEIN;
3:	2lw6-A	4.7	2.4	65	80	18	PDB	MOLECULE: AVRPIZ-T PROTEIN;
4:	2myv-A	4.4	2.2	57	79	16	PDB	MOLECULE: UNCHARACTERIZED PROTEIN;
5:	2mm2-A	4.4	2.4	54	65	13	PDB	MOLECULE: TOXB;
6:	6fub-B	4.3	2.6	57	93	16	PDB	MOLECULE: AVR-PIK PROTEIN;
7:	2myw-A	3.6	2.5	54	79	11	PDB	MOLECULE: AVR-PIA PROTEIN;

Figure 6.19 Dali homology search using PWL2 as query.

First seven hits of Dali search indicated MAX effectors.

The PWL2/OsHIPP43 interface partially resembles the binding interface formed between AVR1-CO39 and RGA5-HMA. In both complexes, the interaction between backbone atoms of the β2 strand of the effector and the β2 of the HMA domain forms a significant interface between the proteins (**Figure 6.20 B**). In contrast, the PWL2/OsHIPP43 binding interface is completely different from the one observed between AVR-PikD and Pikp-HMA, where the C-terminal β4 strand of Pikp-HMA forms an antiparallel β-sheet with β3 strand of AVR-PikD, positioning the effector on the opposite site of the HMA (**Figure 6.20 C**). The interaction interface of PWL2/OsHIPP43 complex is more intricate than described for other effector/HMA structures, which might underlie the differences in correlation between the cell death response and strength of binding between the effector and its HMA interactor observed here.

6.3.3 Binding between PWL2 and OsHIPP43 cannot be easily compromised

In the field, plant-pathogen interactions undergo a constant evolutionary arms race, where pathogens can escape perception by plant immune receptors by deleting or mutating effectors. AVR-Pik effectors occur in an allelic series, where only certain variants are recognised by certain Pik-1/Pik-2 receptors. It has been shown that single mutations introduced in the interfaces of the effectors were sufficient to disrupt the binding between the effector and the integrated Pik-1-HMA domain in vitro, which correlated with lack of response in in planta assays. No synonymous mutations have been observed between the alleles of AVR-Pik effectors, suggesting strong positive selection towards escaping perception (De la Concepcion et al., 2018). Introducing several structure-guided single and triple mutations into sequence of PWL2, with the aim of interfering with OsHIPP43 binding, did not prevent recognition of PWL2 in planta by the chimeric Pikm-1^{OsHIPP43} receptor. Only the septuple mutant was able to break the binding in vitro and escape perception in the cell death assay. However, introducing such extreme changes in the protein resulted in altered biophysical properties of PWL2, as shown by analytical size-exclusion chromatography. These data suggest that introducing the Pikm-1^{OsHIPP43} chimeric receptor in plants by generating stable transformants might provide a durable resistance towards *M. oryzae* carrying PWL2 effectors. Breaking the interactions between PWL2 and OsHIPP43 has proven challenging, and cannot be achieved unless extreme changes are introduced into the effector. Such changes might result in loss of effector function, which could affect the overall fitness of the pathogen making it an unfavourable evolutionary path.

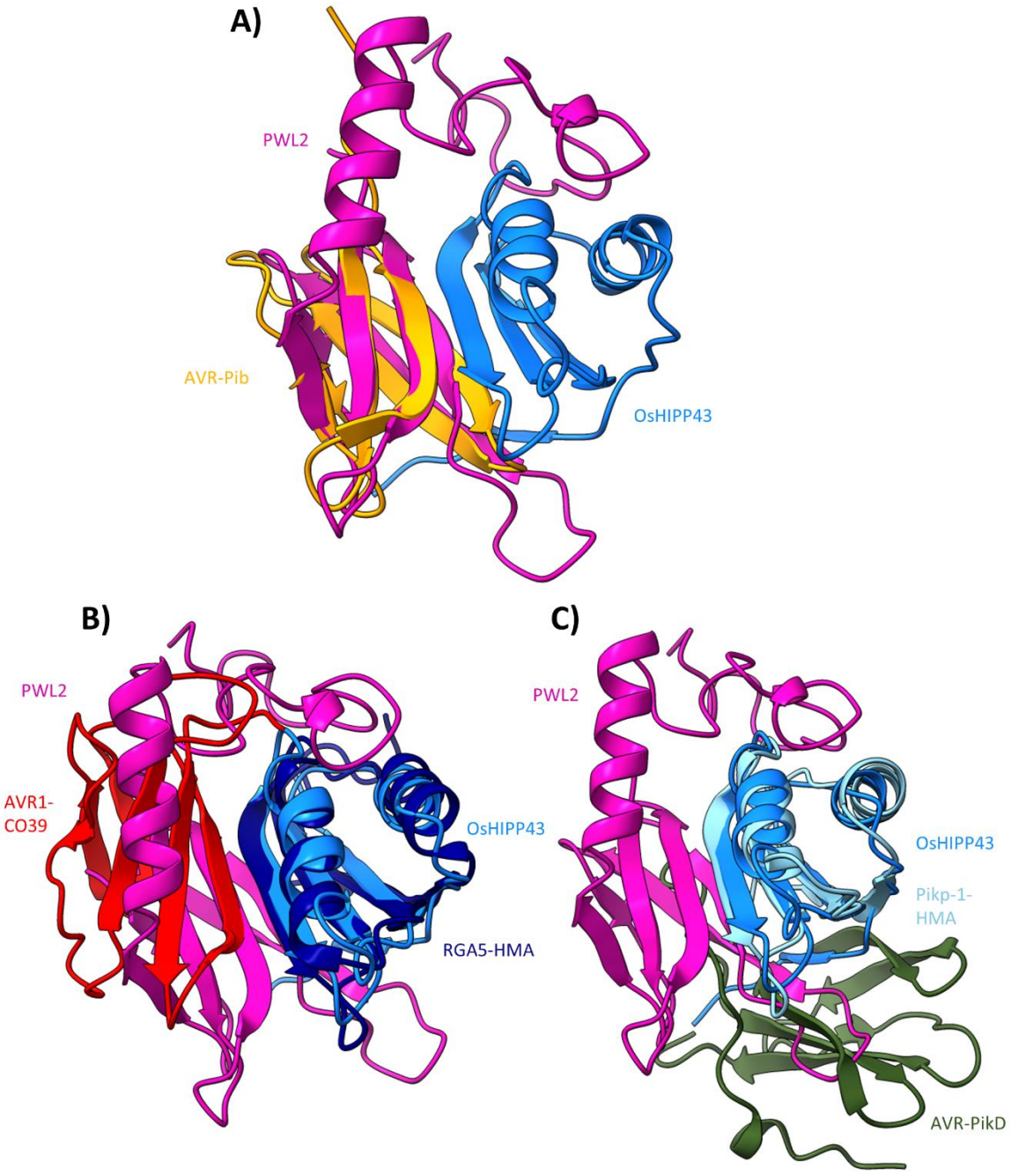

Figure 6.20 Superposition of selected structures with PWL2/OsHIP43 complex.

A) *PWL2/OsHIPP43 and AVR-Pib.* ***B)*** *PWL2/OsHIPP43 and AVR1-CO39/RGA5-HMA.* ***C)*** *PWL2/OsHIPP43 and AVR-PikD/Pikp-HMA.*

7

Recognition specificity of chimeric receptor Pikm-1^{OsHIPP43}

7 Recognition specificity of chimeric receptor Pikm-1^{OsHIPP43}

7.1 Introduction

PWL2 belongs to a larger PWL effector family, whose other members include PWL1, PWL3 and PWL4 (Kang et al., 1995). PWL2 shares amino acid sequence similarity to PWL1, PWL3 and PWL4 of 79%, 42% and 62%, respectively (signal peptide of these effectors was not included in the analysis, **Figure 7.1**). Initially, PWL1 and PWL2 were described as host determinant factors (*Magnaporthe* strains carrying PWL1 and PWL2 were unable to infect weeping lovegrass), whereas PWL3 and PWL4 were described as non-functional. Further analysis revealed that PWL4 encoded a functional protein when its expression was driven from the PWL1 or PWL2 promoter, with *Magnaporthe* carrying pPWL1::PWL4 or pPWL2::PWL4 being non-pathogenic on weeping lovegrass, however this was not demonstrated for PWL3. PWL3 and PWL4 were mapped to the same genetic locus, but PWL1 and PWL2 are located at two different loci, suggesting only PWL3 and PWL4 are allelic (Kang et al., 1995).

The PWL effectors are widely distributed across *M. oryzae* populations, including various host-specific lineages that infect plants from different genera, including *Oryza, Triticum, Digitaria, Setaria, Eleusine, Eragrostis* and more (Dr. Thorsten Langner, personal communication). Due to its widespread distribution, the PWL effector family is an interesting target for engineering resistance in crops. As highlighted in Chapter 6, conserved residues within the PWL effector family are potentially important for interaction between PWL2 and OsHIPP43 (**Figure 7.1,** indicated in red boxes). This suggests that PWL1, PWL3 and PWL4 could potentially bind to OsHIPP43.

In this Chapter, I set out to purify the effectors PWL1, PWL3 and PWL4, and measure their affinity to OsHIPP43 in vitro. I also investigated whether PWL1, PWL3 and PWL4 can be perceived in planta by chimeric receptor Pikm-1^{OsHIPP43}. These studies will shed light on the specificity of the Pikm-1^{OsHIPP43} receptor, and its potential utility for deploying in the field.

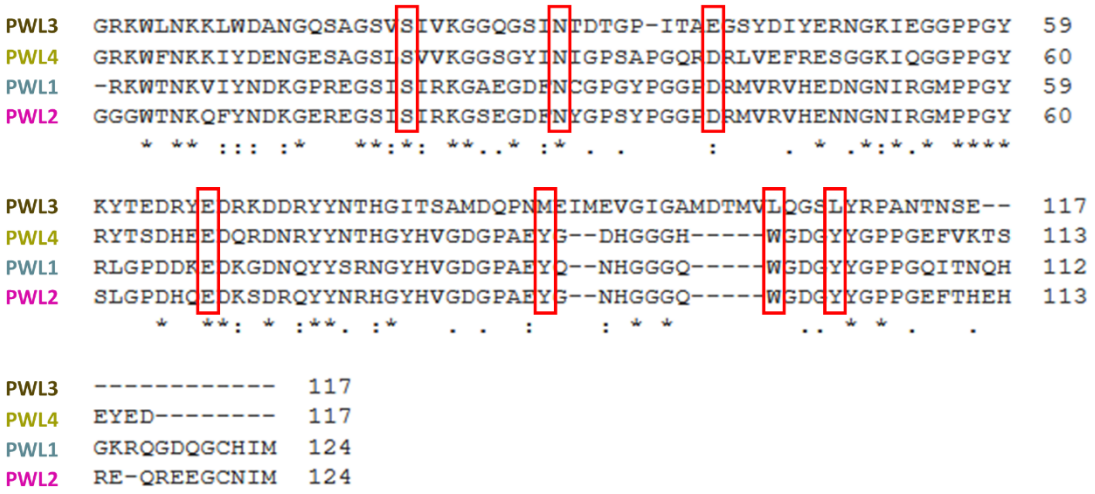

Figure 7.1 Alignment of PWL effector family.

Alignment of PWL1, PWL2, PWL3 and PWL4 effectors using Clustal Omega. Signal peptides of the effectors were not included in the analysis. Red boxes indicate residues identified as important for interaction in PWL2/OsHIPP43 complex, described in Chapter 6.

7.2 Results

7.2.1 Purification of PWL1 and PWL4

To enable the biophysical characterisation of binding between PWL1, PWL3 and PWL4 to OsHIPP43, I first set out to purify these effectors from *E. coli.* Initial expression and purification trials of PWL1 and PWL3 revealed that they are not stable in vitro, and they degrade to more stable products truncated by 13 and 10 amino acids respectively at their C-terminus (Dr. Abbas Maqbool, personal communication). A construct for expression of 6xHis-GB1-PWL1Δ13 was kindly provided by Dr. Abbas Maqbool. To generate constructs for PWL3Δ10 and PWL4 expression, I PCR-amplified the gene (using constructs provided by Dr. Vincent Were as template) and cloned into pOPIN expression vectors (pPGN-C (Bentham et al., 2021b)) using Golden Gate and including 6xHis-MBP and 6xHis-GB1 tags, respectively. In case of PWL3Δ10, an MBP tag was used to boost the protein expression, as fusion with a GB1 tag did not result in sufficient yield (data not shown). The expression and purification of PWL1Δ13 and PWL4 effectors were conducted as described for PWL2-3 in Chapter 4 (**p. 106)**. Both purifications yielded high amounts of protein, although some contamination was observed that may represent additional degradation (**Figure 7.2 A, B**). Attempts were made to prepare samples to minimise the presence of degradation. The identity of each protein was confirmed by intact mass spectrometry (**Figure 7.2 C, D**) and both PWL1Δ13 and PWL4 showed similar features to PWL2 when analysed by circular dichroism spectroscopy (**Figure 7.3**), suggesting a similar fold. Together, these data show that PWL1Δ13 and PWL4 are suitable for further experiments.

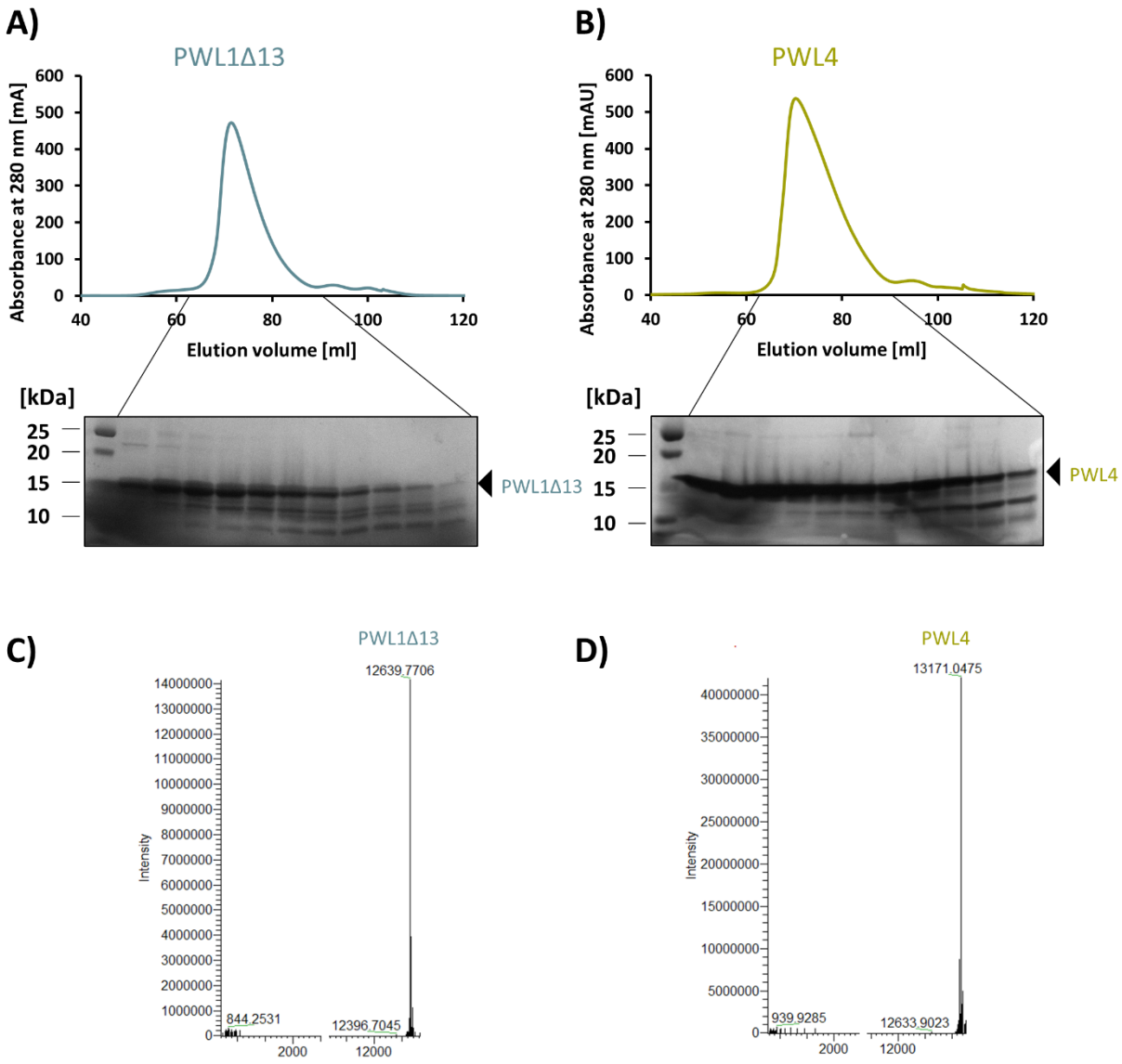

Figure 7.2 Purification of PWL effectors from *E. coli*.

*SDS-PAGE gels showing fractions from final size-exclusion chromatography (SEC) from **A)** PWL1Δ13 and **B)** PWL4 purifications. **C)** Measured intact mass (12639.77 Da) of PWL1Δ13 almost exactly matches the predicted mass (12638.83 Da). **D)** Measured intact mass (13171.05 Da) of PWL4 exactly matches the predicted mass (13171.06 Da).*

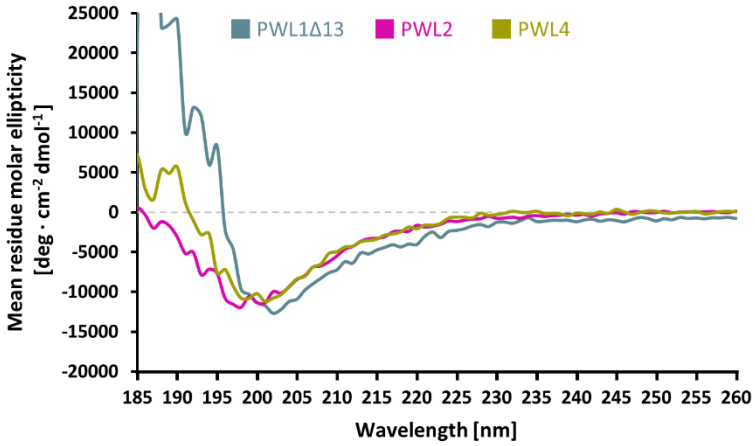

Figure 7.3 CD spectrum of PWL1Δ13, PWL2 and PWL4.

Analysis of the spectrum suggests that all the proteins adopt similar folding pattern. PWL2 spectrum is identical as presented in Chapter 4, here included for comparison.

7.2.2 Purification of PWL3

Expression and purification of PWL3 proved to be more challenging. Initial expression in *E. coli* did not give sufficient yield for further experiments, even upon scaling up the production (16 L of medium vs regular 8 L, see Materials and Methods, **p. 56**) (**Figure 7.4 A**). After further purification steps (tag cleavage and removal), the protein was still significantly contaminated (**Figure 7.4 B**), although this contamination could be separated by a final size-exclusion chromatography (SEC) step (**Figure 7.4 C**). Peptide mapping analysis by mass spectrometry showed the lower molecular mass band on the gel comprised PWL3Δ10, therefore fractions in lanes 6 - 10 on the SDS-PAGE gel from the final SEC purification step (**Figure 7.4 C**) were selected for further analysis. Due to time constraints the purification of PWL3 could not be optimised. However, enough PWL3 was produced for preliminary ITC experiments.

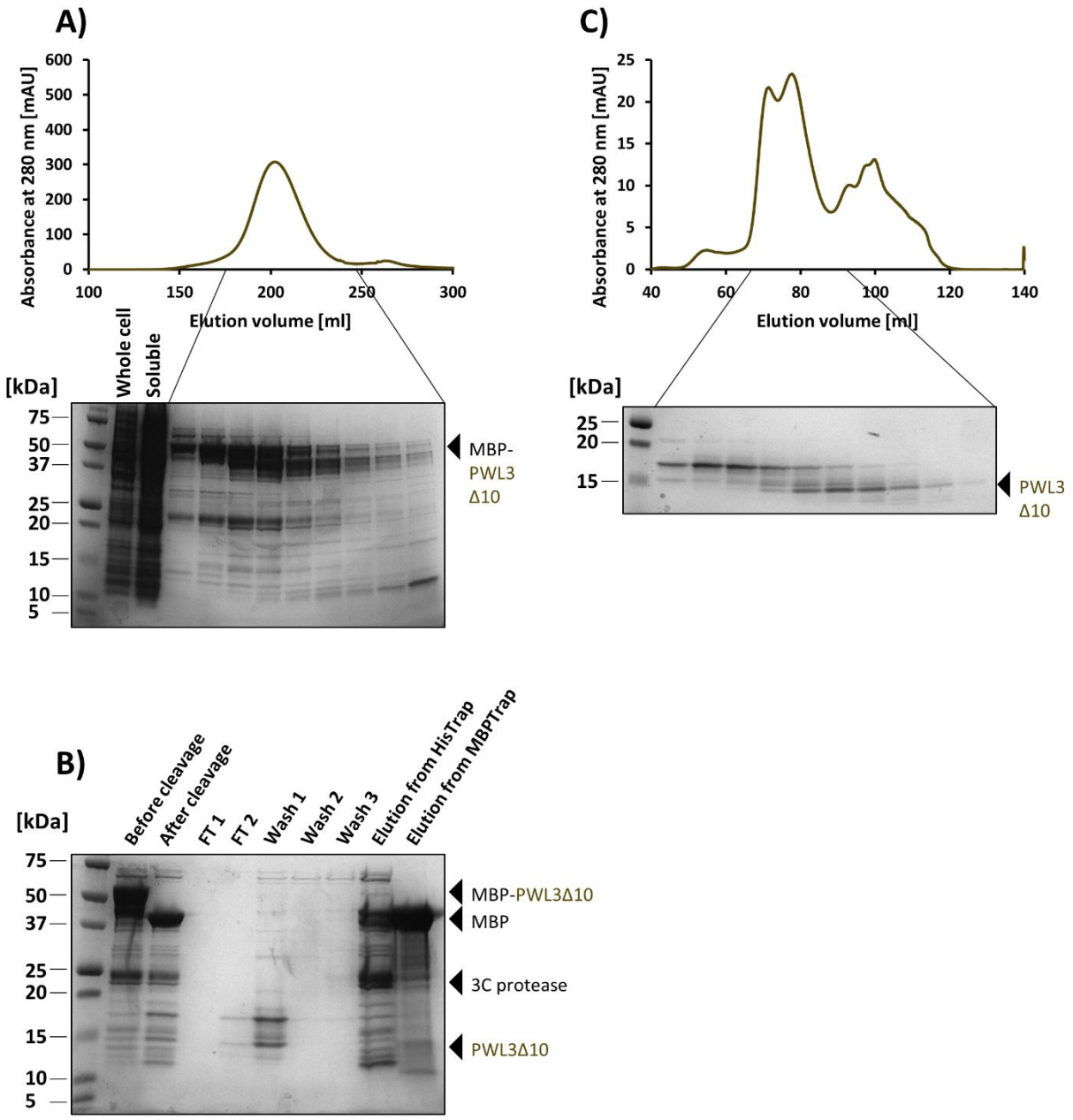

Figure 7.4 Purification of PWL3Δ10 from *E. coli.*

A) *SDS-PAGE gel showing Whole cell and Soluble fractions from E. coli expressing pOPIN-M:PWL3Δ10. Further lanes show fractions corresponding to the indicated fragment of SEC trace.* ***B)*** *SDS-PAGE gel showing fractions before and after cleavage of the tag, and subsequent steps of manual purification.* ***C)*** *SDS-PAGE gel showing fractions from final SEC.*

7.2.3 PWL1, PWL3 and PWL4 bind OsHIPP43 in vitro

As for PWL2 alleles, PWL2-2 and PWL2-3 (Chapter 4), I also did not use analytical SEC for a qualitative assessment of an interaction between PWL effectors and OsHIPP43, and proceeded immediately to the ITC analysis. The experiments were set up as described for PWL2 in Chapter 4 with the effectors placed in the experimental cell at concentration of 20 µM, and OsHIPP43 was placed in the syringe at 300 µM (for details see Materials and Methods, **p. 59**). The isotherms obtained were subsequently analysed with the AFFINIMeter software. Both PWL1Δ13 and PWL4 displayed binding to OsHIPP43 in vitro, with K_d = 147 nM and K_d = 124 nM, respectively (**Figure 7.5**). Both effectors also demonstrated high heat exchange upon binding to OsHIPP43: ΔH = -81.5 kcal/mol and ΔH = -80.2 kcal/mol for PWL1Δ13 and PWL4 respectively. These values are very similar to the values obtained of PWL2 binding to OsHIP43 (K_d = 191 nM and ΔH = -67.6 kcal/mol).

Analysis of interaction between PWL3Δ10 and OsHIPP43 could not be optimised due to time constrains, and insufficient amount of purified PWL3Δ10. However, the preliminary data collected was analysed with the AFFINIMeter software. This analysis showed that PWL3Δ10 binds OsHIPP43 with K_d = 1.04 µM (**Figure 7.6**), which is one order of magnitude less than measured for other effectors in this study. The heat exchange for the PWL3Δ10/OsHIP43 interaction was around two times lower than measured for other PWL effectors, with a value of ΔH = -35.5 kcal/mol. These results need repetition, optimisation and validation. However, this work is beyond the scope of this thesis.

Although characterisation of the PWL3Δ10/OsHIPP43 binding requires further optimisation and confirmation, these results show that all the PWL effectors tested: PWL1Δ13, PWL3Δ10 and PWL4 display affinity to the OsHIPP43 in vitro, and PWL1Δ13 and PWL4 binds the OsHIPP43 with the same strength as PWL2. To see if in vitro binding correlates with response in planta, I sought to determine whether the chimeric Pikm-1^{OsHIPP43} receptor could respond to PWL1, PWL3 and PWL4 in cell death assay.

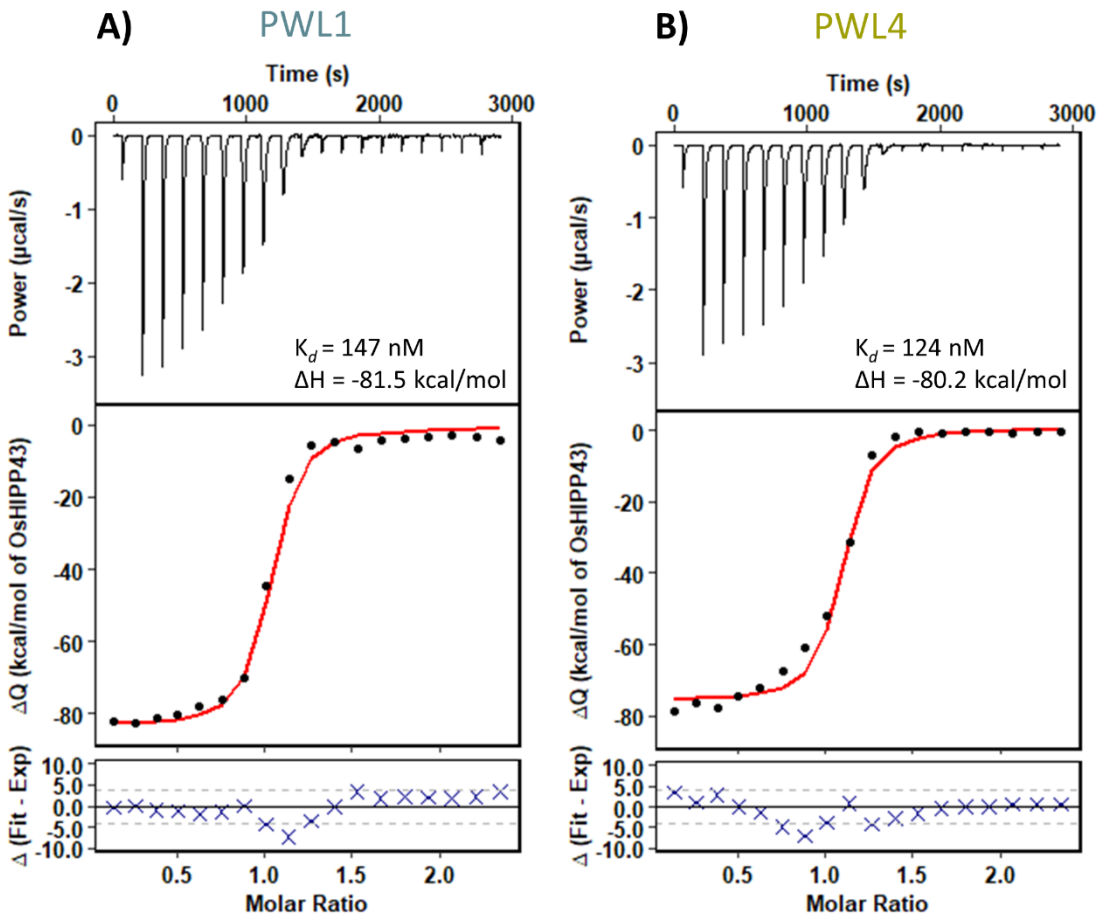

Figure 7.5 PWL1 and PWL4 bind OsHIPP43 with nanomolar affinity.

A) *PWL1Δ13 and* ***B)*** *PWL4 interact with OsHIPP43 in vitro. Upper panel- representative isotherm showing heat exchange upon the injection of the HMA into the cell containing the effector. Middle panel- Integrated heats of injection from the technical replicates and global fit to a single site binding model calculated using AFFINImeter. Lower panel- calculated difference between predicted value of measurement (by global fit) and actual measurement.*

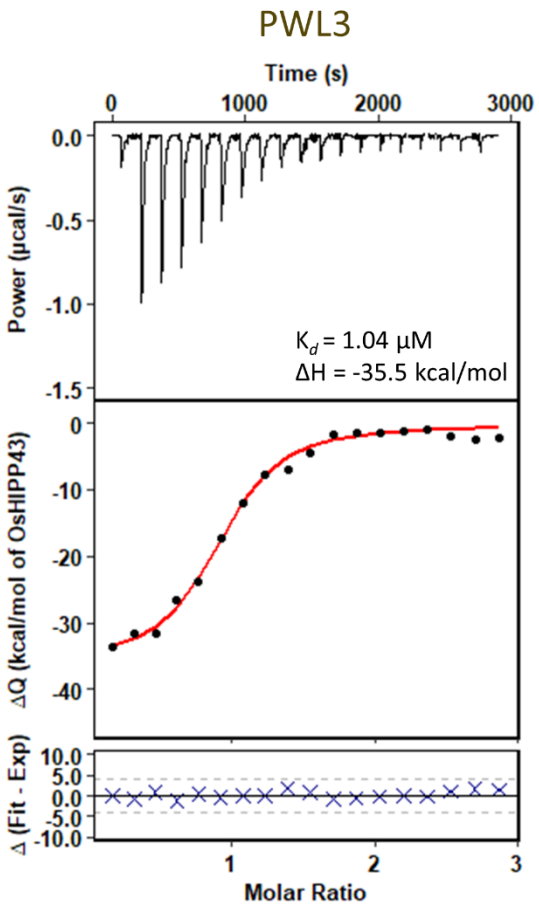

Figure 7.6 PWL3 binds OsHIPP43 with micromolar affinity.

Upper panel- representative isotherm showing heat exchange upon the injection of the HMA into the cell containing the effector. Middle panel- Integrated heats of injection from the technical replicates and global fit to a single site binding model calculated using AFFINImeter. Lower panel- calculated difference between predicted value of measurement (by global fit) and actual measurement.

7.2.4 In planta recognition of PWL1, PWL3 and PWL4 by chimeric Pikm-1^{OsHIPP43}

I cloned the full-length sequences of PWL1, PWL3 and PWL4, only lacking the signal peptides, into plant expression vectors via Golden Gate cloning with a C-terminal 4xMyc tag, and under control of the AtUbi10 promoter for cell death assays. Subsequently, I co-expressed these effectors with Pikm-1^{OsHIPP43} and Pikp-2 receptors in *N. benthamiana* leaves, along with PWL2 and AVR-PikD that served as a positive and negative control, respectively.

Each of the effectors PWL1, PWL2, PWL3 and PWL4, but not AVR-PikD, were recognised by the chimeric Pikm-1^{OsHIPP43} receptor and triggered strong cell death upon co-expression (**Figure 7.7 A**). Analysis by western blot showed the presence of PWL1, PWL2 and AVR-PikD could be detected, but not PWL3 and PWL4, indicating that these two effectors might be less stable on overexpression in planta and not suitable for detection by western blot analysis.

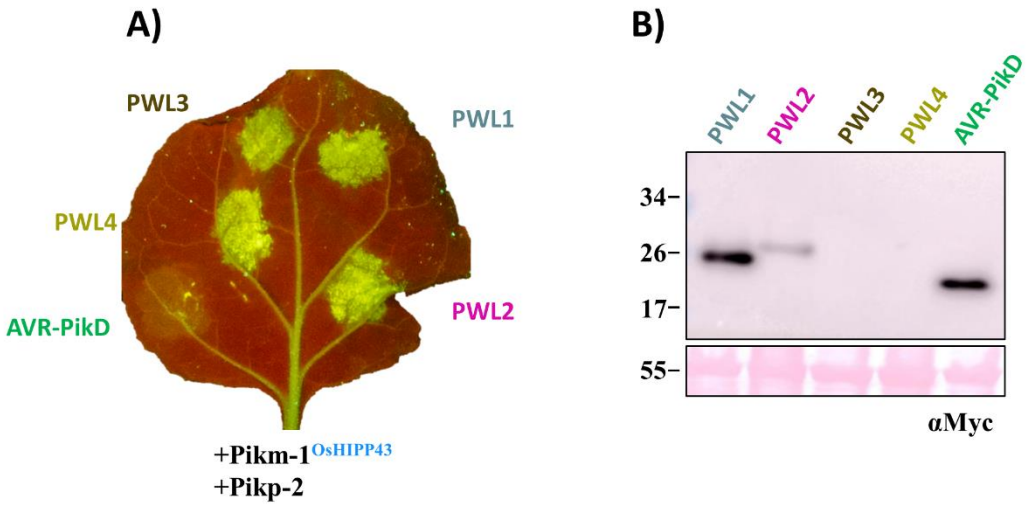

Figure 7.7 PWL1, PWL2, PWL3 and PWL4 are perceived by the chimeric Pikm-1^{OsHIPP43} receptor.

Indicated proteins were transiently overexpressed using agroinfiltration. ***A)*** *Leaf picture was taken at 5 dpi under the UV light, which allows to visualise the cell death response as green fluorescence.* ***B)*** *Western blot showing that PWL1, PWL2 and AVR-PikD were expressed and accumulated to detectable level. PWL3 and PWL4 could not be detected, despite triggering a response in the cell death assay.*

To troubleshoot this, I cloned and tested C-terminally truncated and N-terminally tagged variants of PWL3 and PWL4: PWL3Δ10:Myc, PWL4Δ3:Myc, PWL4Δ7:Myc, Myc:PWL3 and Myc:PWL4. For consistency, I also cloned corresponding constructs for other effectors: PWL1Δ11:Myc, PWL2Δ10:Myc, Myc:PWL1 and Myc:PWL2. I used wild type PWL2:Myc and PWL2^{SNDEYWY} as positive and negative control, respectively. The presence of all the effector variants was perceived by Pikm-1^{OsHIPP43}/Pikp-2 (apart from PWL2^{SNDEYWY}) (**Figure 7.8 A, C**). However, consistent with previous result, PWL3 and PWL4 constructs could not be detected on western blot (**Figure 7.8 B, D**). Interestingly, N-terminally tagged Myc:PWL1 and Myc:PWL2 also could not be detected on western blot (**Figure 7.8 B, D**), suggesting that N-terminal tagging of PWL effectors is not suitable for western blot analysis.

Taken together, these results show that the chimeric Pikm-1^{OsHIPP43} receptor can perceive a wide range of effectors belonging to the PWL family, which further strengthens its potential utility for deployment in the field.

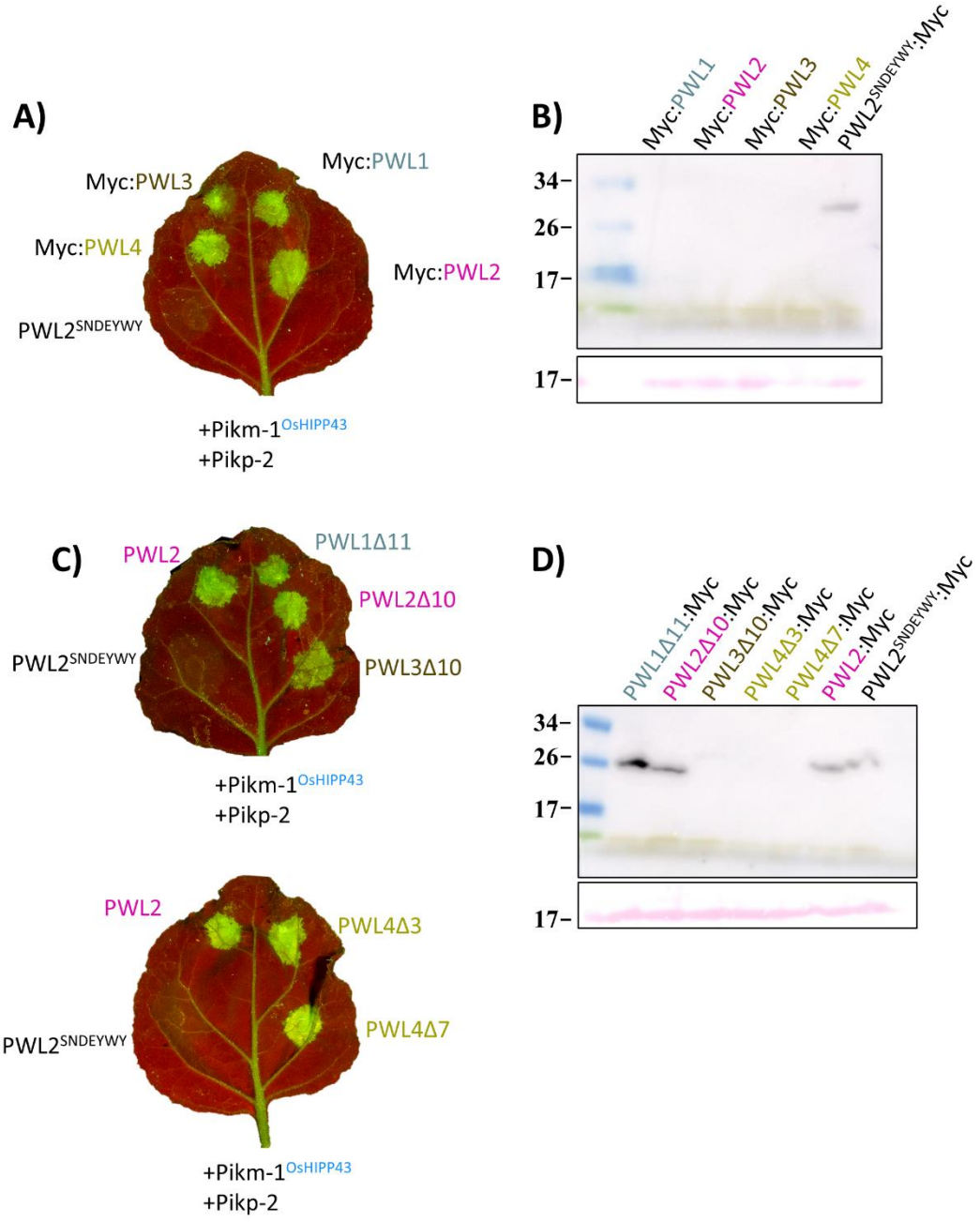

Figure 7.8 Truncated and diffrentially tagged PWL effectors are perceived by Pikm-1^{OsHIPP43}.

Indicated proteins were transiently overexpressed using agroinfiltration. ***A) C)*** *Leaf picture was taken at 5 dpi under the UV light, which allows to visualise the cell death response as green fluorescence.* ***B)*** *Western blot showing that N-terminally tagged PWL effectors are not detectable with this technique.* ***D)*** *Western blot showing that PWL1Δ11, PWL2Δ10, PWL2 and PWL2^{SNDEYWY} were expressed and accumulated to detectable level. PWL3Δ10 and PWL4Δ3 and PWL4Δ7 could not be detected, despite triggering a response in the cell death assay.*

7.3 Discussion

The sequences of the PWL1, PWL3 and PWL4 effectors are divergent from the PWL2, only sharing 79%, 42% and 62% similarity with PWL2, respectively. In this Chapter, I demonstrated that all the PWL effectors interact with OsHIPP43. The PWL1, PWL3 and PWL4 effectors each bind to OsHIPP43 in vitro within the micro- to nano-molar range, and all the effectors are recognised by the chimeric Pikm-1^{OsHIPP43} receptor when transiently expressed in planta. Together, these data suggest that PWL effectors, despite diverse sequences, retain binding to the potential target, probably due to the structure conservation. This strengthens the hypothesis that OsHIPP43 could be an actual biological target of PWL effectors.

7.3.1 What makes OsHIPP43 an interesting target for PWL effectors?

To better understand its role in pathogenicity, it is important to elucidate the biological function of OsHIPP43. Analysis reported by de Abreu Neto and colleagues (de Abreu-Neto et al., 2013) showed that expression of OsHIPP43 was downregulated in Fe deficiency, but was not altered in response to Cd, Pb or Cr (VI) deficiency, suggesting that OsHIPP43 might be involved specifically in iron homeostasis in plants. It would be interesting to see whether its expression would be elevated in presence of higher iron concentrations. If so, it would be possible that OsHIPP43 is responsible for detoxification of plant cells by removing excess Fe. The canonical metal binding motif in HMA proteins consists of MxCxxC residues (where x represents any amino acid). This motif is degenerated in the integrated HMA domains (Maqbool et al., 2015), but is conserved and potentially functional in OsHIPP43 (formed by residues MDCEGC). This is expected, as all the HIPP proteins are thought to be involved in heavy metal homeostasis, therefore should possess the ability to bind the heavy metal atoms. However, I did not detect any heavy metal atom in the crystal structure of OsHIPP43, and instead, a disulphide bond was found in the metal-binding loop.

The presence of this disulphide bond might be an artifact of protein production in a heterologous system that specifically supports the disulphide bond formation. However, it is possible that special environment conditions (e.g., redox potential) are required for a heavy metal to bind. In the crystal structure, the metal binding loop of OsHIPP43 is facing away from the PWL2 binding interface, and it seems likely that the role of the effector is not to compromise metal binding in the HMA protein. AVR-PikD has been shown to stabilise its HMA targets in planta (Oikawa et al., 2020). It would be interesting to see whether PWL2 also stabilises OsHIPP43. Such stabilisation, without compromising the metal binding ability might promote removal of toxic ions from the host cell, which would be beneficial for the pathogen. A similar mechanism has been reported for another rice pathogen, *Xanthomonas oryzae pv oryzae* (Xoo) (Yuan et al., 2010), the causal agent of rice blight disease. Xoo

is sensitive to Cu, and many pesticides based on copper proved to be effective in controlling rice blight. Xoo secretes an effector that activates transcription of rice susceptibility gene Xa13 which in turn, together with copper transporters COPT1 and COPT5, promotes removal of toxic Cu from plant cells.

7.3.2 HMA proteins as susceptibility factors

HMA-containing proteins have been reported to be susceptibility factors multiple times (Oikawa et al., 2020). AtHIPP3 is expressed in Arabidopsis upon inoculation with *Pseudomonas syringae pv tomato* (but not when challenged with *P. syringae hrc*- mutant which is unable to deliver effectors. Overexpression of AtHIPP3 affects expression of ca. 400 other genes. Analysis of expression patterns revealed that it might play a role in negative regulation of the salicylate-dependent pathway (Zschiesche et al., 2015). Intriguingly, some HIPPs have been shown to be susceptibility factors for a wide range of pathogens (Radakovic et al., 2018). AtHIPP27 is important for the nematode *Heterodera schachtii*, as its expression level was significantly elevated in syncytia and Arabidopsis *hipp27* knockout mutants were significantly less susceptible, although their level of basal resistance, as measured by expression of defence marker genes and ROS burst upon flg22 treatment, remained the same (Radakovic et al., 2018). NbHIPP26 from *N. benthamiana* interacts with the TGB1 protein from Potato mop-top virus (PMTV) and plays a role in viral long-distance movement throughout the plant tissues (Cowan et al., 2018). OsHIPP05 from rice was described as a major susceptibility factor upon challenging with rice blast. Knocking out HIPP05 in rice conferred increased resistance to *M. oryzae*, and Arabidopsis lines overexpressing HIPP05 become susceptible to the pathogen (switching from non-host to a host status) (Nakao et al., 2011).

7.3.3 Effectors from the PWL family might be structurally conserved

Retaining binding to a putative biological target likely requires that effectors display similar structural features, despite low sequence homology. The CD spectrum of PWL1 and PWL4 was similar that of PWL2, indicating that PWL1 and PWL4 may also be highly unstrucutred before binding to a target like OsHIPP43. Further experiments, such as limited trypsin digest, are required to confirm this hypothesis.

AlphaFold2 is a recent breakthrough in the field of protein fold prediction (Jumper et al., 2021). It can predict protein structures with high accuracy, even when no homologous model is available. I used AlphaFold2 to predict the structures of PWL1, PWL3 and PWL4. The analysis revealed that all the PWL effectors are predicted to contain the MAX fold (**Figure 7.9 A**), supporting the hypothesis that they retained the same structural features despite diverging in sequence. Structure comparison revealed that PWL1, PWL3 and PWL4 are very similar to crystal structure of PWL2 with

RMSDs of 0.866 Å, 0.949 Å and 0.980 Å, over 49, 66, 56 atoms respectively. Interestingly, the C-terminal part of all the effectors was predicted to be largely unstructured (**Figure 7.9 B**). Determination of crystal structures of PWL1, PWL3 and PWL4 in complex with OsHIPP43 is not only important to confirm these predictions, but will also allow for the elucidation of how the polymorphic residues in different PWLs are accommodated in the complex, or whether they differentially contribute to binding. An alternative approach to confirm that the binding interface is conserved between the PWL effectors is to find a combination of mutations (based on the PWL2/OsHIPP43 structure) that disrupts the interaction between PWL2 and OsHIPP43, without affecting biophysical properties of the effector, and subsequently test whether the same mutations would disrupt binding between OsHIPP43 and PWL1, PWL3 and PWL4. However, this work is beyond the scope of this thesis.

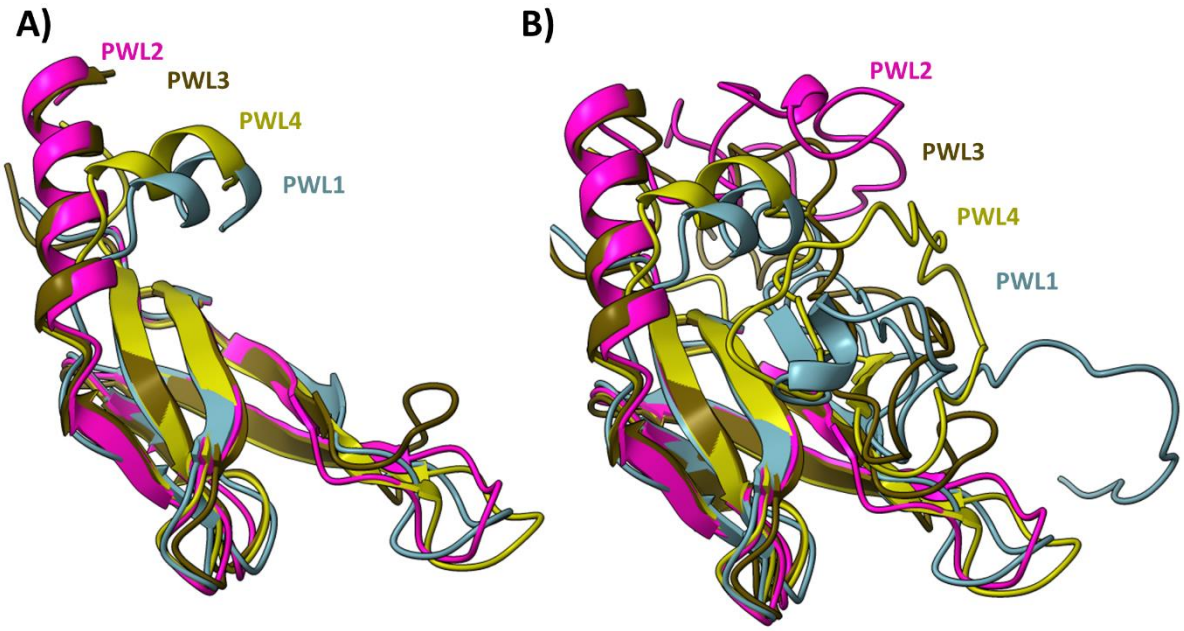

Figure 7.9 Structure prediction of PWL1, PWL3 and PWL4.

A) *AlphaFold2 prediction of PWL1, PWL3 and PWL4 revealed that all these effectors possess a MAX fold highly similar to the one present in crystal structure of PWL2.* ***B)*** *PWL1, PWL3 and PWL4 effectors are predicted to contain largely unstructured C-terminal region, similarly as observed in crystal structure of PWL2.*

The chimeric receptor Pikm-1^{OsHIPP43} can perceive all tested members of PWL effector family. This includes the PWL3 effector that is only 42% similar to the PWL2 in sequence and binds to the OsHIPP43 with seemingly lower affinity (within the micromolar range). Despite the lower apparent binding affinity of PWL3 to OsHIPP43, the Pikm-1^{OsHIPP43} seems an excellent candidate for field deployment, as it still promotes cell death and may confer resistance to wide range of *M. oryzae*

strains that express PWL effectors. This resistance may not be easily overcome by the pathogen, as multiple alterations of the sequence cannot break the interaction between the PWL effector and OsHIPP43, unless the biophysical properties of the effector (i.e., the fold) are changed. Gene loss may be necessary to escape perception, which might come with a fitness cost and decreased pathogenicity at the population level.

Taken together, these results demonstrate the potential of using potential biological targets of pathogen effectors as integrated domains in engineering novel resistance in plants. It will be interesting to test whether stable expression of Pikm-1^{OsHIPP43}/Pikp-2 in crops such as barley, rice and wheat will provide resistance to *M. oryzae* strains carrying the PWL effectors.

8

The solution structure of AVR-Pias

8 The solution structure of AVR-Pias

8.1 Introduction

Recently discovered genetically linked CC-NLRs Pias-1 and Pias-2 from rice confer resistance to *M. oryzae* strains carrying the AVR-Pias effector (Shimizu et al., 2021). Interestingly, Pias-1 shares 96.6% DNA sequence similarity with RGA4 and displays auto-activity when expressed alone in *N. benthamiana* plants. However, Pias-2 has only 59.8% DNA sequence similarity to RGA5 and possess different domain at its C-terminus, called DUF761 (Domain of Unknown Function 761). When transiently overexpressed together, RGA5 can inhibit the auto-activity of Pias-1, however in presence of Pias-2, the cell death triggered by Pias-1 seems to be enhanced, even in the absence of the effector. This suggests different working model between these two pairs of NLRs (Shimizu et al., 2021).

In rice, Pias-1/Pias-2 perceives the AVR-Pias effector, initially cloned from *M. oryzae* strain 2012-1. AVR-Pias is 91 amino acids in length, and does not share any significant sequence similarity to any other known effector. However, a Toxin18-like motif (12 amino acids) has been predicted at its C-terminus. To date, despite several attempts, no direct interactions between AVR-Pias and Pias-2 have been detected. It is possible that recognition of AVR-Pias by Pias-2 might require an intermediate interactor, as has been observed for AVR-Pii, which is recognised by the corresponding NLR Pii-2 only when it is bound to its interactor Exo70-F3 (Fujisaki et al., 2015, Fujisaki et al., 2017). However, to date, no direct interactors for the AVR-Pias effector have been found, and its biological role has not been elucidated.

In this Chapter, I set out to purify and determine the structure of the AVR-Pias effector. This work might inform the future directions for studies of the Pias/AVR-Pias system.

8.2 Results

8.2.1 AVR-Pias can be purified from *E. coli*

The coding sequence of AVR-Pias effector was synthesised (IDT oligo) and cloned into the pOPIN-M expression vector that fuses N-terminal 6xHis-MBP tag to the protein of interest. The sequence was cloned without the predicted signal peptide, spanning residues Ala-18 to Glu-91. Analysis of the amino acid sequence revealed presence of four cysteine residues, indicating a possibility of at least one disulphide bridge in the protein. Therefore, I chose the *E. coli* SHuffle strain for expression of the construct, as this strain better supports disulphide bond formation in the bacterial cytoplasm. The construct was expressed on a small scale (2 L of LB medium vs. standard 8 L) and subsequent steps to obtain clarified lysate were conducted as described previously (See Material and Methods, **p. 56**). The lysate was incubated with 1 ml of Ni-NTA resin (equilibrated in the lysis buffer) for 20 min and transferred into a gravity-flow column. The resin was washed two times with lysis buffer (5 ml/wash) and the protein was eluted with 1 ml of elution buffer containing 500 mM imidazole. Samples were collected throughout the process and inspected by SDS-PAGE. The 6xHis-MBP-AVR-Pias construct was well expressed and soluble (**Figure 8.1 A**). Although an intense band representing the protein of interest can be observed in the elution fraction, the majority of the protein seemed to be still in the flow through fraction, indicating that the resin used in this process was saturated (**Figure 8.1 A**). The flow through fraction was subsequently loaded on ÄKTAxpress for IMAC coupled with size-exclusion chromatography (SEC), as described for other protein purifications described in this thesis (see Chapter 4 (**p. 91**)) (data not shown). Relevant fractions from the SEC were combined and incubated with 3C protease overnight, and subsequently purified manually using HisTrap™ and MBPTrap columns in tandem. As revealed by SDS-PAGE, AVR-Pias displayed weak affinity to the Ni-NTA resin and was found in the flow through and Wash 1 fractions, when eluted with the low concentration of imidazole (**Figure 8.1 B**). These fractions were combined and submitted for SEC. SDS-PAGE indicated that the final product was smaller (ca. 6 kDa) than expected (8.1 kDa). However, it was of very high purity, as a single band was observed on the gel (**Figure 8.1 C**). The protein was directly submitted for crystallisation trials, as listed in **Table 8-1**

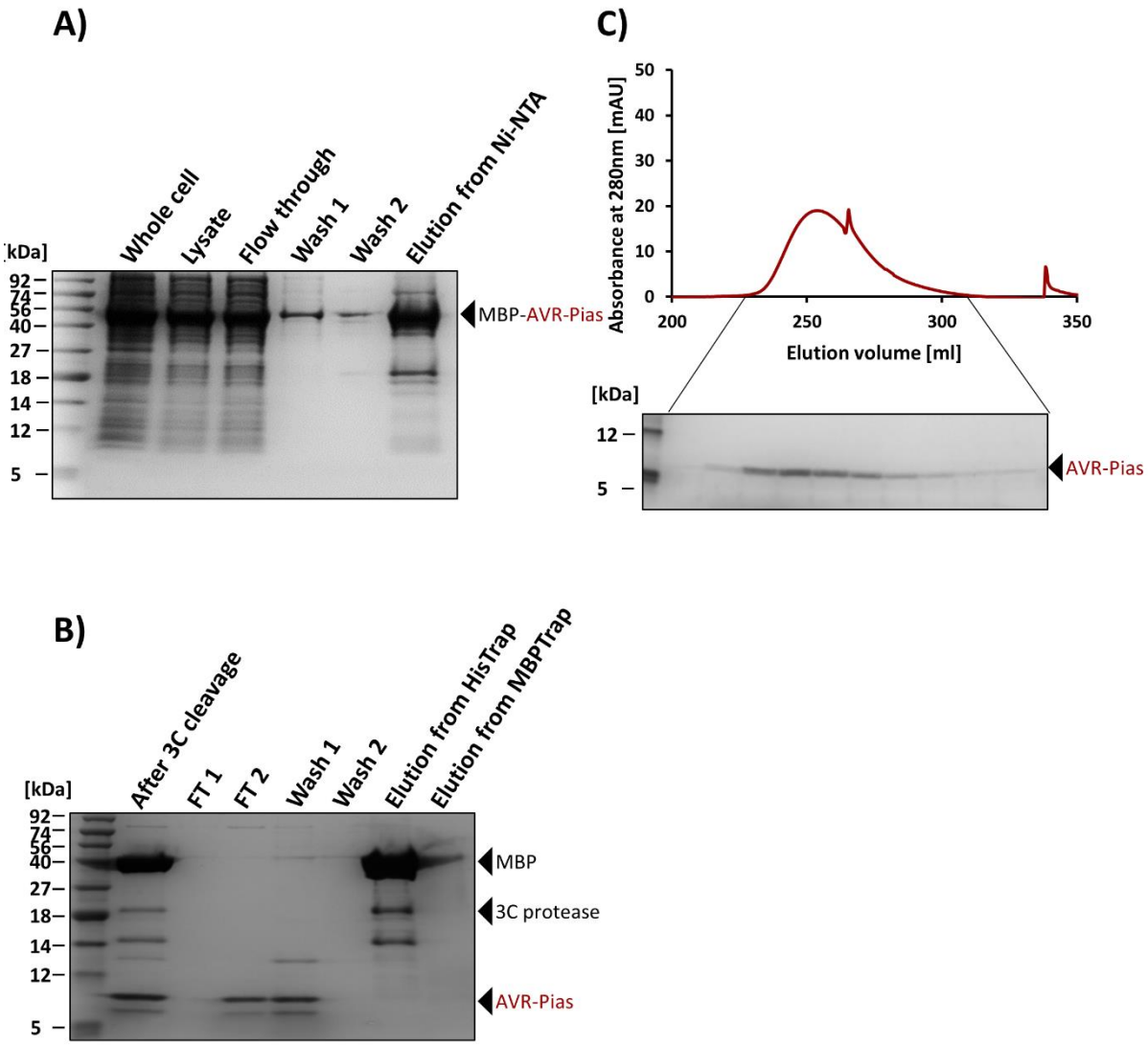

Figure 8.1 Purification of AVR-Pias from *E. coli.*

A) *SDS-PAGE gel showing fractions from consecutive steps of manual purification of 6xHis-MBP:AVR-Pias.* ***B)*** *SDS-PAGE gel showing fractions before and after cleavage of the 6xHis-MBP tag, and subsequent steps of manual purification.* ***C)*** *SDS-PAGE gel showing fractions from final SEC.*

Initial screens resulted in many conditions showing crystalline precipitate, especially in the Morpheus screen (**Figure 8.2**). However, due to its complex mix of precipitant conditions, this screen is not straightforward to optimise. Before proceeding with further crystallisation trials, I sort to confirm the integrity of the purified protein by mass spectrometry, to determine whether the difference in observed and expected mass of the protein was due to protein degradation, or just an artifact of the SDS-PAGE. The purified AVR-Pias effector was submitted for intact mass analysis and tryptic digest mass fingerprinting by The Sainsbury Laboratory Proteomics Team.

Table 8-1 Crystallisation screens and conditions used for crystallisation of AVR-Pias.

Screen	Protein concentration
JCSG	**9 mg/ml and 4.5 mg/ml**
Morpheus	**9 mg/ml and 4.5 mg/ml**
PEGs	**9 mg/ml and 4.5 mg/ml**

All screens are commercially available.

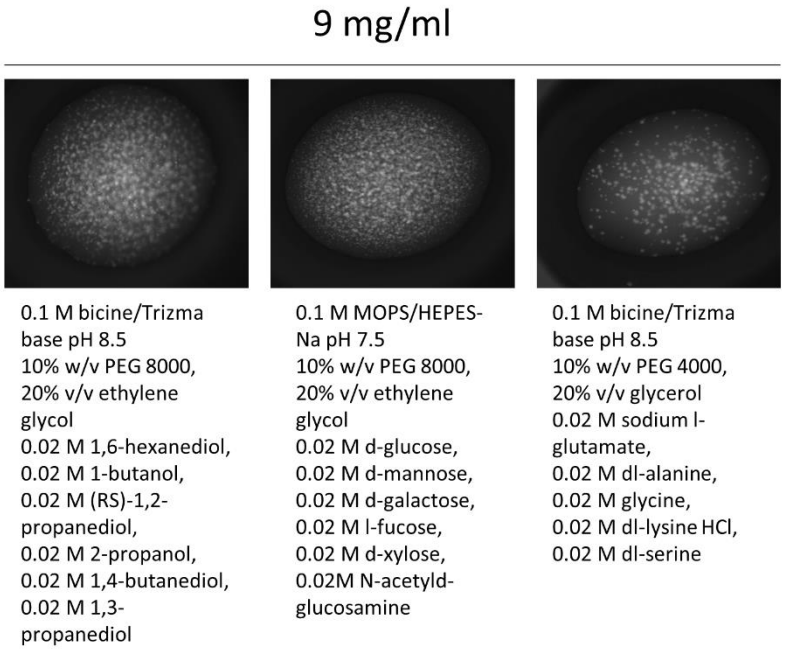

Figure 8.2 Initial crystallisation screens and conditions used for crystallisation of AVR-Pias resulted in crystalline precipitate.

Representative pictures of crystalline precipitates obtained in indicated conditions.

8.2.2 Intact mass spectrometry revealed that AVR-Pias was truncated

The intact mass analysis revealed two major peaks at 5830.78 Da and 5870.81 Da (**Figure 8.3 A**). However, automated analysis did not find the corresponding fragment of the protein that would match these masses. Interestingly, peptide mapping revealed that 96% of the AVR-Pias sequence was present in the sample, with only three residues missing, Asp-35 to Lys-37 (**Figure 8.3 B**). This suggested that AVR-Pias might be unstable at two different sites, and the break down products display similar masses, unresolvable by SDS-PAGE. To further aid the identification of a stable AVR-Pias fragment, I submitted the sequence for in silico analysis by the MoreRONN software (Yang et al., 2005) that predicts the disordered regions of the proteins. This analysis predicted that N-terminal part of AVR-Pias is disordered, with the ordered region only spanning the residues Arg-41 to Glu-91 (**Figure 8.3 C**). Analysis of the protein sequence truncated in that region revealed a mass close to the one observed in mass spectroscopy (5830.78 Da) that spans residues Ser-39 to Glu-91 (predicted mass: 5834.81 Da). I hypothesised that the remaining difference of 4 Da might be a result of potential formation of two disulphide bridges formed by the 4 cysteines present in the sequence. Therefore, I generated a new AVR-Pias construct truncated to include this sequence, generating AVR-Pias$^{39\text{-}91}$, henceforth referred to as AVR-PiasΔ21, due to truncation of further N-terminal 21 amino acids (apart from signal peptide).

A)

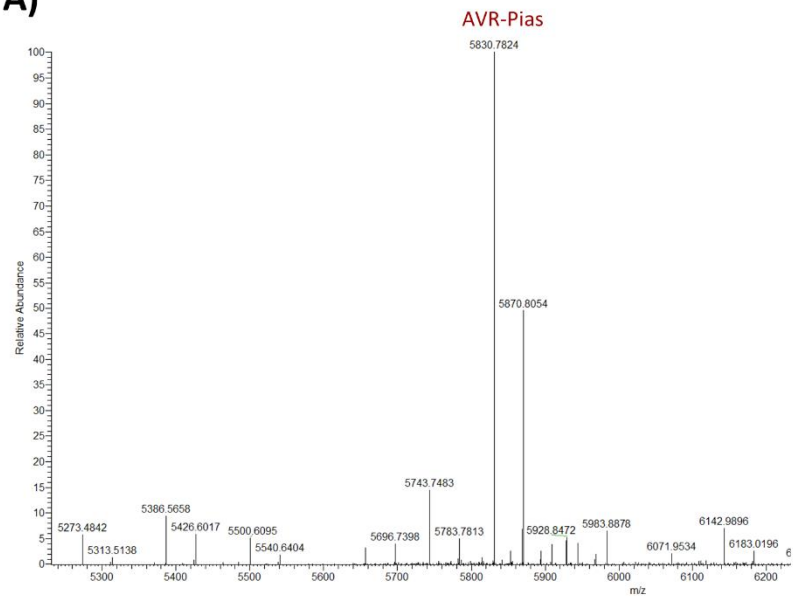

B)

Protein sequence coverage: 96%

Matched peptides shown in ***bold red***.

```
  1 GPAQIQDSST KNPNQVVNRN AKLSSRNLER RNENYWRCVN ICIAGGVFGA
 51 LKFTDITVRD SVHCAGACAA VFGYPE
```

C)

AVR-Pias

View graph Download raw data

```
AQIQDSSTKNPNQVVNRNAKLSSRNLERRNENYWRCVNICIAGGVFGALKFTDITVRDSVHCAGACAAVFGYPE
########################====---
```

Figure 8.3 Mass spectrometry analysis of AVR-Pias revealed an N-terminal truncation.

A) *Intact mass spectrometry analysis of the AVR-Pias showed main peak at 5830.78 Da, which is significantly lower than expected (8141.02 Da)* ***B)*** *Peptide mapping of the AVR-Pias revealed that 96% of the sequence can be detected in the sample.* ***C)*** *Disorder prediction by MoreRONN software. Per-residue scores < 0.4 are denoted as blank spaces (predicted ordered region of the protein), scores >= 0.4 and < 0.5 are shown as '-', scores >= 0.5 and < 0.6 are identified as '=', and scores >= 0.6 are denoted by '#' (predicted disordered region).*

8.2.3 Purification of AVR-PiasΔ21

This coding sequence was introduced into pOPIN-M via In-Fusion cloning and expressed in the *E. coli* SHuffle strain. Subsequent steps of harvesting the cells, sonication and clarification of the lysate were performed as described in Materials and Methods. Clarified lysate was loaded onto ÄKTAxpress system and subjected to tandem IMAC and SEC. SDS-PAGE analysis revealed that the protein was well expressed (**Figure 8.4 A**). Fractions under the elution peak were combined and incubated with 3C protease overnight. Subsequently, the sample was subjected to further purification on HisTrap and MBPTrap columns (in tandem). SDS-PAGE analysis of samples collected throughout the process revealed that AVR-PiasΔ21 displayed higher affinity to the HisTrap column than the full-length construct, and majority of the protein was present in the Wash 1 and Wash 2 fractions (**Figure 8.4 B**). These samples were combined and subjected to SEC, yielding a protein of high purity and yield (**Figure 8.4 C**). The fractions were combined, concentrated, and crystallisations screens set up as listed in **Table 8-2 (p. 189).** Unfortunately, no crystals were obtained from these trials.

The next question to address was whether the AVR-Pias effector was properly folded following expression and purification. To address this, I submitted the protein for CD analysis (the sample was prepared as described in Chapter 4, **p. 94**). Analysis of the obtained spectrum indicated that majority of AVR-Pias is α-helical, displaying characteristic (almost text-book example) positive peak at 192 nm and two negative peaks at 208 nm and 222 nm (Wei et al., 2014). Further analysis with BeStSel software confirmed that large part of the protein is helical (40.8%, data not shown). These results indicate that AVR-PiasΔ21 is at least partially ordered and might be expected to be suitable for crystallisation.

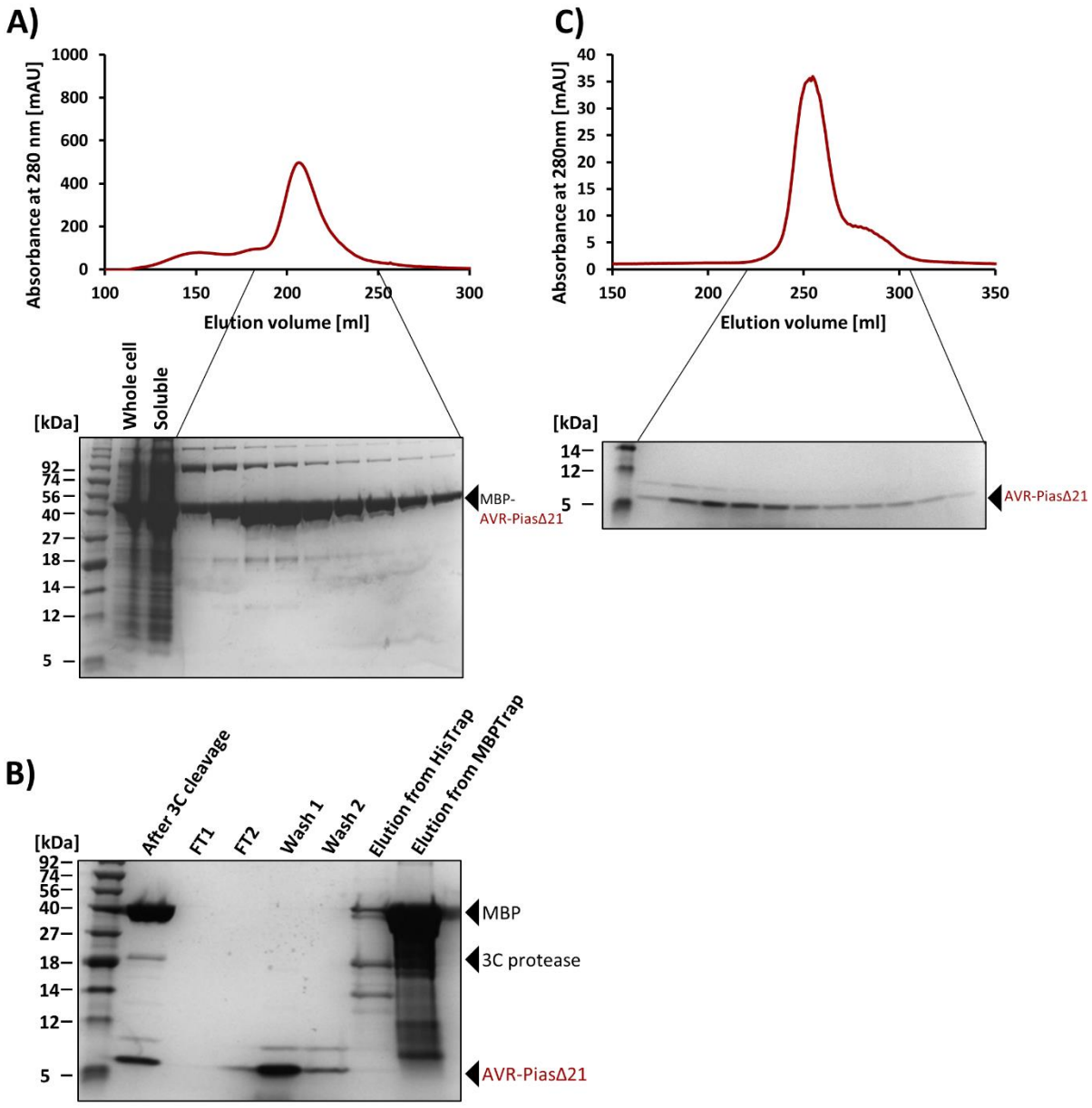

Figure 8.4 Purification of AVR-PiasΔ21 from *E. coli.*

A) *SDS-PAGE gel showing Whole cell and Soluble fraction from E. coli expressing 6xHis-MBP:AVR-PiasΔ21. Further lanes show fractions corresponding to the indicated fragment of SEC trace.* ***B)*** *SDS-PAGE gel showing fractions before and after cleavage of the tag, and subsequent steps of manual purification.* ***C)*** *SDS-PAGE gel showing fractions from final SEC.*

Table 8-2 Crystallisation screens and conditions used for crystallisation of AVR-PiasΔ21.

Screen	Protein concentration
JCSG	**9 mg/ml and 4.5 mg/ml**
Morpheus	**9 mg/ml and 4.5 mg/ml**
KISS	**9 mg/ml and 4.5 mg/ml**

All screens are commercially available, apart from the KISS screen, which has been developed by Biophysical Platform in John Innes Centre.

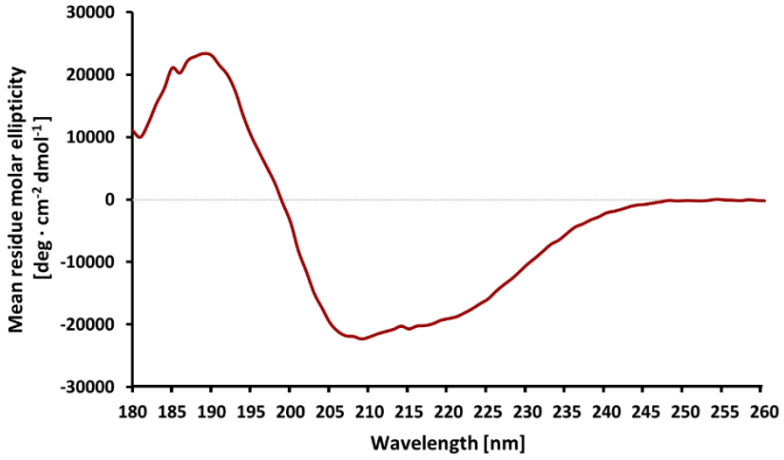

Figure 8.5 CD spectrum of AVR-PiasΔ21.

Analysis of the spectrum suggests that AVR-Pias mostly comprises of α-helices.

Aside from X-ray crystallography, there are other two other major experimental techniques that allow for structure determination of proteins. Nowadays, Cryo-Electron Microscopy (CryoEM) is gaining more and more interest among scientists, mainly due to its constantly improving resolution. However, it is only suitable for big molecular complexes, such as resistosomes, inflammasomes or membrane pores (Tenthorey et al., 2017, Boyd and Bubeck, 2018, Wang et al., 2019a, Hebert, 2019). Molecules (or complexes) smaller than 100 kDa are difficult to find and orient against the noisy background when using normal defocus phase contrast. To investigate the structure of smaller molecules, including small proteins (up to 20 kDa), Nuclear Magnetic Resonance (NMR) can be used. NMR is a technique based on observation and measurement of nuclear spins of individual atoms of a molecule, when placed in a powerful magnetic field. This technique has certain advantages over X-ray crystallography, mainly the lack of a requirement of protein crystals. However, it typically requires labelling the purified proteins with heavy isotopes of nitrogen (^{15}N) or carbon (^{13}C) and high protein stability at room temperature as typically experiments may take days (or even weeks) to collect the required data.

As AVR-PiasΔ21 is a small protein (6 kDa), and I was unable to obtain protein crystals, I explored the potential of using NMR studies to obtain its structure using this method. To achieve this aim, the sample was sent to our collaborators at Centre de Biochimie Structurale, Université de Montpellier, France. The data collection and AVR-Pias structure calculation were performed by Dr. Andre Padilla at Université de Montpellier, France (for details, see Materials and Methods). Initially, the submitted and analysed sample was not labelled with any heavy isotopes. The initial analysis allows to assess, whether the protein is suitable for NMR studies, e.g., whether it is stable in room temperature for long time and can be concentrated to higher concentration that would allow for collection of quality data. Interestingly, AVR-Pias was very stable, which allowed for significantly prolonged data collection and structure determination, using only scarce natural abundance of heavy isotopes. Notably, the prolonged data collection was possible due to low demand on the NMR spectrometer, as we sent the sample just before the first Covid-19 lockdown.

However, to confirm the results, I set out to produce and purify AVR-PiasΔ21 labelled with N^{15}. Briefly, *E. coli* SHuffle cells were transformed with pOPIN-M:AVR-PiasΔ21 construct and grown in minimal medium M9, supplemented with labelled $^{15}NH_4Cl$ (for details, see Materials and Methods). The subsequent purification steps were performed as described for AVR-PiasΔ21. The final SEC gave a high yield of pure protein (**Figure 8.6**), which was concentrated to 2 mg/ml, flash frozen in liquid nitrogen and sent to our collaborators.

The structure of AVR-PiasΔ21 was successfully determined and reported to us, along with the key refinement statistics (**Table 8-3**).

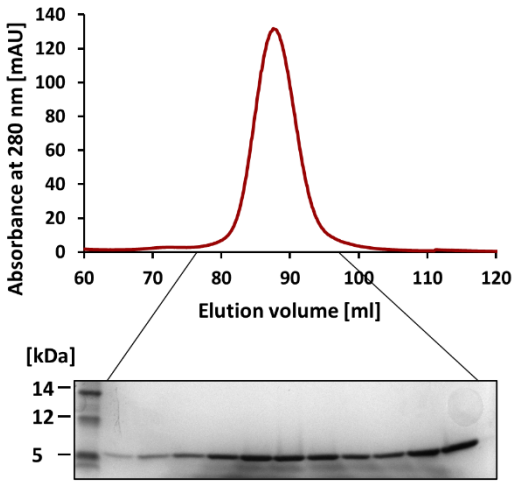

Figure 8.6 Final size-exclusion chromatography step of purification of ^{15}N-labelled AVR-PiasΔ21.

SDS-PAGE shows fractions corresponding to the indicated SEC trace.

Table 8-3 Refinement statistics for NMR structure of AVR-Pias.

	AVR-Pias
NMR distance and dihedral constraints	
Distance constraints	
Total NOE	1201
Intra-residue	264
Inter-residue	
Sequential ($\|i-j\|=1$)	324
Medium-range ($\|i-j\|<4$)	323
Long-range ($\|i-j\|>5$)	290
Hydrogen bonds	28
Disulfide bonds	6
Total dihedral angle restraints	
ϕ	37
ψ	37
χ_1	19
Structure statistics	
Violations (mean and s.d.)	
Max. distance constraint violation (Å)	0.14 ± 0.01
Max. dihedral angle violation (°)	1.72 ± 0.52
Deviations from idealized geometry	
Bond lengths (Å)	0.0099 ± 0.0003
Bond angles (°)	1.1648 ± 0.0423
Impropers (°)	1.2906 ± 0.0975
Ramachandran plot (%)	
Most favoured region	89.1
Additionally allowed region	8.7
Generously allowed region	2.2
Disallowed region	0.0
Average pairwise *r.m.s.* deviation (Å)**	
Backbone	0.33 ± 0.08
Heavy	0.92 ± 0.17

** "Pairwise r.m.s. deviation calculated among 20 refined structures for residues 10-52."

(AVR-Pias, 0.5 mM, 25 mM NaPhosphate pH 6.8, 150 mM NaCl, 1mM DTT, 293 K, 800 MHz)

8.2.4 The solution structure of AVR-Pias

The structure of AVR-PiasΔ21 (henceforth, for simplicity, referred to as AVR-Pias) revealed a novel class of *M. oryzae* effector that comprises of two anti-parallel α-helices, stapled together by two disulphide bridges (**Figure 8.7 A**). The N-terminal fragment of purified AVR-Pias is disordered, spanning the fragment Gly^{-2} to Arg-45 (the Gly^{-2} is the first remaining residue after cleavage of the 6xHis-MBP tag, a part of "Gly-Pro scar"). The α1 helix spans residues Arg-46 to Gly-60, and the α2 helix spans residues Ser-76 to Ala-85. The two helices are joined by a loop region, which lacks any secondary structure features. The helices are stabilised by presence of two S-S bridges, formed by pairs Cys-53/Cys-83, and Cys-57/Cys-79, which is in agreement with the obtained mass spectrometry result. Analysis of positions of charged residues did not reveal any major charged patches on the surface of the effector (**Figure 8.7 B**) that have been shown to be important for interactions in other effectors (Zhang et al., 2018). However, several charged amino acids are facing towards outside of the AVR-Pias structure, which may play a role in interaction with a potential target. A homology search using the Dali server (Holm, 2020) did not find any significantly similar structures (**Figure 8.8**). This may be due to relatively simple structure of this effector that allows many helical fragments of a given protein to be compared with AVR-Pias.

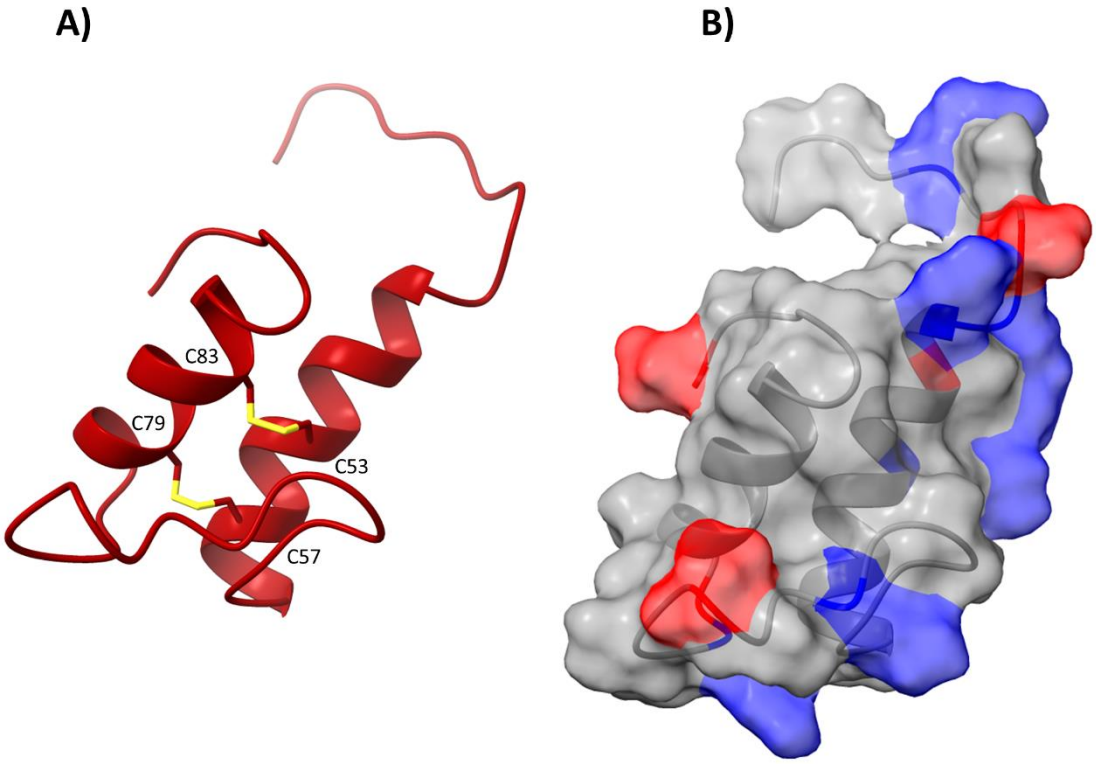

Figure 8.7 NMR Structure of AVR-Pias.

A) *AVR-Pias consists of two α-helices stapled together with two disulphide bridges (in yellow).* ***B)*** *Analysis of location of charged residues revealed no major charged patches on the surface of AVR-Pias, although several single charged residues are exposed, and may play a role in potential interactions. Negatively charged residues (Asp and Glu) are shown in red, positively charged residues (Lys and Arg) are shown in blue.*

No:	Chain	Z	rmsd	lali	nres	%id	PDB	Description
1:	5w7g-A	3.2	2.4	37	131	8	PDB	MOLECULE: ORF140;
2:	5g4y-A	3.1	2.4	37	147	5	PDB	MOLECULE: CHEMOTAXIS PROTEIN;
3:	6ofa-A	3.1	1.9	32	32	13	PDB	MOLECULE: WASABI RECEPTOR TOXIN;
4:	6ajf-A	3.0	2.6	39	901	13	PDB	MOLECULE: DRUG EXPORTERS OF THE RND SUPERFAMILY-LIKE PROTEI
5:	2wit-A	3.0	4.3	48	531	8	PDB	MOLECULE: GLYCINE BETAINE TRANSPORTER BETP;
6:	7jsj-A	2.9	3.0	41	468	12	PDB	MOLECULE: SOLUTE CARRIER FAMILY 13 MEMBER 5;
7:	6wgm-A	2.9	5.0	43	305	12	PDB	MOLECULE: TRAP-TYPE C4-DICARBOXYLATE TRANSPORT SYSTEM, PERI
8:	2lo0-A	2.9	4.4	37	45	3	PDB	MOLECULE: UNCHARACTERIZED PROTEIN;
9:	6ux5-A	2.9	2.9	41	50	5	PDB	MOLECULE: U-ACTITOXIN-AEQ5A;
10:	6o3q-A	2.8	2.5	37	49	14	PDB	MOLECULE: VICILIN;

Figure 8.8 Dali homology search did not find any significant similarity of AVR-Pias to other known structures.

8.3 Discussion

In this Chapter, I set out to purify and determine the structure of the newly identified *M. oryzae* effector AVR-Pias. I identified a stable fragment of this effector for in vitro work, and purified it in both native forms and with ^{15}N labelling. For structure determination by NMR, I collaborated with researchers at The Université de Montpellier, France.

To date, all the determined and published structures of *M. oryzae* effectors belong to the MAX family, due to the characteristic fold present in their structure, even if they share low sequence similarity (Franceschetti et al., 2017, Bentham et al., 2021a). Analysis of the AVR-Pias structure revealed a new structural class of effectors in *M. oryzae*, characterised by presence of two α-helices stapled together with two disulphide bonds.

8.3.1 Correlation of sequence conservation with the structure

AVR-Pias is well spread across different *M. oryzae* host-specific lineages, including lineages infecting rice, wheat, *Lollium, Digitaria* and *Eleusine* (Dr. Thorsten Langner, personal communication). Protein sequence alignment across these isolates shows that the four cysteines forming the two S-S bonds are highly conserved, indicating that they may be crucial for effector stability and function (**Figure 8.9**). Other highly conserved residues include Gly-60 and Gly-61, which are located at the end of the α1, and Phe-68 and Arg-74, present within the loop region. The properties of glycine residues make them less suited to helical structures, and Gly-60/Gly-61 may enable helix termination and formation of the loop. For Phe-68 and Arg-74, it is possible the loop between the two helices is important for the biological activity of AVR-Pias, and the two helices stabilised by two S-S bridges are a scaffold for the effector and mainly contribute to protein stability. This hypothesis requires further testing, for example by identifying the host cell target of AVR-Pias and performing biophysical analysis of complex formation.

Another highly conserved set of residues are Leu-43, Arg-45, and Arg-46. These residues are located in the disordered region, immediately preceding the α1-helix. They form a characteristic LxxR motif, which is a potential cleavage site for the Kex2 protease (Li et al., 2017). Kex2 is an endogenous protease conserved across fungi, with a canonical cleavage site defined as dibasic RR or KR (in AVR-Pias the sequence is LERR). This protease has been suggested to play role in maturation of the effectors, before they are secreted into plants. In the AVR-Pias structure, we observe that the α1 helix starts immediately after this motif, therefore it can be hypothesised that the mature form of AVR-Pias spans the residues Arg-46 to Ala-91 and the N-terminal part of the effectors is a pro-domain that might play a role in appropriate folding of the effector or effector trafficking. This would classify AVR-Pias as K2PP (Kex2-processed pro-domain) effector (Outram et al., 2021).

Confirmation of the role of Kex2 cleavage-mediated maturation of the AVR-Pias is beyond the scope of this thesis. Kex2 has been shown to cleave effectors from different fungi, including *Parastagonospora nodorum* (SnTox3 effector) and *Fusarium oxysporum f. sp. lycopersici* (effectors SIX1, SIX4 and SIX6) (Outram et al., 2021), and the potential Kex2 cleavage site has been found in a range of effectors from different fungi, including *Puccinia graminis*, *Ustilago maydis*, *Verticillium dahlia* and *M. oryzae* (Outram et al., 2021).

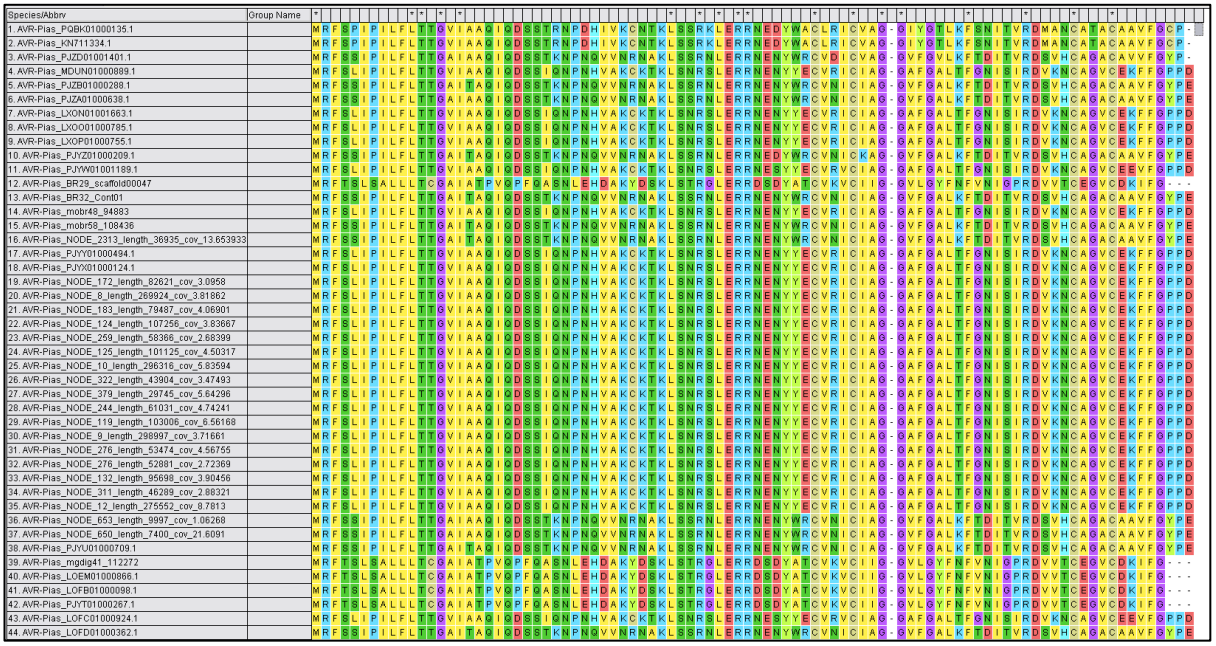

Figure 8.9 AVR-Pias is prevalent in pathogen population.

Sequence alignment of AVR-Pias sequences shown high sequence conservation. Only sequences with similarity higher than 90% were taken into the alignment. Analysis conducted by Dr. Thorsten Langner.

8.3.2 Finding the interactor for AVR-Pias is crucial for establishing its activity

The majority of fungal plant pathogen effectors share low sequence identity with each other, or with other proteins with established activities, therefore prediction of their function remains challenging. The few exceptions are effectors containing known-function-related motifs or domains, such as Slp1 or Ecp6 with LysM domain or necrosis and ethylene-inducing peptide 1 (Nep1)-like proteins (NLPs) (Mentlak et al., 2012, Sanchez-Vallet et al., 2013, Giraldo and Valent, 2013, Lo Presti et al., 2015). AVR-Pias does not share any significant sequence similarity to any other know protein, and a structure-based homology search did not identify any characteristic domain folds. To determine the role of AVR-Pias in the pathogenesis, it is crucial to find its interactor.

Two common methods can be used in search for protein interactions, Yeast-2-Hybrid (Y2H) and Immunoprecipitation coupled with Mass Spectrometry (IP-MS). Y2H has been recently successfully used to identify the interactors of SAP05 effector from Aster Yellows phytoplasma- two distinct transcription factors SPL and GATA (Huang et al., 2021). Further, the authors showed that SAP05 binds and mediates the degradation of these transcription factors via lysine ubiquitination-independent mechanism, which leads to delayed plant ageing and simultaneous proliferation of plant tissue. Moreover, using structure guided approach, they were able to eliminate the susceptibility factor in the plant host (Huang et al., 2021). An alternative approach to interactor identification is to perform immunoprecipitation of a tagged effector from transgenic crop (expressing the effector of interest) and subsequently analysing the sample using mass spectrometry. This approach identified Exo70-F3 as interactor of *M. oryzae* effector AVR-Pii (Fujisaki et al., 2015). Subsequently, is has been shown that Exo70-F3 also binds to the integrated NOI domain of Pii-1 receptor (Fujisaki et al., 2017), revealing the mechanism of indirect recognition of the effector to activate the plant immune system.

Identification of the AVR-Pias host target is beyond the scope of this thesis. However, generation of stable barley transgenic lines expressing AVR-Pias:FLAG is in progress. In future, I will perform the IP-MS experiment to identify interactors of AVR-Pias. In case of SnTox3 effector, it has been shown that the mature protein was triggering much stronger response when delivered into its host, therefore the pro-domain was interfering the process of recognition. The currently generated transformants express the full length (without the signal peptide), which may interfere with potential interactions, but at the same time could be crucial for appropriate protein folding. Therefore, an alternative approach might be considered in the future. In case of finding the potential interactor, further studies will be needed to confirm and characterise the interaction, including crystallisation of the complex. Learning from the structure of AVR-Pias, further truncation (after the Kex2 cleavage site) of the protein may be advisable, to ensure that the protein in the sample is well ordered and, perhaps, more suited to crystallisation.

9

General Discussion

9 General Discussion

9.1 Plant diseases can become pandemic too

Plant pathogens pose a constant threat to food production all over the world. Increased globalisation allows for rapid spread of pathogens, not only between different countries, but also between different continents, which can change an emergence into a pandemic. Moreover, a changing climate can enable pathogens to thrive in new regions, which were previously not available to them. A changing climate can also support host jumps and alteration of host range (Thines, 2019). *Magnaporthe oryzae* is a model example of such a globally spreading pathogen. Aside from being a major threat to rice production worldwide, an increasing number of cases are emerging of wheat blast (Islam et al., 2020). In 2016, wheat blast was reported in Bangladesh for the first time, where it had a significant impact on crop yield, with knock-on effects to the country's overall economy (Islam et al., 2016). Since 2020, wheat blast has also been reported in Africa, with the first cases occurring in Zambia (Tembo et al., 2020, Singh et al., 2021). Recently, wheat blast has also emerged in other countries, including Tanzania and Zimbabwe (Dr. Joe Win, personal communication). This is a prime example of how pathogens can adapt to ever changing environments and spread globally, along with human movement across the world. Such occurrences emphasize the need of studying plant-pathogen interactions and widening our arsenal of resistance potential against disease if we want to improve food security.

9.2 Pathogen's effector repertoire can be structurally diverse

To enable this, further studies are required on both the pathogen and the plant side of the interaction. Structural information about the effectors can help with elucidation of their function and aid discovery of new effector candidates. Through protein modelling, structural data can also be used to predict potential effectors, which is more powerful approach than sequence alone. In Chapters 6 and 8, I present new structures of *M. oryzae* effectors, PWL2 and AVR-Pias, respectively. Shared with other *M. oryzae* effectors, for which structures have been determined and published to date, PWL2 belongs to the MAX effector family despite little recognisable sequence homology with other MAX effectors. AVR-Pias is a recently identified effector, perceived by the NLR pair Pias-1/Pias-2 (Shimizu et al., 2021). The NMR structure of AVR-Pias revealed this effector adopts a completely different fold comparing to the MAX effectors, and therefore represents a new class of effectors in the rice blast fungus that may have novel targets. This latter hypothesis requires further investigation, but it would seem likely that we are only just beginning to uncover the structural complexity of the *M. oryzae* effector repertoire.

9.3 One model does not fit them all

NLRs are plant immune receptors that can function as singletons, pairs, or in networks. Paired NLRs have evolved to carry out specialised functions, with one of the pair acting as the sensor and the other as the helper. Perhaps the best studied NLR pairs to date, RGA4/RGA5 and RPS4/RRS1, have been described to work via negative regulation mechanism (Cesari et al., 2014b, Williams et al., 2014). Until recently, it has been generalised and assumed this model might apply to most paired NLRs. In Chapter 3, I showed that the negative regulation model does not apply to the Pikp-1/Pikp-2 NLR pair, which seems to work via tightly regulated cooperation. This emphasises the diversity of NLR mechanisms, and indicates that we still lack knowledge about mechanistic features of NLRs. It seems likely that the ZAR1 resistosome is not a universal mechanism of CC-NLRs oligomerisation and different NLRs may work via different mechanisms.

One striking difference between the Pik-1/Pik-2 pair, and RGA5/4 and RRS1/RPS4 pairs is the position of the integrated domain in the sensor NLR. In the Pik pair, the integrated domain is located between the CC and NB-ARC domains, whereas in RGA5/4 and RRS1/RPS4 pairs it is located at the C-terminus, after the LRRs. It remains an open question whether the position of the integrated domain in the architecture of the NLR can be correlated with the mode of action; is the position of the integrated domain in the Pik pair a determinant for their cooperative mode of function?

9.4 The discovery of the integrated domains (IDs) offers new insights into plant immunity and NLR engineering

IDs have been suggested to have evolved as “integrated decoys” (Cesari et al., 2014a), displaying features of natural effector targets. This has generated hypotheses concerning potential virulence-associated targets for the effectors in promoting disease. Frequently, it has been shown that the virulence-associated targets of effectors can act as susceptibility factors, and deleting them can increase plants resistance to disease. This strategy is potentially useful for engineering resistance, however, it may come at a cost. Effector targets are biologically relevant proteins (Wang and Jiao, 2019, Huang et al., 2021), therefore deleting them, or knocking them down, might have deleterious effects on plant health and development. To avoid this, an alternative approach could involve engineering these susceptibility factors to reduce their binding to the effector, but retain their biological function (Huang et al., 2021). To achieve this, structural information about effector/target complexes may be crucial. The results presented in Chapter 6 showed that interactions between PWL2 and OsHIPP43 cannot be easily compromised, however attempts to date to break the interaction have only been made by mutating the effector. It would be interesting to see whether mutating residues in OsHIPP43 could break or reduce the binding between these

two proteins. Although the biological role of OsHIPP43 remains to be elucidated, the PWL2 binding interface is located away from the metal binding loop. It could be possible to engineer an OsHIPP43 variant that would still perform its biological function, but would not be targeted by the effectors from the PWL family.

An alternative approach to increasing resistance is engineering perception of effectors. Integrated domains of NLRs are a very interesting target for this approach. It has been suggested that integration of non-canonical domains into the NLR architecture not only allows direct recognition of selected effectors, but it also enables improved tolerance for sequence alterations during the course of evolution (Baggs et al., 2017, Białas et al., 2018). This allows NLRs to adapt to rapidly evolving pathogens without compromising the role of NLRs in immunity. Mutations within the integrated domains could be tolerated in context of full-length NLRs, although the extent to which these alterations may happen remains unclear. In Chapters 5 and 7, I showed that integration of HMA domain of OsHIPP43 protein into Pikm-1 chassis allowed perception of PWL effectors in a transient expression system in *N. benthamiana* plants. These results showed an entire integrated domain can be swapped within an NLR to generate a novel recognition specificity in plant NLRs, providing an important proof-of-concept that engineering of NLRs can be taken further than mutation of individual amino acid residues.

The full extent to which integrated domains can be altered is currently unknown, but there are some potential limitations to this system. Swapping the Pikm-1-HMA domain for OsHIPP43-HMA caused auto-activity of the NLR pair (expression with Pikm-2). Moreover, it has been shown that even single point mutations within the HMA domain of Pik proteins can cause auto-activity of the system (De la Concepcion et al., 2021a). In Chapter 5, I showed that this auto-activity can be alleviated by mismatching the allele of the helper NLR (Pikm-2 for Pikp-2). However, whether this approach can mitigate any auto-activity that arises from the integration of any new domain remains to be determined. To date, any changes introduced in the integrated domain of Pik proteins were performed by structure-guided mutations of single amino acids or, as presented in this work, by swapping the entire HMA domain for another HMA domain. It would be interesting to investigate whether other effector targets with folds different to HMAs could be also incorporated into the Pikm-1 chassis and change the recognition specificity of the receptor. This approach might be limited by the size of the integrated domain and/or the perceived effector, due to position of the integrated domain. For example, target domains may cause a steric clash with the neighbouring CC or NB-ARC domain affecting the intramolecular interaction within the receptor. Moreover, an effector significantly larger than AVR-Pik or the PWL effectors may clash with the CC and/or NB-ARC domains and not be able to interact with the integrated domain limiting the use of the system.

Pathogens whose effectors became AVR genes (are recognized by cognate plant NLRs) are unable to infect their host. Therefore, these pathogens are under constant selection pressure which favours the strains that acquired mutations in the avr genes that allow them to evade the recognition, preferably without losing the ability of binding the biological target (Bentham et al., 2021a). This can be exemplified by presence of the stealthy effector allele AVR-PikF, that binds its target OsHIPP19, but is not perceived by any known Pik accession (Maidment et al., 2021). Deploying engineered receptors with integrated effector targets may generate plants that cannot be infected by pathogens carrying the cognate effectors. Mutations in these effectors may not be favoured as they could compromise binding to their host target. In this case, selection pressure may lead to complete loss of effector genes and hence to occurrence of presence/absence phenotypes. This mechanism has been suggested for *M. oryzae* AVR-Pik effectors, which are present only in the rice-infecting lineages of the blast fungus (Bentham et al., 2021a). However, the loss of an effector can result in decreased pathogenicity and reduced fitness of the pathogen at the population level.

9.5 New recognition specificity does not always correlate with resistance in the field

Engineered receptors that display new recognition specificities in transient expression systems do not always confer new resistance towards pathogens when stably expressed in plants. For example, swapping the restriction site in the PBS1 decoy kinase (cleavage of PBS1 is recognised by the NLR RPS5) resulted in new recognition specificity and activated immune responses in transient expression system (Kim et al., 2016). However, it did not confer full resistance in Arabidopsis, unless the decoy was overexpressed and localised at the plasma membrane (Pottinger et al., 2020, Pottinger and Innes, 2020). In a second example, engineering the recognition interface of Pikp-1-HMA/AVR-PikD onto RGA5-HMA showed that the mutated HMA domain could bind AVR-PikD, AVR1-CO39 and AVR-Pia in vitro and in a transient expression system (Cesari et al., 2021). However, the engineered RGA5 did not confer resistance in rice to *M. oryzae* strain carrying AVR-PikD. Finally, the chimeric receptor RRS1-$R^{SH/AA}$-GATA was designed to be targeted and degraded by phytoplasma effector SAP05, which would lead to derepression of auto-active RRS1-R^{slh1} that can trigger cell death responses in RPS4-dependent manner. This strategy was shown to be successful in a transient expression system, but stable transformants of Arabidopsis carrying these three proteins did not display full resistance when challenged with the phytoplasma expressing the SAP05 effector (Wang et al., 2021b). In contrast to these studies, stable expression of Pikp-$1^{SNK\text{-}EKE}$ in rice conferred resistance to *M. oryzae* strains carrying the previously unrecognised AVR-PikF effector (Ryohei Terauchi, personal communication; manuscript in preparation), proving that alteration of the HMA domain in Pik-1 is a promising platform for engineering novel resistance in plants, especially when

it can be supported by in-depth structural analysis of the interaction. Together, these studies show that a cell death response in a transient expression system may not always correlate with resistance in target plants, and chimeric receptors need to be validated in stable transgenic lines.

Validation of the engineered NLRs described in this thesis a is an essential next step. For this, stable transgenic lines of barley, rice and wheat expressing the chimeric Pikm-1^{OsHIPP43}/Pikp-2 receptor will be generated and challenged with pathogen strains expressing PWL2 effectors. It will be important to closely monitor physiological phenotypes that might occur as a result of expression of the chimeric proteins. Although only the HMA region of the OsHIPP43 was incorporated into the Pikm-1 background, it retains an intact metal-binding loop, which might interfere with plant's heavy metal homeostasis. Such potential interference may be the reason why the heavy metal binding motif in the integrated HMA domains (including both Pik and RGA5 NLRs) is degenerate. This region has been also shown to be responsible for the observed auto-activity of chimeric Pik receptors with an ancient HMA domain incorporated (Bialas et al., 2021). The emerging question is: why has the OsHIPP43 sequence not been incorporated into Pik, RGA, or other HMA-containing NLR backgrounds so far during the course of evolution? It may be that this specific interaction is yet to evolve to be compatible with the NLR system, hence the resistance against PWL2 found in weeping lovegrass may adapt a different strategy to recognise the effector. This hypothesis is supported by the location of allelic/polymorphic residues in the PWL2 crystal structure being distanced from the OsHIPP43 interface (presented in Chapter 6, **p. 143**), and the fact that unrecognised alleles of PWL2-2 and PWL2-3 strongly bind to OsHIPP43 (presented in Chapter 4, **p. 111**).

9.6 GMO acceptance is slowly increasing worldwide

Even if the chimeric Pikm-1^{OsHIPP43} receptor confers novel resistance in transgenic crops, its commercialisation and deployment in the field may meet significant obstacles. As a synthetic protein, it does not exist naturally and therefore can only be introduced into elite cultivars via genetic modification. Various genetic modification tools now exist that work successfully in rice (reviewed in (Mishra et al., 2018)). This includes CRISPR/Cas9 that is constantly being improved and enables precise genetic manipulation. However, genetically edited crops are still under tight regulation with various levels of approval in different regions of the world. In certain countries (mainly USA), the level of GMO acceptance and cultivation is high, and overall, it is increasing worldwide. Over the last 25 years, GM crop production has increased ca. 100 times (Brookes and Barfoot, 2013, Mathur et al., 2017). However, the majority of the GM crops (with the four main GM crops: soybean, maize, cotton and canola as a prime examples) are not destined for direct human consumption. Most of the GM soybean is used for oil production and feeding livestock, and maize

usage is shifting to ethanol production rather than animal feed (Wallington et al., 2012, Klopfenstein et al., 2013, Ranum et al., 2014). The best example for genetically modified crop targeted for human consumption is Golden Rice that expresses β-carotene; a pre-cursor of vitamin A (Moghissi et al., 2016, Bohn et al., 2019). In several countries Golden Rice has been approved for human consumption, but not for cultivation (these two aspects of GMO commercialisation are regulated separately). Unfortunately, many countries, including the European Union, do not approve consumption of GM products. The cultivation of GM plants within the EU is dependent on countries' own policies, however the only gene edited crop grown in Europe is insect-resistant maize MON810, which is currently only allowed in Portugal and Spain (Turnbull et al., 2021). Regrettably, although some African countries approve GM technologies (with South Africa as a leader), the main GM resisting countries include Zambia, Zimbabwe, and Tanzania, which would potentially benefit the most, especially in the light of recent wheat blast outbreaks. In Asia, several countries allow cultivation of specific GM crops, with India and China being the world's leaders in GM cotton production. Very recently (July 2021), The Philippines became the first country that allows commercial cultivation of Golden Rice, in addition to its consumption.

9.7 Closing remarks

In conclusion, the work presented in this thesis extends our knowledge of *M. oryzae* effectors, describing a potentially new effector class. Moreover, it contributes to our understanding of the plant immune system and explores its potential towards novel resistance in crops through engineering NLRs, driven by the discovery of putative effector targets. Given the improving precision of gene editing and increasing GM technology approval by governments and society, rational design of NLRs can provide real solutions for sustainable combating plant diseases and contribute globally to future food security.

References

ADACHI, H., CONTRERAS, M. P., HARANT, A., WU, C. H., DEREVNINA, L., SAKAI, T., DUGGAN, C., MORATTO, E., BOZKURT, T. O., MAQBOOL, A., WIN, J. & KAMOUN, S. 2019a. An N-terminal motif in NLR immune receptors is functionally conserved across distantly related plant species. *Elife,* 8.

ADACHI, H., DEREVNINA, L. & KAMOUN, S. 2019b. NLR singletons, pairs, and networks: evolution, assembly, and regulation of the intracellular immunoreceptor circuitry of plants. *Curr Opin Plant Biol,* 50**,** 121-131.

ADE, J., DEYOUNG, B. J., GOLSTEIN, C. & INNES, R. W. 2007. Indirect activation of a plant nucleotide binding site-leucine-rich repeat protein by a bacterial protease. *Proc Natl Acad Sci U S A,* 104**,** 2531-6.

AFROZ, A., CHAUDHRY, Z., RASHID, U., ALI, G. M., NAZIR, F., IQBAL, J. & KHAN, M. R. 2010. Enhanced resistance against bacterial wilt in transgenic tomato (Lycopersicon esculentum) lines expressing the Xa21 gene. *Plant Cell, Tissue and Organ Culture (PCTOC),* 104**,** 227-237.

ALLEN, R. L., BITTNER-EDDY, P. D., GRENVILLE-BRIGGS, L. J., MEITZ, J. C., REHMANY, A. P., ROSE, L. E. & BEYNON, J. L. 2004. Host-parasite coevolutionary conflict between Arabidopsis and downy mildew. *Science,* 306**,** 1957-60.

ANDERSEN, E. J., NEPAL, M. P., PURINTUN, J. M., NELSON, D., MERMIGKA, G. & SARRIS, P. F. 2020. Wheat Disease Resistance Genes and Their Diversification Through Integrated Domain Fusions. *Front Genet,* 11**,** 898.

ARNESANO, F., BANCI, L., BERTINI, I., HUFFMAN, D. L. & O'HALLORAN, T. V. 2001. Solution structure of the Cu(I) and apo forms of the yeast metallochaperone, Atx1. *Biochemistry,* 40**,** 1528-39.

ARORA, S., STEUERNAGEL, B., GAURAV, K., CHANDRAMOHAN, S., LONG, Y., MATNY, O., JOHNSON, R., ENK, J., PERIYANNAN, S., SINGH, N., ASYRAF MD HATTA, M., ATHIYANNAN, N., CHEEMA, J., YU, G., KANGARA, N., GHOSH, S., SZABO, L. J., POLAND, J., BARIANA, H., JONES, J. D. G., BENTLEY, A. R., AYLIFFE, M., OLSON, E., XU, S. S., STEFFENSON, B. J., LAGUDAH, E. & WULFF, B. B. H. 2019. Resistance gene cloning from a wild crop relative by sequence capture and association genetics. *Nat Biotechnol,* 37**,** 139-143.

ASAI, S., SHIRASU, K. & JONES, J. D. G. 2015. Hyaloperonospora arabidopsidis (Downy Mildew) Infection Assay in Arabidopsis. *Bio-protocol,* 5**,** e1627.

ASHIKAWA, I., HAYASHI, N., ABE, F., WU, J. & MATSUMOTO, T. 2012. Characterization of the rice blast resistance gene Pik cloned from Kanto51. *Molecular Breeding,* 30**,** 485-494.

ASHIKAWA, I., HAYASHI, N., YAMANE, H., KANAMORI, H., WU, J., MATSUMOTO, T., ONO, K. & YANO, M. 2008. Two adjacent nucleotide-binding site-leucine-rich repeat class genes are required to confer Pikm-specific rice blast resistance. *Genetics,* 180**,** 2267-76.

AXTELL, M. J. & STASKAWICZ, B. J. 2003. Initiation of RPS2-Specified Disease Resistance in Arabidopsis Is Coupled to the AvrRpt2-Directed Elimination of RIN4. *Cell,* 112**,** 369-377.

BAGGS, E., DAGDAS, G. & KRASILEVA, K. V. 2017. NLR diversity, helpers and integrated domains: making sense of the NLR IDentity. *Curr Opin Plant Biol,* 38**,** 59-67.

BAI, S., LIU, J., CHANG, C., ZHANG, L., MAEKAWA, T., WANG, Q., XIAO, W., LIU, Y., CHAI, J., TAKKEN, F. L., SCHULZE-LEFERT, P. & SHEN, Q. H. 2012. Structure-function analysis of barley NLR immune receptor MLA10 reveals its cell compartment specific activity in cell death and disease resistance. *PLoS Pathog,* 8**,** e1002752.

BAILEY, P. C., SCHUDOMA, C., JACKSON, W., BAGGS, E., DAGDAS, G., HAERTY, W., MOSCOU, M. & KRASILEVA, K. V. 2018. Dominant integration locus drives continuous diversification of plant immune receptors with exogenous domain fusions. *Genome Biology,* 19**,** 23.

BARRAGAN, C. A., WU, R., KIM, S.-T., XI, W., HABRING, A., HAGMANN, J., VAN DE WEYER, A.-L., ZAIDEM, M., HO, W. W. H., WANG, G., BEZRUKOV, I., WEIGEL, D. & CHAE, E. 2019. RPW8/HR repeats control NLR activation in Arabidopsis thaliana. *PLOS Genetics,* 15**,** e1008313.

BARTHO, J. D., DEMITRI, N., BELLINI, D., FLACHOWSKY, H., PEIL, A., WALSH, M. A. & BENINI, S. 2019. The structure of Erwinia amylovora AvrRpt2 provides insight into protein maturation and induced resistance to fire blight by Malus × robusta 5. *Journal of structural biology,* 206**,** 233-242.

BAUDIN, M., HASSAN, J. A., SCHREIBER, K. J. & LEWIS, J. D. 2017. Analysis of the ZAR1 Immune Complex Reveals Determinants for Immunity and Molecular Interactions. *Plant Physiol,* 174**,** 2038-2053.

BEILSTEN-EDMANDS, J., WINTER, G., GILDEA, R., PARKHURST, J., WATERMAN, D. & EVANS, G. 2020. Scaling diffraction data in the DIALS software package: algorithms and new approaches for multi-crystal scaling. *Acta Crystallographica Section D,* 76**,** 385-399.

BENDAHMANE, A., FARNHAM, G., MOFFETT, P. & BAULCOMBE, D. C. 2002. Constitutive gain-of-function mutants in a nucleotide binding site-leucine rich repeat protein encoded at the Rx locus of potato. *Plant J,* 32**,** 195-204.

BENTHAM, A., BURDETT, H., ANDERSON, P. A., WILLIAMS, S. J. & KOBE, B. 2017. Animal NLRs provide structural insights into plant NLR function. *Ann Bot,* 119**,** 827-702.

BENTHAM, A. R., DE LA CONCEPCION, J. C., MUKHI, N., ZDRZALEK, R., DRAEGER, M., GORENKIN, D., HUGHES, R. K. & BANFIELD, M. J. 2020. A molecular roadmap to the plant immune system. *J Biol Chem,* 295**,** 14916-14935.

BENTHAM, A. R., PETIT-HOUDENOT, Y., WIN, J., CHUMA, I., TERAUCHI, R., BANFIELD, M. J., KAMOUN, S. & LANGNER, T. 2021a. A single amino acid polymorphism in a conserved effector of the multihost blast fungus pathogen expands host-target binding spectrum. *bioRxiv***,** 2021.03.15.435478.

BENTHAM, A. R., YOULES, M., MENDEL, M. N., VARDEN, F. A., CONCEPCION, J. C. D. L. & BANFIELD, M. J. 2021b. pOPIN-GG: A resource for modular assembly in protein expression vectors. *bioRxiv***,** 2021.08.10.455798.

BENTHAM, A. R., ZDRZALEK, R., DE LA CONCEPCION, J. C. & BANFIELD, M. J. 2018. Uncoiling CNLs: Structure/Function Approaches to Understanding CC Domain Function in Plant NLRs. *Plant Cell Physiol,* 59**,** 2398-2408.

BERNOUX, M., BURDETT, H., WILLIAMS, S. J., ZHANG, X., CHEN, C., NEWELL, K., LAWRENCE, G. J., KOBE, B., ELLIS, J. G., ANDERSON, P. A. & DODDS, P. N. 2016. Comparative Analysis of the Flax Immune Receptors L6 and L7 Suggests an Equilibrium-Based Switch Activation Model. *Plant Cell,* 28**,** 146-59.

BERNOUX, M., VE, T., WILLIAMS, S., WARREN, C., HATTERS, D., VALKOV, E., ZHANG, X., ELLIS, J. G., KOBE, B. & DODDS, P. N. 2011. Structural and functional analysis of a plant resistance protein TIR domain reveals interfaces for self-association, signaling, and autoregulation. *Cell Host Microbe,* 9**,** 200-211.

BERROW, N. S., ALDERTON, D., SAINSBURY, S., NETTLESHIP, J., ASSENBERG, R., RAHMAN, N., STUART, D. I. & OWENS, R. J. 2007. A versatile ligation-independent cloning method suitable for high-throughput expression screening applications. *Nucleic Acids Res,* 35**,** e45.

BEVAN, M. W., UAUY, C., WULFF, B. B., ZHOU, J., KRASILEVA, K. & CLARK, M. D. 2017. Genomic innovation for crop improvement. *Nature,* 543**,** 346-354.

BI, G., SU, M., LI, N., LIANG, Y., DANG, S., XU, J., HU, M., WANG, J., ZOU, M., DENG, Y., LI, Q., HUANG, S., LI, J., CHAI, J., HE, K., CHEN, Y. H. & ZHOU, J. M. 2021. The ZAR1 resistosome is a calcium-permeable channel triggering plant immune signaling. *Cell,* 184**,** 3528-3541 e12.

BIALAS, A., LANGNER, T., HARANT, A., CONTRERAS, M. P., STEVENSON, C. E., LAWSON, D. M., SKLENAR, J., KELLNER, R., MOSCOU, M. J., TERAUCHI, R., BANFIELD, M. J. & KAMOUN, S. 2021. Two NLR immune receptors acquired high-affinity binding to a fungal effector through convergent evolution of their integrated domain. *Elife,* 10.

BIAŁAS, A., ZESS, E. K., DE LA CONCEPCION, J. C., FRANCESCHETTI, M., PENNINGTON, H. G., YOSHIDA, K., UPSON, J. L., CHANCLUD, E., WU, C.-H., LANGNER, T., MAQBOOL, A., VARDEN, F. A., DEREVNINA, L., BELHAJ, K., FUJISAKI, K., SAITOH, H., TERAUCHI, R., BANFIELD, M. J. &

KAMOUN, S. 2018. Lessons in Effector and NLR Biology of Plant-Microbe Systems. *Molecular Plant-Microbe Interactions®,* 31**,** 34-45.

BIELSKA, E., HIGUCHI, Y., SCHUSTER, M., STEINBERG, N., KILARU, S., TALBOT, N. J. & STEINBERG, G. 2014. Long-distance endosome trafficking drives fungal effector production during plant infection. *Nat Commun,* 5**,** 5097.

BOEVINK, P. C., WANG, X., MCLELLAN, H., HE, Q., NAQVI, S., ARMSTRONG, M. R., ZHANG, W., HEIN, I., GILROY, E. M., TIAN, Z. & BIRCH, P. R. J. 2016. A Phytophthora infestans RXLR effector targets plant PP1c isoforms that promote late blight disease. *Nat Commun,* 7**,** 10311.

BÖHM, H., ALBERT, I., FAN, L., REINHARD, A. & NÜRNBERGER, T. 2014. Immune receptor complexes at the plant cell surface. *Curr Opin Plant Biol,* 20**,** 47-54.

BOHN, T., DESMARCHELIER, C., EL, S. N., KEIJER, J., VAN SCHOTHORST, E., RÜHL, R. & BOREL, P. 2019. β-Carotene in the human body: metabolic bioactivation pathways – from digestion to tissue distribution and excretion. *Proceedings of the Nutrition Society,* 78**,** 68-87.

BOLLER, T. & FELIX, G. 2009. A renaissance of elicitors: perception of microbe-associated molecular patterns and danger signals by pattern-recognition receptors. *Annu Rev Plant Biol,* 60**,** 379-406.

BOMBLIES, K. & WEIGEL, D. 2007. Hybrid necrosis: autoimmunity as a potential gene-flow barrier in plant species. *Nat Rev Genet,* 8**,** 382-93.

BONARDI, V., TANG, S., STALLMANN, A., ROBERTS, M., CHERKIS, K. & DANGL, J. L. 2011. Expanded functions for a family of plant intracellular immune receptors beyond specific recognition of pathogen effectors. *Proc Natl Acad Sci U S A,* 108**,** 16463-8.

BORG, M., MITTAG, T., PAWSON, T., TYERS, M., FORMAN-KAY, J. D. & CHAN, H. S. 2007. Polyelectrostatic interactions of disordered ligands suggest a physical basis for ultrasensitivity. *Proc Natl Acad Sci U S A,* 104**,** 9650-5.

BORGIA, A., BORGIA, M. B., BUGGE, K., KISSLING, V. M., HEIDARSSON, P. O., FERNANDES, C. B., SOTTINI, A., SORANNO, A., BUHOLZER, K. J., NETTELS, D., KRAGELUND, B. B., BEST, R. B. & SCHULER, B. 2018. Extreme disorder in an ultrahigh-affinity protein complex. *Nature,* 555**,** 61-66.

BOTELLA, M. A., PARKER, J. E., FROST, L. N., BITTNER-EDDY, P. D., BEYNON, J. L., DANIELS, M. J., HOLUB, E. B. & JONES, J. D. 1998. Three genes of the Arabidopsis RPP1 complex resistance locus recognize distinct Peronospora parasitica avirulence determinants. *Plant Cell,* 10**,** 1847-60.

BOUTEMY, L. S., KING, S. R. F., WIN, J., HUGHES, R. K., CLARKE, T. A., BLUMENSCHEIN, T. M. A., KAMOUN, S. & BANFIELD, M. J. 2011. Structures of Phytophthora RXLR effector proteins: a conserved but adaptable fold underpins functional diversity. *J Biol Chem,* 286**,** 35834-35842.

BOYD, C. M. & BUBECK, D. 2018. Advances in cryoEM and its impact on β-pore forming proteins. *Current Opinion in Structural Biology,* 52**,** 41-49.

BOZKURT, T. O., SCHORNACK, S., WIN, J., SHINDO, T., ILYAS, M., OLIVA, R., CANO, L. M., JONES, A. M., HUITEMA, E., VAN DER HOORN, R. A. & KAMOUN, S. 2011. Phytophthora infestans effector AVRblb2 prevents secretion of a plant immune protease at the haustorial interface. *Proc Natl Acad Sci U S A,* 108**,** 20832-7.

BROOKES, G. & BARFOOT, P. 2013. The global income and production effects of genetically modified (GM) crops 1996–2011. *GM Crops & Food,* 4**,** 74-83.

BROZ, P. & DIXIT, V. M. 2016. Inflammasomes: mechanism of assembly, regulation and signalling. *Nature Reviews Immunology,* 16**,** 407-420.

BURDETT, H., BENTHAM, A. R., WILLIAMS, S. J., DODDS, P. N., ANDERSON, P. A., BANFIELD, M. J. & KOBE, B. 2019a. The Plant "Resistosome": Structural Insights into Immune Signaling. *Cell Host Microbe,* 26**,** 193-201.

BURDETT, H., KOBE, B. & ANDERSON, P. A. 2019b. Animal NLRs continue to inform plant NLR structure and function. *Arch Biochem Biophys,* 670**,** 58-68.

BÜTTNER, D. 2016. Behind the lines-actions of bacterial type III effector proteins in plant cells. *FEMS Microbiol Rev,* 40**,** 894-937.

CARTER, M. E., HELM, M., CHAPMAN, A. V. E., WAN, E., RESTREPO SIERRA, A. M., INNES, R. W., BOGDANOVE, A. J. & WISE, R. P. 2019. Convergent Evolution of Effector Protease Recognition by Arabidopsis and Barley. *Mol Plant Microbe Interact,* 32**,** 550-565.

CASEY, L. W., LAVRENCIC, P., BENTHAM, A. R., CESARI, S., ERICSSON, D. J., CROLL, T., TURK, D., ANDERSON, P. A., MARK, A. E., DODDS, P. N., MOBLI, M., KOBE, B. & WILLIAMS, S. J. 2016. The CC domain structure from the wheat stem rust resistance protein Sr33 challenges paradigms for dimerization in plant NLR proteins. *Proc Natl Acad Sci U S A*.

CASTEL, B., NGOU, P. M., CEVIK, V., REDKAR, A., KIM, D. S., YANG, Y., DING, P. & JONES, J. D. G. 2019. Diverse NLR immune receptors activate defence via the RPW8-NLR NRG1. *New Phytol,* 222**,** 966-980.

CERESINI, P. C., CASTROAGUDÍN, V. L., RODRIGUES, F., RIOS, J. A., EDUARDO AUCIQUE-PÉREZ, C., MOREIRA, S. I., ALVES, E., CROLL, D. & MACIEL, J. L. N. 2018. Wheat Blast: Past, Present, and Future. *Annu Rev Phytopathol,* 56**,** 427-456.

CESARI, S. 2017. Multiple strategies for pathogen perception by plant immune receptors. *New Phytol*.

CESARI, S., BERNOUX, M., MONCUQUET, P., KROJ, T. & DODDS, P. N. 2014a. A novel conserved mechanism for plant NLR protein pairs: the "integrated decoy" hypothesis. *Front Plant Sci,* 5**,** 606.

CESARI, S., KANZAKI, H., FUJIWARA, T., BERNOUX, M., CHALVON, V., KAWANO, Y., SHIMAMOTO, K., DODDS, P., TERAUCHI, R. & KROJ, T. 2014b. The NB-LRR proteins RGA4 and RGA5 interact functionally and physically to confer disease resistance. *EMBO J,* 33**,** 1941-59.

CESARI, S., MOORE, J., CHEN, C., WEBB, D., PERIYANNAN, S., MAGO, R., BERNOUX, M., LAGUDAH, E. S. & DODDS, P. N. 2016. Cytosolic activation of cell death and stem rust resistance by cereal MLA-family CC-NLR proteins. *Proc Natl Acad Sci U S A,* 113**,** 10204-9.

CESARI, S., THILLIEZ, G., RIBOT, C., CHALVON, V., MICHEL, C., JAUNEAU, A., RIVAS, S., ALAUX, L., KANZAKI, H., OKUYAMA, Y., MOREL, J. B., FOURNIER, E., THARREAU, D., TERAUCHI, R. & KROJ, T. 2013. The rice resistance protein pair RGA4/RGA5 recognizes the Magnaporthe oryzae effectors AVR-Pia and AVR1-CO39 by direct binding. *Plant Cell,* 25**,** 1463-81.

CESARI, S., XI, Y., DECLERCK, N., CHALVON, V., MAMMRI, L., PUGNIÈRE, M., HENRIQUET, C., DE GUILLEN, K., PADILLA, A. & KROJ, T. 2021. Design of a new effector recognition specificity in a plant NLR immune receptor by molecular engineering of its integrated decoy domain. *bioRxiv***,** 2021.04.24.441256.

CHAE, E., BOMBLIES, K., KIM, S. T., KARELINA, D., ZAIDEM, M., OSSOWSKI, S., MARTÍN-PIZARRO, C., LAITINEN, R. A., ROWAN, B. A., TENENBOIM, H., LECHNER, S., DEMAR, M., HABRING-MÜLLER, A., LANZ, C., RÄTSCH, G. & WEIGEL, D. 2014. Species-wide genetic incompatibility analysis identifies immune genes as hot spots of deleterious epistasis. *Cell,* 159**,** 1341-51.

CHAE, E., TRAN, D. T. N. & WEIGEL, D. 2016. Cooperation and Conflict in the Plant Immune System. *PLOS Pathogens,* 12**,** e1005452.

CHANG, C., YU, D., JIAO, J., JING, S., SCHULZE-LEFERT, P. & SHEN, Q. H. 2013. Barley MLA immune receptors directly interfere with antagonistically acting transcription factors to initiate disease resistance signaling. *Plant Cell,* 25**,** 1158-73.

CHEN, C., JOST, M., CLARK, B., MARTIN, M., MATNY, O., STEFFENSON, B. J., FRANCKOWIAK, J. D., MASCHER, M., SINGH, D., PEROVIC, D., RICHARDSON, T., PERIYANNAN, S., LAGUDAH, E. S., PARK, R. F. & DRACATOS, P. M. 2021. BED domain-containing NLR from wild barley confers resistance to leaf rust. *Plant Biotechnol J,* 19**,** 1206-1215.

CHEN, J., PENG, P., TIAN, J., HE, Y., ZHANG, L., LIU, Z., YIN, D. & ZHANG, Z. 2015. Pike, a rice blast resistance allele consisting of two adjacent NBS–LRR genes, was identified as a novel allele at the Pik locus. *Molecular Breeding,* 35**,** 117.

CHEN, V. B., ARENDALL, W. B., 3RD, HEADD, J. J., KEEDY, D. A., IMMORMINO, R. M., KAPRAL, G. J., MURRAY, L. W., RICHARDSON, J. S. & RICHARDSON, D. C. 2010. MolProbity: all-atom structure validation for macromolecular crystallography. *Acta Crystallogr D Biol Crystallogr,* 66**,** 12-21.

CHOU, S., KRASILEVA, K. V., HOLTON, J. M., STEINBRENNER, A. D., ALBER, T. & STASKAWICZ, B. J. 2011. Hyaloperonospora arabidopsidis ATR1 effector is a repeat protein with distributed recognition surfaces. *Proc Natl Acad Sci U S A,* 108**,** 13323-8.

CHUNG, E. H., DA CUNHA, L., WU, A. J., GAO, Z., CHERKIS, K., AFZAL, A. J., MACKEY, D. & DANGL, J. L. 2011. Specific threonine phosphorylation of a host target by two unrelated type III effectors activates a host innate immune receptor in plants. *Cell Host Microbe,* 9**,** 125-36.

CHUNG, E. H., EL-KASMI, F., HE, Y., LOEHR, A. & DANGL, J. L. 2014. A plant phosphoswitch platform repeatedly targeted by type III effector proteins regulates the output of both tiers of plant immune receptors. *Cell Host Microbe,* 16**,** 484-94.

COLLEMARE, J., O'CONNELL, R. & LEBRUN, M.-H. 2019. Nonproteinaceous effectors: the terra incognita of plant–fungal interactions. *New Phytologist,* 223**,** 590-596.

COLLIER, S. M., HAMEL, L. P. & MOFFETT, P. 2011. Cell death mediated by the N-terminal domains of a unique and highly conserved class of NB-LRR protein. *Mol Plant Microbe Interact,* 24**,** 918-31.

COWAN, G. H., ROBERTS, A. G., JONES, S., KUMAR, P., KALYANDURG, P. B., GIL, J. F., SAVENKOV, E. I., HEMSLEY, P. A. & TORRANCE, L. 2018. Potato Mop-Top Virus Co-Opts the Stress Sensor HIPP26 for Long-Distance Movement. *Plant Physiol,* 176**,** 2052-2070.

DE ABREU-NETO, J. B., TURCHETTO-ZOLET, A. C., DE OLIVEIRA, L. F., ZANETTINI, M. H. & MARGIS-PINHEIRO, M. 2013. Heavy metal-associated isoprenylated plant protein (HIPP): characterization of a family of proteins exclusive to plants. *FEBS J,* 280**,** 1604-16.

DE GUILLEN, K., ORTIZ-VALLEJO, D., GRACY, J., FOURNIER, E., KROJ, T. & PADILLA, A. 2015. Structure Analysis Uncovers a Highly Diverse but Structurally Conserved Effector Family in Phytopathogenic Fungi. *PLoS Pathog,* 11**,** e1005228.

DE LA CONCEPCION, J. C., BENJUMEA, J. V., BIAŁAS, A., TERAUCHI, R., KAMOUN, S. & BANFIELD, M. J. 2021a. Functional diversification gave rise to allelic specialization in a rice NLR immune receptor pair. *bioRxiv***,** 2021.06.25.449940.

DE LA CONCEPCION, J. C., FRANCESCHETTI, M., MACLEAN, D., TERAUCHI, R., KAMOUN, S. & BANFIELD, M. J. 2019. Protein engineering expands the effector recognition profile of a rice NLR immune receptor. *Elife,* 8.

DE LA CONCEPCION, J. C., FRANCESCHETTI, M., MAQBOOL, A., SAITOH, H., TERAUCHI, R., KAMOUN, S. & BANFIELD, M. J. 2018. Polymorphic residues in rice NLRs expand binding and response to effectors of the blast pathogen. *Nat Plants,* 4**,** 576-585.

DE LA CONCEPCION, J. C., MAIDMENT, J. H. R., LONGYA, A., XIAO, G., FRANCESCHETTI, M. & BANFIELD, M. J. 2021b. The allelic rice immune receptor Pikh confers extended resistance to strains of the blast fungus through a single polymorphism in the effector binding interface. *PLoS Pathog,* 17**,** e1009368.

DE LA FUENTE VAN BENTEM, S., VOSSEN, J. H., DE VRIES, K. J., VAN WEES, S., TAMELING, W. I., DEKKER, H. L., DE KOSTER, C. G., HARING, M. A., TAKKEN, F. L. & CORNELISSEN, B. J. 2005. Heat shock protein 90 and its co-chaperone protein phosphatase 5 interact with distinct regions of the tomato I-2 disease resistance protein. *Plant J,* 43**,** 284-98.

DEAN, R., VAN KAN, J. A., PRETORIUS, Z. A., HAMMOND-KOSACK, K. E., DI PIETRO, A., SPANU, P. D., RUDD, J. J., DICKMAN, M., KAHMANN, R., ELLIS, J. & FOSTER, G. D. 2012. The Top 10 fungal pathogens in molecular plant pathology. *Mol Plant Pathol,* 13**,** 414-30.

DEREVNINA, L., CONTRERAS, M. P., ADACHI, H., UPSON, J., CRUCES, A. V., XIE, R., SKLENAR, J., MENKE, F. L. H., MUGFORD, S. T., MACLEAN, D., MA, W., HOGENHOUT, S., GOVERSE, A., MAQBOOL, A., WU, C.-H. & KAMOUN, S. 2021. Plant pathogens convergently evolved to

counteract redundant nodes of an NLR immune receptor network. *bioRxiv*, 2021.02.03.429184.

DINESH-KUMAR, S. P., THAM, W. H. & BAKER, B. J. 2000. Structure-function analysis of the tobacco mosaic virus resistance gene N. *Proc Natl Acad Sci U S A,* 97**,** 14789-94.

DODDS, P. N., LAWRENCE, G. J., CATANZARITI, A. M., AYLIFFE, M. A. & ELLIS, J. G. 2004. The Melampsora lini AvrL567 avirulence genes are expressed in haustoria and their products are recognized inside plant cells. *Plant Cell,* 16**,** 755-68.

DODDS, P. N., LAWRENCE, G. J., CATANZARITI, A. M., TEH, T., WANG, C. I., AYLIFFE, M. A., KOBE, B. & ELLIS, J. G. 2006. Direct protein interaction underlies gene-for-gene specificity and coevolution of the flax resistance genes and flax rust avirulence genes. *Proc Natl Acad Sci U S A,* 103**,** 8888-93.

DONG, A., XU, X., EDWARDS, A. M., CHANG, C., CHRUSZCZ, M., CUFF, M., CYMBOROWSKI, M., DI LEO, R., EGOROVA, O., EVDOKIMOVA, E., FILIPPOVA, E., GU, J., GUTHRIE, J., IGNATCHENKO, A., JOACHIMIAK, A., KLOSTERMANN, N., KIM, Y., KORNIYENKO, Y., MINOR, W., QUE, Q., SAVCHENKO, A., SKARINA, T., TAN, K., YAKUNIN, A., YEE, A., YIM, V., ZHANG, R., ZHENG, H., AKUTSU, M., ARROWSMITH, C., AVVAKUMOV, G. V., BOCHKAREV, A., DAHLGREN, L. G., DHE-PAGANON, S., DIMOV, S., DOMBROVSKI, L., FINERTY, P., JR., FLODIN, S., FLORES, A., GRÄSLUND, S., HAMMERSTRÖM, M., HERMAN, M. D., HONG, B. S., HUI, R., JOHANSSON, I., LIU, Y., NILSSON, M., NEDYALKOVA, L., NORDLUND, P., NYMAN, T., MIN, J., OUYANG, H., PARK, H. W., QI, C., RABEH, W., SHEN, L., SHEN, Y., SUKUMARD, D., TEMPEL, W., TONG, Y., TRESAGUES, L., VEDADI, M., WALKER, J. R., WEIGELT, J., WELIN, M., WU, H., XIAO, T., ZENG, H. & ZHU, H. 2007. In situ proteolysis for protein crystallization and structure determination. *Nat Methods,* 4**,** 1019-21.

DONG, S., RAFFAELE, S. & KAMOUN, S. 2015. The two-speed genomes of filamentous pathogens: waltz with plants. *Curr Opin Genet Dev,* 35**,** 57-65.

DUXBURY, Z., MA, Y., FURZER, O. J., HUH, S. U., CEVIK, V., JONES, J. D. & SARRIS, P. F. 2016. Pathogen perception by NLRs in plants and animals: Parallel worlds. *Bioessays,* 38**,** 769-81.

EITAS, T. K. & DANGL, J. L. 2010. NB-LRR proteins: pairs, pieces, perception, partners, and pathways. *Curr Opin Plant Biol,* 13**,** 472-7.

EL KASMI, F., CHUNG, E. H., ANDERSON, R. G., LI, J., WAN, L., EITAS, T. K., GAO, Z. & DANGL, J. L. 2017. Signaling from the plasma-membrane localized plant immune receptor RPM1 requires self-association of the full-length protein. *Proc Natl Acad Sci U S A,* 114**,** E7385-E7394.

EL KASMI, F., HORVATH, D. & LAHAYE, T. 2018. Microbial effectors and the role of water and sugar in the infection battle ground. *Curr Opin Plant Biol,* 44**,** 98-107.

ELLIS, J. G., LAWRENCE, G. J., LUCK, J. E. & DODDS, P. N. 1999. Identification of regions in alleles of the flax rust resistance gene L that determine differences in gene-for-gene specificity. *Plant Cell,* 11**,** 495-506.

EMSLEY, P., LOHKAMP, B., SCOTT, W. G. & COWTAN, K. 2010. Features and development of Coot. *Acta Crystallogr D Biol Crystallogr,* 66**,** 486-501.

ENGELSDORF, T., WILL, C., HOFMANN, J., SCHMITT, C., MERRITT, B. B., RIEGER, L., FRENGER, M. S., MARSCHALL, A., FRANKE, R. B., PATTATHIL, S. & VOLL, L. M. 2017. Cell wall composition and penetration resistance against the fungal pathogen Colletotrichum higginsianum are affected by impaired starch turnover in Arabidopsis mutants. *J Exp Bot,* 68**,** 701-713.

ENGLER, C., KANDZIA, R. & MARILLONNET, S. 2008. A one pot, one step, precision cloning method with high throughput capability. *PLoS One,* 3**,** e3647.

ENGLER, C., YOULES, M., GRUETZNER, R., EHNERT, T. M., WERNER, S., JONES, J. D., PATRON, N. J. & MARILLONNET, S. 2014. A golden gate modular cloning toolbox for plants. *ACS Synth Biol,* 3**,** 839-43.

ESEOLA, A. B., RYDER, L. S., OSES-RUIZ, M., FINDLAY, K., YAN, X., CRUZ-MIRELES, N., MOLINARI, C., GARDUNO-ROSALES, M. & TALBOT, N. J. 2021. Investigating the cell and developmental

biology of plant infection by the rice blast fungus Magnaporthe oryzae. *Fungal Genet Biol,* 154**,** 103562.

ESSUMAN, K., SUMMERS, D. W., SASAKI, Y., MAO, X., YIM, A. K. Y., DIANTONIO, A. & MILBRANDT, J. 2018. TIR Domain Proteins Are an Ancient Family of NAD(+)-Consuming Enzymes. *Curr Biol,* 28**,** 421-430 e4.

EVANS, P. R. & MURSHUDOV, G. N. 2013. How good are my data and what is the resolution? *Acta Crystallographica Section D,* 69**,** 1204-1214.

FARNHAM, G. & BAULCOMBE, D. C. 2006. Artificial evolution extends the spectrum of viruses that are targeted by a disease-resistance gene from potato. *Proceedings of the National Academy of Sciences,* 103**,** 18828-18833.

FAUSTIN, B., LARTIGUE, L., BRUEY, J. M., LUCIANO, F., SERGIENKO, E., BAILLY-MAITRE, B., VOLKMANN, N., HANEIN, D., ROUILLER, I. & REED, J. C. 2007. Reconstituted NALP1 inflammasome reveals two-step mechanism of caspase-1 activation. *Mol Cell,* 25**,** 713-24.

FIGUEROA BETTS, M., MANNING, V. A., CARDWELL, K. B., PANDELOVA, I. & CIUFFETTI, L. M. 2011. The importance of the N-terminus for activity of Ptr ToxB, a chlorosis-inducing host-selective toxin produced by Pyrenophora tritici-repentis. *Physiological and Molecular Plant Pathology,* 75**,** 138-145.

FIRMAN, T. & GHOSH, K. 2018. Sequence charge decoration dictates coil-globule transition in intrinsically disordered proteins. *J Chem Phys,* 148**,** 123305.

FISHER, M. C., HENK, D. A., BRIGGS, C. J., BROWNSTEIN, J. S., MADOFF, L. C., MCCRAW, S. L. & GURR, S. J. 2012. Emerging fungal threats to animal, plant and ecosystem health. *Nature,* 484**,** 186-94.

FLOR, H. H. 1971. Current Status of the Gene-For-Gene Concept. *Annual Review of Phytopathology,* 9**,** 275-296.

FRANCESCHETTI, M., MAQBOOL, A., JIMENEZ-DALMARONI, M. J., PENNINGTON, H. G., KAMOUN, S. & BANFIELD, M. J. 2017. Effectors of Filamentous Plant Pathogens: Commonalities amid Diversity. *Microbiol Mol Biol Rev,* 81.

FU, B. & VENDRUSCOLO, M. 2015. Structure and Dynamics of Intrinsically Disordered Proteins. *Adv Exp Med Biol,* 870**,** 35-48.

FUJISAKI, K., ABE, Y., ITO, A., SAITOH, H., YOSHIDA, K., KANZAKI, H., KANZAKI, E., UTSUSHI, H., YAMASHITA, T., KAMOUN, S. & TERAUCHI, R. 2015. Rice Exo70 interacts with a fungal effector, AVR-Pii, and is required for AVR-Pii-triggered immunity. *Plant J,* 83**,** 875-87.

FUJISAKI, K., ABE, Y., KANZAKI, E., ITO, K., UTSUSHI, H., SAITOH, H., BIAŁAS, A., BANFIELD, M. J., KAMOUN, S. & TERAUCHI, R. 2017. An unconventional NOI/RIN4 domain of a rice NLR protein binds host EXO70 protein to confer fungal immunity. *bioRxiv***,** 239400.

FURST, U., ZENG, Y., ALBERT, M., WITTE, A. K., FLIEGMANN, J. & FELIX, G. 2020. Perception of Agrobacterium tumefaciens flagellin by FLS2(XL) confers resistance to crown gall disease. *Nat Plants,* 6**,** 22-27.

GAO, Z., CHUNG, E. H., EITAS, T. K. & DANGL, J. L. 2011. Plant intracellular innate immune receptor Resistance to Pseudomonas syringae pv. maculicola 1 (RPM1) is activated at, and functions on, the plasma membrane. *Proc Natl Acad Sci U S A,* 108**,** 7619-24.

GHISLAIN, M., BYARUGABA, A. A., MAGEMBE, E., NJOROGE, A., RIVERA, C., ROMAN, M. L., TOVAR, J. C., GAMBOA, S., FORBES, G. A., KREUZE, J. F., BAREKYE, A. & KIGGUNDU, A. 2019. Stacking three late blight resistance genes from wild species directly into African highland potato varieties confers complete field resistance to local blight races. *Plant Biotechnol J,* 17**,** 1119-1129.

GIANNAKOPOULOU, A., STEELE, J. F., SEGRETIN, M. E., BOZKURT, T. O., ZHOU, J., ROBATZEK, S., BANFIELD, M. J., PAIS, M. & KAMOUN, S. 2015. Tomato I2 Immune Receptor Can Be Engineered to Confer Partial Resistance to the Oomycete Phytophthora infestans in Addition to the Fungus Fusarium oxysporum. *Mol Plant Microbe Interact,* 28**,** 1316-29.

GILDEA, R. J. & WINTER, G. 2018. Determination of Patterson group symmetry from sparse multi-crystal data sets in the presence of an indexing ambiguity. *Acta Crystallographica Section D,* 74**,** 405-410.

GIRALDO, M. C. & VALENT, B. 2013. Filamentous plant pathogen effectors in action. *Nat Rev Microbiol,* 11**,** 800-14.

GITSCHIER, J., MOFFAT, B., REILLY, D., WOOD, W. I. & FAIRBROTHER, W. J. 1998. Solution structure of the fourth metal-binding domain from the Menkes copper-transporting ATPase. *Nat Struct Biol,* 5**,** 47-54.

GRIEBEL, T., MAEKAWA, T. & PARKER, J. E. 2014. NOD-like receptor cooperativity in effector-triggered immunity. *Trends Immunol,* 35**,** 562-70.

GRUND, E., TREMOUSAYGUE, D. & DESLANDES, L. 2019. Plant NLRs with Integrated Domains: Unity Makes Strength. *Plant Physiol,* 179**,** 1227-1235.

GUNASEKARAN, K., TSAI, C. J. & NUSSINOV, R. 2004. Analysis of ordered and disordered protein complexes reveals structural features discriminating between stable and unstable monomers. *J Mol Biol,* 341**,** 1327-41.

GÜNTERT, P. 2004. Automated NMR structure calculation with CYANA. *Methods Mol Biol,* 278**,** 353-78.

GUO, L., ZHANG, Y., MA, M., LIU, Q., ZHANG, Y., PENG, Y. & LIU, J. 2018. Crystallization of the rice immune receptor RGA5A_S with the rice blast fungus effector AVR1-CO39 prepared via mixture and tandem strategies. *Acta Crystallogr F Struct Biol Commun,* 74**,** 262-267.

GUO, X., ZHONG, D., XIE, W., HE, Y., ZHENG, Y., LIN, Y., CHEN, Z., HAN, Y., TIAN, D., LIU, W., WANG, F., WANG, Z. & CHEN, S. 2019. Functional Identification of Novel Cell Death-inducing Effector Proteins from Magnaporthe oryzae. *Rice (N Y),* 12**,** 59.

GUTIERREZ, J. R., BALMUTH, A. L., NTOUKAKIS, V., MUCYN, T. S., GIMENEZ-IBANEZ, S., JONES, A. M. & RATHJEN, J. P. 2010. Prf immune complexes of tomato are oligomeric and contain multiple Pto-like kinases that diversify effector recognition. *Plant J,* 61**,** 507-18.

HAMEL, L. P., SEKINE, K. T., WALLON, T., SUGIWAKA, Y., KOBAYASHI, K. & MOFFETT, P. 2016. The Chloroplastic Protein THF1 Interacts with the Coiled-Coil Domain of the Disease Resistance Protein N' and Regulates Light-Dependent Cell Death. *Plant Physiol,* 171**,** 658-74.

HAO, W., COLLIER, S. M., MOFFETT, P. & CHAI, J. 2013. Structural basis for the interaction between the potato virus X resistance protein (Rx) and its cofactor Ran GTPase-activating protein 2 (RanGAP2). *J Biol Chem,* 288**,** 35868-76.

HARRIS, C. J., SLOOTWEG, E. J., GOVERSE, A. & BAULCOMBE, D. C. 2013. Stepwise artificial evolution of a plant disease resistance gene. *Proc Natl Acad Sci U S A,* 110**,** 21189-94.

HE, J., YE, W., CHOI, D. S., WU, B., ZHAI, Y., GUO, B., DUAN, S., WANG, Y., GAN, J., MA, W. & MA, J. 2019. Structural analysis of Phytophthora suppressor of RNA silencing 2 (PSR2) reveals a conserved modular fold contributing to virulence. *Proc Natl Acad Sci U S A,* 116**,** 8054-8059.

HEBERT, H. 2019. CryoEM: a crystals to single particles round-trip. *Current Opinion in Structural Biology,* 58**,** 59-67.

HELM, M., QI, M., SARKAR, S., YU, H., WHITHAM, S. A. & INNES, R. W. 2019. Engineering a Decoy Substrate in Soybean to Enable Recognition of the Soybean Mosaic Virus NIa Protease. *Mol Plant Microbe Interact,* 32**,** 760-769.

HERMSEN, J. G. T. 1963. The genetic basis of hybrid necrosis in wheat. *Genetica,* 33**,** 245-287.

HOLM, L. 2020. Using Dali for Protein Structure Comparison. *Methods Mol Biol,* 2112**,** 29-42.

HORSEFIELD, S., BURDETT, H., ZHANG, X., MANIK, M. K., SHI, Y., CHEN, J., QI, T., GILLEY, J., LAI, J. S., RANK, M. X., CASEY, L. W., GU, W., ERICSSON, D. J., FOLEY, G., HUGHES, R. O., BOSANAC, T., VON ITZSTEIN, M., RATHJEN, J. P., NANSON, J. D., BODEN, M., DRY, I. B., WILLIAMS, S. J., STASKAWICZ, B. J., COLEMAN, M. P., VE, T., DODDS, P. N. & KOBE, B. 2019. NAD(+) cleavage activity by animal and plant TIR domains in cell death pathways. *Science,* 365**,** 793-799.

HOU, S., LIU, Z., SHEN, H. & WU, D. 2019. Damage-Associated Molecular Pattern-Triggered Immunity in Plants. *Front Plant Sci,* 10**,** 646.

HOWLES, P., LAWRENCE, G., FINNEGAN, J., MCFADDEN, H., AYLIFFE, M., DODDS, P. & ELLIS, J. 2005. Autoactive alleles of the flax L6 rust resistance gene induce non-race-specific rust resistance associated with the hypersensitive response. *Mol Plant Microbe Interact,* 18**,** 570-82.

HU, Z., YAN, C., LIU, P., HUANG, Z., MA, R., ZHANG, C., WANG, R., ZHANG, Y., MARTINON, F., MIAO, D., DENG, H., WANG, J., CHANG, J. & CHAI, J. 2013. Crystal structure of NLRC4 reveals its autoinhibition mechanism. *Science,* 341**,** 172-5.

HU, Z., ZHOU, Q., ZHANG, C., FAN, S., CHENG, W., ZHAO, Y., SHAO, F., WANG, H. W., SUI, S. F. & CHAI, J. 2015. Structural and biochemical basis for induced self-propagation of NLRC4. *Science,* 350**,** 399-404.

HUA, L., WU, J., CHEN, C., WU, W., HE, X., LIN, F., WANG, L., ASHIKAWA, I., MATSUMOTO, T., WANG, L. & PAN, Q. 2012. The isolation of Pi1, an allele at the Pik locus which confers broad spectrum resistance to rice blast. *Theor Appl Genet,* 125**,** 1047-55.

HUANG, J., SI, W., DENG, Q., LI, P. & YANG, S. 2014. Rapid evolution of avirulence genes in rice blast fungus Magnaporthe oryzae. *BMC Genet,* 15**,** 45.

HUANG, W., MACLEAN, A. M., SUGIO, A., MAQBOOL, A., BUSSCHER, M., CHO, S.-T., KAMOUN, S., KUO, C.-H., IMMINK, R. G. H. & HOGENHOUT, S. A. 2021. Parasitic modulation of host development by ubiquitin-independent protein degradation. *Cell*.

HUH, S. U., CEVIK, V., DING, P., DUXBURY, Z., MA, Y., TOMLINSON, L., SARRIS, P. F. & JONES, J. D. G. 2017. Protein-protein interactions in the RPS4/RRS1 immune receptor complex. *PLoS Pathog,* 13**,** e1006376.

HURNI, S., BRUNNER, S., STIRNWEIS, D., HERREN, G., PEDITTO, D., MCINTOSH, R. A. & KELLER, B. 2014. The powdery mildew resistance gene Pm8 derived from rye is suppressed by its wheat ortholog Pm3. *Plant J,* 79**,** 904-13.

INOUE, Y., VY, T. T. P., YOSHIDA, K., ASANO, H., MITSUOKA, C., ASUKE, S., ANH, V. L., CUMAGUN, C. J. R., CHUMA, I., TERAUCHI, R., KATO, K., MITCHELL, T., VALENT, B., FARMAN, M. & TOSA, Y. 2017. Evolution of the wheat blast fungus through functional losses in a host specificity determinant. *Science,* 357**,** 80-83.

ISHIGA, Y., UPPLAPAPTI, S. R. & MYSORE, K. S. 2013. Expression analysis reveals a role for hydrophobic or epicuticular wax signals in pre-penetration structure formation of Phakopsora pachyrhizi. *Plant Signaling & Behavior,* 8**,** e26959.

ISLAM, M. T., CROLL, D., GLADIEUX, P., SOANES, D. M., PERSOONS, A., BHATTACHARJEE, P., HOSSAIN, M. S., GUPTA, D. R., RAHMAN, M. M., MAHBOOB, M. G., COOK, N., SALAM, M. U., SUROVY, M. Z., SANCHO, V. B., MACIEL, J. L., NHANIJUNIOR, A., CASTROAGUDIN, V. L., REGES, J. T., CERESINI, P. C., RAVEL, S., KELLNER, R., FOURNIER, E., THARREAU, D., LEBRUN, M. H., MCDONALD, B. A., STITT, T., SWAN, D., TALBOT, N. J., SAUNDERS, D. G., WIN, J. & KAMOUN, S. 2016. Emergence of wheat blast in Bangladesh was caused by a South American lineage of Magnaporthe oryzae. *BMC Biol,* 14**,** 84.

ISLAM, M. T., GUPTA, D. R., HOSSAIN, A., ROY, K. K., HE, X., KABIR, M. R., SINGH, P. K., KHAN, M. A. R., RAHMAN, M. & WANG, G.-L. 2020. Wheat blast: a new threat to food security. *Phytopathology Research,* 2.

ISLAM, M. T., KIM, K. H. & CHOI, J. 2019. Wheat Blast in Bangladesh: The Current Situation and Future Impacts. *Plant Pathol J,* 35**,** 1-10.

ISPOLATOV, I. & DOEBELI, M. 2009. SPECIATION DUE TO HYBRID NECROSIS IN PLANT–PATHOGEN MODELS. *Evolution,* 63**,** 3076-3084.

JACOB, P., KIM, N. H., WU, F., EL-KASMI, F., CHI, Y., WALTON, W. G., FURZER, O. J., LIETZAN, A. D., SUNIL, S., KEMPTHORN, K., REDINBO, M. R., PEI, Z.-M., WAN, L. & DANGL, J. L. 2021a. Plant “helper” immune receptors are Ca²⁺-permeable nonselective cation channels. *Science,* 373**,** 420-425.

JACOB, P., KIM, N. H., WU, F., EL-KASMI, F., CHI, Y., WALTON, W. G., FURZER, O. J., LIETZAN, A. D., SUNIL, S., KEMPTHORN, K., REDINBO, M. R., PEI, Z. M., WAN, L. & DANGL, J. L. 2021b. Plant

"helper" immune receptors are Ca(2+)-permeable nonselective cation channels. *Science,* 373**,** 420-425.

JIA, Y., MCADAMS, S. A., BRYAN, G. T., HERSHEY, H. P. & VALENT, B. 2000. Direct interaction of resistance gene and avirulence gene products confers rice blast resistance. *EMBO J,* 19**,** 4004-14.

JIANG, R. H., TRIPATHY, S., GOVERS, F. & TYLER, B. M. 2008. RXLR effector reservoir in two Phytophthora species is dominated by a single rapidly evolving superfamily with more than 700 members. *Proc Natl Acad Sci U S A,* 105**,** 4874-9.

JIANG, S., YAO, J., MA, K.-W., ZHOU, H., SONG, J., HE, S. Y. & MA, W. 2013. Bacterial Effector Activates Jasmonate Signaling by Directly Targeting JAZ Transcriptional Repressors. *PLOS Pathogens,* 9**,** e1003715.

JONES, J. D. & DANGL, J. L. 2006. The plant immune system. *Nature,* 444**,** 323-9.

JONES, J. D., VANCE, R. E. & DANGL, J. L. 2016. Intracellular innate immune surveillance devices in plants and animals. *Science,* 354.

JUBIC, L. M., SAILE, S., FURZER, O. J., EL KASMI, F. & DANGL, J. L. 2019. Help wanted: helper NLRs and plant immune responses. *Curr Opin Plant Biol,* 50**,** 82-94.

JUMPER, J., EVANS, R., PRITZEL, A., GREEN, T., FIGURNOV, M., RONNEBERGER, O., TUNYASUVUNAKOOL, K., BATES, R., ŽÍDEK, A., POTAPENKO, A., BRIDGLAND, A., MEYER, C., KOHL, S. A. A., BALLARD, A. J., COWIE, A., ROMERA-PAREDES, B., NIKOLOV, S., JAIN, R., ADLER, J., BACK, T., PETERSEN, S., REIMAN, D., CLANCY, E., ZIELINSKI, M., STEINEGGER, M., PACHOLSKA, M., BERGHAMMER, T., BODENSTEIN, S., SILVER, D., VINYALS, O., SENIOR, A. W., KAVUKCUOGLU, K., KOHLI, P. & HASSABIS, D. 2021. Highly accurate protein structure prediction with AlphaFold. *Nature,* 596**,** 583-589.

JUPE, F., WITEK, K., VERWEIJ, W., ŚLIWKA, J., PRITCHARD, L., ETHERINGTON, G. J., MACLEAN, D., COCK, P. J., LEGGETT, R. M., BRYAN, G. J., CARDLE, L., HEIN, I. & JONES, J. D. G. 2013. Resistance gene enrichment sequencing (RenSeq) enables reannotation of the NB-LRR gene family from sequenced plant genomes and rapid mapping of resistance loci in segregating populations. *The Plant Journal,* 76**,** 530-544.

KAMOUN, S., FURZER, O., JONES, J. D., JUDELSON, H. S., ALI, G. S., DALIO, R. J., ROY, S. G., SCHENA, L., ZAMBOUNIS, A., PANABIÈRES, F., CAHILL, D., RUOCCO, M., FIGUEIREDO, A., CHEN, X. R., HULVEY, J., STAM, R., LAMOUR, K., GIJZEN, M., TYLER, B. M., GRÜNWALD, N. J., MUKHTAR, M. S., TOMÉ, D. F., TÖR, M., VAN DEN ACKERVEKEN, G., MCDOWELL, J., DAAYF, F., FRY, W. E., LINDQVIST-KREUZE, H., MEIJER, H. J., PETRE, B., RISTAINO, J., YOSHIDA, K., BIRCH, P. R. & GOVERS, F. 2015. The Top 10 oomycete pathogens in molecular plant pathology. *Mol Plant Pathol,* 16**,** 413-34.

KANG, S., SWEIGARD, J. A. & VALENT, B. 1995. The PWL host specificity gene family in the blast fungus Magnaporthe grisea. *Mol Plant Microbe Interact,* 8**,** 939-48.

KANYUKA, K. & RUDD, J. J. 2019. Cell surface immune receptors: the guardians of the plant's extracellular spaces. *Curr Opin Plant Biol,* 50**,** 1-8.

KANZAKI, H., YOSHIDA, K., SAITOH, H., FUJISAKI, K., HIRABUCHI, A., ALAUX, L., FOURNIER, E., THARREAU, D. & TERAUCHI, R. 2012. Arms race co-evolution of Magnaporthe oryzae AVR-Pik and rice Pik genes driven by their physical interactions. *Plant J,* 72**,** 894-907.

KARASOV, T. L., CHAE, E., HERMAN, J. J. & BERGELSON, J. 2017. Mechanisms to Mitigate the Trade-Off between Growth and Defense. *Plant Cell,* 29**,** 666-680.

KASCHANI, F., SHABAB, M., BOZKURT, T., SHINDO, T., SCHORNACK, S., GU, C., ILYAS, M., WIN, J., KAMOUN, S. & VAN DER HOORN, R. A. 2010. An effector-targeted protease contributes to defense against Phytophthora infestans and is under diversifying selection in natural hosts. *Plant Physiol,* 154**,** 1794-804.

KASCHANI, F. & VAN DER HOORN, R. A. 2011. A model of the C14-EPIC complex indicates hotspots for a protease-inhibitor arms race in the oomycete-potato interaction. *Plant Signal Behav,* 6**,** 109-12.

KAWANO, Y., AKAMATSU, A., HAYASHI, K., HOUSEN, Y., OKUDA, J., YAO, A., NAKASHIMA, A., TAKAHASHI, H., YOSHIDA, H., WONG, H. L., KAWASAKI, T. & SHIMAMOTO, K. 2010. Activation of a Rac GTPase by the NLR family disease resistance protein Pit plays a critical role in rice innate immunity. *Cell Host Microbe,* 7**,** 362-75.

KAWASHIMA, C. G., GUIMARAES, G. A., NOGUEIRA, S. R., MACLEAN, D., COOK, D. R., STEUERNAGEL, B., BAEK, J., BOUYIOUKOS, C., MELO BDO, V., TRISTAO, G., DE OLIVEIRA, J. C., RAUSCHER, G., MITTAL, S., PANICHELLI, L., BACOT, K., JOHNSON, E., IYER, G., TABOR, G., WULFF, B. B., WARD, E., RAIRDAN, G. J., BROGLIE, K. E., WU, G., VAN ESSE, H. P., JONES, J. D. & BROMMONSCHENKEL, S. H. 2016. A pigeonpea gene confers resistance to Asian soybean rust in soybean. *Nat Biotechnol,* 34**,** 661-5.

KEEGAN, R. M. & WINN, M. D. 2007. Automated search-model discovery and preparation for structure solution by molecular replacement. *Acta Crystallographica Section D,* 63**,** 447-457.

KEEGAN, R. M. & WINN, M. D. 2008. MrBUMP: an automated pipeline for molecular replacement. *Acta Crystallographica Section D,* 64**,** 119-124.

KELLEY, L. A., MEZULIS, S., YATES, C. M., WASS, M. N. & STERNBERG, M. J. E. 2015. The Phyre2 web portal for protein modeling, prediction and analysis. *Nature Protocols,* 10**,** 845-858.

KIM, S. H., QI, D., ASHFIELD, T., HELM, M. & INNES, R. W. 2016. Using decoys to expand the recognition specificity of a plant disease resistance protein. *Science,* 351**,** 684-687.

KING, S. R., MCLELLAN, H., BOEVINK, P. C., ARMSTRONG, M. R., BUKHAROVA, T., SUKARTA, O., WIN, J., KAMOUN, S., BIRCH, P. R. & BANFIELD, M. J. 2014. Phytophthora infestans RXLR effector PexRD2 interacts with host MAPKKK ε to suppress plant immune signaling. *Plant Cell,* 26**,** 1345-59.

KLOPFENSTEIN, T. J., ERICKSON, G. E. & BERGER, L. L. 2013. Maize is a critically important source of food, feed, energy and forage in the USA. *Field Crops Research,* 153**,** 5-11.

KOFOED, E. M. & VANCE, R. E. 2011. Innate immune recognition of bacterial ligands by NAIPs determines inflammasome specificity. *Nature,* 477**,** 592-5.

KORADI, R., BILLETER, M. & WÜTHRICH, K. 1996. MOLMOL: a program for display and analysis of macromolecular structures. *J Mol Graph,* 14**,** 51-5, 29-32.

KOURELIS, J., MALIK, S., MATTINSON, O., KRAUTER, S., KAHLON, P. S., PAULUS, J. K. & VAN DER HOORN, R. A. L. 2020. Evolution of a guarded decoy protease and its receptor in solanaceous plants. *Nat Commun,* 11**,** 4393.

KOURELIS, J. & VAN DER HOORN, R. A. L. 2018. Defended to the Nines: 25 Years of Resistance Gene Cloning Identifies Nine Mechanisms for R Protein Function. *Plant Cell,* 30**,** 285-299.

KRASILEVA, K. V., DAHLBECK, D. & STASKAWICZ, B. J. 2010. Activation of an Arabidopsis resistance protein is specified by the in planta association of its leucine-rich repeat domain with the cognate oomycete effector. *Plant Cell,* 22**,** 2444-58.

KRISSINEL, E. 2010. Crystal contacts as nature's docking solutions. *Journal of Computational Chemistry,* 31**,** 133-143.

KRISSINEL, E. 2015. Stock-based detection of protein oligomeric states in jsPISA. *Nucleic Acids Research,* 43**,** W314-W319.

KRISSINEL, E. & HENRICK, K. 2007. Inference of macromolecular assemblies from crystalline state. *J Mol Biol,* 372**,** 774-97.

KROJ, T., CHANCLUD, E., MICHEL-ROMITI, C., GRAND, X. & MOREL, J. B. 2016. Integration of decoy domains derived from protein targets of pathogen effectors into plant immune receptors is widespread. *New Phytol,* 210**,** 618-26.

KUNWAR, S., IRIARTE, F., FAN, Q., EVARISTO DA SILVA, E., RITCHIE, L., NGUYEN, N. S., FREEMAN, J. H., STALL, R. E., JONES, J. B., MINSAVAGE, G. V., COLEE, J., SCOTT, J. W., VALLAD, G. E., ZIPFEL, C., HORVATH, D., WESTWOOD, J., HUTTON, S. F. & PARET, M. L. 2018. Transgenic Expression of EFR and Bs2 Genes for Field Management of Bacterial Wilt and Bacterial Spot of Tomato. *Phytopathology,* 108**,** 1402-1411.

LACOMBE, S., ROUGON-CARDOSO, A., SHERWOOD, E., PEETERS, N., DAHLBECK, D., VAN ESSE, H. P., SMOKER, M., RALLAPALLI, G., THOMMA, B. P., STASKAWICZ, B., JONES, J. D. & ZIPFEL, C. 2010. Interfamily transfer of a plant pattern-recognition receptor confers broad-spectrum bacterial resistance. *Nat Biotechnol,* 28**,** 365-9.

LANGNER, T., BIAŁAS, A. & KAMOUN, S. 2018. The Blast Fungus Decoded: Genomes in Flux. *mBio,* 9.

LANGNER, T., HARANT, A., GOMEZ-LUCIANO, L. B., SHRESTHA, R. K., MALMGREN, A., LATORRE, S. M., BURBANO, H. A., WIN, J. & KAMOUN, S. 2021. Genomic rearrangements generate hypervariable mini-chromosomes in host-specific isolates of the blast fungus. *PLoS Genet,* 17**,** e1009386.

LASKOWSKI, R. A., MOSS, D. S. & THORNTON, J. M. 1993. Main-chain Bond Lengths and Bond Angles in Protein Structures. *Journal of Molecular Biology,* 231**,** 1049-1067.

LEE, A. H., HURLEY, B., FELSENSTEINER, C., YEA, C., CKURSHUMOVA, W., BARTETZKO, V., WANG, P. W., QUACH, V., LEWIS, J. D., LIU, Y. C., BÖRNKE, F., ANGERS, S., WILDE, A., GUTTMAN, D. S. & DESVEAUX, D. 2012. A bacterial acetyltransferase destroys plant microtubule networks and blocks secretion. *PLoS Pathog,* 8**,** e1002523.

LEE, D., BOURDAIS, G., YU, G., ROBATZEK, S. & COAKER, G. 2015. Phosphorylation of the Plant Immune Regulator RPM1-INTERACTING PROTEIN4 Enhances Plant Plasma Membrane H^+-ATPase Activity and Inhibits Flagellin-Triggered Immune Responses in Arabidopsis. *Plant Cell,* 27**,** 2042-56.

LEE, H.-Y., MANG, H., CHOI, E.-H., SEO, Y.-E., KIM, M.-S., OH, S., KIM, S.-B. & CHOI, D. 2020a. Genome-wide functional analysis of hot pepper immune receptors reveals an autonomous NLR cluster in seed plants. *bioRxiv***,** 2019.12.16.878959.

LEE, H.-Y., MANG, H., CHOI, E., SEO, Y.-E., KIM, M.-S., OH, S., KIM, S.-B. & CHOI, D. 2021. Genome-wide functional analysis of hot pepper immune receptors reveals an autonomous NLR clade in seed plants. *New Phytologist,* 229**,** 532-547.

LEE, H.-Y., SEO, Y.-E., LEE, J. H., LEE, S. E., OH, S., KIM, J., JUNG, S., KIM, H., PARK, H., KIM, S., MANG, H. & CHOI, D. 2020b. Plant NLR targets P-type ATPase for executing plasma membrane depolarization leading to calcium influx and cell death. *bioRxiv***,** 2020.08.30.274688.

LEONELLI, L., PELTON, J., SCHOEFFLER, A., DAHLBECK, D., BERGER, J., WEMMER, D. E. & STASKAWICZ, B. 2011. Structural Elucidation and Functional Characterization of the Hyaloperonospora arabidopsidis Effector Protein ATR13. *PLOS Pathogens,* 7**,** e1002428.

LI, J., WANG, Q., LI, C., BI, Y., FU, X. & WANG, R. 2019. Novel haplotypes and networks of AVR-Pik alleles in Magnaporthe oryzae. *BMC Plant Biol,* 19**,** 204.

LI, Q., YI, L., HOI, K. H., MAREK, P., GEORGIOU, G. & IVERSON, B. L. 2017. Profiling Protease Specificity: Combining Yeast ER Sequestration Screening (YESS) with Next Generation Sequencing. *ACS Chem Biol,* 12**,** 510-518.

LIU, J., ELMORE, J. M., LIN, Z. J. & COAKER, G. 2011. A receptor-like cytoplasmic kinase phosphorylates the host target RIN4, leading to the activation of a plant innate immune receptor. *Cell Host Microbe,* 9**,** 137-46.

LIU, J. H., YANG, J. Y., HSU, D. W., LAI, Y. H., LI, Y. P., TSAI, Y. R. & HOU, M. H. 2019. Crystal Structure-Based Exploration of Arginine-Containing Peptide Binding in the ADP-Ribosyltransferase Domain of the Type III Effector XopAI Protein. *Int J Mol Sci,* 20.

LIU, W., LIU, J., TRIPLETT, L., LEACH, J. E. & WANG, G. L. 2014. Novel insights into rice innate immunity against bacterial and fungal pathogens. *Annu Rev Phytopathol,* 52**,** 213-41.

LIU, X., INOUE, H., HAYASHI, N., JIANG, C.-J. & TAKATSUJI, H. 2015. CC-NBS-LRR-Type R Proteins for Rice Blast Commonly Interact with Specific WRKY Transcription Factors. *Plant Molecular Biology Reporter,* 34**,** 533-537.

LO PRESTI, L. & KAHMANN, R. 2017. How filamentous plant pathogen effectors are translocated to host cells. *Curr Opin Plant Biol,* 38**,** 19-24.

LO PRESTI, L., LANVER, D., SCHWEIZER, G., TANAKA, S., LIANG, L., TOLLOT, M., ZUCCARO, A., REISSMANN, S. & KAHMANN, R. 2015. Fungal effectors and plant susceptibility. *Annu Rev Plant Biol,* 66**,** 513-45.

LOBSTEIN, J., EMRICH, C. A., JEANS, C., FAULKNER, M., RIGGS, P. & BERKMEN, M. 2012. SHuffle, a novel Escherichia coli protein expression strain capable of correctly folding disulfide bonded proteins in its cytoplasm. *Microb Cell Fact,* 11**,** 56.

LONGYA, A., CHAIPANYA, C., FRANCESCHETTI, M., MAIDMENT, J. H. R., BANFIELD, M. J. & JANTASURIYARAT, C. 2019. Gene Duplication and Mutation in the Emergence of a Novel Aggressive Allele of the AVR-Pik Effector in the Rice Blast Fungus. *Mol Plant Microbe Interact,* 32**,** 740-749.

LU, Y. & TSUDA, K. 2021. Intimate Association of PRR- and NLR-Mediated Signaling in Plant Immunity. *Mol Plant Microbe Interact,* 34**,** 3-14.

LUDWIG, N., REISSMANN, S., SCHIPPER, K., GONZALEZ, C., ASSMANN, D., GLATTER, T., MORETTI, M., MA, L. S., REXER, K. H., SNETSELAAR, K. & KAHMANN, R. 2021. A cell surface-exposed protein complex with an essential virulence function in Ustilago maydis. *Nat Microbiol,* 6**,** 722-730.

MA, S., LAPIN, D., LIU, L., SUN, Y., SONG, W., ZHANG, X., LOGEMANN, E., YU, D., WANG, J., JIRSCHITZKA, J., HAN, Z., SCHULZE-LEFERT, P., PARKER, J. E. & CHAI, J. 2020. Direct pathogen-induced assembly of an NLR immune receptor complex to form a holoenzyme. *Science,* 370.

MA, Y., GUO, H., HU, L., MARTINEZ, P. P., MOSCHOU, P. N., CEVIK, V., DING, P., DUXBURY, Z., SARRIS, P. F. & JONES, J. D. G. 2018. Distinct modes of derepression of an Arabidopsis immune receptor complex by two different bacterial effectors. *Proc Natl Acad Sci U S A,* 115**,** 10218-10227.

MACHO, A. P. & ZIPFEL, C. 2014. Plant PRRs and the activation of innate immune signaling. *Mol Cell,* 54**,** 263-72.

MACKEY, D., HOLT, B. F., 3RD, WIIG, A. & DANGL, J. L. 2002. RIN4 interacts with Pseudomonas syringae type III effector molecules and is required for RPM1-mediated resistance in Arabidopsis. *Cell,* 108**,** 743-54.

MAEKAWA, T., CHENG, W., SPIRIDON, L. N., TOLLER, A., LUKASIK, E., SAIJO, Y., LIU, P., SHEN, Q. H., MICLUTA, M. A., SOMSSICH, I. E., TAKKEN, F. L. W., PETRESCU, A. J., CHAI, J. & SCHULZE-LEFERT, P. 2011. Coiled-coil domain-dependent homodimerization of intracellular barley immune receptors defines a minimal functional module for triggering cell death. *Cell Host Microbe,* 9**,** 187-199.

MAIDMENT, J. H. R., FRANCESCHETTI, M., MAQBOOL, A., SAITOH, H., JANTASURIYARAT, C., KAMOUN, S., TERAUCHI, R. & BANFIELD, M. J. 2021. Multiple variants of the fungal effector AVR-Pik bind the HMA domain of the rice protein OsHIPP19, providing a foundation to engineer plant defense. *J Biol Chem,* 296**,** 100371.

MANSFIELD, J., GENIN, S., MAGORI, S., CITOVSKY, V., SRIARIYANUM, M., RONALD, P., DOW, M., VERDIER, V., BEER, S. V., MACHADO, M. A., TOTH, I., SALMOND, G. & FOSTER, G. D. 2012. Top 10 plant pathogenic bacteria in molecular plant pathology. *Mol Plant Pathol,* 13**,** 614-29.

MAQBOOL, A., HUGHES, R. K., DAGDAS, Y. F., TREGIDGO, N., ZESS, E., BELHAJ, K., ROUND, A., BOZKURT, T. O., KAMOUN, S. & BANFIELD, M. J. 2016. Structural Basis of Host Autophagy-related Protein 8 (ATG8) Binding by the Irish Potato Famine Pathogen Effector Protein PexRD54. *J Biol Chem,* 291**,** 20270-20282.

MAQBOOL, A., SAITOH, H., FRANCESCHETTI, M., STEVENSON, C. E., UEMURA, A., KANZAKI, H., KAMOUN, S., TERAUCHI, R. & BANFIELD, M. J. 2015. Structural basis of pathogen recognition by an integrated HMA domain in a plant NLR immune receptor. *Elife,* 4.

MARTIN, R., QI, T., ZHANG, H., LIU, F., KING, M., TOTH, C., NOGALES, E. & STASKAWICZ, B. J. 2020. Structure of the activated ROQ1 resistosome directly recognizing the pathogen effector XopQ. *Science,* 370**,** eabd9993.

MATHUR, V., JAVID, L., KULSHRESTHA, S., MANDAL, A. & REDDY, A. A. 2017. World Cultivation of Genetically Modified Crops: Opportunities and Risks. *In:* LICHTFOUSE, E. (ed.) *Sustainable Agriculture Reviews.* Cham: Springer International Publishing.

MCCOY, A. J., GROSSE-KUNSTLEVE, R. W., ADAMS, P. D., WINN, M. D., STORONI, L. C. & READ, R. J. 2007. Phaser crystallographic software. *Journal of Applied Crystallography,* 40**,** 658-674.

MCPHERSON, A. 2017. Protein Crystallization. *In:* WLODAWER, A., DAUTER, Z. & JASKOLSKI, M. (eds.) *Protein Crystallography: Methods and Protocols.* New York, NY: Springer New York.

MELOTTO, M., ZHANG, L., OBLESSUC, P. R. & HE, S. Y. 2017. Stomatal Defense a Decade Later. *Plant Physiol,* 174**,** 561-571.

MENDES, B. M. J., CARDOSO, S. C., BOSCARIOL-CAMARGO, R. L., CRUZ, R. B., MOURÃO FILHO, F. A. A. & BERGAMIN FILHO, A. 2010. Reduction in susceptibility to Xanthomonas axonopodis pv. citri in transgenic Citrus sinensis expressing the rice Xa21 gene. *Plant Pathology,* 59**,** 68-75.

MENTLAK, T. A., KOMBRINK, A., SHINYA, T., RYDER, L. S., OTOMO, I., SAITOH, H., TERAUCHI, R., NISHIZAWA, Y., SHIBUYA, N., THOMMA, B. P. & TALBOT, N. J. 2012. Effector-mediated suppression of chitin-triggered immunity by magnaporthe oryzae is necessary for rice blast disease. *Plant Cell,* 24**,** 322-35.

MESTRE, P. & BAULCOMBE, D. C. 2006. Elicitor-mediated oligomerization of the tobacco N disease resistance protein. *Plant Cell,* 18**,** 491-501.

MEUNIER, E. & BROZ, P. 2017. Evolutionary Convergence and Divergence in NLR Function and Structure. *Trends Immunol,* 38**,** 744-757.

MICSONAI, A., BULYÁKI, É. & KARDOS, J. 2021. BeStSel: From Secondary Structure Analysis to Protein Fold Prediction by Circular Dichroism Spectroscopy. *In:* CHEN, Y. W. & YIU, C.-P. B. (eds.) *Structural Genomics: General Applications.* New York, NY: Springer US.

MICSONAI, A., WIEN, F., KERNYA, L., LEE, Y. H., GOTO, Y., REFREGIERS, M. & KARDOS, J. 2015. Accurate secondary structure prediction and fold recognition for circular dichroism spectroscopy. *Proc Natl Acad Sci U S A,* 112**,** E3095-103.

MISHRA, R., JOSHI, R. K. & ZHAO, K. 2018. Genome Editing in Rice: Recent Advances, Challenges, and Future Implications. *Front Plant Sci,* 9**,** 1361.

MOGHISSI, A. A., PEI, S. & LIU, Y. 2016. Golden rice: scientific, regulatory and public information processes of a genetically modified organism. *Crit Rev Biotechnol,* 36**,** 535-41.

MUKHI, N., BROWN, H., GORENKIN, D., DING, P., BENTHAM, A., JONES, J. & BANFIELD, M. 2021. Perception of structurally distinct effectors by the integrated WRKY domain of a plant immune receptor. *bioRxiv***,** 2021.07.28.454147.

MUKHI, N., GORENKIN, D. & BANFIELD, M. J. 2020. Exploring folds, evolution and host interactions: understanding effector structure/function in disease and immunity. *New Phytol,* 227**,** 326-333.

MURSHUDOV, G. N., SKUBAK, P., LEBEDEV, A. A., PANNU, N. S., STEINER, R. A., NICHOLLS, R. A., WINN, M. D., LONG, F. & VAGIN, A. A. 2011. REFMAC5 for the refinement of macromolecular crystal structures. *Acta Crystallographica Section D,* 67**,** 355-367.

NAKAO, M., NAKAMURA, R., KITA, K., INUKAI, R. & ISHIKAWA, A. 2011. Non-host resistance to penetration and hyphal growth of Magnaporthe oryzae in Arabidopsis. *Sci Rep,* 1**,** 171.

NARUSAKA, M., HATAKEYAMA, K., SHIRASU, K. & NARUSAKA, Y. 2014. Arabidopsis dual resistance proteins, both RPS4 and RRS1, are required for resistance to bacterial wilt in transgenic Brassica crops. *Plant Signal Behav,* 9**,** e29130.

NEDERVEEN, A. J., DORELEIJERS, J. F., VRANKEN, W., MILLER, Z., SPRONK, C. A., NABUURS, S. B., GUNTERT, P., LIVNY, M., MARKLEY, J. L., NILGES, M., ULRICH, E. L., KAPTEIN, R. & BONVIN, A. M. 2005. RECOORD: a recalculated coordinate database of 500+ proteins from the PDB using restraints from the BioMagResBank. *Proteins,* 59**,** 662-72.

NEMRI, A., SAUNDERS, D. G., ANDERSON, C., UPADHYAYA, N. M., WIN, J., LAWRENCE, G. J., JONES, D. A., KAMOUN, S., ELLIS, J. G. & DODDS, P. N. 2014. The genome sequence and effector complement of the flax rust pathogen Melampsora lini. *Front Plant Sci,* 5**,** 98.

NISHIMURA, M. T., ANDERSON, R. G., CHERKIS, K. A., LAW, T. F., LIU, Q. L., MACHIUS, M., NIMCHUK, Z. L., YANG, L., CHUNG, E. H., EL KASMI, F., HYUNH, M., OSBORNE NISHIMURA, E., SONDEK, J. E. & DANGL, J. L. 2017. TIR-only protein RBA1 recognizes a pathogen effector to regulate cell death in Arabidopsis. *Proc Natl Acad Sci U S A,* 114**,** E2053-E2062.

NTOUKAKIS, V., SAUR, I. M., CONLAN, B. & RATHJEN, J. P. 2014. The changing of the guard: the Pto/Prf receptor complex of tomato and pathogen recognition. *Curr Opin Plant Biol,* 20**,** 69-74.

NYARKO, A., SINGARAPU, K. K., FIGUEROA, M., MANNING, V. A., PANDELOVA, I., WOLPERT, T. J., CIUFFETTI, L. M. & BARBAR, E. 2014. Solution NMR structures of Pyrenophora tritici-repentis ToxB and its inactive homolog reveal potential determinants of toxin activity. *J Biol Chem,* 289**,** 25946-56.

OFIR, G., HERBST, E., BAROZ, M., COHEN, D., MILLMAN, A., DORON, S., TAL, N., MALHEIRO, D. B. A., MALITSKY, S., AMITAI, G. & SOREK, R. 2021. Antiviral activity of bacterial TIR domains via signaling molecules that trigger cell death. *bioRxiv***,** 2021.01.06.425286.

OIKAWA, K., FUJISAKI, K., SHIMIZU, M., TAKEDA, T., SAITOH, H., HIRABUCHI, A., HIRAKA, Y., BIAŁAS, A., LANGNER, T., KELLNER, R., BOZKURT, T. O., CESARI, S., KROJ, T., MAIDMENT, J. H. R., BANFIELD, M. J., KAMOUN, S. & TERAUCHI, R. 2020. The blast pathogen effector AVR-Pik binds and stabilizes rice heavy metal-associated (HMA) proteins to co-opt their function in immunity. *bioRxiv***,** 2020.12.01.406389.

ORTIZ, D., DE GUILLEN, K., CESARI, S., CHALVON, V., GRACY, J., PADILLA, A. & KROJ, T. 2017. Recognition of the Magnaporthe oryzae Effector AVR-Pia by the Decoy Domain of the Rice NLR Immune Receptor RGA5. *Plant Cell,* 29**,** 156-168.

OSE, T., OIKAWA, A., NAKAMURA, Y., MAENAKA, K., HIGUCHI, Y., SATOH, Y., FUJIWARA, S., DEMURA, M., SONE, T. & KAMIYA, M. 2015. Solution structure of an avirulence protein, AVR-Pia, from Magnaporthe oryzae. *J Biomol NMR,* 63**,** 229-35.

OUTRAM, M. A., SUNG, Y. C., YU, D., DAGVADORJ, B., RIMA, S. A., JONES, D. A., ERICSSON, D. J., SPERSCHNEIDER, J., SOLOMON, P. S., KOBE, B. & WILLIAMS, S. J. 2021. The crystal structure of SnTox3 from the necrotrophic fungus Parastagonospora nodorum reveals a unique effector fold and provides insight into Snn3 recognition and pro-domain protease processing of fungal effectors. *New Phytol,* 231**,** 2282-2296.

PANDEY, P., LEARY, A. Y., TUMTAS, Y., SAVAGE, Z., DAGVADORJ, B., DUGGAN, C., YUEN, E. L., SANGUANKIATTICHAI, N., TAN, E., KHANDARE, V., CONNERTON, A. J., YUNUSOV, T., MADALINSKI, M., MIRKIN, F. G., SCHORNACK, S., DAGDAS, Y., KAMOUN, S. & BOZKURT, T. O. 2021. An oomycete effector subverts host vesicle trafficking to channel starvation-induced autophagy to the pathogen interface. *Elife,* 10.

PANSTRUGA, R. & MOSCOU, M. J. 2020. What is the Molecular Basis of Nonhost Resistance? *Mol Plant Microbe Interact,* 33**,** 1253-1264.

PARK, C. H., CHEN, S., SHIRSEKAR, G., ZHOU, B., KHANG, C. H., SONGKUMARN, P., AFZAL, A. J., NING, Y., WANG, R., BELLIZZI, M., VALENT, B. & WANG, G. L. 2012. The Magnaporthe oryzae effector AvrPiz-t targets the RING E3 ubiquitin ligase APIP6 to suppress pathogen-associated molecular pattern-triggered immunity in rice. *Plant Cell,* 24**,** 4748-62.

PARK, C. H., SHIRSEKAR, G., BELLIZZI, M., CHEN, S., SONGKUMARN, P., XIE, X., SHI, X., NING, Y., ZHOU, B., SUTTIVIRIYA, P., WANG, M., UMEMURA, K. & WANG, G. L. 2016. The E3 Ligase APIP10 Connects the Effector AvrPiz-t to the NLR Receptor Piz-t in Rice. *PLoS Pathog,* 12**,** e1005529.

PENNISI, E. 2010. Armed and dangerous. *Science,* 327**,** 804-5.

PERMYAKOV, S. E., MILLETT, I. S., DONIACH, S., PERMYAKOV, E. A. & UVERSKY, V. N. 2003. Natively unfolded C-terminal domain of caldesmon remains substantially unstructured after the effective binding to calmodulin. *Proteins,* 53**,** 855-62.

PETIT-HOUDENOT, Y., LANGNER, T., HARANT, A., WIN, J. & KAMOUN, S. 2020. A Clone Resource of Magnaporthe oryzae Effectors That Share Sequence and Structural Similarities Across Host-Specific Lineages. *Molecular Plant-Microbe Interactions®,* 33**,** 1032-1035.

PETTERSEN, E. F., GODDARD, T. D., HUANG, C. C., MENG, E. C., COUCH, G. S., CROLL, T. I., MORRIS, J. H. & FERRIN, T. E. 2021. UCSF ChimeraX: Structure visualization for researchers, educators, and developers. *Protein Sci,* 30**,** 70-82.

PINEIRO, A., MUNOZ, E., SABIN, J., COSTAS, M., BASTOS, M., VELAZQUEZ-CAMPOY, A., GARRIDO, P. F., DUMAS, P., ENNIFAR, E., GARCIA-RIO, L., RIAL, J., PEREZ, D., FRAGA, P., RODRIGUEZ, A. & COTELO, C. 2019. AFFINImeter: A software to analyze molecular recognition processes from experimental data. *Anal Biochem,* 577**,** 117-134.

POTTINGER, S. E., BAK, A., MARGETS, A., HELM, M., TANG, L., CASTEEL, C. & INNES, R. W. 2020. Optimizing the PBS1 Decoy System to Confer Resistance to Potyvirus Infection in Arabidopsis and Soybean. *Mol Plant Microbe Interact*.

POTTINGER, S. E. & INNES, R. W. 2020. RPS5-Mediated Disease Resistance: Fundamental Insights and Translational Applications. *Annu Rev Phytopathol*.

QI, D., DEYOUNG, B. J. & INNES, R. W. 2012. Structure-function analysis of the coiled-coil and leucine-rich repeat domains of the RPS5 disease resistance protein. *Plant Physiol,* 158**,** 1819-32.

QI, T., SEONG, K., THOMAZELLA, D. P. T., KIM, J. R., PHAM, J., SEO, E., CHO, M. J., SCHULTINK, A. & STASKAWICZ, B. J. 2018. NRG1 functions downstream of EDS1 to regulate TIR-NLR-mediated plant immunity in Nicotiana benthamiana. *Proc Natl Acad Sci U S A,* 115**,** E10979-E10987.

RADAKOVIC, Z. S., ANJAM, M. S., ESCOBAR, E., CHOPRA, D., CABRERA, J., SILVA, A. C., ESCOBAR, C., SOBCZAK, M., GRUNDLER, F. M. W. & SIDDIQUE, S. 2018. Arabidopsis HIPP27 is a host susceptibility gene for the beet cyst nematode Heterodera schachtii. *Mol Plant Pathol*.

RAFFAELE, S., FARRER, R. A., CANO, L. M., STUDHOLME, D. J., MACLEAN, D., THINES, M., JIANG, R. H. Y., ZODY, M. C., KUNJETI, S. G., DONOFRIO, N. M., MEYERS, B. C., NUSBAUM, C. & KAMOUN, S. 2010. Genome evolution following host jumps in the Irish potato famine pathogen lineage. *Science (New York, N.Y.),* 330**,** 1540-3.

RAFFAELE, S. & KAMOUN, S. 2012. Genome evolution in filamentous plant pathogens: why bigger can be better. *Nat Rev Microbiol,* 10**,** 417-30.

RAIRDAN, G. J. & MOFFETT, P. 2006. Distinct domains in the ARC region of the potato resistance protein Rx mediate LRR binding and inhibition of activation. *Plant Cell,* 18**,** 2082-93.

RANUM, P., PEÑA-ROSAS, J. P. & GARCIA-CASAL, M. N. 2014. Global maize production, utilization, and consumption. *Annals of the New York Academy of Sciences,* 1312**,** 105-112.

RICHARD, M. M. S. & TAKKEN, F. L. W. 2017. Plant Autoimmunity: When Good Things Go Bad. *Curr Biol,* 27**,** R361-r363.

ROBERTS, M., TANG, S., STALLMANN, A., DANGL, J. L. & BONARDI, V. 2013. Genetic requirements for signaling from an autoactive plant NB-LRR intracellular innate immune receptor. *PLoS Genet,* 9**,** e1003465.

RODRIGUEZ-MORENO, L., SONG, Y. & THOMMA, B. P. 2017. Transfer and engineering of immune receptors to improve recognition capacities in crops. *Curr Opin Plant Biol,* 38**,** 42-49.

SAIJO, Y., LOO, E. P. & YASUDA, S. 2018. Pattern recognition receptors and signaling in plant-microbe interactions. *Plant J,* 93**,** 592-613.

SANCHEZ-VALLET, A., SALEEM-BATCHA, R., KOMBRINK, A., HANSEN, G., VALKENBURG, D. J., THOMMA, B. P. & MESTERS, J. R. 2013. Fungal effector Ecp6 outcompetes host immune receptor for chitin binding through intrachain LysM dimerization. *Elife,* 2**,** e00790.

SARRIS, P. F., CEVIK, V., DAGDAS, G., JONES, J. D. & KRASILEVA, K. V. 2016. Comparative analysis of plant immune receptor architectures uncovers host proteins likely targeted by pathogens. *BMC Biol,* 14**,** 8.

SARRIS, P. F., DUXBURY, Z., HUH, S. U., MA, Y., SEGONZAC, C., SKLENAR, J., DERBYSHIRE, P., CEVIK, V., RALLAPALLI, G., SAUCET, S. B., WIRTHMUELLER, L., MENKE, F. L. H., SOHN, K. H. & JONES, J. D. G. 2015. A Plant Immune Receptor Detects Pathogen Effectors that Target WRKY Transcription Factors. *Cell,* 161**,** 1089-1100.

SAUNDERS, D. G., WIN, J., CANO, L. M., SZABO, L. J., KAMOUN, S. & RAFFAELE, S. 2012. Using hierarchical clustering of secreted protein families to classify and rank candidate effectors of rust fungi. *PLoS One,* 7**,** e29847.

SAUR, I. M. L., BAUER, S., LU, X. & SCHULZE-LEFERT, P. 2019. A cell death assay in barley and wheat protoplasts for identification and validation of matching pathogen AVR effector and plant NLR immune receptors. *Plant Methods,* 15**,** 118.

SAVARY, S., WILLOCQUET, L., PETHYBRIDGE, S. J., ESKER, P., MCROBERTS, N. & NELSON, A. 2019. The global burden of pathogens and pests on major food crops. *Nature Ecology & Evolution,* 3**,** 430-439.

SCHNEIDER, D. R., SARAIVA, A. M., AZZONI, A. R., MIRANDA, H. R., DE TOLEDO, M. A., PELLOSO, A. C. & SOUZA, A. P. 2010. Overexpression and purification of PWL2D, a mutant of the effector protein PWL2 from Magnaporthe grisea. *Protein Expr Purif,* 74**,** 24-31.

SCHOLTHOF, K. B., ADKINS, S., CZOSNEK, H., PALUKAITIS, P., JACQUOT, E., HOHN, T., HOHN, B., SAUNDERS, K., CANDRESSE, T., AHLQUIST, P., HEMENWAY, C. & FOSTER, G. D. 2011. Top 10 plant viruses in molecular plant pathology. *Mol Plant Pathol,* 12**,** 938-54.

SCHOONBEEK, H. J., WANG, H. H., STEFANATO, F. L., CRAZE, M., BOWDEN, S., WALLINGTON, E., ZIPFEL, C. & RIDOUT, C. J. 2015. Arabidopsis EF-Tu receptor enhances bacterial disease resistance in transgenic wheat. *New Phytol,* 206**,** 606-13.

SCHREIBER, K. J., BENTHAM, A., WILLIAMS, S. J., KOBE, B. & STASKAWICZ, B. J. 2016. Multiple Domain Associations within the Arabidopsis Immune Receptor RPP1 Regulate the Activation of Programmed Cell Death. *PLoS Pathog,* 12**,** e1005769.

SEGRETIN, M. E., PAIS, M., FRANCESCHETTI, M., CHAPARRO-GARCIA, A., BOS, J. I., BANFIELD, M. J. & KAMOUN, S. 2014. Single amino acid mutations in the potato immune receptor R3a expand response to Phytophthora effectors. *Mol Plant Microbe Interact,* 27**,** 624-37.

SETO, D., KOULENA, N., LO, T., MENNA, A., GUTTMAN, D. S. & DESVEAUX, D. 2017. Expanded type III effector recognition by the ZAR1 NLR protein using ZED1-related kinases. *Nat Plants,* 3**,** 17027.

SHAO, F., GOLSTEIN, C., ADE, J., STOUTEMYER, M., DIXON, J. E. & INNES, R. W. 2003. Cleavage of Arabidopsis PBS1 by a bacterial type III effector. *Science,* 301**,** 1230-3.

SHARMA, R., RADULY, Z., MISKEI, M. & FUXREITER, M. 2015. Fuzzy complexes: Specific binding without complete folding. *FEBS Lett,* 589**,** 2533-42.

SHEN, Y. & BAX, A. 2013. Protein backbone and sidechain torsion angles predicted from NMR chemical shifts using artificial neural networks. *J Biomol NMR,* 56**,** 227-41.

SHIMIZU, M., HIRABUCHI, A., SUGIHARA, Y., ABE, A., TAKEDA, T., KOBAYASHI, M., HIRAKA, Y., KANZAKI, E., OIKAWA, K., SAITOH, H., LANGNER, T., BANFIELD, M. J., KAMOUN, S. & TERAUCHI, R. 2021. A genetically linked pair of NLR immune receptors show contrasting patterns of evolution. *bioRxiv***,** 2021.09.01.458560.

SINGH, P. K., GAHTYARI, N. C., ROY, C., ROY, K. K., HE, X., TEMBO, B., XU, K., JULIANA, P., SONDER, K., KABIR, M. R. & CHAWADE, A. 2021. Wheat Blast: A Disease Spreading by Intercontinental Jumps and Its Management Strategies. *Front Plant Sci,* 12**,** 710707.

SKUBÁK, P., ARAÇ, D., BOWLER, M. W., CORREIA, A. R., HOELZ, A., LARSEN, S., LEONARD, G. A., MCCARTHY, A. A., MCSWEENEY, S., MUELLER-DIECKMANN, C., OTTEN, H., SALZMAN, G. & PANNU, N. S. 2018. A new MR-SAD algorithm for the automatic building of protein models from low-resolution X-ray data and a poor starting model. *IUCrJ,* 5**,** 166-171.

SKUBÁK, P. & PANNU, N. S. 2013. Automatic protein structure solution from weak X-ray data. *Nature Communications,* 4**,** 2777.

SLOOTWEG, E. J., SPIRIDON, L. N., ROOSIEN, J., BUTTERBACH, P., POMP, R., WESTERHOF, L., WILBERS, R., BAKKER, E., BAKKER, J., PETRESCU, A. J., SMANT, G. & GOVERSE, A. 2013. Structural determinants at the interface of the ARC2 and leucine-rich repeat domains control the activation of the plant immune receptors Rx1 and Gpa2. *Plant Physiol,* 162**,** 1510-28.

SONG, J., WIN, J., TIAN, M., SCHORNACK, S., KASCHANI, F., ILYAS, M., VAN DER HOORN, R. A. L. & KAMOUN, S. 2009. Apoplastic effectors secreted by two unrelated eukaryotic plant pathogens target the tomato defense protease Rcr3. *Proceedings of the National Academy of Sciences,* 106**,** 1654-1659.

SPERSCHNEIDER, J., DODDS, P. N., GARDINER, D. M., SINGH, K. B. & TAYLOR, J. M. 2018. Improved prediction of fungal effector proteins from secretomes with EffectorP 2.0. *Mol Plant Pathol,* 19**,** 2094-2110.

SPERSCHNEIDER, J., GARDINER, D. M., DODDS, P. N., TINI, F., COVARELLI, L., SINGH, K. B., MANNERS, J. M. & TAYLOR, J. M. 2016. EffectorP: predicting fungal effector proteins from secretomes using machine learning. *New Phytol,* 210**,** 743-61.

STEELE, J. F. C., HUGHES, R. K. & BANFIELD, M. J. 2019. Structural and biochemical studies of an NB-ARC domain from a plant NLR immune receptor. *PLoS One,* 14**,** e0221226.

STEINBRENNER, A. D., GORITSCHNIG, S. & STASKAWICZ, B. J. 2015. Recognition and activation domains contribute to allele-specific responses of an Arabidopsis NLR receptor to an oomycete effector protein. *PLoS Pathog,* 11**,** e1004665.

STEUERNAGEL, B., PERIYANNAN, S. K., HERNÁNDEZ-PINZÓN, I., WITEK, K., ROUSE, M. N., YU, G., HATTA, A., AYLIFFE, M., BARIANA, H., JONES, J. D., LAGUDAH, E. S. & WULFF, B. B. 2016. Rapid cloning of disease-resistance genes in plants using mutagenesis and sequence capture. *Nat Biotechnol,* 34**,** 652-5.

STIRNWEIS, D., MILANI, S. D., BRUNNER, S., HERREN, G., BUCHMANN, G., PEDITTO, D., JORDAN, T. & KELLER, B. 2014. Suppression among alleles encoding nucleotide-binding-leucine-rich repeat resistance proteins interferes with resistance in F1 hybrid and allele-pyramided wheat plants. *Plant J,* 79**,** 893-903.

SWEIGARD, J. A., CARROLL, A. M., KANG, S., FARRALL, L., CHUMLEY, F. G. & VALENT, B. 1995. Identification, cloning, and characterization of PWL2, a gene for host species specificity in the rice blast fungus. *Plant Cell,* 7**,** 1221-33.

TAKKEN, F. L., ALBRECHT, M. & TAMELING, W. I. 2006. Resistance proteins: molecular switches of plant defence. *Curr Opin Plant Biol,* 9**,** 383-90.

TAKKEN, F. L. & GOVERSE, A. 2012. How to build a pathogen detector: structural basis of NB-LRR function. *Curr Opin Plant Biol,* 15**,** 375-84.

TAMELING, W. I., VOSSEN, J. H., ALBRECHT, M., LENGAUER, T., BERDEN, J. A., HARING, M. A., CORNELISSEN, B. J. & TAKKEN, F. L. 2006. Mutations in the NB-ARC domain of I-2 that impair ATP hydrolysis cause autoactivation. *Plant Physiol,* 140**,** 1233-45.

TAMELING, W. I. L., ELZINGA, S. D. J., DARMIN, P. S., VOSSEN, J. H., TAKKEN, F. L. W., HARING, M. A. & CORNELISSEN, B. J. C. 2002. The Tomato R Gene Products I-2 and Mi-1 Are Functional ATP Binding Proteins with ATPase Activity. *The Plant Cell,* 14**,** 2929-2939.

TANG, M., NING, Y., SHU, X., DONG, B., ZHANG, H., WU, D., WANG, H., WANG, G. L. & ZHOU, B. 2017. The Nup98 Homolog APIP12 Targeted by the Effector AvrPiz-t is Involved in Rice Basal Resistance Against Magnaporthe oryzae. *Rice (N Y),* 10**,** 5.

TEMBO, B., MULENGA, R. M., SICHILIMA, S., M'SISKA, K. K., MWALE, M., CHIKOTI, P. C., SINGH, P. K., HE, X., PEDLEY, K. F., PETERSON, G. L., SINGH, R. P. & BRAUN, H. J. 2020. Detection and characterization of fungus (Magnaporthe oryzae pathotype Triticum) causing wheat blast disease on rain-fed grown wheat (Triticum aestivum L.) in Zambia. *PLOS ONE,* 15**,** e0238724.

TENTHOREY, J. L., HALOUPEK, N., LOPEZ-BLANCO, J. R., GROB, P., ADAMSON, E., HARTENIAN, E., LIND, N. A., BOURGEOIS, N. M., CHACON, P., NOGALES, E. & VANCE, R. E. 2017. The structural basis of flagellin detection by NAIP5: A strategy to limit pathogen immune evasion. *Science,* 358**,** 888-893.

THINES, M. 2019. An evolutionary framework for host shifts – jumping ships for survival. *New Phytologist,* 224**,** 605-617.

TIAN, J., XU, G. & YUAN, M. 2020. Towards Engineering Broad-Spectrum Disease-Resistant Crops. *Trends Plant Sci,* 25**,** 424-427.

TIAN, M., BENEDETTI, B. & KAMOUN, S. 2005. A Second Kazal-like protease inhibitor from Phytophthora infestans inhibits and interacts with the apoplastic pathogenesis-related protease P69B of tomato. *Plant Physiol,* 138**,** 1785-93.

TIAN, M., HUITEMA, E., DA CUNHA, L., TORTO-ALALIBO, T. & KAMOUN, S. 2004. A Kazal-like extracellular serine protease inhibitor from Phytophthora infestans targets the tomato pathogenesis-related protease P69B. *J Biol Chem,* 279**,** 26370-7.

TIAN, M., WIN, J., SONG, J., VAN DER HOORN, R., VAN DER KNAAP, E. & KAMOUN, S. 2007. A Phytophthora infestans cystatin-like protein targets a novel tomato papain-like apoplastic protease. *Plant Physiol,* 143**,** 364-77.

TOBI, D. & BAHAR, I. 2005. Structural changes involved in protein binding correlate with intrinsic motions of proteins in the unbound state. *Proc Natl Acad Sci U S A,* 102**,** 18908-13.

TORUÑO, T. Y., STERGIOPOULOS, I. & COAKER, G. 2016. Plant-Pathogen Effectors: Cellular Probes Interfering with Plant Defenses in Spatial and Temporal Manners. *Annu Rev Phytopathol,* 54**,** 419-41.

TOWNSEND, P. D., DIXON, C. H., SLOOTWEG, E. J., SUKARTA, O. C. A., YANG, A. W. H., HUGHES, T. R., SHARPLES, G. J., PALSSON, L. O., TAKKEN, F. L. W., GOVERSE, A. & CANN, M. J. 2018. The intracellular immune receptor Rx1 regulates the DNA-binding activity of a Golden2-like transcription factor. *J Biol Chem,* 293**,** 3218-3233.

TRAN, D. T. N., CHUNG, E. H., HABRING-MULLER, A., DEMAR, M., SCHWAB, R., DANGL, J. L., WEIGEL, D. & CHAE, E. 2017. Activation of a Plant NLR Complex through Heteromeric Association with an Autoimmune Risk Variant of Another NLR. *Curr Biol,* 27**,** 1148-1160.

TRIPATHI, J. N., LORENZEN, J., BAHAR, O., RONALD, P. & TRIPATHI, L. 2014. Transgenic expression of the rice Xa21 pattern-recognition receptor in banana (Musa sp.) confers resistance to Xanthomonas campestris pv. musacearum. *Plant Biotechnol J,* 12**,** 663-73.

TURNBULL, C., LILLEMO, M. & HVOSLEF-EIDE, T. A. K. 2021. Global Regulation of Genetically Modified Crops Amid the Gene Edited Crop Boom - A Review. *Front Plant Sci,* 12**,** 630396.

UVERSKY, V. N. 2010. The mysterious unfoldome: structureless, underappreciated, yet vital part of any given proteome. *J Biomed Biotechnol,* 2010**,** 568068.

UVERSKY, V. N. 2019. Intrinsically Disordered Proteins and Their “Mysterious” (Meta)Physics. *Frontiers in Physics,* 7.

UVERSKY, V. N., GILLESPIE, J. R. & FINK, A. L. 2000. Why are "natively unfolded" proteins unstructured under physiologic conditions? *Proteins,* 41**,** 415-27.

UVERSKY, V. N., GILLESPIE, J. R., MILLETT, I. S., KHODYAKOVA, A. V., VASILIEV, A. M., CHERNOVSKAYA, T. V., VASILENKO, R. N., KOZLOVSKAYA, G. D., DOLGIKH, D. A., FINK, A. L., DONIACH, S. & ABRAMOV, V. M. 1999. Natively unfolded human prothymosin alpha adopts partially folded collapsed conformation at acidic pH. *Biochemistry,* 38**,** 15009-16.

UVERSKY, V. N., PERMYAKOV, S. E., ZAGRANICHNY, V. E., RODIONOV, I. L., FINK, A. L., CHERSKAYA, A. M., WASSERMAN, L. A. & PERMYAKOV, E. A. 2002. Effect of zinc and temperature on the conformation of the gamma subunit of retinal phosphodiesterase: a natively unfolded protein. *J Proteome Res,* 1**,** 149-59.

VAID, N. & LAITINEN, R. A. E. 2019. Diverse paths to hybrid incompatibility in Arabidopsis. *Plant J,* 97**,** 199-213.

VAN DER HOORN, R. A. & KAMOUN, S. 2008. From Guard to Decoy: a new model for perception of plant pathogen effectors. *Plant Cell,* 20**,** 2009-17.

VAN ESSE, H. P., REUBER, T. L. & VAN DER DOES, D. 2020. Genetic modification to improve disease resistance in crops. *New Phytol,* 225**,** 70-86.

VAN OOIJEN, G., MAYR, G., KASIEM, M. M., ALBRECHT, M., CORNELISSEN, B. J. & TAKKEN, F. L. 2008. Structure-function analysis of the NB-ARC domain of plant disease resistance proteins. *J Exp Bot,* 59**,** 1383-97.

VARDEN, F. A., SAITOH, H., YOSHINO, K., FRANCESCHETTI, M., KAMOUN, S., TERAUCHI, R. & BANFIELD, M. J. 2019. Cross-reactivity of a rice NLR immune receptor to distinct effectors from the rice blast pathogen Magnaporthe oryzae provides partial disease resistance. *J Biol Chem,* 294**,** 13006-13016.

VONRHEIN, C., FLENSBURG, C., KELLER, P., SHARFF, A., SMART, O., PACIOREK, W., WOMACK, T. & BRICOGNE, G. 2011. Data processing and analysis with the autoPROC toolbox. *Acta Crystallographica Section D,* 67**,** 293-302.

WALLINGTON, T. J., ANDERSON, J. E., MUELLER, S. A., KOLINSKI MORRIS, E., WINKLER, S. L., GINDER, J. M. & NIELSEN, O. J. 2012. Corn Ethanol Production, Food Exports, and Indirect Land Use Change. *Environmental Science & Technology,* 46**,** 6379-6384.

WAN, L., ESSUMAN, K., ANDERSON, R. G., SASAKI, Y., MONTEIRO, F., CHUNG, E. H., OSBORNE NISHIMURA, E., DIANTONIO, A., MILBRANDT, J., DANGL, J. L. & NISHIMURA, M. T. 2019. TIR domains of plant immune receptors are NAD(+)-cleaving enzymes that promote cell death. *Science,* 365**,** 799-803.

WANG, G., ROUX, B., FENG, F., GUY, E., LI, L., LI, N., ZHANG, X., LAUTIER, M., JARDINAUD, M. F., CHABANNES, M., ARLAT, M., CHEN, S., HE, C., NOEL, L. D. & ZHOU, J. M. 2015a. The Decoy Substrate of a Pathogen Effector and a Pseudokinase Specify Pathogen-Induced Modified-Self Recognition and Immunity in Plants. *Cell Host Microbe,* 18**,** 285-95.

WANG, G., ROUX, B., FENG, F., GUY, E., LI, L., LI, N., ZHANG, X., LAUTIER, M., JARDINAUD, M. F., CHABANNES, M., ARLAT, M., CHEN, S., HE, C., NOËL, L. D. & ZHOU, J. M. 2015b. The Decoy Substrate of a Pathogen Effector and a Pseudokinase Specify Pathogen-Induced Modified-Self Recognition and Immunity in Plants. *Cell Host Microbe,* 18**,** 285-95.

WANG, G. F., JI, J., EL-KASMI, F., DANGL, J. L., JOHAL, G. & BALINT-KURTI, P. J. 2015c. Molecular and functional analyses of a maize autoactive NB-LRR protein identify precise structural requirements for activity. *PLoS Pathog,* 11**,** e1004674.

WANG, J., HU, M., WANG, J., QI, J., HAN, Z., WANG, G., QI, Y., WANG, H. W., ZHOU, J. M. & CHAI, J. 2019a. Reconstitution and structure of a plant NLR resistosome conferring immunity. *Science,* 364.

WANG, J., WANG, J., HU, M., WU, S., QI, J., WANG, G., HAN, Z., QI, Y., GAO, N., WANG, H. W., ZHOU, J. M. & CHAI, J. 2019b. Ligand-triggered allosteric ADP release primes a plant NLR complex. *Science,* 364.

WANG, Q., LI, Y., KOSAMI, K.-I., LIU, C., LI, J., ZHANG, D., MIKI, D. & KAWANO, Y. 2021a. Three conserved hydrophobic residues in the CC domain of Pit contribute to its plasma membrane localization and immune induction. *bioRxiv***,** 2021.07.31.454611.

WANG, R., NING, Y., SHI, X., HE, F., ZHANG, C., FAN, J., JIANG, N., ZHANG, Y., ZHANG, T., HU, Y., BELLIZZI, M. & WANG, G. L. 2016. Immunity to Rice Blast Disease by Suppression of Effector-Triggered Necrosis. *Curr Biol,* 26**,** 2399-2411.

WANG, S., HUANG, W., DUXBURY, Z., HOGENHOUT, S. A. & JONES, J. D. G. 2021b. Novel effector recognition capacity engineered into a paired NLR complex. *bioRxiv***,** 2021.09.06.459143.

WANG, W. & JIAO, F. 2019. Effectors of Phytophthora pathogens are powerful weapons for manipulating host immunity. *Planta,* 250**,** 413-425.

WANG, Y. & WANG, Y. 2018. Trick or Treat: Microbial Pathogens Evolved Apoplastic Effectors Modulating Plant Susceptibility to Infection. *Molecular Plant-Microbe Interactions®,* 31**,** 6-12.

WANG, Y., ZHANG, Q., SUN, M. A. & GUO, D. 2011. High-accuracy prediction of bacterial type III secreted effectors based on position-specific amino acid composition profiles. *Bioinformatics,* 27**,** 777-84.

WEBER, E., ENGLER, C., GRUETZNER, R., WERNER, S. & MARILLONNET, S. 2011. A modular cloning system for standardized assembly of multigene constructs. *PLoS One,* 6**,** e16765.

WEI, Y., THYPARAMBIL, A. A. & LATOUR, R. A. 2014. Protein helical structure determination using CD spectroscopy for solutions with strong background absorbance from 190 to 230nm. *Biochim Biophys Acta,* 1844**,** 2331-7.

WERNIMONT, A. & EDWARDS, A. 2009. In situ proteolysis to generate crystals for structure determination: an update. *PLoS One,* 4**,** e5094.

WHISSON, S. C., BOEVINK, P. C., MOLELEKI, L., AVROVA, A. O., MORALES, J. G., GILROY, E. M., ARMSTRONG, M. R., GROUFFAUD, S., VAN WEST, P., CHAPMAN, S., HEIN, I., TOTH, I. K., PRITCHARD, L. & BIRCH, P. R. 2007. A translocation signal for delivery of oomycete effector proteins into host plant cells. *Nature,* 450**,** 115-8.

WICKHAM, H. 2016. ggplot2: Elegant Graphics for Data Analysis. *Springer-Verlag New York.*

WILLIAMS, S. J., SOHN, K. H., WAN, L., BERNOUX, M., SARRIS, P. F., SEGONZAC, C., VE, T., MA, Y., SAUCET, S. B., ERICSSON, D. J., CASEY, L. W., LONHIENNE, T., WINZOR, D. J., ZHANG, X., COERDT, A., PARKER, J. E., DODDS, P. N., KOBE, B. & JONES, J. D. 2014. Structural basis for assembly and function of a heterodimeric plant immune receptor. *Science,* 344**,** 299-303.

WILLIAMS, S. J., SORNARAJ, P., DECOURCY-IRELAND, E., MENZ, R. I., KOBE, B., ELLIS, J. G., DODDS, P. N. & ANDERSON, P. A. 2011. An autoactive mutant of the M flax rust resistance protein has a preference for binding ATP, whereas wild-type M protein binds ADP. *Mol Plant Microbe Interact,* 24**,** 897-906.

WIN, J., KRASILEVA, K. V., KAMOUN, S., SHIRASU, K., STASKAWICZ, B. J. & BANFIELD, M. J. 2012. Sequence Divergent RXLR Effectors Share a Structural Fold Conserved across Plant Pathogenic Oomycete Species. *PLOS Pathogens,* 8**,** e1002400.

WINN, M. D., BALLARD, C. C., COWTAN, K. D., DODSON, E. J., EMSLEY, P., EVANS, P. R., KEEGAN, R. M., KRISSINEL, E. B., LESLIE, A. G., MCCOY, A., MCNICHOLAS, S. J., MURSHUDOV, G. N., PANNU, N. S., POTTERTON, E. A., POWELL, H. R., READ, R. J., VAGIN, A. & WILSON, K. S. 2011. Overview of the CCP4 suite and current developments. *Acta Crystallogr D Biol Crystallogr,* 67**,** 235-42.

WINN, M. D., MURSHUDOV, G. N. & PAPIZ, M. Z. 2003. Macromolecular TLS refinement in REFMAC at moderate resolutions. *Methods Enzymol,* 374**,** 300-21.

WITEK, K., JUPE, F., WITEK, A. I., BAKER, D., CLARK, M. D. & JONES, J. D. G. 2016. Accelerated cloning of a potato late blight–resistance gene using RenSeq and SMRT sequencing. *Nature Biotechnology,* 34**,** 656-660.

WOOD, K. J., NUR, M., GIL, J., FLETCHER, K., LAKEMAN, K., GANN, D., GOTHBERG, A., KHUU, T., KOPETZKY, J., NAQVI, S., PANDYA, A., ZHANG, C., MAISONNEUVE, B., PEL, M. & MICHELMORE, R. 2020. Effector prediction and characterization in the oomycete pathogen Bremia lactucae reveal host-recognized WY domain proteins that lack the canonical RXLR motif. *PLOS Pathogens,* 16**,** e1009012.

WROBLEWSKI, T., SPIRIDON, L., MARTIN, E. C., PETRESCU, A. J., CAVANAUGH, K., TRUCO, M. J., XU, H., GOZDOWSKI, D., PAWLOWSKI, K., MICHELMORE, R. W. & TAKKEN, F. L. W. 2018. Genome-wide functional analyses of plant coiled-coil NLR-type pathogen receptors reveal essential roles of their N-terminal domain in oligomerization, networking, and immunity. *PLoS Biol,* 16**,** e2005821.

WU, C. H., ABD-EL-HALIEM, A., BOZKURT, T. O., BELHAJ, K., TERAUCHI, R., VOSSEN, J. H. & KAMOUN, S. 2017. NLR network mediates immunity to diverse plant pathogens. *Proc Natl Acad Sci U S A,* 114**,** 8113-8118.

WU, C. H., BELHAJ, K., BOZKURT, T. O., BIRK, M. S. & KAMOUN, S. 2016. Helper NLR proteins NRC2a/b and NRC3 but not NRC1 are required for Pto-mediated cell death and resistance in Nicotiana benthamiana. *New Phytol,* 209**,** 1344-52.

WU, C. H., DEREVNINA, L. & KAMOUN, S. 2018. Receptor networks underpin plant immunity. *Science,* 360**,** 1300-1301.

WU, C. H., KRASILEVA, K. V., BANFIELD, M. J., TERAUCHI, R. & KAMOUN, S. 2015. The "sensor domains" of plant NLR proteins: more than decoys? *Front Plant Sci,* 6**,** 134.

WU, Z., LI, M., DONG, O. X., XIA, S., LIANG, W., BAO, Y., WASTENEYS, G. & LI, X. 2019. Differential regulation of TNL-mediated immune signaling by redundant helper CNLs. *New Phytol,* 222**,** 938-953.

XU, F., KAPOS, P., CHENG, Y. T., LI, M., ZHANG, Y. & LI, X. 2014. NLR-associating transcription factor bHLH84 and its paralogs function redundantly in plant immunity. *PLoS Pathog,* 10**,** e1004312.

XUE, B., DUNKER, A. K. & UVERSKY, V. N. 2012. Orderly order in protein intrinsic disorder distribution: disorder in 3500 proteomes from viruses and the three domains of life. *J Biomol Struct Dyn,* 30**,** 137-49.

YAENO, T., LI, H., CHAPARRO-GARCIA, A., SCHORNACK, S., KOSHIBA, S., WATANABE, S., KIGAWA, T., KAMOUN, S. & SHIRASU, K. 2011. Phosphatidylinositol monophosphate-binding interface in the oomycete RXLR effector AVR3a is required for its stability in host cells to modulate plant immunity. *Proceedings of the National Academy of Sciences,* 108**,** 14682-14687.

YAMAMOTO, E., TAKASHI, T., MORINAKA, Y., LIN, S., WU, J., MATSUMOTO, T., KITANO, H., MATSUOKA, M. & ASHIKARI, M. 2010. Gain of deleterious function causes an autoimmune response and Bateson–Dobzhansky–Muller incompatibility in rice. *Molecular Genetics and Genomics,* 283**,** 305-315.

YANG, Z. R., THOMSON, R., MCNEIL, P. & ESNOUF, R. M. 2005. RONN: the bio-basis function neural network technique applied to the detection of natively disordered regions in proteins. *Bioinformatics,* 21**,** 3369-3376.

YOSHIDA, K., SAITOH, H., FUJISAWA, S., KANZAKI, H., MATSUMURA, H., YOSHIDA, K., TOSA, Y., CHUMA, I., TAKANO, Y., WIN, J., KAMOUN, S. & TERAUCHI, R. 2009. Association genetics reveals three novel avirulence genes from the rice blast fungal pathogen Magnaporthe oryzae. *Plant Cell,* 21**,** 1573-91.

YOSHIDA, K., SAUNDERS, D. G. O., MITSUOKA, C., NATSUME, S., KOSUGI, S., SAITOH, H., INOUE, Y., CHUMA, I., TOSA, Y., CANO, L. M., KAMOUN, S. & TERAUCHI, R. 2016. Host specialization of the blast fungus Magnaporthe oryzae is associated with dynamic gain and loss of genes linked to transposable elements. *BMC Genomics,* 17**,** 370.

YU, Z., SHEN, K., NEWCOMBE, G., FAN, J. & CHEN, Q. 2019. Leaf Cuticle Can Contribute to Non-Host Resistance to Poplar Leaf Rust. *Forests,* 10**,** 870.

YUAN, B., ZHAI, C., WANG, W., ZENG, X., XU, X., HU, H., LIN, F., WANG, L. & PAN, Q. 2011. The Pik-p resistance to Magnaporthe oryzae in rice is mediated by a pair of closely linked CC-NBS-LRR genes. *Theor Appl Genet,* 122**,** 1017-28.

YUAN, M., CHU, Z., LI, X., XU, C. & WANG, S. 2010. The bacterial pathogen Xanthomonas oryzae overcomes rice defenses by regulating host copper redistribution. *Plant Cell,* 22**,** 3164-76.

YUE, J. X., MEYERS, B. C., CHEN, J. Q., TIAN, D. & YANG, S. 2012. Tracing the origin and evolutionary history of plant nucleotide-binding site-leucine-rich repeat (NBS-LRR) genes. *New Phytol,* 193**,** 1049-1063.

ZHAI, C., LIN, F., DONG, Z., HE, X., YUAN, B., ZENG, X., WANG, L. & PAN, Q. 2011. The isolation and characterization of Pik, a rice blast resistance gene which emerged after rice domestication. *New Phytol,* 189**,** 321-34.

ZHAI, C., ZHANG, Y., YAO, N., LIN, F., LIU, Z., DONG, Z., WANG, L. & PAN, Q. 2014. Function and interaction of the coupled genes responsible for Pik-h encoded rice blast resistance. *PLoS One,* 9**,** e98067.

ZHAI, K., DENG, Y., LIANG, D., TANG, J., LIU, J., YAN, B., YIN, X., LIN, H., CHEN, F., YANG, D., XIE, Z., LIU, J. Y., LI, Q., ZHANG, L. & HE, Z. 2019. RRM Transcription Factors Interact with NLRs and Regulate Broad-Spectrum Blast Resistance in Rice. *Mol Cell,* 74**,** 996-1009.e7.

ZHANG, H., ZHANG, X., LIU, J., NIU, Y., CHEN, Y., HAO, Y., ZHAO, J., SUN, L., WANG, H., XIAO, J. & WANG, X. 2020. Characterization of the Heavy-Metal-Associated Isoprenylated Plant Protein (HIPP) Gene Family from Triticeae Species. *Int J Mol Sci,* 21.

ZHANG, L., CHEN, S., RUAN, J., WU, J., TONG, A. B., YIN, Q., LI, Y., DAVID, L., LU, A., WANG, W. L., MARKS, C., OUYANG, Q., ZHANG, X., MAO, Y. & WU, H. 2015. Cryo-EM structure of the activated NAIP2-NLRC4 inflammasome reveals nucleated polymerization. *Science,* 350**,** 404-9.

ZHANG, T., FARAGGI, E., LI, Z. & ZHOU, Y. 2013a. Intrinsically semi-disordered state and its role in induced folding and protein aggregation. *Cell Biochem Biophys,* 67**,** 1193-205.

ZHANG, X., BERNOUX, M., BENTHAM, A. R., NEWMAN, T. E., VE, T., CASEY, L. W., RAAYMAKERS, T. M., HU, J., CROLL, T. I., SCHREIBER, K. J., STASKAWICZ, B. J., ANDERSON, P. A., SOHN, K. H., WILLIAMS, S. J., DODDS, P. N. & KOBE, B. 2017a. Multiple functional self-association interfaces in plant TIR domains. *Proc Natl Acad Sci U S A,* 114**,** E2046-E2052.

ZHANG, X., DODDS, P. N. & BERNOUX, M. 2017b. What Do We Know About NOD-Like Receptors in Plant Immunity? *Annu Rev Phytopathol,* 55**,** 205-229.

ZHANG, X., HE, D., ZHAO, Y., CHENG, X., ZHAO, W., TAYLOR, I. A., YANG, J., LIU, J. & PENG, Y. L. 2018. A positive-charged patch and stabilized hydrophobic core are essential for avirulence function of AvrPib in the rice blast fungus. *Plant J,* 96**,** 133-146.

ZHANG, Z. M., ZHANG, X., ZHOU, Z. R., HU, H. Y., LIU, M., ZHOU, B. & ZHOU, J. 2013b. Solution structure of the Magnaporthe oryzae avirulence protein AvrPiz-t. *J Biomol NMR,* 55**,** 219-23.

ZHENG, C., LIU, Y., SUN, F., ZHAO, L. & ZHANG, L. 2021. Predicting Protein–Protein Interactions Between Rice and Blast Fungus Using Structure-Based Approaches. *Frontiers in Plant Science,* 12.

ZSCHIESCHE, W., BARTH, O., DANIEL, K., BOHME, S., RAUSCHE, J. & HUMBECK, K. 2015. The zinc-binding nuclear protein HIPP3 acts as an upstream regulator of the salicylate-dependent plant immunity pathway and of flowering time in Arabidopsis thaliana. *New Phytol,* 207**,** 1084-96.

Appendix

PLOS ONE

RESEARCH ARTICLE

The rice NLR pair Pikp-1/Pikp-2 initiates cell death through receptor cooperation rather than negative regulation

Rafał Zdrzałek[1], **Sophien Kamoun**[2], **Ryohei Terauchi**[3,4], **Hiromasa Saitoh**[5]*, **Mark J. Banfield**[1]*

1 Department of Biological Chemistry, John Innes Centre, Norwich, United Kingdom, **2** The Sainsbury Laboratory, University of East Anglia, Norwich, United Kingdom, **3** Division of Genomics and Breeding, Iwate Biotechnology Research Centre, Iwate, Japan, **4** Laboratory of Crop Evolution, Graduate School of Agriculture, Kyoto University, Kyoto, Japan, **5** Laboratory of Plant Symbiotic and Parasitic Microbes, Department of Molecular Microbiology, Faculty of Life Sciences, Tokyo University of Agriculture, Tokyo, Japan

* hs206173@nodai.ac.jp (HS); mark.banfield@jic.ac.uk (MB)

Citation: Zdrzałek R, Kamoun S, Terauchi R, Saitoh H, Banfield MJ (2020) The rice NLR pair Pikp-1/Pikp-2 initiates cell death through receptor cooperation rather than negative regulation. PLoS ONE 15(9): e0238616. https://doi.org/10.1371/journal.pone.0238616

Editor: Richard A. Wilson, University of Nebraska-Lincoln, UNITED STATES

Received: June 22, 2020

Accepted: August 20, 2020

Published: September 15, 2020

Data Availability Statement: All relevant data are within the manuscript and its Supporting Information files

Funding: This work was supported by the UKRI Biotechnology and Biological Sciences Research Council (BBSRC) Norwich Research Park Biosciences Doctoral Training Partnership, UK [grant BB/M011216/1 (RZ, MJB)]; the UKRI BBSRC, UK [grants BB/P012574, BB/M02198X (MJB, SK)]; the European Research Council [ERC; proposal 743165 (SK, MJB)]; the John Innes

Abstract

Plant NLR immune receptors are multidomain proteins that can function as specialized sensor/helper pairs. Paired NLR immune receptors are generally thought to function via negative regulation, where one NLR represses the activity of the second and detection of pathogen effectors relieves this repression to initiate immunity. However, whether this mechanism is common to all NLR pairs is not known. Here, we show that the rice NLR pair Pikp-1/Pikp-2, which confers resistance to strains of the blast pathogen *Magnaporthe oryzae* (syn. *Pyricularia oryzae*) expressing the AVR-PikD effector, functions via receptor cooperation, with effector-triggered activation requiring both NLRs to trigger the immune response. To investigate the mechanism of Pikp-1/Pikp-2 activation, we expressed truncated variants of these proteins, and made mutations in previously identified NLR sequence motifs. We found that any domain truncation, in either Pikp-1 or Pikp-2, prevented cell death in the presence of AVR-PikD, revealing that all domains are required for activity. Further, expression of individual Pikp-1 or Pikp-2 domains did not result in cell death. Mutations in the conserved P-loop and MHD sequence motifs in both Pikp-1 and Pikp-2 prevented cell death activation, demonstrating that these motifs are required for the function of the two partner NLRs. Finally, we showed that Pikp-1 and Pikp-2 associate to form homo- and hetero-complexes in planta in the absence of AVR-PikD; on co-expression the effector binds to Pikp-1 generating a tri-partite complex. Taken together, we provide evidence that Pikp-1 and Pikp-2 form a fine-tuned system that is activated by AVR-PikD via receptor cooperation rather than negative regulation.

Foundation (MJB); the Japan Society for the Promotion of Science (JSPS KAKENHI; proposal 18K05657, 15H05779, and 20H00421 (RT)), and by the Strategic Research Project from Tokyo University of Agriculture (HS). The funders had no role in study design, data collection and analysis, decision to publish, or preparation of the manuscript.

Competing interests: The authors have declared that no competing interests exist.

Introduction

Like animals, plants are constantly threatened by pathogens and pests. To defend themselves, they have evolved a sophisticated immune system that relies on both cell surface and intracellular receptors [1, 2]. The majority of cloned resistance genes are intracellular immune receptors that belong to the nucleotide-binding, leucine-rich repeat (NLR) superfamily [3]. NLRs activate immunity leading to disease resistance following recognition of pathogen elicitors, typically effectors delivered into host cells to promote pathogenesis [4]. NLR-mediated immunity can include localised cell death known as the Hypersensitive Response (HR) [5], which contributes to limiting pathogen spread through host tissue.

The canonical architecture of plant NLRs consists of an N-terminal Toll/Interleukin-1 receptor homology (TIR) domain or coiled-coil (CC) domain ((including the RPW8-like CC, CC_R), establishing the TIR-NLR, CC-NLR and CC_R-NLR families), a central NB-ARC domain (Nucleotide-binding adaptor and APAF-1, R proteins, and CED-4), and a C-terminal leucine-rich repeat (LRR) domain. Conceptual frameworks for the roles of each domain are established, although their precise role may vary from one NLR to another [6]. In brief, the N-terminal TIR or CC domains are thought to be involved in triggering cell death following effector perception, with recent studies suggesting a nucleotide hydrolase activity (for TIRs [7–9]) and membrane-perturbation (for oligomeric CCs [10, 11]). The NB-ARC domain acts as a molecular switch with the conformation of the protein stabilised by the bound nucleotide, ADP or ATP [12–15]. Within the NB-ARC domain, several well-conserved sequence motifs are known, with the "P-loop" and "MHD" motifs located to the nucleotide binding site [16, 17]. Mutations in these motifs have diverse effects on NLR activity. For example, mutations within the P-loop motif impair nucleotide binding, and often result in loss of protein function [18–20]. Mutations in this motif can also prevent self-association and affect localisation [21]. Mutations within the MHD motif frequently lead to constitutive activity (often called auto-activation [22–26]). The C-terminal LRR domain has a role in auto-inhibition [27–29], a function shared with animal NLRs [30–32], but can also define effector recognition specificity [33].

NLRs can function as singletons, capable of both perceiving effectors and executing a response [34, 35]. This activity may require non-NLR interactors [36–40] or oligomerisation [41, 42]. However, many NLRs require a second NLR for function, with three major classes described [43, 44]. In each class, one of the NLRs functions as a "sensor" to detect the presence of the effector, whereas the second acts as a "helper", and is required for cell death activity. For genetically linked sensor-helper NLR pairs, expression is driven from a shared promoter, and both proteins are required for effector perception [45]. Interestingly, in many genetically linked NLR pairs, the sensor NLR contains an additional integrated domain that directly binds a pathogen effector [46–50]. Integrated domains in NLRs have been found across all flowering plants [51–53]. The separation of sensor/helper functions within NLR pairs may have evolutionary advantages, for example increasing tolerance to point mutations in the sensor [54].

CC-NLRs RGA5 and RGA4 from rice, and TIR-NLRs RRS1 and RPS4 from *Arabidopsis* are well established models in the study of genetically linked NLR pairs [45, 48, 55]. RGA5 and RRS1 are the sensor NLRs (harbouring an integrated HMA (Heavy Metal Associated) domain and integrated WRKY domain respectively), and RGA4 and RPS4 are the helpers. In both systems, the helper NLRs appear to be auto-active when expressed alone in heterologous expression systems, and this auto-activity is suppressed on co-expression with the sensor NLR. Effector perception relieves suppression and initiates receptor activity [45, 56].

In rice, the CC-NLR pair Pik-1 and Pik-2 confers resistance to *Magnaporthe oryzae* (syn. *Pyricularia oryzae*) carrying the AVR-Pik effector. Similar to RGA5, Pik-1 has an integrated HMA domain, but unlike RGA5 this is positioned between the CC and NB-ARC domain,

rather than after the LRR. The Pik-1 integrated HMA domain directly binds the AVR-Pik effector [50]. However, how recognition of the effector translates into an immune response in the context of full-length receptors is unclear, as is the nature of any pre-activation state of the Pik-1/Pik-2 proteins. Further, which NLR domains are necessary and sufficient for immune signalling in this pair is unknown.

We previously showed that the AVR-Pik elicited hypersensitive cell death mediated by the Pik NLR pair can be recapitulated using transient expression in leaves of the model plant *Nicotiana benthamiana* [50, 57, 58]. In this study, we investigated the roles and requirements of domains in the Pik NLR alleles Pikp-1 and Pikp-2 in planta using the *N. benthamiana* experimental system. We show that intact, full-length, Pikp-1 and Pikp-2 are necessary for a cell death response upon effector perception. Truncation of any domain results in lack of effector-dependent cell death compared to wild-type. Further, expression of any specific NLR domain, or combination of domains, does not result in cell death. We also show that native P-loop and MHD-like motifs are required in both Pikp-1 and Pikp-2 proteins for receptor activity. Finally, we demonstrate that Pikp-1 and Pikp-2 are able to form homo- and hetero-complexes in planta in the absence of the AVR-PikD. Upon binding of the AVR-PikD effector, a tri-partite complex is formed that may represent the activated state of the receptor.

Materials and Methods

Cloning

Domesticated sequences of full-length Pikp-1 and Pikp-2 (as described in [58]), and MLA10, were assembled into the pICH47751 vector under the control of the *mas* promoter and with C-terminal epitope tags (3x FLAG tag, V-5 tag or 6xHA tag accordingly) using the Golden Gate system [59]. To obtain Pikp-1 and Pikp-2 individual domains and truncation variants, relevant sequences were amplified by PCR using the plasmids above as templates, and assembled into the pICH47751 vector under control of CaMV35S promoter and with C-terminal epitope tags (6xHis + 3xFlag (HellFire (HF)) for Pikp-1 derivatives and 6xHA for Pikp-2 derivatives) using the Golden Gate system. Myc:AVR-PikD and Myc:AVR-PikD^{H46E} constructs used were as described in [58]. All DNA constructs were confirmed by sequencing and transformed into *Agrobacterium tumefaciens* strain GV3101 via electroporation.

Mutagenesis

To generate Pikp mutants (P-loop and MHD-like motifs), we introduced mutations into the relevant NB-ARC domain modules using site-directed mutagenesis. Subsequently these domain constructs were used to generate full length NLRs by assembly using the Golden Gate system. Each of the constructs were assembled with the CaMV35S promoter with relevant tags (6xHis + 3xFlag (HellFire (HF)) for Pikp-1 derivatives and 6xHA tag for Pikp-2 derivatives).

Cell death assays

Agrobacterium tumefaciens strain GV3101 carrying the appropriate constructs were suspended in infiltration buffer (10 mM MgCl2, 10 mM MES, pH 5.6, 150 mM acetosyringone) and mixed prior to infiltration at the following final OD_{600}: NLRs and NLR-derivatives 0.4, effectors 0.6, P19 (silencing suppressor) 0.1. Bacteria were infiltrated into leaves of ~4 weeks old *N. benthamiana* plants using a 1ml needleless syringe. At 5 days post infiltration (dpi), detached leaves were imaged under UV light on the abaxial side, and visually scored for cell death response (see below). To confirm protein expression, representative infiltration spots were prepared, frozen in liquid nitrogen, ground to a fine powder, mixed with extraction buffer (see

below) in 2 ml/g ratio, centrifuged, mixed with loading dye and loaded on an SDS-PAGE gel for western blot analysis.

Cell death scoring

Pictures of the leaves at 5 dpi were taken as described previously [57] and cell death (visible as green fluorescence area under the UV light) was scored according to the scale presented in [50]. The dot plots were generated using R v3.4.3 (https://www.r-project.org/) and the graphic package ggplot2 [60]. Dots represent the individual datapoints and the size of larger circles is proportional to the number of dots within that score. Dots of the same colour within one plot come from the same biological repeat. All positive and negative controls were also scored and are represented on relevant plots. As positive and negative controls were included on most leaves there are more data points for these samples.

Co-Immunoprecipitation

Protein extraction was conducted as described in [61] with minor modifications. Extraction buffer GTEN (10% glycerol, 25 mM Tris, pH 7.5, 1 mM EDTA, 150 mM NaCl), 2% w/v PVPP, 10 mM DTT, 1× protease inhibitor cocktail (Sigma), 0.1% Tween 20 (Sigma) was added to frozen tissue in 2 ml/g ratio. The sample was resuspended and centrifuged for 30 min (4500g) at 4˚C. The supernatant was filtered through a 0.45 μm filter. Anti-FLAG M2 magnetic beads (Sigma, M8823) were washed with the IP buffer (GTEN + 0.1% Tween 20), resuspended, and added to protein extracts (20 μl of resin per 1.5 ml of extract). Samples were incubated for an hour at 4˚C with gentle shaking. Following incubation, the resin was separated using magnetic stand and washed 5 times with IP buffer. For elution, beads were mixed with 30 μl of Loading Dye and incubated at 70˚C for 10 min. Finally, samples were centrifuged and loaded on a precast gradient gel (4–20%, Expedeon) for western blot analysis.

Western blot

Western blots were performed as described previously [61]. Following SDS-PAGE, proteins were transferred onto PVDF membrane using Trans-Blot Turbo Transfer Kit (Biorad) and blocked in 5% milk in TBS-T (50mM Tris-HCl, 150mM NaCl, 0.1% Tween20, pH 8.0) at 4˚C for at least 1 hour. Respective primary HRP-conjugated antibodies (α-FLAG: Cohesion Biosciences, CPA9020; α-HA: Invitrogen, #26183-HRP; α-V-5: Invitrogen, #MA5-15253-HRP; α-Myc (9E10): Santa Cruz Biotechnology, SC-40) were applied for overnight incubation (4˚C). Membranes were then rinsed with TBS-T. Proteins were detected using ECL Extreme reagents (Expedeon) in chemiluminescence CCD camera (ImageQuant LAS 500).

Results

Each domain of Pikp-1 and Pikp-2 is required for receptor activation

To investigate the roles and requirements for individual domains of Pikp-1 (CC, HMA, NB-ARC and LRR) and Pikp-2 (CC, NB-ARC and LRR) in triggering cell death, we transiently expressed each of these in *N. benthamiana* using *Agrobacterium tumefaciens* mediated transformation (henceforth agroinfiltration). All constructs were tagged at their C-terminus with the HellFire tag (6xHis + 3xFlag (HF), for Pikp-1 domains) or HA tag (for Pikp-2 domains). The boundaries of the domains used were as defined in [50].

We found that each of the individual domains of either Pikp-1 or Pikp-2 were unable to trigger cell death when expressed alone, or in the presence of the corresponding paired NLR and/or effector (Fig 1 and 2 and S1 Fig in S1 File). We confirmed that all the proteins

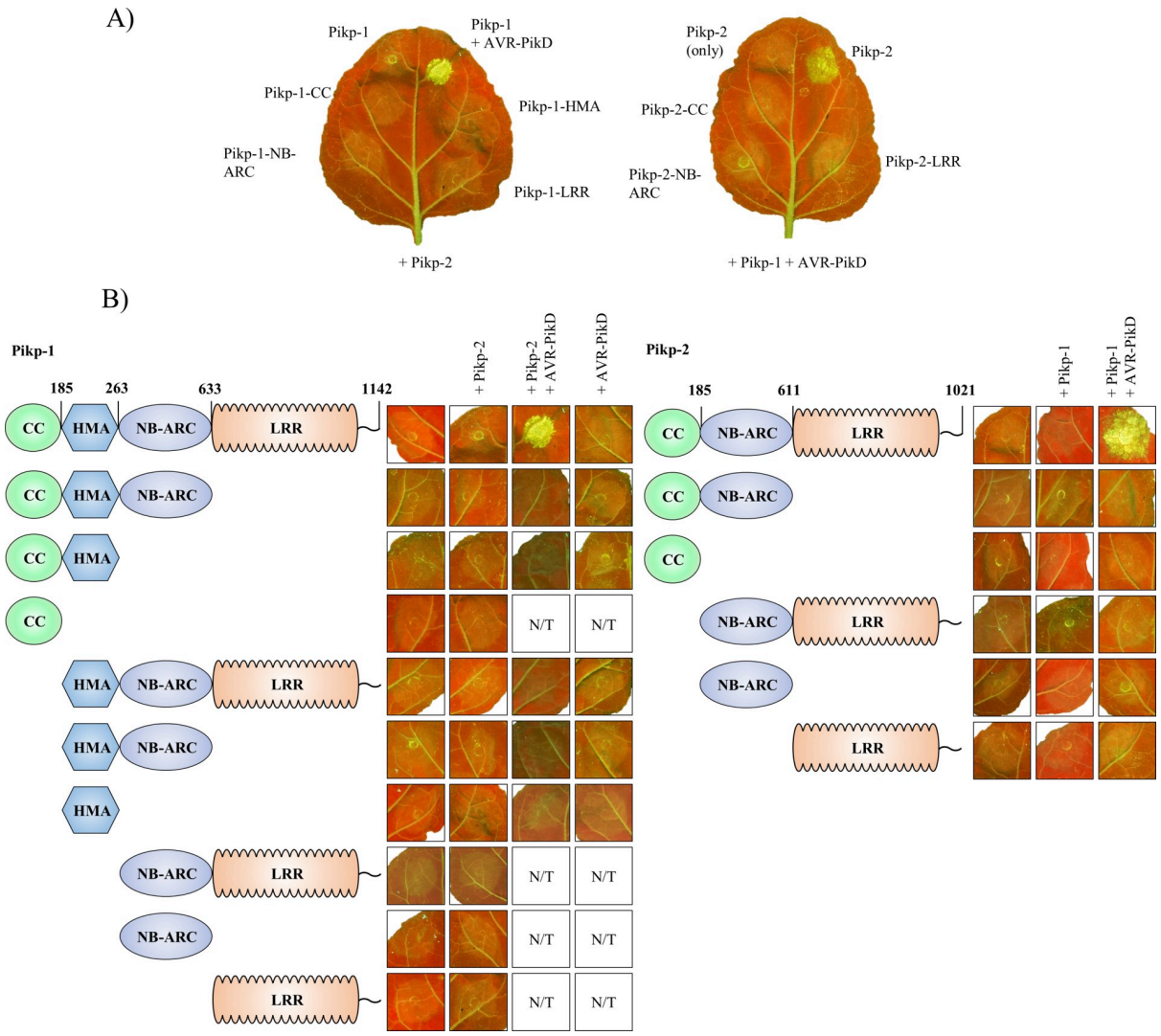

Fig 1. Each domain of Pikp-1 and Pikp-2 is required for receptor activation. A) Representative *N. benthamiana* leaves showing that expression of the individual domains of Pikp-1 (left) or Pikp-2 (right) were unable to elicit a cell death response in presence of the corresponding paired NLR (for Pikp-1) or paired NLR and effector (for Pikp-2). Pikp-1+Pikp-2+AVR-PikD is shown as a positive control. **B)** Representative agroinfiltration spots show that the truncated variants of Pikp-1 (left) or Pikp-2 (right) were unable to elicit a cell death response, either when overexpressed alone, or in the presence of corresponding full-length NLR and/or effector. Combinations of constructs without HMA domain were not tested (N/T) in presence of the effector.

https://doi.org/10.1371/journal.pone.0238616.g001

accumulated to detectable levels using western blot analysis (S2 Fig in S1 File). We then systematically truncated Pikp-1 or Pikp-2 at relevant domain boundaries, and expressed these alone or in the presence of the corresponding paired NLR and/or effector, to search for any minimum functional unit (Figs 1B and 2A and 2B and S1 Fig in S1 File). As it has been shown previously that AVR-PikD binds directly to the HMA domain of Pikp-1 [50], we did not test truncation variants of Pikp-1 without the HMA domain or Pikp-2 variants in the presence of the effector. In all cases tested no cell death was observed, despite the proteins accumulating in plant tissues (S2 Fig in S1 File). The only combination that gave cell death was the positive control of full length Pikp-1 and Pikp-2 in the presence of AVR-PikD. These results show that the Pikp-1/Pikp-2 pair work together to deliver a cell death response on effector perception, and all domains are required for activity.

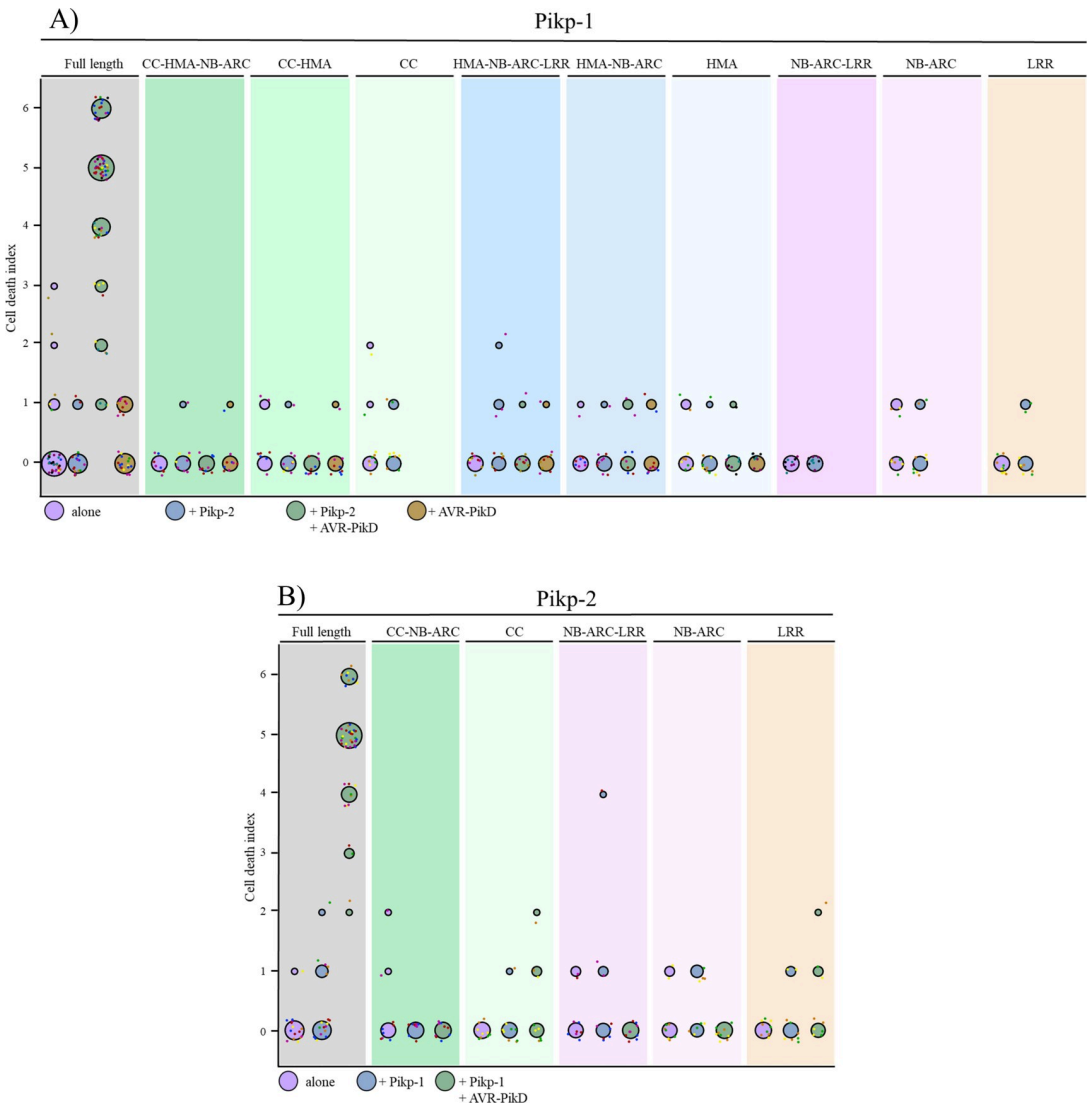

Fig 2. Each domain of Pikp-1 and Pikp-2 is required for receptor activation. Cell death quantification for the infiltration combinations of Fig 1 shown as dot plots, for Pikp-1 **(A)** and Pikp-2 **(B)** respectively. Each of the dots has a distinct colour corresponding to the biological replicate, and are plotted around the cell death score for visualization purposes. Each set of infiltrations were repeated in 3 biological replicates with at least 2–3 technical replicates. The size of the central dot at each cell death value is proportional to the number of replicates of the sample with that score.

https://doi.org/10.1371/journal.pone.0238616.g002

Conserved NB-ARC domain sequence motifs are required for Pikp-1 and Pikp-2 activity

Next, we tested whether previously characterised sequence motifs within the nucleotide-binding pocket of the Pikp-1 and Pikp-2 NB-ARC domains are required for receptor activity. Firstly, we generated mutations in the P-loop motifs of Pikp-1 and Pikp-2 (Pikp-1^{K296R} and Pikp-2^{K217R}). Such mutations restrict nucleotide binding, and have previously been shown to impair NLR function [18, 19, 62, 63]. On expression in *N. benthamiana* via agroinfiltration, we found that these mutations abolish cell death activity in planta, including when expressed in the presence of the paired NLR and the AVR-PikD effector (Fig 3 and S3A Fig in S1 File). This reveals that an intact P-loop motif is required in both Pikp-1 and Pikp-2 for activity.

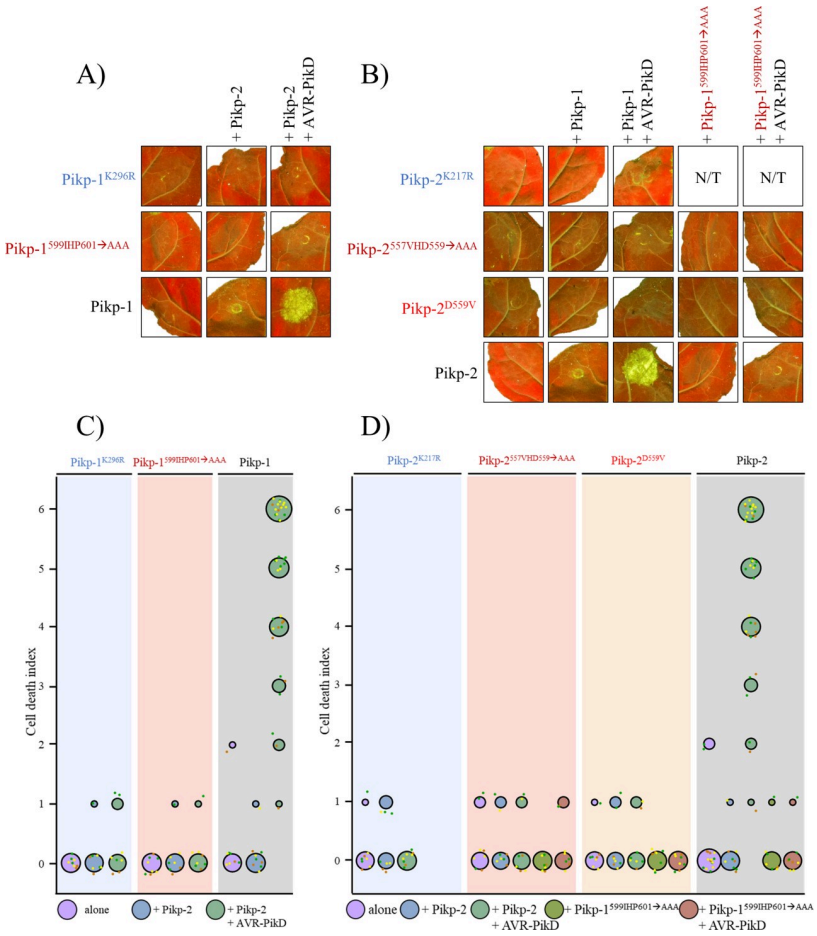

Fig 3. Conserved NB-ARC domain sequence motifs are required for Pikp-1 and Pikp-2 activity. A) Mutation of the P-loop motif of Pikp-1 (Pikp-1^{K296R}) results in loss of cell death response upon effector perception. Mutation of the Pikp-1 MHD-like motif (Pikp-$1^{599IHP601\rightarrow AAA}$) does not lead to auto-activity when overexpressed alone, or in the presence of corresponding intact NLR. Further, this mutant was also unable to trigger a cell death response when co-expressed with AVR-PikD. **B)** Mutation of the P-loop motif of Pikp-2 (Pikp-2^{K217R}) results in loss of cell death response upon effector perception. Mutation of the Pikp-2 MHD-like motif (Pikp-$2^{557VHD559\rightarrow AAA}$ and Pikp-2^{D559V}) does not lead to auto-activity when overexpressed alone, in the presence of corresponding intact NLR, or its MHD-like mutant. Further, these mutants were also unable to trigger a cell death response when co-expressed with AVR-PikD. Each set of infiltrations were repeated in 3 biological replicates with at least 2–3 technical replicates within each. The square showing the infiltration spot for wild type Pikp-1+Pikp-2 was as-used in Fig 1B. Squares representing Pikp-$1^{599IHP601\rightarrow AAA}$+Pikp-2 and Pikp-$1^{599IHP601\rightarrow AAA}$+Pikp-2+AVR-PikD are the same on both panels, presented for comparison. **C)** and **D)** Cell death quantification for each infiltration shown as dot plots. Each of the dots has a distinct colour corresponding to the biological replicate, and are plotted around the cell death score for visualization purposes. The size of the central dot at each cell death value is proportional to the number of replicates of the sample with that score. The data for Pikp-1+Pikp-2 (wild type) is a subset of the previous experiment (Fig 2A and 2B), used here for comparison. The data shown for Pikp-1+Pikp-2, Pikp-1+Pikp-2+AVR-PikD, Pikp-$1^{599IHP601}$+Pikp-2 and Pikp-$1^{599IHP601}$+Pikp-2+AVR-PikD are the same in both panels, presented for comparison.

https://doi.org/10.1371/journal.pone.0238616.g003

Expression of all proteins was confirmed by western blot analysis (S3B Fig in S1 File). Secondly, we generated mutations in the "MHD" motifs of Pikp-1 and Pikp-2. Although classically defined as Methionine-Histidine-Aspartate (MHD), the residues that comprise this motif in plant NLRs can vary. Here we will refer to this as the MHD-like motif. In Pikp-1, the MHD-like motif residues are Ile-His-Pro (IHP), while in Pikp-2 they are Val-His-Asp (VHD). Mutations within this NLR motif frequently lead to auto-activation and cell death in the absence of pathogen perception [64–66]. To determine the importance of the MHD-like motif for Pikp-1

and Pikp-2 activity, we generated triple alanine mutants of each protein (Pikp-1$^{599IHP601\rightarrow AAA}$, and Pikp-2$^{557VHD559\rightarrow AAA}$) and a Pikp-2^{D559V} mutant. On expression in *N. benthamiana* via agroinfiltration, we found that expression of these mutants alone did not result in auto-activity and cell death (Fig 3). We also found that any combination of the MHD-like motif mutants with wild-type or mutant paired NLRs, with or without the AVR-PikD effector, did not result in cell death (Fig 3B and 3D). These results show that the native MHD-like motifs of Pikp-1 and Pikp-2 are required to trigger cell death. All proteins were expressed to detectable levels, as confirmed by western blot analysis (S3B Fig in S1 File).

Pikp-1 and Pikp-2 form homo- and hetero-complexes in planta

Paired NLRs can form homo- and hetero-complexes in planta [45, 48]. To investigate whether Pikp-1 and Pikp-2 can also homo- and/or hetero-associate, both in the absence and in the presence of the effector, we performed in planta co-immunoprecipitation (co-IP) assays. To test for homo-complex formation we expressed differentially tagged Pikp-1 constructs (FLAG tag and V-5 tag), or Pikp-2 constructs (FLAG tag and HA tag) in *N. benthamiana* via agroinfiltration, followed by immunoprecipitation with α-FLAG resin. The barley NLR MLA10 (expressed with a FLAG tag) served as a negative control for interactions. Each FLAG-tagged protein was expressed, and immunoprecipitated as expected (lower panels, Fig 4A and 4B). For Pikp-1, we observe co-immunoprecipitation of Pikp-1:V-5 with Pikp-1:FLAG, but not with MLA10:FLAG, and Pikp-1:V-5 did not show non-specific interaction with the resin when expressed alone (Fig 4A). Similar results were obtained for Pikp-2 (Fig 4B), where Pikp-2:HA immunoprecipitated Pikp-2:FLAG on co-expression. Faint bands of Pikp-2:HA were also observed with MLA10:FLAG. However, a similar band can be observed where Pikp-2:HA is expressed alone, indicating a weak non-specific binding to the resin. The presence of the AVR-PikD effector (or the mutant AVR-PikD^{H46E} as a negative control) does not affect the homo-association of Pikp-1 or Pikp-2 (S4 Fig in S1 File).

We then tested whether Pikp-1 and Pikp-2 can form hetero-complexes. Using the resources described above, we co-expressed the proteins and performed α-FLAG pull downs. We show that Pikp-2:HA co-immunoprecipitated with Pikp-1:FLAG, but not with MLA10:FLAG,

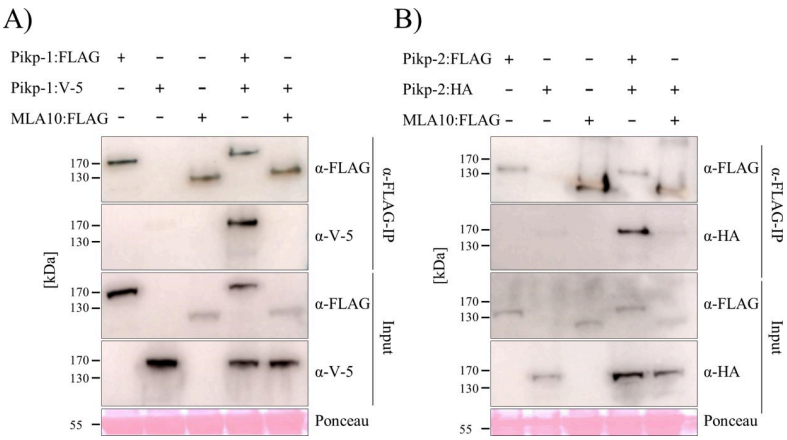

Fig 4. Pikp-1 and Pikp-2 form homo-complexes. A) Pikp-1:FLAG, Pikp-1:V-5 and MLA10:FLAG and **B)** Pikp-2:FLAG, Pikp-2:HA and MLA10:FLAG were expressed alone or in the combinations shown. Subsequently, anti-FLAG immunoprecipitation (α-FLAG-IP) was performed, followed by western blot analysis with relevant antibodies to detect the proteins (upper panel). The lower panel confirms presence of all the proteins prior to immunoprecipitation. Experiments were repeated at least 3 times with similar results.

https://doi.org/10.1371/journal.pone.0238616.g004

indicating that these NLRs specifically hetero-associate (Fig 5A). We also tested whether co-expression with AVR-PikD affects the formation of Pikp-1/Pikp-2 hetero-complexes. We co-expressed Pikp-1:V-5, Pikp-2:FLAG and Myc:AVR-PikD followed by α-FLAG pull down (note: in this case Pikp-2:FLAG is immunoprecipitated). All three proteins could be detected after α-FLAG pull down (Fig 5B). We suggest that Pikp-2 associates with Pikp-1, which is also bound to the AVR-PikD effector, forming tri-partite complex. Co-expression with the AVR--PikD^{H46E} mutant was used as a negative control for effector interaction.

Discussion

Genetically linked NLR pairs are emerging as an important class of immune receptor in plants. Established models for paired NLR receptors suggest they function via negative regulation where a sensor NLR, that often carries an integrated domain, represses the activity of the second. Binding of pathogen effectors to the sensor NLR relieves this negative regulation. In this study, we show that the rice NLR pair Pikp-1/Pikp-2 differs from this model and works via receptor cooperation. Pikp-2 is not auto-active when expressed in the absence of Pikp-1. Both Pikp-1 and Pikp-2 are required to trigger cell death upon binding of the AVR-PikD effector to the integrated HMA domain of Pikp-1, and all the domains are indispensable for this activity. Further, we determined the requirements for conserved NB-ARC domain sequence motifs, the P-loop and MHD-like motifs. Finally, we find Pikp-1 and Pikp-2 can form homo- and hetero-complexes that are likely important for function.

The expression of individual domains of a number of NLRs can result in cell death. In particular, CC domains and other N-terminal truncations can induce cell death when expressed in planta [19, 42, 67–70]. This is thought to reflect oligomerization of the CC domains, resulting in minimal functional units that can trigger cell death. However, the CC domains of either

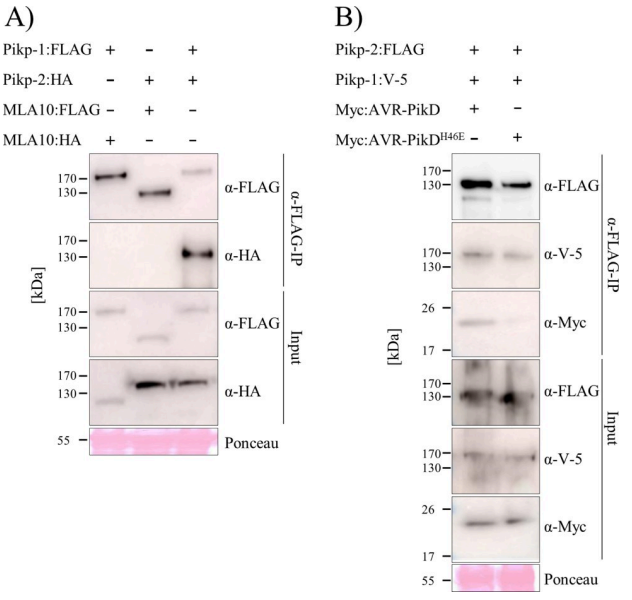

Fig 5. Pikp-1 and Pikp-2 form hetero-complexes prior to and upon recognition of AVR-PikD. A) Pikp-1:FLAG, Pikp-2:HA, MLA10:FLAG and MLA10:HA and **B)** Pikp-2:FLAG, Pikp-1:V-5, Myc:AVR-PikD and Myc:AVR-PikD^{H46E} were expressed in the combinations shown. Subsequently, anti-FLAG immunoprecipitation (α-FLAG-IP) was performed, followed by western blot analysis with relevant antibodies to detect the proteins (upper panel). The lower panel confirms presence of all the proteins prior to immunoprecipitation. Experiments were repeated at least 3 times with similar results.

https://doi.org/10.1371/journal.pone.0238616.g005

Pikp-1 or Pikp-2 did not display cell death inducing activity. This likely reflects an inability of these domains to adopt a configuration that supports cell death when expressed alone. Further, we did not observe cell death on expression of full-length Pikp-1 with the Pikp-2 CC domain (with or without AVR-PikD). We consider this a biologically relevant test for CC domain-mediated cell death in a paired NLR compared to co-expression of the CC domains with short epitope tags, or fused to GFP/YFP (a strategy required to observe cell death for some CC domains [38, 39, 71], but not used here). It is possible that further studies may identify a Pikp-1 or Pikp-2 CC domain construct that supports cell death, as studies with MLA10 family NLRs showed that a single amino acid change can make the difference between observing cell death or not [69], and chimeric NLRs with swaps within the CC domains can result in cell death [72].

Considering NLR regions other than the N-terminal domains, expression of the NB-ARC from Rx resulted in cell death [73]. However, we did not observe this phenotype on expression of the NB-ARC domains of Pikp1 or Pikp-2. For the NLR RPS5, it was shown that a CC-NB-ARC construct can elicit cell death [40], but this may be due to deletion of the LRR domain that may have a role in auto-inhibition prior to effector detection [28]. We did not observe cell death following deletion of the LRR domains of Pikp-1 or Pikp-2. Together, our data shows that full-length Pikp proteins, and perception of the effector, are required for cell death activity in planta. This is an effective strategy to prevent mis-regulation of receptor activity in the absence of the pathogen, but highlights the need for additional studies to understand the molecular mechanistic basis of Pikp activation, and the diversity of paired NLR function more generally.

Although the P-loop motif is required for NLRs reported to work as singletons [18, 20], it is not always necessary for paired and networked NLRs [45, 56, 74]. In genetically linked pairs RGA5/RGA4 and RRS1/RPS4, the helper NLR requires an intact P-loop for cell death, but not the sensor [45, 56]. In CC_R-type helper NLRs, such as ADR1 and NRG1 (which function downstream of several other NLRs, but are not genetically linked [75]), an intact P-loop motif may not be required [76, 77]. Pikp-1 and Pikp-2 appear to function similar to the NRC network of solanaceous plants, where both sensor and helper NLRs require a native P-loop motif for function [74]. So why do Pikp-1 and Pikp-2 both require a native P-loop? It maybe this just provides an additional layer of regulation. It is also possible that mutations in the P-loop affect protein folding by preventing ADP binding, and Pikp-1 is more sensitive to this than other sensor NLRs studied, or that ADP/ATP exchange is more important for transducing effector binding by the HMA integrated domain in Pikp-1, possibly determined by the unusual position of the integrated domain between the CC and NB-ARC domain in this NLR.

Residues of the MHD-like motif are involved in binding ADP in the inactive state of NLRs [12, 78], and mutations in this motif can lead to auto-activity [22, 23]. Mutations in the MHD-like motif of Pikp-1 and Pikp-2 are not auto-active, and result in a loss of cell death activity when expressed with the AVR-PikD effector. In RGA5 and RGA4, residues of the MHD-like motif are LHH and TYG, respectively, and the presence of a Glycine (G) in the third position of RGA4 was shown to be linked to RGA4 auto-activity, whereas introducing mutations into MHD-like motif of RGA5 did not abolish its ability to repress RGA4 [45]. The most straightforward explanation for why changes at the MHD-like motif in Pikp-1 and Pikp-2 results in a loss of any cell death activity, rather than autoactivation, is that these mutations do not support the protein confirmation required, perhaps in the context of this NLR pair specifically. It is also possible that mutations in the P-loop and MHD-like motifs affect the ability of the receptors to form biologically relevant protein complexes that support activity.

Plant NLRs can form both homo- and hetero-complexes both prior to and after effector recognition [21, 40, 42, 79, 80], or undergo effector induced oligomerisation [81]. In addition

to the CC domains of CC-NLRs, the N-terminal TIR domains of TIR-NLRs have been shown to oligomerise [82–84]. Recently, the structure of full-length ZAR1 revealed the role of oligomerisation in activation of a full-length NLR [11]. Here, we have shown that Pikp-1 and Pikp-2 form both homo- and hetero-complexes in the absence and presence of the AVR-PikD effector. However, the conformation of the proteins, their stoichiometry, and their specific arrangement within the complexes, remain to be determined. Various models are possible for the active complex including a Pikp-1/Pikp-2 dimer, a higher order oligomer including multiple copies of the dimer, or a structure where Pikp-1 initiates the oligomerisation of Pikp-2 similar to the mechanism seen for NAIP2/NLRC4 [85] and NAIP5/NLRC4 [86].

In summary, our findings reveal that the Pikp-1/Pikp-2 NLR pair function via receptor cooperation rather than a suppression/activation mechanism, and signalling in planta requires the full-length proteins with native sequences at the P-loop and MHD-like sequence motifs. This suggests multiple mechanisms of regulation exist for NLRs. It is important to further investigate these mechanisms if we are to fully understand NLR function and use this to engineer improved disease resistance phenotypes in crops.

Supporting information

S1 File.
(DOCX)

S1 Raw images.
(PDF)

Acknowledgments

We thank Juan Carlos De la Concepcion and Josephine Maidment for help with cloning. We also thank Thorsten Langner and Hiroaki Adachi for comments on the manuscript.

Author Contributions

Conceptualization: Rafał Zdrzałek, Sophien Kamoun, Ryohei Terauchi, Hiromasa Saitoh, Mark J. Banfield.

Funding acquisition: Sophien Kamoun, Ryohei Terauchi, Hiromasa Saitoh, Mark J. Banfield.

Investigation: Rafał Zdrzałek, Hiromasa Saitoh.

Methodology: Rafał Zdrzałek.

Project administration: Sophien Kamoun, Ryohei Terauchi, Hiromasa Saitoh, Mark J. Banfield.

Supervision: Mark J. Banfield.

Writing – original draft: Rafał Zdrzałek, Mark J. Banfield.

Writing – review & editing: Rafał Zdrzałek, Sophien Kamoun, Ryohei Terauchi, Hiromasa Saitoh, Mark J. Banfield.

References

1. Cesari S. Multiple strategies for pathogen perception by plant immune receptors. New Phytol. 2017.
2. Couto D, Zipfel C. Regulation of pattern recognition receptor signalling in plants. Nat Rev Immunol. 2016; 16(9):537–52.

3. Kourelis J, van der Hoorn RAL. Defended to the Nines: 25 Years of Resistance Gene Cloning Identifies Nine Mechanisms for R Protein Function. Plant Cell. 2018; 30(2):285–99.
4. El Kasmi F, Horvath D, Lahaye T. Microbial effectors and the role of water and sugar in the infection battle ground. Curr Opin Plant Biol. 2018; 44:98–107.
5. Dodds PN, Rathjen JP. Plant immunity: towards an integrated view of plant-pathogen interactions. Nat Rev Genet. 2010; 11(8):539–48.
6. Sukarta OCA, Slootweg EJ, Goverse A. Structure-informed insights for NLR functioning in plant immunity. Semin Cell Dev Biol. 2016; 56:134–49.
7. Horsefield S, Burdett H, Zhang X, Manik MK, Shi Y, Chen J, et al. NAD(+) cleavage activity by animal and plant TIR domains in cell death pathways. Science. 2019; 365(6455):793–9.
8. Wan L, Essuman K, Anderson RG, Sasaki Y, Monteiro F, Chung EH, et al. TIR domains of plant immune receptors are NAD(+)-cleaving enzymes that promote cell death. Science. 2019; 365 (6455):799–803.
9. Essuman K, Summers DW, Sasaki Y, Mao X, Yim AKY, DiAntonio A, et al. TIR Domain Proteins Are an Ancient Family of NAD(+)-Consuming Enzymes. Curr Biol. 2018; 28(3):421–30 e4.
10. Burdett H, Bentham AR, Williams SJ, Dodds PN, Anderson PA, Banfield MJ, et al. The Plant "Resistosome": Structural Insights into Immune Signaling. Cell Host Microbe. 2019; 26(2):193–201.
11. Wang J, Hu M, Wang J, Qi J, Han Z, Wang G, et al. Reconstitution and structure of a plant NLR resistosome conferring immunity. Science. 2019; 364(6435).
12. Wang J, Wang J, Hu M, Wu S, Qi J, Wang G, et al. Ligand-triggered allosteric ADP release primes a plant NLR complex. Science. 2019; 364(6435).
13. Zhang X, Dodds PN, Bernoux M. What Do We Know About NOD-Like Receptors in Plant Immunity? Annu Rev Phytopathol. 2017; 55:205–29.
14. Bernoux M, Burdett H, Williams SJ, Zhang X, Chen C, Newell K, et al. Comparative Analysis of the Flax Immune Receptors L6 and L7 Suggests an Equilibrium-Based Switch Activation Model. Plant Cell. 2016; 28(1):146–59.
15. Tameling WI, Vossen JH, Albrecht M, Lengauer T, Berden JA, Haring MA, et al. Mutations in the NB-ARC domain of I-2 that impair ATP hydrolysis cause autoactivation. Plant Physiol. 2006; 140(4):1233–45.
16. Albrecht M, Takken FL. Update on the domain architectures of NLRs and R proteins. Biochem Biophys Res Commun. 2006; 339(2):459–62.
17. Meyers BC, Dickerman AW, Michelmore RW, Sivaramakrishnan S, Sobral BW, Young ND. Plant disease resistance genes encode members of an ancient and diverse protein family within the nucleotide-binding superfamily. Plant J. 1999; 20(3):317–32.
18. Bai S, Liu J, Chang C, Zhang L, Maekawa T, Wang Q, et al. Structure-function analysis of barley NLR immune receptor MLA10 reveals its cell compartment specific activity in cell death and disease resistance. PLoS Pathog. 2012; 8(6):e1002752.
19. Howles P, Lawrence G, Finnegan J, McFadden H, Ayliffe M, Dodds P, et al. Autoactive alleles of the flax L6 rust resistance gene induce non-race-specific rust resistance associated with the hypersensitive response. Mol Plant Microbe Interact. 2005; 18(6):570–82.
20. Dinesh-Kumar SP, Tham WH, Baker BJ. Structure-function analysis of the tobacco mosaic virus resistance gene N. Proc Natl Acad Sci U S A. 2000; 97(26):14789–94.
21. El Kasmi F, Chung EH, Anderson RG, Li J, Wan L, Eitas TK, et al. Signaling from the plasma-membrane localized plant immune receptor RPM1 requires self-association of the full-length protein. Proc Natl Acad Sci U S A. 2017; 114(35):E7385–E94.
22. Li J, Huang H, Zhu M, Huang S, Zhang W, Dinesh-Kumar SP, et al. A Plant Immune Receptor Adopts a Two-Step Recognition Mechanism to Enhance Viral Effector Perception. Mol Plant. 2019; 12(2):248–62.
23. Roberts M, Tang S, Stallmann A, Dangl JL, Bonardi V. Genetic requirements for signaling from an autoactive plant NB-LRR intracellular innate immune receptor. PLoS Genet. 2013; 9(4):e1003465.
24. Gao Z, Chung EH, Eitas TK, Dangl JL. Plant intracellular innate immune receptor Resistance to Pseudomonas syringae pv. maculicola 1 (RPM1) is activated at, and functions on, the plasma membrane. Proc Natl Acad Sci U S A. 2011; 108(18):7619–24.
25. Kawano Y, Akamatsu A, Hayashi K, Housen Y, Okuda J, Yao A, et al. Activation of a Rac GTPase by the NLR family disease resistance protein Pit plays a critical role in rice innate immunity. Cell Host Microbe. 2010; 7(5):362–75.
26. Bendahmane A, Farnham G, Moffett P, Baulcombe DC. Constitutive gain-of-function mutants in a nucleotide binding site-leucine rich repeat protein encoded at the Rx locus of potato. Plant J. 2002; 32 (2):195–204.

27. Slootweg EJ, Spiridon LN, Roosien J, Butterbach P, Pomp R, Westerhof L, et al. Structural determinants at the interface of the ARC2 and leucine-rich repeat domains control the activation of the plant immune receptors Rx1 and Gpa2. Plant Physiol. 2013; 162(3):1510–28.

28. Qi D, DeYoung BJ, Innes RW. Structure-function analysis of the coiled-coil and leucine-rich repeat domains of the RPS5 disease resistance protein. Plant Physiol. 2012; 158(4):1819–32.

29. Rairdan GJ, Moffett P. Distinct domains in the ARC region of the potato resistance protein Rx mediate LRR binding and inhibition of activation. Plant Cell. 2006; 18(8):2082–93.

30. Burdett H, Kobe B, Anderson PA. Animal NLRs continue to inform plant NLR structure and function. Arch Biochem Biophys. 2019; 670:58–68.

31. Bentham A, Burdett H, Anderson PA, Williams SJ, Kobe B. Animal NLRs provide structural insights into plant NLR function. Ann Bot. 2017; 119(5):827–702.

32. Hu Z, Zhou Q, Zhang C, Fan S, Cheng W, Zhao Y, et al. Structural and biochemical basis for induced self-propagation of NLRC4. Science. 2015; 350(6259):399–404.

33. Jia Y, McAdams SA, Bryan GT, Hershey HP, Valent B. Direct interaction of resistance gene and avirulence gene products confers rice blast resistance. EMBO J. 2000; 19(15):4004–14.

34. Adachi H, Derevnina L, Kamoun S. NLR singletons, pairs, and networks: evolution, assembly, and regulation of the intracellular immunoreceptor circuitry of plants. Curr Opin Plant Biol. 2019; 50:121–31.

35. Cesari S, Moore J, Chen C, Webb D, Periyannan S, Mago R, et al. Cytosolic activation of cell death and stem rust resistance by cereal MLA-family CC-NLR proteins. Proc Natl Acad Sci U S A. 2016; 113 (36):10204–9.

36. Townsend PD, Dixon CH, Slootweg EJ, Sukarta OCA, Yang AWH, Hughes TR, et al. The intracellular immune receptor Rx1 regulates the DNA-binding activity of a Golden2-like transcription factor. J Biol Chem. 2018; 293(9):3218–33.

37. Leibman-Markus M, Pizarro L, Schuster S, Lin ZJD, Gershony O, Bar M, et al. The intracellular nucleotide-binding leucine-rich repeat receptor (SlNRC4a) enhances immune signalling elicited by extracellular perception. Plant Cell Environ. 2018; 41(10):2313–27.

38. Baudin M, Hassan JA, Schreiber KJ, Lewis JD. Analysis of the ZAR1 Immune Complex Reveals Determinants for Immunity and Molecular Interactions. Plant Physiol. 2017; 174(4):2038–53.

39. Hamel LP, Sekine KT, Wallon T, Sugiwaka Y, Kobayashi K, Moffett P. The Chloroplastic Protein THF1 Interacts with the Coiled-Coil Domain of the Disease Resistance Protein N' and Regulates Light-Dependent Cell Death. Plant Physiol. 2016; 171(1):658–74.

40. Ade J, DeYoung BJ, Golstein C, Innes RW. Indirect activation of a plant nucleotide binding site-leucine-rich repeat protein by a bacterial protease. Proc Natl Acad Sci U S A. 2007; 104(7):2531–6.

41. Saur IM, Conlan BF, Rathjen JP. The N-terminal domain of the tomato immune protein Prf contains multiple homotypic and Pto kinase interaction sites. J Biol Chem. 2015; 290(18):11258–67.

42. Wang GF, Ji J, El-Kasmi F, Dangl JL, Johal G, Balint-Kurti PJ. Molecular and functional analyses of a maize autoactive NB-LRR protein identify precise structural requirements for activity. PLoS Pathog. 2015; 11(2):e1004674.

43. Jubic LM, Saile S, Furzer OJ, El Kasmi F, Dangl JL. Help wanted: helper NLRs and plant immune responses. Curr Opin Plant Biol. 2019; 50:82–94.

44. Wu CH, Derevnina L, Kamoun S. Receptor networks underpin plant immunity. Science. 2018; 360 (6395):1300–1.

45. Cesari S, Kanzaki H, Fujiwara T, Bernoux M, Chalvon V, Kawano Y, et al. The NB-LRR proteins RGA4 and RGA5 interact functionally and physically to confer disease resistance. EMBO J. 2014; 33 (17):1941–59.

46. Guo L, Cesari S, de Guillen K, Chalvon V, Mammri L, Ma M, et al. Specific recognition of two MAX effectors by integrated HMA domains in plant immune receptors involves distinct binding surfaces. Proc Natl Acad Sci U S A. 2018; 115(45):11637–42.

47. Ortiz D, de Guillen K, Cesari S, Chalvon V, Gracy J, Padilla A, et al. Recognition of the Magnaporthe oryzae Effector AVR-Pia by the Decoy Domain of the Rice NLR Immune Receptor RGA5. Plant Cell. 2017; 29(1):156–68.

48. Huh SU, Cevik V, Ding P, Duxbury Z, Ma Y, Tomlinson L, et al. Protein-protein interactions in the RPS4/RRS1 immune receptor complex. PLoS Pathog. 2017; 13(5):e1006376.

49. Zhang ZM, Ma KW, Gao L, Hu Z, Schwizer S, Ma W, et al. Mechanism of host substrate acetylation by a YopJ family effector. Nat Plants. 2017; 3:17115.

50. Maqbool A, Saitoh H, Franceschetti M, Stevenson CE, Uemura A, Kanzaki H, et al. Structural basis of pathogen recognition by an integrated HMA domain in a plant NLR immune receptor. Elife. 2015;4.

51. Kroj T, Chanclud E, Michel-Romiti C, Grand X, Morel JB. Integration of decoy domains derived from protein targets of pathogen effectors into plant immune receptors is widespread. New Phytol. 2016; 210 (2):618–26.

52. Sarris PF, Cevik V, Dagdas G, Jones JD, Krasileva KV. Comparative analysis of plant immune receptor architectures uncovers host proteins likely targeted by pathogens. BMC Biol. 2016; 14:8.

53. Cesari S, Bernoux M, Moncuquet P, Kroj T, Dodds PN. A novel conserved mechanism for plant NLR protein pairs: the "integrated decoy" hypothesis. Front Plant Sci. 2014; 5:606.

54. Baggs E, Dagdas G, Krasileva KV. NLR diversity, helpers and integrated domains: making sense of the NLR IDentity. Curr Opin Plant Biol. 2017; 38:59–67.

55. Ma Y, Guo H, Hu L, Martinez PP, Moschou PN, Cevik V, et al. Distinct modes of derepression of an Arabidopsis immune receptor complex by two different bacterial effectors. Proc Natl Acad Sci U S A. 2018; 115(41):10218–27.

56. Williams SJ, Sohn KH, Wan L, Bernoux M, Sarris PF, Segonzac C, et al. Structural basis for assembly and function of a heterodimeric plant immune receptor. Science. 2014; 344(6181):299–303.

57. De la Concepcion JC, Franceschetti M, MacLean D, Terauchi R, Kamoun S, Banfield MJ. Protein engineering expands the effector recognition profile of a rice NLR immune receptor. Elife. 2019;8.

58. De la Concepcion JC, Franceschetti M, Maqbool A, Saitoh H, Terauchi R, Kamoun S, et al. Polymorphic residues in rice NLRs expand binding and response to effectors of the blast pathogen. Nat Plants. 2018; 4(8):576–85.

59. Engler C, Kandzia R, Marillonnet S. A one pot, one step, precision cloning method with high throughput capability. PLoS One. 2008; 3(11):e3647.

60. Wickham H. ggplot2: Elegant Graphics for Data Analysis. Springer-Verlag New York. 2016.

61. Win J, Kamoun S, Jones AM. Purification of effector-target protein complexes via transient expression in Nicotiana benthamiana. Methods Mol Biol. 2011; 712:181–94.

62. Williams SJ, Sornaraj P, deCourcy-Ireland E, Menz RI, Kobe B, Ellis JG, et al. An autoactive mutant of the M flax rust resistance protein has a preference for binding ATP, whereas wild-type M protein binds ADP. Mol Plant Microbe Interact. 2011; 24(8):897–906.

63. Tameling WIL, Elzinga SDJ, Darmin PS, Vossen JH, Takken FLW, Haring MA, et al. The Tomato R Gene Products I-2 and Mi-1 Are Functional ATP Binding Proteins with ATPase Activity. The Plant Cell. 2002; 14(11):2929–39.

64. Takken FL, Goverse A. How to build a pathogen detector: structural basis of NB-LRR function. Curr Opin Plant Biol. 2012; 15(4):375–84.

65. van Ooijen G, Mayr G, Kasiem MM, Albrecht M, Cornelissen BJ, Takken FL. Structure-function analysis of the NB-ARC domain of plant disease resistance proteins. J Exp Bot. 2008; 59(6):1383–97.

66. de la Fuente van Bentem S, Vossen JH, de Vries KJ, van Wees S, Tameling WI, Dekker HL, et al. Heat shock protein 90 and its co-chaperone protein phosphatase 5 interact with distinct regions of the tomato I-2 disease resistance protein. Plant J. 2005; 43(2):284–98.

67. Lee H-Y, Mang H, Choi E-H, Seo Y-E, Kim M-S, Oh S, et al. Genome-wide functional analysis of hot pepper immune receptors reveals an autonomous NLR cluster in seed plants. bioRxiv. 2020:2019.12.16.878959.

68. Wroblewski T, Spiridon L, Martin EC, Petrescu AJ, Cavanaugh K, Truco MJ, et al. Genome-wide functional analyses of plant coiled-coil NLR-type pathogen receptors reveal essential roles of their N-terminal domain in oligomerization, networking, and immunity. PLoS Biol. 2018; 16(12):e2005821.

69. Casey LW, Lavrencic P, Bentham AR, Cesari S, Ericsson DJ, Croll T, et al. The CC domain structure from the wheat stem rust resistance protein Sr33 challenges paradigms for dimerization in plant NLR proteins. Proc Natl Acad Sci U S A. 2016.

70. Maekawa T, Cheng W, Spiridon LN, Toller A, Lukasik E, Saijo Y, et al. Coiled-coil domain-dependent homodimerization of intracellular barley immune receptors defines a minimal functional module for triggering cell death. Cell Host Microbe. 2011; 9(3):187–99.

71. Krasileva KV, Dahlbeck D, Staskawicz BJ. Activation of an Arabidopsis resistance protein is specified by the in planta association of its leucine-rich repeat domain with the cognate oomycete effector. Plant Cell. 2010; 22(7):2444–58.

72. Adachi H, Contreras MP, Harant A, Wu CH, Derevnina L, Sakai T, et al. An N-terminal motif in NLR immune receptors is functionally conserved across distantly related plant species. Elife. 2019;8.

73. Rairdan GJ, Collier SM, Sacco MA, Baldwin TT, Boettrich T, Moffett P. The coiled-coil and nucleotide binding domains of the Potato Rx disease resistance protein function in pathogen recognition and signaling. Plant Cell. 2008; 20(3):739–51.

74. Wu CH, Abd-El-Haliem A, Bozkurt TO, Belhaj K, Terauchi R, Vossen JH, et al. NLR network mediates immunity to diverse plant pathogens. Proc Natl Acad Sci U S A. 2017; 114(30):8113–8.

75. Castel B, Ngou PM, Cevik V, Redkar A, Kim DS, Yang Y, et al. Diverse NLR immune receptors activate defence via the RPW8-NLR NRG1. New Phytol. 2019; 222(2):966–80.

76. Wu Z, Li M, Dong OX, Xia S, Liang W, Bao Y, et al. Differential regulation of TNL-mediated immune signaling by redundant helper CNLs. New Phytol. 2019; 222(2):938–53.

77. Bonardi V, Tang S, Stallmann A, Roberts M, Cherkis K, Dangl JL. Expanded functions for a family of plant intracellular immune receptors beyond specific recognition of pathogen effectors. Proc Natl Acad Sci U S A. 2011; 108(39):16463–8.

78. Steele JFC, Hughes RK, Banfield MJ. Structural and biochemical studies of an NB-ARC domain from a plant NLR immune receptor. PLoS One. 2019; 14(8):e0221226.

79. Ntoukakis V, Saur IM, Conlan B, Rathjen JP. The changing of the guard: the Pto/Prf receptor complex of tomato and pathogen recognition. Curr Opin Plant Biol. 2014; 20:69–74.

80. Gutierrez JR, Balmuth AL, Ntoukakis V, Mucyn TS, Gimenez-Ibanez S, Jones AM, et al. Prf immune complexes of tomato are oligomeric and contain multiple Pto-like kinases that diversify effector recognition. Plant J. 2010; 61(3):507–18.

81. Mestre P, Baulcombe DC. Elicitor-mediated oligomerization of the tobacco N disease resistance protein. Plant Cell. 2006; 18(2):491–501.

82. Zhang X, Bernoux M, Bentham AR, Newman TE, Ve T, Casey LW, et al. Multiple functional self-association interfaces in plant TIR domains. Proc Natl Acad Sci U S A. 2017; 114(10):E2046–E52.

83. Schreiber KJ, Bentham A, Williams SJ, Kobe B, Staskawicz BJ. Multiple Domain Associations within the Arabidopsis Immune Receptor RPP1 Regulate the Activation of Programmed Cell Death. PLoS Pathog. 2016; 12(7):e1005769.

84. Bernoux M, Ve T, Williams S, Warren C, Hatters D, Valkov E, et al. Structural and functional analysis of a plant resistance protein TIR domain reveals interfaces for self-association, signaling, and autoregulation. Cell Host Microbe. 2011; 9(3):200–11.

85. Zhang L, Chen S, Ruan J, Wu J, Tong AB, Yin Q, et al. Cryo-EM structure of the activated NAIP2-NLRC4 inflammasome reveals nucleated polymerization. Science. 2015; 350(6259):404–9.

86. Tenthorey JL, Haloupek N, Lopez-Blanco JR, Grob P, Adamson E, Hartenian E, et al. The structural basis of flagellin detection by NAIP5: A strategy to limit pathogen immune evasion. Science. 2017; 358 (6365):888–93.